

1994

# STRUCTURAL INTEGRITY ASSESSMENT USING VIBRATION DATA

SALAWU, OLUSEGUN SAHEED

<http://hdl.handle.net/10026.1/2614>

---

<http://dx.doi.org/10.24382/3861>

University of Plymouth

---

*All content in PEARL is protected by copyright law. Author manuscripts are made available in accordance with publisher policies. Please cite only the published version using the details provided on the item record or document. In the absence of an open licence (e.g. Creative Commons), permissions for further reuse of content should be sought from the publisher or author.*

**STRUCTURAL INTEGRITY ASSESSMENT USING  
VIBRATION DATA**

**By**

**O. S. SALAWU, BSc, MSc (Eng)**

**PhD THESIS**

**JULY 1994**

*This copy of the thesis has been supplied on condition that anyone who consults it is understood to recognise that its copyright rests with its author and that no quotation from the thesis and no information derived from it may be published without the author's prior written consent.*

© O. S. Salawu, 1994.

**STRUCTURAL INTEGRITY ASSESSMENT USING VIBRATION DATA**

by

**OLUSEGUN SAHEED SALAWU, B.Sc, M.Sc (Eng.)**

A thesis submitted to the University of Plymouth  
in partial fulfilment for the degree of

**DOCTOR OF PHILOSOPHY**

School of Civil and Structural Engineering  
Faculty of Technology

July 1994.

UNIVERSITY OF PLYMOUTH  
LIBRARY SERVICES

ITEM  
NO.

900 0058077

CLASS  
NO.

T620.1127 SAL

CARD  
NO.

X702927472

90 0205807 7



REFERENCE ONLY

## **ACKNOWLEDGEMENT**

The author acknowledges with thanks the following people and organisations who have made this work possible:

Dr. C. Williams, Director of Studies, for providing the opportunity to undertake the research and for his help during the course of the project.

The University of Plymouth for funding the research.

Mr. P. J. Hewson for his advice and interest.

Technical Staff, School of Civil and Structural Engineering, for their help during the experimental phase of the project. In particular, Keith Stott, Ian Morgan and Brian Worley for their assistance during the field tests.

Department of Transport, Devon County Council and Mott MacDonald Special Services for their support in connection with the full-scale testing of Deep Lane bridge.

Somerset Consulting Engineers (consulting division of the Environment Department, Somerset County Council) for supplying structural details of Holway Road bridge and their assistance during full-scale tests on the bridge.

The Institution of Civil Engineers for providing a scholarship enabling me to participate at the 2nd Computational Structures Technology Conference, Athens, 1994.

WS Atkins Engineering Services, Bristol Office, for their support for the project.

My fellow researchers in the School for their help, at various times and in various ways, during the research period.

My family for their support and encouragement.

## AUTHOR'S DECLARATION

At no time during the registration for the degree of Doctor of Philosophy has the author been registered for any other award in any University. The dissertation is based entirely on independent work by the author. All the work and ideas recorded are original except where acknowledged in the text or by reference to published literature.

The following conferences, at which papers were presented, were attended by the author:

- (a) 11th International Modal Analysis Conference, Florida, Feb. 1-4, 1993.
- (b) 2nd International Conference on Computational Structures Technology, Athens, Greece, Aug. 30th - Sep. 1st, 1994.

Based in whole or part on the work described in this thesis, the following papers have been published:

'Damage Detection Using Experimental Modal Analysis - A Comparison of Some Methods'  
Salawu, O. S. and Williams, C.  
Proceedings of the 11th International Modal Analysis Conference, Kissimmee, Florida, Vol. 1, pp. 254-260, 1993.

'Hydraulic Actuators Deliver Controllable Excitation for the Analysis of Large Structures'  
Salawu, O. S. and Williams, C.  
Noise & Vibration Worldwide, Vol. 24, No. 5, pp. 15-18, 1993.

'Forced Vibration Testing of a Highway Bridge'  
Salawu, O. S. and Williams, C.  
Noise & Vibration Worldwide, Vol. 24, No. 6, pp. 14-15, 1993.

'Damage Location using Vibration Mode Shapes'  
Salawu, O. S. and Williams, C.  
Proceedings of the 12th International Modal Analysis Conference, Honolulu, Hawaii, Vol. 1, pp. 933-939, 1994.

'Modal Identification of a Full-Scale Highway Bridge'  
Williams, C. and Salawu, O. S.  
Proceedings of the 12th International Modal Analysis Conference, Honolulu, Hawaii, Vol. 1, pp. 724-730, 1994.

'An Excitation System for Dynamic Testing of Large Structures'  
Salawu, O. S. and Williams, C.  
Journal of Testing and Evaluation, Vol. 22, No. 4, pp. 370-375, July 1994.

**'A Review of Full Scale Dynamic Testing of Bridge Structures'**

Salawu, O. S. and Williams, C.

To appear in *Engineering Structures*, 1995.

**'Bridge Assessment Using Forced Vibration Testing'**

Salawu, O. S. and Williams, C.

To appear in *Journal of Structural Engineering*, American Society of Civil Engineers, February 1995.

**'Development and Use of an Excitation System for Dynamic Testing of Large Structures'**

Williams, C., Salawu, O. S. and Tsang, W. F.

International Conference on Advances in Engineering Measurements, Edinburgh, 30th Aug. - 1st Sept, 1994.

**'Comparison of Results from Vibration Testing and Finite Element Analysis of a Highway Bridge'**

Salawu, O. S., Williams, C. and Hewson, P. J.

Second International Conference on Computational Structures Technology, Athens, Greece, 30th August - 1st Sept., 1994.

*Published in Computational Structural Engineering for Practice (editors: M. Papadrakakis and B. H. V. Topping), Civil Comp Press, Edinburgh, 1994, pp. 61-69.*

**'Concepts of Condition Assessment of Bridges using Vibration Testing and Analysis'**

Williams, C. and Salawu, O. S.

Centenary Year Bridge Conference, Cardiff, 26th - 30th September, 1994.

**'Non-Destructive Evaluation of Constructed Facilities using Vibration Testing'**

Salawu, O. S.

*INSIGHT: The Journal of the British Institute of Non-Destructive Testing*, Vol. 36, No. 8, 1994.

**'An Integrity Index Method for Structural Assessment of Engineering Structures using Modal Testing'**

Salawu, O. S.

Submitted to *Modal Analysis: The International Journal of Analytical and Experimental Modal Analysis*, 1994.

Signature.....

Date.....28/7/94

# **STRUCTURAL INTEGRITY ASSESSMENT USING VIBRATION DATA**

**By**

**Olusegun Saheed Salawu**

## **ABSTRACT**

Engineering structures need to be assessed as part of activities to ensure their continued serviceability. Global methods of assessment which also give an indication of local conditions are most attractive since they are cost effective and flexible. A suitable method with these attributes is vibration monitoring which involves relating dynamic properties, or changes in them, to the integrity of the assessed structure. The present study investigates the application of vibration testing to structural integrity assessment of civil engineering structures.

A survey of existing methods of damage detection, location and quantification in structures using vibration testing was conducted. Evaluation of the performance of some of the more promising methods was conducted using both simulated and experimental data. The results revealed that the damage identification process could be enhanced if appropriate modes are used. To this end, a new function, called Modal Sensitivity Values, has been proposed for identifying damage sensitive modes to be included in damage detection and location methods. It was also found that some success could be achieved if system identification and model updating procedures are applied to the problem of damage detection in structures. The literature survey revealed that most of the available methods are not applicable to general structural systems and are often limited by the damage model assumed. A new method, called Integrity Index Damage Location method, of assessing structural integrity using vibration data has also been proposed. The method is applicable to any structure and any damage type that affects the integrity/stiffness of the structure. Performance evaluation of the method using both numerical and experimental data is presented.

Full-scale forced vibration tests were conducted before and after repairs on two reinforced concrete highway bridges. The vibrator used during the tests was developed during the research project and details of its development and operation are given in the thesis. As a background to the tests, a review of full-scale dynamic testing of bridge structures was conducted. Results from the tests were used to investigate the effectiveness of forced vibration testing as an integrity monitoring tool. It was found that the repair works caused slight (less than 5%) changes in the natural frequencies while there was no definite trend in the changes to the modal damping ratios. Comparison of frequency response functions and mode shapes, using modal analysis procedures, was found to give an indication of the presence and location of the repairs. The integrity assessment method proposed was also able to identify some of the affected parts of the structures.

Results from the full-scale tests were also compared with predictions from finite element analysis. Good correlation was obtained between the measured and calculated natural frequencies and mode shapes, thus enabling validation of the analytical models within limits of the model assumptions and experimental errors. The results demonstrate the importance of accurate representation of boundary conditions. They (results) also showed that the vertical stiffness of new bearings installed on one of the bridges is not as high as was assumed in the design.

# LIST OF CONTENTS

<i>Copyright Statement</i>	
<i>Title page</i>	
<i>Acknowledgement</i>	iv
<i>Author's Declaration</i>	v
<i>Abstract</i>	vii
<i>List of Contents</i>	viii
<i>List of Figures</i>	xiii
<i>List of Tables</i>	xvi
<i>Notations</i>	xviii
<i>Abbreviations</i>	xxi
<b>1 INTRODUCTION</b>	<b>1</b>
1.1 General Background	1
1.2 Objectives and Outline of This Work	3
<b>2 A REVIEW OF FULL-SCALE DYNAMIC TESTING OF BRIDGE STRUCTURES</b>	<b>6</b>
2.1 Introduction	6
2.2 Reasons for Full-Scale Dynamic Testing	8
2.3 Ambient Vibration Testing	9
2.4 Forced Vibration Testing	16
2.4.1 Eccentric rotating mass vibrators	17
2.4.2 Electro-hydraulic vibrators	19
2.4.3 Impactors	22
2.4.4 Other excitation mechanisms	26
2.5 Concluding Remarks	29
<b>3 A REVIEW OF METHODS OF DAMAGE DETECTION AND INTEGRITY ASSESSMENT USING VIBRATION DATA</b>	<b>32</b>
3.1 Introduction	32
3.2 Theoretical Background	34
3.3 Methods Based on Measuring Natural Frequency Changes	37

3.3.1	Effects of structural damage on natural frequency	37
3.3.2	Damage detection and location using natural frequency changes	39
3.4	Damage Detection and Location using Mode Shape Data	43
3.5	Methods Based on Measuring Changes in Damping Values	47
3.6	Mathematical Model Error Localization Schemes	50
3.7	Other Damage Location Methods	54
3.9	Factors to Consider	57
3.9	Conclusions	61
<b>4</b>	<b>EVALUATION OF SOME DAMAGE LOCATION METHODS</b>	<b>64</b>
4.1	Introduction	64
4.2	Methods Utilizing Modal Data	65
4.2.1	MAC, COMAC and MSV	65
4.2.2	Eigenparameter method	67
4.2.3	Curvature mode shape method	69
4.2.4	Mode shape relative difference method	70
4.3	Methods Based on Model Updating Procedures	70
4.3.1	Matrix cursor method	70
4.3.2	Identification of system matrices	74
4.3.3	Stiffness error matrix method	76
4.4	Cantilever Beam	77
4.4.1	Damage simulation	78
4.4.2	Results from the analysis	79
4.5	Experimental Steel Beam	79
4.5.1	Experimental arrangement	79
4.5.2	Damage cases	81
4.5.3	Test results	83
4.6	Performance of the Methods	84
4.6.1	Methods based on modal data	84
4.6.1.1	Cantilever beam	84
4.6.1.2	Steel beam	93
4.6.2	Model updating methods	98
4.6.2.1	Cantilever beam	99
4.6.2.2	Steel beam	106

4.7	Conclusions	108
<b>5</b>	<b>THE INTEGRITY INDEX DAMAGE LOCATION METHOD</b>	<b>110</b>
5.1	Introduction	110
5.2	Development and Implementation	111
5.2.1	Global Integrity Index	111
5.2.2	Local Integrity Indices	113
5.3	Evaluation of the Method using Simulated Data	114
5.3.1	Cantilever beam	116
5.3.2	Eight degrees of freedom (8-DOF) mass-spring system	118
5.4	Evaluation of the Method using Experimental Data	123
5.4.1	Simply supported steel beam	123
5.4.2	3-storey frame model structure	124
5.5	Conclusions	127
<b>6</b>	<b>TEST EQUIPMENT AND ANALYSIS PROCEDURES</b>	<b>128</b>
6.1	Introduction	128
6.2	An Excitation System for Full-Scale Testing	130
6.2.1	Description of system	130
6.2.2	Excitation signal generation	134
6.2.2.1	Signal source	134
6.2.2.2	Signal types	134
6.2.3	Hydraulic jack and pumps	135
6.2.4	The test frame/rig	136
6.2.5	Weight carrying system	138
6.2.6	Performance characteristics	140
6.2.6.1	Correlation between input signal, load response and stroke response	142
6.2.6.2	Characteristics of the load generated	144
6.2.6.3	Characteristics of the stroke response	146
6.3	Data Acquisition and Recording System	147
6.3.1	Response transducers	147
6.3.2	Signal conditioning equipment	148
6.3.3	Signal monitoring and recording equipment	149
6.3.4	PC based data acquisition system	150

6.4	Analysis of Vibration Data	150
6.4.1	Discrete Fourier transform	151
6.4.2	Signal processing errors	154
6.4.3	Frequency response function calculation	157
6.4.4	Signal analysis equipment	159
6.5	Modal Parameter Extraction	160
6.5.1	Inverse method	163
6.5.2	Direct least squares method	164
6.5.3	Improved amplitude fitting method	165
6.5.4	Implementation of the methods	167
6.6	Repeatability and Accuracy of Results from Test System	168
6.6.1	Effect of temperature on signal acquisition and recording equipment	170
6.6.2	Effect of random environmental factors	173
6.7	Conclusions	180
<b>7</b>	<b>FULL-SCALE TESTING OF DEEP LANE BRIDGE</b>	<b>182</b>
7.1	Introduction	182
7.2	Description of Bridge	182
7.3	The Repair Scheme	185
7.4	Full-Scale Testing	186
7.4.1	Equipment	188
7.4.2	Measurement locations	188
7.4.3	Test procedure	190
7.4.4	Data analysis	192
7.5	Theoretical Vibration Analysis	197
7.6	Experimental Results and Comparison with Theoretical Results	199
7.7	Discussion of Experimental Results	204
7.7.1	Frequency response functions	206
7.7.2	Natural frequency and damping values	212
7.7.3	Mode shapes, MAC and MSV	214
7.7.4	COMAC and Integrity Indices	219
7.8	Conclusions	223

<b>8</b>	<b>FULL-SCALE TESTING OF HOLWAY ROAD BRIDGE</b>	<b>224</b>
8.1	Introduction	224
8.2	Description of Bridge	224
8.3	The Repair Work	225
8.4	Finite Element Modelling and Pre-Test Analyses	227
8.5	Measurement Procedures	231
8.6	Discussion of Experimental Results	232
	8.6.1 Frequency response function (FRF)	237
	8.6.2 Natural frequencies and damping values	237
	8.6.3 MAC, MSV and mode shapes	240
	8.6.4 COMAC and Integrity Indices	241
8.7	Comparison of Analytical and Experimental Results	245
8.8	Conclusions	252
<b>9</b>	<b>SUMMARY, CONCLUSIONS AND RECOMMENDATIONS</b>	<b>253</b>
9.1	Full-Scale Testing	253
9.2	Analytical Model Validation	254
9.3	Structural Assessment using Vibration Data	255
9.4	Recommendations for Future Work	259
	<b>REFERENCES</b>	<b>260</b>
	<b>APPENDIX - METEOROLOGICAL DATA DURING FULL-SCALE TESTS</b>	<b>279</b>

## LIST OF FIGURES

### CHAPTER 2

2.1	Stages involved in vibration testing	7
2.2	Relationship between fundamental frequency and span for concrete bridges (Alvarez et al, 1993)	15
2.3	Rotating mass vibrator (after Shepherd and Reay, 1967)	18
2.4	A simple impact device	23
2.5	Transient excitation	27

### CHAPTER 3

3.1	Changes in frequency, damping and temperature in short-term tests (Askegaard and Mossing, 1988)	59
3.2	Long-term changes in frequency, damping and temperature (Askegaard and Mossing, 1988)	59

### CHAPTER 4

4.1	Section of a general structure	65
4.2	Eigenparameter plots	68
4.3	Matrix cursor example	73
4.4	Cantilever beam model	77
4.5	Experimental arrangement for beam tests	81
4.6	Diagrammatic representation of induced damage - steel beam	82
4.7	Mode shapes for steel beam	85
4.8	Identification of sensitive modes using MSV and frequency changes - cantilever beam	87
4.9	Eigenparameter plots for all damage cases - cantilever beam	89
4.10	Absolute difference in curvature mode shapes - cantilever beam	91
4.11	Plots of relative difference in displacement mode shapes - cantilever beam	92
4.12	Displacement eigenparameter plots for steel beam	95
4.13	Absolute difference in curvature mode shapes - steel beam	96
4.14	Relative difference in displacement mode shapes - steel beam	97
4.15	Comparison of FRFs from original and identified system matrices of cantilever beam	99
4.16	Damage location plots for cantilever beam using all six modes: case 2	101
4.17	Damage location plots for cantilever beam using the matrix cursor method with six modes	102
4.18	Damage location plots for cantilever beam using stiffness error matrix method with six modes	103
4.19	Damage location plots for cantilever beam using the matrix cursor method: case 3	104
4.20	Damage location plots for cantilever beam using stiffness error matrix method: case 3	105
4.21	Damage location plot for steel beam using the matrix cursor method	106
4.22	Damage location plots for steel beam using stiffness error matrix method	107

## CHAPTER 5

5.1	Flowchart for identifying damage locations using the Integrity Index method	115
5.2	8-DOF system	119
5.3	Eigenvalues [(rad/sec.) <sup>2</sup> ] of 8-DOF system	120
5.4	Eigenvectors of 8-DOF system	120
5.5	Elevation of the model structure (after Beck, 1991)	125

## CHAPTER 6

6.1	Instrumentation layout for dynamic tests	129
6.2	Block diagram of excitation system	131
6.3	Excitation system on location	132
6.4	The electro-hydraulic vibrator used in full-scale tests	133
6.5	Side view of the test frame	138
6.6	Weight carrying system	139
6.7	Block diagram of experimental set-up to determine characteristics of vibrator	141
6.8	Coherence function between excitation signal and response from load cell	142
6.9	Phase of the signal from the load cell relative to the excitation signal	143
6.10	Coherence function between excitation signal and stroke amplitude	143
6.11	Sample amplitude response of the load generated	145
6.12	Coherence function between transducer (accelerometer) and input load	146
6.13	Auto-spectrum of stroke	147
6.14	Partitioning of time history	153
6.15	Overlapp averaging	154
6.16	Single input-output system	157
6.17	Real and imaginary parts of receptance	164
6.18	Flow chart of the module used to implement the modified IAF method	169
6.19	Experimental set-up for signal acquisition system calibration	171
6.20	Inclination of accelerometers	171
6.21	Set-up of test to investigate effect of random experimental errors on test and analysis techniques	174

## CHAPTER 7

7.1	Photograph showing Deep Lane bridge	183
7.2	Side elevation and cross-section of Deep Lane bridge (dimensions in mm)	184
7.3	Location of the repairs	187
7.4	Measurement locations (dimensions in mm)	189
7.5	FRFs from sine sweep test	191
7.6	Typical plots of FRF amplitude and coherence from tests before the repairs	193
7.7	Typical plots of FRF amplitude and coherence from tests after the repairs	194
7.8	Example of curve-fit - point 11 : before repairs	195
7.9	Example of curve-fit - point 46 : before repairs	195
7.10	Example of curve-fit - point 4 : after repairs	196
7.11	Example of curve-fit - reference point, test 8 : after repairs	196

7.12	Finite element model of Deep Lane bridge	198
7.13	Comparison of experimental and analytical mode shapes	202
7.14	FRFs measured at the reference point before the repairs	207
7.15	FRFs measured at the reference point after the repairs	208
7.16	Comparison of the magnitudes of FRF : Deep Lane bridge	209
7.17	Comparison of the squares of the imaginary part : Deep Lane bridge	210
7.18	Comparison of the squares of the real part : Deep Lane bridge	211
7.19	Comparison of mode shapes before and after repairs : Deep Lane bridge	215
7.20	Modal Assurance Criterion (MAC) values of Deep Lane bridge	218

## CHAPTER 8

8.1	Side elevation and deck cross-section of Holway Road bridge (dimensions in mm)	226
8.2	Finite element model of Holway Road bridge	228
8.3	Layout of measurement points used (dimensions in mm)	233
8.4	Sample FRF plot from tests before bearing replacement	234
8.5	Example of curve-fitting	235
8.6	Typical FRFs measured at the reference point	236
8.7	Comparison of FRFs before and after bearing replacement	238
8.8	Comparison of experimental mode shapes before and after bearing replacement	242
8.9	Comparison of analytical and experimental mode shapes before bearing replacement	248
8.10	Comparison of analytical and experimental mode shapes after bearing replacement	250

## APPENDIX

A.1	Variation in ambient conditions in Plymouth during tests on Deep Lane bridge	282
-----	--	-----

## LIST OF TABLES

### CHAPTER 4

4.1	Natural frequencies of the cantilever beam	80
4.2	Natural frequencies obtained from beam tests	83
4.3	Viscous damping ratios obtained from beam tests	84
4.4	MAC and MSV for the cantilever beam	86
4.5	COMAC values for the cantilever beam	88
4.6	MAC and MSV for steel beam	94
4.7	COMAC values for steel beam	94

### CHAPTER 5

5.1	Global Integrity Indices for cantilever beam	116
5.2	Local Integrity Indices for cantilever beam	117
5.3	Natural frequencies of 8-DOF system for different damage cases	121
5.4	Global Integrity Indices for 8-DOF system	122
5.5	Local Integrity Indices for 8-DOF system	122
5.6	Global Integrity Indices for steel beam	124
5.7	Local Integrity Indices for steel beam	124
5.8	Modal parameters of 3-storey model structure	126
5.9	Global and Local Integrity Indices for 3-storey model structure	127

### CHAPTER 6

6.1	System calibration factors	173
6.2	Repeatability of results: comparison of natural frequencies (Hz)	176
6.3	Repeatability of results: comparison of modal damping values (% of critical damping)	177
6.4	Repeatability of results: comparison of MAC values	178
6.5	Identified values of effective modulus of elasticity	180

### CHAPTER 7

7.1	Comparison of analytical and experimental frequencies of Deep Lane bridge	201
7.2	Comparison of natural frequencies and damping ratios obtained before and after repairs to Deep Lane bridge	213
7.3	Modal Sensitivity Values (MSV) of Deep Lane bridge	218
7.4	Coordinate Modal Assurance Criterion (COMAC) values of Deep Lane bridge	220
7.5	Local Integrity Indices of Deep Lane bridge	222

### CHAPTER 8

8.1	Comparison of frequencies for partial and full vertical restraint at abutments	230
8.2	MAC matrix for partial and full vertical restraint at abutment	230
8.3	Comparison of natural frequencies and damping ratios obtained before and after bearing replacement on Holway Road bridge	239
8.4	Modal Assurance Criterion (MAC) values of Holway Road bridge	240
8.5	Modal Sensitivity Values (MSV) of Holway Road bridge	240

8.6	COMAC values and Local Integrity Indices	244
8.7	Comparison of analytical and experimental frequencies of Holway Road bridge	246
8.8	MAC matrix for analytical and experimental models before bearing replacement	246
8.9	MAC matrix for analytical and experimental models after bearing replacement	247
8.10	MSV for analytical and experimental models	247

## APPENDIX

A.1	Environmental variables for Wednesday, 14th October, 1992	280
A.2	Environmental variables for Thursday, 15th October, 1992	280
A.3	Environmental variables for Tuesday, 25th May, 1993	281
A.4	Environmental variables for Wednesday, 26th May, 1993	281
A.5	Meteorological data during tests on Holway Road bridge	283

## NOTATIONS

$A_{ikr}$	modal constant for the $r$ th mode at measurement point $i$ for excitation at point $k$
[A]	sensitivity matrix
$a$	weighting factor
{B}	vector of measured changes in FRF, modulus of FRF or phase difference
$b$	number of data blocks
{b}	vector of damage parameters
[C]	physical viscous damping matrix
$c_r$	modal viscous damping ratio
[c]	diagonal modal viscous damping matrix
$E$	modulus of elasticity
$E'$	effective modulus of elasticity
$E_c$	static modulus of elasticity
$E_d$	dynamic modulus of elasticity
$E_{c,28}$	static modulus of elasticity at 28 days
{F(t)}	vector of externally applied time dependent forces
{F(j $\omega$ )}	complex Fourier transform of {F(t)}
$f$	frequency variable (Hz)
$f_{NYQ}$	Nyquist frequency
$f_r$	natural frequency (Hz) of the $r$ th mode
$G_{uu}(f)$	one-sided auto-spectral density function of $u(t)$
$G_{vv}(f)$	one-sided auto-spectral density function of $v(t)$
$G_{uv}(jf)$	one-sided cross-spectral density function of $u(t)$ and $v(t)$
$g$	gravitational acceleration ( $g \approx 9.81 \text{ m/s}^2$ )
$H_1(jf)$	frequency response function estimator
$H_2(jf)$	frequency response function estimator
$H_{ik}(j\omega)$	element of [H(j $\omega$ )] at row $i$ and column $k$
[H(j $\omega$ )]	frequency response function matrix
$h$	length of a beam element (distance between two consecutive measurement points)
$I$	second moment of area
Im(X)	imaginary part of a complex function X
$j$	imaginary part ( $j^2 = -1$ )
[K]	physical stiffness matrix
[K <sup>H</sup> ]	'hybrid' stiffness matrix
[ $\Delta$ K]	stiffness error matrix
$k_r$	modal stiffness for mode $r$
[k]	diagonal modal stiffness matrix
$L$	total number of correlated mode pairs
$l$	length of beam
$M$	bending moment at a section
[M]	physical mass matrix
$m$	number of measured modes
$m_r$	modal mass for mode $r$
[m]	diagonal modal mass matrix
$n$	total number of measured degrees of freedom
$P_r$	modal participation factor for mode $r$
[P]	matrix projection operator
$Q$	magnitude of frequency response function
Re(X)	real part of a complex function X

$\{RD\}$	relative difference between two displacement eigenvectors
$T$	record length of a time history segment
$T_T$	total length of a signal
$t$	time variable
$U(jf)$	complex Fourier transform of $u(t)$
$\{U\}$	eigenparameter vector
$u$	number of error locations
$u(t)$	time history of a random process $u$
$V(jf)$	complex Fourier transform of $v(t)$
$v(t)$	time history of a random process $v$
$v''$	curvature
$W$	constant parameter
$\{X(t)\}$	physical coordinate displacement vector
$\{X(j\omega)\}$	complex Fourier transform of $\{X(t)\}$
$\{X'(t)\}$	physical coordinate velocity vector
$\{X'(j\omega)\}$	complex Fourier transform of $\{X'(t)\}$
$\{X''(t)\}$	physical coordinate acceleration vector
$\{X''(j\omega)\}$	complex Fourier transform of $\{X''(t)\}$
$[ ]$	matrix
$\{ \}$	vector
$( )$	element of matrix or vector
$[\alpha_M]$	approximation to the mass error matrix
$[\alpha_S]$	approximation to the stiffness error matrix
$[\delta_S]$	approximation to the stiffness error matrix
$[\epsilon_S]$	approximation to the stiffness error matrix
$\lambda$	eigenvalue
$\gamma_{uv}^2$	coherence function between $u$ and $v$
$\xi$	modal viscous damping ratio
$\Sigma$	summation sign
$[\Psi]$	mode shape matrix
$\{\phi\}$	mode shape/eigenvector
$\{\phi'\}$	normal velocity vector
$\{\phi''\}$	normal acceleration vector
$(\phi_{ir})$	element of $r$ th mode shape at point $i$
$(\phi_{kr})$	element of $r$ th mode shape at point $k$
$\omega$	frequency variable (radians/seconds)
$\omega_r$	natural frequency (radians/seconds) of the $r$ th mode
$M$	mass per unit length of beam

### Subscripts

A	data set $A$
B	data set $B$
D	damaged structure
i	measurement point
k	excitation point
l	lth correlated mode pair
O	undamaged structure
q	qth mode
r	rth mode
z	zth mode
u	a random process $u$
v	a random process $v$

### Superscripts

-1	ordinary inverse of a matrix
T	matrix transpose
†	pseudo-inverse of a matrix
*	complex conjugate

## ABBREVIATIONS

ADC	Analogue to Digital Conversion
COMAC	Coordinate Modal Assurance Criterion
COV	Covariance
DFT	Discrete Fourier Transform
DLS	Direct Least Squares
DOF	Degrees of Freedom
FE	Finite Element
FFT	Fast Fourier Transform
FRF	Frequency Response Function
FT	Fourier Transform
GI	Global (Integrity) Index
IAF	Improved Amplitude Fitting
LI	Local (Integrity) Index
MAC	Modal Assurance Criterion
MDOF	Multi-Degree-of-Freedom
MSV	Modal Sensitivity Values
SDOF	Single-Degree-of-Freedom
STD	Standard Deviation
SVD	Singular Value Decomposition

# CHAPTER ONE

## INTRODUCTION

### 1.1 General Background

With increasing stock of constructed facilities, most of the work conducted by engineers of infrastructure owners will involve maintenance of existing structures. An important part of a maintenance programme is structural assessment to ensure that the integrity of the structures is preserved. Williams (1992b) has reported a situation where fatal structural failure was averted as a result of periodic structural assessment. Structural integrity assessment of engineering structures is necessary if they suffer damage or deterioration, when they have to carry loads higher than originally anticipated, when doubts about their capacity to sustain current or future loads exist and generally to ensure that the structures are fit for the intended purposes. Regular inspection and assessment enable early detection of damage/deterioration and therefore allow timely planning of remedial action to arrest further deterioration, thereby reducing or avoiding human, social and economic costs. Current structural assessment procedures usually rely on visual inspections and location dependent (nondestructive, pseudo-nondestructive and destructive) methods.

A typical assessment programme, for any structure, would usually start with a visual inspection of the structure. If observed features (e.g. presence of cracks, delamination, corrosion) suggest structural distress, further investigations are conducted. The exact nature and degree of complexity of these investigations depend on the aims of the investigations, the visually observed features and available resources. Collation and interpretation of inspection and test results and calculations to assess structural condition are tasks that always accompany an assessment programme irrespective of the specific methods used.

The visual inspection stage and test methods (Iffland and Birnstiel, 1993, have presented an extensive list / bibliography summarising most of the currently used test methods) adopted in subsequent investigations often lead to some problems with the use of these procedures. According to Cabrera (1988), many of the detailed investigations carried out for evaluation of bridge performance have shown that the intrinsic properties measured (using current methods) on site do not seem, on the whole, to correlate with performance.

Other limitations of current assessment procedures include: 1) concealed and inaccessible parts of the structure are difficult, if not impossible, to inspect; 2) the quality of the process is often dependent on the inspection personnel's experience and knowledge; 3) results from one (local) area of a structure does not necessarily represent the condition at another area; and 4) as a result of (3), it would be necessary to take measurements at a large number of points so as to have a good representation of the global structural condition. These constraints imply that the process is time consuming, labour intensive and expensive.

In view of the above limitations, a better approach to structural assessment would be a procedure that is not location dependent and involves the participation of the complete structure under investigation. Any distress or loss of integrity can be detected by measuring global parameters at a few easily accessible points on the structure. Since the measured properties are global, the measurement points can be chosen to suit the test situation. Static load testing used to be the only full-scale global test method for assessing the condition of built structures. However, it requires extensive (and cumbersome) site preparation involving application of large loads (for example, see Bakht and Jaeger, 1992). Other disadvantages include high cost, potential for damaging the test structure (Tilly, 1988) and the possibility of producing results that may be difficult to measure (Savage and Hewlett, 1978).

A more attractive global test method is dynamic (vibration) testing. Vibration testing does not require a large force input since dynamic amplification of the modest input loads would ensure generation of measurable response. The basic principle in using vibration monitoring to assess structural integrity relies on the fact that dynamic response is a sensitive indicator of the physical integrity of any structure. This is discussed in more detail in chapter three. Occurrence of defects reduces structural rigidity which leads to changes in dynamic properties such as natural frequencies. Thus, results of tests conducted at different times offer the possibility of monitoring changes in structural condition with time.

System and modal parameters, which characterize the behaviour and condition of the structure, can be obtained from the measured dynamic response. The most reliable experimental results in civil engineering are obtained by using large scale specimens/prototypes which give a true representation of actual site conditions (Kroggel, 1993). Experimental data obtained from a full-scale structure still in service provide valuable information which aid understanding of structural behaviour and are useful in validating theoretical models before such models are utilized in predicting future behaviour. Such data also add to the database on structural performance of similar structures. Current analytical and design procedures can be refined using the performance database so that design of new structures is improved.

## **1.2 Objectives and Outline of This Work**

The main objective of the research is to investigate the suitability of using data obtained from vibration testing in integrity assessment of civil engineering structures. To achieve this, it was necessary to study the performance of some methods for detecting and locating

damage. This required evaluating the methods using numerical and experimental (laboratory and field) data. Highway bridges were used as the test structures for the full-scale field tests. The choice of bridges was influenced by the current programme of structural assessment to ensure Britain's highway bridges on designated routes are capable of carrying loads from the 40 tonne trucks to be introduced in 1999. It was also intended to gain a better understanding of the dynamic behaviour of large civil engineering structures from the test results and comparison of the results with predictions from theoretical models. Although bridges were used as the test structures, the procedures adopted are applicable to other types of structures. The layout of the thesis, with respect to the approach adopted in conducting the research, is described in the remaining paragraphs of this chapter.

As a background to the full-scale tests conducted, a review of dynamic testing of bridge structures is presented in the next chapter. The review covers reasons for conducting full-scale tests, the available types of dynamic testing and a discussion on the types of excitation systems used in forced vibration testing.

The justification for using vibration data in structural assessment and various approaches proposed for detecting, locating and quantifying damage in structures are reviewed in chapter three. The discussions are meant to give an overview and unified perspective, while highlighting the potentials and limitations, of integrity assessment using vibration data. Chapter four presents a critical study of the performance of some damage detection and location methods using both simulated and laboratory data. Development and evaluation of a new method of damage detection/integrity assessment are discussed in chapter five. The performance evaluation was conducted using results from theoretical simulations and laboratory testing.

Details of equipment used, test and data analysis procedures adopted during full-scale tests conducted are discussed in chapter six. Also included in chapter six is a discussion on the configuration and performance characteristics of the system developed for generating vertical excitation during full-scale tests. In chapters seven and eight, results from experimental and theoretical vibration analyses of two full-scale highway bridges are presented. Integrity assessment of the bridges, based on results of tests conducted before and after repair works, using the approaches described in chapters three to five is also discussed in these chapters. Conclusions from the research and recommendations for future work are given in chapter nine.

## **CHAPTER TWO**

### **A REVIEW OF FULL-SCALE DYNAMIC TESTING OF BRIDGE STRUCTURES**

#### **2.1 Introduction**

Dynamic field tests have been carried out on bridges since the late 19th century (Kato and Shimada, 1981). Many of the early tests were conducted as part of safety inspection of railway bridges and involved monitoring bridge vibrations. Modern test methods are sophisticated extensions of these early investigations. Most of the more recent tests have been concerned with improving analysis and design procedures, assessment of bridge design code provisions and monitoring the in-service behaviour of bridges. These test objectives underline the importance of vibration testing.

A simplistic view of dynamic testing is to consider it as a procedure for determining the resonance (natural) frequencies of a structure. Each natural frequency has a vibration mode shape which corresponds to the deflected shape when the structure is vibrating at that frequency. Every vibration mode has an associated damping value which is a measure of energy dissipation. The natural frequency, vibration mode shape and damping value of a mode are sometimes referred to as the modal parameters of the particular mode. In the literature, dynamic tests involving identification of modal parameters are also termed modal tests or modal surveys. Other parameters such as modal mass, modal stiffness, system mass and system stiffness can also be identified from the measured vibration response. The basic stages involved in dynamic testing are illustrated in Figure 2.1. Although the stages have been shown as distinct phases, it should be noted that modern test configurations

usually incorporate a number of procedures within a single device.

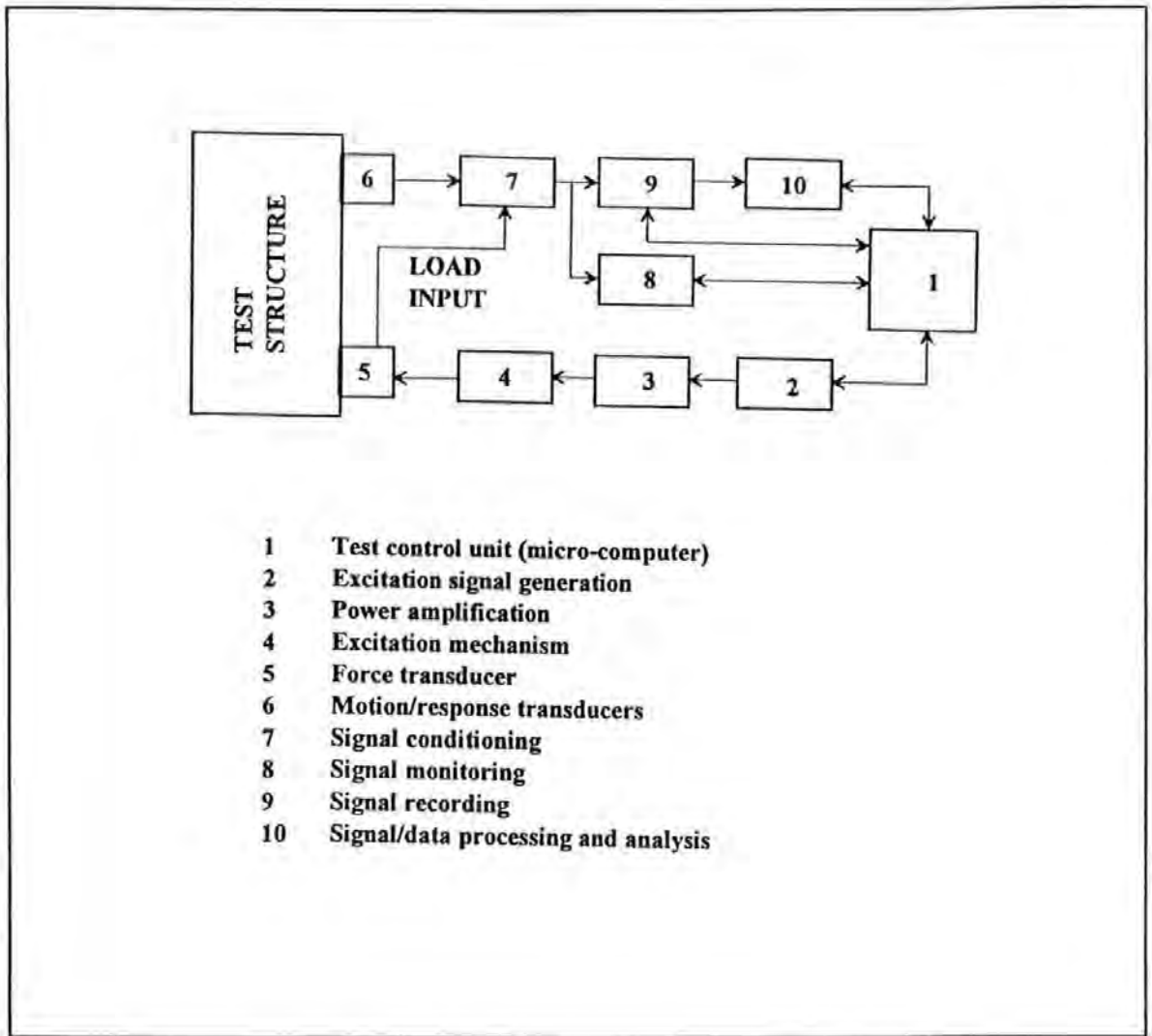


**Figure 2.1 Stages involved in vibration testing**

The two main types of dynamic tests are ambient and forced vibration testing. The basis of the classification adopted here is the degree of control over the input excitation. Dynamic testing methods without any control on the input are classified as ambient vibration testing. Thus, stages 2 - 5 in Figure 2.1 will not be present in the test set-up. Forced vibration testing incorporates those methods where the vibration is artificially induced. Methods where the excitation is artificially induced but is not and/or cannot be measured are also categorized under forced vibration testing. Examples of these are excitation by explosions and vehicle impact. The review in this chapter starts with a

discussion of some of the reasons for conducting full-scale dynamic tests. Ambient vibration testing and forced vibration testing are respectively discussed in sections 2.3 and 2.4.

## **2.2 Reasons for Full-Scale Dynamic Testing**

There are various reasons for conducting full-scale dynamic testing. Some of these are :

1. **Dynamic measurements on a full-scale structure serve to increase the database on dynamic behaviour of similar structures. The database can be useful in predicting the response of new structures. Since full-scale tests can be expensive, this database becomes invaluable in procedures utilizing test data to evaluate and improve current analytical methods.**
2. **To determine the integrity of a structure after the occurrence of an overload. If the nature of loading causing the overload is unknown, results of the dynamic tests may be used to determine the type of loading (Tsang and Rider, 1988). The same approach can also be used to assess the effectiveness of remedial works (Williams, 1990; 1992a) and repair materials (Slařtan and Pietrzko, 1993a; 1993b).**
3. **To validate theoretical models of structures. Mathematical models of real structures usually involve significant assumptions especially with regard to boundary conditions, material and inertia properties. Moreover, as the structural system becomes more complex and sophisticated, it becomes more difficult to understand its mechanisms, and, therefore, to develop an appropriate model which will give a good prediction of its dynamic response (Nalitolela et al, 1990). Comparison and correlation of theoretical predictions with measured response will lead to a better understanding of the structure, better defined safety margins, less conservative**

assumptions and hence, more economical designs.

4. To assess the integrity of a structure when higher loading levels are envisaged either due to a change of use, higher environmental loading or an increase in allowable loading. A possible application of this approach is in the current assessment of some highway bridges in the U.K. to check their ability to withstand 40 tonne trucks to be introduced in 1999. According to Proulx et al (1992), dynamic testing is more reliable than other methods to evaluate the dynamic amplification factor since it (dynamic testing) yields information, on the dynamic properties of the structure, that can be used in structural assessment and design of repair work.
5. The overall condition of a structure can be monitored by regular measurement of its dynamic response. Changes, as a result of deterioration, in the system parameters - mass, stiffness and damping - lead to changes in the vibrational response and these can be measured using standard dynamic testing techniques. Results of tests have shown that the size of damage is proportional to the magnitudes of observed changes in identified system parameters (Tsai and Yang, 1988).
6. As a trouble shooting tool to verify that behaviour of a given system conforms to that expected. This provides performance information on the completed structure and also yields useful data for future designs. Dynamic testing has historically been used by engineers to study structural vibration problems.

### **2.3 Ambient Vibration Testing**

Most of the published work on full-scale dynamic testing have used the ambient vibration testing method. This is due, among other factors, to the ease of measuring the vibration response while the structure is still in service, increasing availability of robust data

acquisition and storage systems, elimination of the need for special excitation devices and the possibility of correlating structural vibration response with the normal service loading. The literature on ambient vibration testing of highway bridges is extensive. In this section, some of the reported tests are presented. The list is by no means exhaustive but the papers reviewed are meant to illustrate the different test approaches employed and the main results obtained.

In ambient vibration testing, the input excitation is not under the control of the test engineer. The loading could be from either wind, waves, vehicular or pedestrian traffic or any other service loading. Since the magnitude of the input is unknown, certain assumptions have to be made about its nature. The basic assumption of the method is that the excitation forces are a stationary random process, having an acceptably flat frequency spectrum (Taškov, 1988). If this assumption holds, then the vibration response of any structure subjected to such effects will contain all the normal modes. Ambient vibration testing implicitly assumes response data alone could be used to estimate vibration parameters.

In most cases, the nature of the input excitation can only be approximated by statistical descriptions or by assuming the excitation spectrum to be concentrated within a frequency range. If the loading spectrum is limited to a narrow band of frequencies, only a limited picture of the dynamics of the structure can be monitored (Williams, 1992a). Inadequate knowledge of the input force also implies generalised mass and stiffness cannot be derived. A theoretical justification of ambient vibration testing has been proposed by James et al (1992).

During the 1970s, the Transport Research Laboratory conducted series of full-scale

vibration tests on motorway bridges to re-assess bridge loading rules and to gain a better understanding of the dynamic behaviour of bridges. As part of the series, Eyre and Smith (1977) measured the dynamic response of Tinsley viaduct due to excitation from normal vehicular traffic and a 30 tonne control vehicle driven at speeds of 13, 18, 22 and 27 m/sec. The viaduct is a two-level, twenty span steel structure with a total length of 1032m. The measurements were made on the eighteenth span of the upper level using cantilever deflection gauges. It was found that the superstructure deflected as a continuous beam and that the principal bending and torsional vibration frequencies were in the range 1.80Hz to 3.60Hz and 1.31Hz to 1.84Hz respectively.

Ambient vibration testing of the Tamar suspension bridge has been reported by Williams (1983). The dynamic response was monitored when the bridge was excited by a wind of between 7 and 12m/s speed and a fairly continuous flow of traffic. Seismometers were used at 17 locations for the measurements. Ten natural frequencies in the range 0.3Hz - 2.75Hz were identified. Although analytical mode shapes were given, experimentally determined mode shapes and damping values were not reported. Seismometers were also used by Taškov (1988) to measure the wind induced oscillations of the Špilje lake bridge, Yugoslavia.

The traffic induced vibration of some 18 bridges were studied by Ward (1984). Vertical vibrations were recorded on the ground approaches to the bridges and at locations close to the mid-span. The approach measurements were made to provide an estimate of the energy input to the bridges and to identify unambiguously the natural frequencies of the bridges. Estimates of the damping values were obtained by treating the time histories as a series of transient vibration records associated with the passage of each vehicle across the bridges. It was found that most of the energy associated with the traffic loading were confined

within the frequency range 0 - 30Hz.

The Golden Gate suspension bridge, California, has been the subject of a number of investigations to monitor the structural dynamic behaviour and give warning of any impending disaster (Vincent, 1958). Recently, extensive experimental investigations have been conducted (Abdel-Ghaffar and Scanlan, 1985a; 1985b) on the bridge to determine effective damping, three-dimensional mode shapes and resonant frequencies. Excitation was from wind, ocean waves and vehicular traffic. 20 vertical, 18 torsional, 33 lateral and 20 longitudinal modes were identified (frequency range 0 - 1.5 Hz) from simultaneous measurement of vertical, lateral and longitudinal vibration of the suspended structure. The measured mode shapes and frequencies showed good agreement with the results of both 2- and 3-dimensional finite element analyses. McLamore et al (1971) also studied the dynamic characteristics of two suspension bridges using ambient vibration methods.

Preliminary vibration tests of the 866m long Foyle bridge (Northern Ireland) have been reported by Leith et al (1987) and Sloan et al (1992). The monitoring system was automated and could be programmed to gather data either at a preset timetable or when certain environmental conditions were fulfilled. The results showed that the lower frequency end (< 0.2Hz) of the relative displacement spectrum was caused by traffic crossing the bridge.

Dynamic response monitoring during normal bridge traffic was carried out by Creed (1987) on a six span concrete motorway bridge. Eight vertical accelerometers were used in pairs to assess mode shapes and check bearing motion at the supports. The measured natural frequencies for a given span were found to be repeatable to within 2.5% though the mode shape ratios were only repeatable to within 35 - 40%. The measured natural frequencies

also showed good agreement (within 3.5%) with finite element analysis predictions. Ambient vibration testing was also used by Pardeon et al (1981) and Baumgärtner and Waubke (1993) to study respectively the dynamic behaviour of a steel truss bridge and a steel-concrete arch bridge.

Brownjohn et al (1987) conducted ambient vibration tests on the Humber suspension bridge to determine vertical, lateral and torsional vibrational characteristics of the deck and towers. It was found that while many vertical and lateral modes occurred at close frequencies, they were not related. Though there were relatively few predominantly longitudinal modes, there was significant longitudinal participation in most main span vertical modes. This interaction between different vibration modes was also observed by Abdel-Ghaffar and Scanlan (1985a) and more recently by Owen and Blakeborough (1993) and Ventura et al (1994). From the correlation between wind speed and modal amplitude, Brownjohn et al (1987) suggested that low frequency excitation is mainly wind induced while response upwards of about 2Hz is mainly traffic induced. Although reliable frequency values were obtained, the modal damping values were believed to be over-estimated due to signal processing errors involved in analysing response from ambient vibration. Similar conclusions about damping estimates were also expressed by Mazurek and DeWolf (1990).

Using a different data acquisition method, Littler and Ellis (1987) also conducted vibration tests on the Humber bridge. The estimated natural frequencies and mode shapes were in agreement with the results of Brownjohn et al (1987). Detailed discussions of a number of modal surveys, using ambient excitation, that were conducted on suspension and cable stayed bridges can be found in Brownjohn (1988).

During the modal testing of Kessock bridge, Owen and Blakeborough (1993) obtained

mode shapes from low frequency resolution measurements taken during the day while natural frequencies were identified from overnight recordings using a finer frequency resolution. This approach was taken to achieve a reasonable compromise between frequency resolution, recording period and number of averages. However, modal parameters of closely spaced modes were still inadequately identified primarily due to the problems associated with ambient testing and the low sophistication of the modal identification algorithm used.

Results from an extensive programme of testing to determine the dynamic characteristics of a slant-leg steel frame pedestrian overpass were reported by Rivas-Gomes (1993). Excitation of the bridge was by people jumping and running on the deck in such a way that maximum response was produced. The tests were conducted to validate analytical models developed for the bridge and assess design assumptions. It was found that the dynamic response of the structure was governed by the rocking oscillations of the foundations (massive concrete supports on top of vertical drilled piers). The results demonstrate the fact that boundary conditions are the main determinants of the behaviour of some statically indeterminate structures and that assumptions about rigidity of the supports are critical for supports at which fixed moments and horizontal thrusts are expected to be developed.

Alvarez et al (1993) have produced a relationship (Figure 2.2) between the fundamental natural frequency and span length of concrete bridges. The relationship was deduced from results of dynamic tests on 174 rail and highway bridges of span length ranging from 7.4m to 150m. A quick initial estimate of the first natural frequency can be obtained from the curve. For multi-span bridges, response of the longest span would tend to dominate the fundamental frequency.

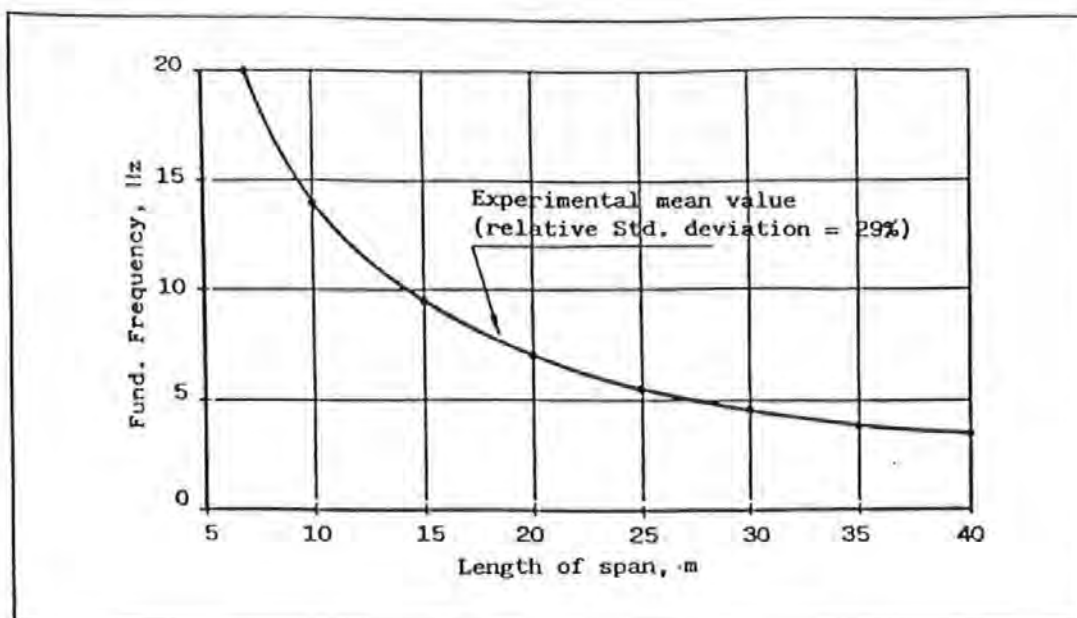


**Figure 2.2 Relationship between fundamental frequency and span for concrete bridges (Alvarez et al, 1993)**

Although reliable frequency and mode shape data can be obtained (Srinivasan et al, 1984) from ambient testing, estimated damping values are prone to errors. The errors in the damping estimates are due to a combination of factors such as the (possible) nonstationarity of the excitation process, signal processing and data analysis procedures necessary to extract modal parameters and the insufficient excitation of some modes (Bendat and Piersol, 1986; Brownjohn et al, 1987; Carne et al, 1988; Jeary, 1992; Littler, 1988). Brownjohn (1988, chapter 10) has discussed the problems of obtaining reliable damping estimates from ambient vibration testing.

The frequency response function (sections 3.2, 6.4) changes depending on the amplitude of the input excitation. This leads to variation in damping estimates since damping depends on vibration amplitudes. Hence, results from low level excitation (as in ambient testing) might not be appropriate to predict the dynamic response to high level excitation (Abdel-Ghaffar and Scanlan, 1985a). Coupled with this is the considerable degree of non-linearity exhibited by many real-life structures.

To achieve better results, it is necessary to use higher energy excitation techniques which can excite all the modes of interest. Thus, the only alternative to ambient vibration testing is to conduct forced vibration testing using properly designed excitation systems which can produce desired loading spectra. According to Kroggel (1993), artificial excitation is sometimes the only means of obtaining accurate and reproducible dynamic parameters. Tests on offshore structures (Gundy et al, 1980) using both ambient and forced vibration methods have shown that damping and frequencies can be measured more accurately with forced vibration and that the higher modes can only be excited to measurable levels by artificial excitation. Dynamic tests involving artificial excitation are discussed in the next section.

#### **2.4 Forced Vibration Testing**

This involves application of input excitation of known force levels at known frequencies. The input is thus under the control of the experimentalist. Forced vibration tests have the advantage of suppressing effects of extraneous noise in the measured structural response. The input loading can be altered to suit test requirements. Also included in this category are tests in which the input is controlled but not measured. The physical means through which the excitation is realised maybe termed a vibrator, vibrator exciter, exciter or shaker. It is a device used for transmitting a time varying force into the structure. Forced vibration testing is based on the classical fact that if the loads on a structure are known and the resulting motion can be measured, then it should be possible to estimate the structural properties.

In full-scale testing of large structures, vibrators are generally of the contacting type i.e. the exciter stays in contact with the test structure *throughout* the testing period. In such

applications, they are physically mounted onto the structure. However, non-contacting devices such as impactors have also been successfully used on some large structures. Appropriate contacting vibrators are usually of the eccentric rotating mass or electro-hydraulic type. Brief description of the general characteristics of eccentric rotating mass vibrators, electro-hydraulic vibrators and impactors are included in the review. Further details on the configuration and operating principles of these machines can be found in Clements et al (1988) and Unholtz (1988). Also discussed in this section are some other types of excitation mechanisms in which the input force is not measured.

The number of reported forced vibration tests is less than that reported for ambient vibration testing. A factor contributing to this is the difficulty in constructing suitable excitation systems that can generate sufficient excitation forces at low frequencies, especially for long span slender bridges. The papers reviewed form a subset of the published literature and have been chosen to highlight types of excitation systems used, the main conclusions from the tests and the various test procedures adopted.

#### **2.4.1 Eccentric rotating mass vibrators**

An early form of contacting vibrator is the eccentric rotating mass vibrator which is a reaction type mechanical vibration machine. These vibrators have been used for some years to excite large civil engineering structures (Ellis et al, 1977; Jeary and Sparks, 1977). The eccentric mass vibrator generates vibratory force by using a rotating shaft carrying a mass whose centre-of-mass is displaced from the centre-of-rotation of the shaft. The motion generating the force can be circular or rectilinear (in which case, the term 'moving mass vibrator' is more appropriate). The magnitude of the applied force is constant for a particular setting of mass, rotational speed and the out of balance displacement.

The machine can be operated at different frequencies by changing the rotational speed of the shaft. Adequate shaft speed control is necessary in order to have satisfactory results. The simplest reaction type machine uses a single rotating mass. Machines with more than one rotating mass are also available (Ellis et al, 1977). An example is shown in Figure 2.3. These have the advantage of generating forces in more than one direction (when motion is rectilinear). These exciters are capable of delivering only sinusoidally varying forces that are proportional to the square of the rotational speed so that reliable excitation can only be achieved above 1Hz (Brownjohn, 1988).

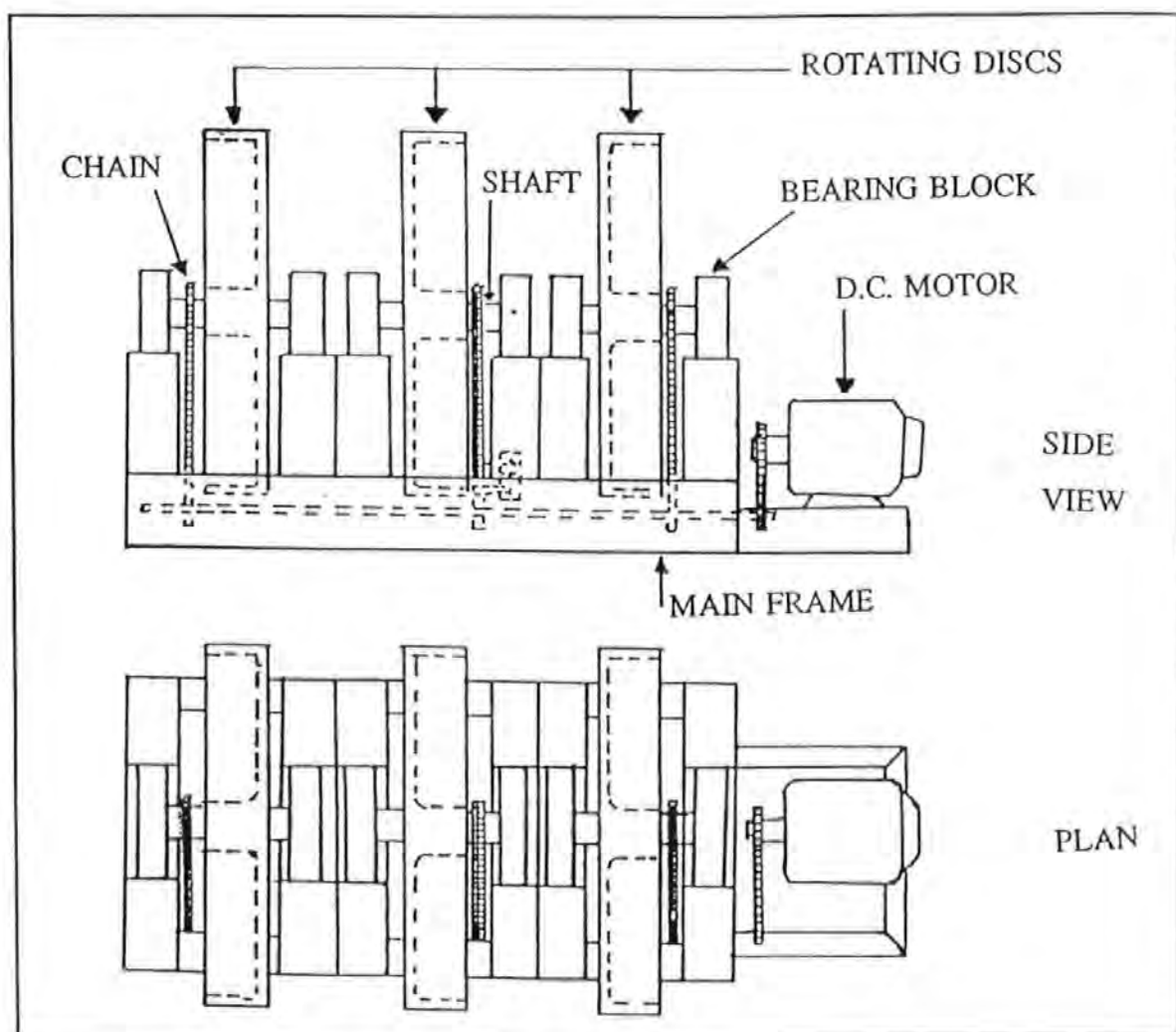


Figure 2.3 Rotating mass vibrator (after Shepherd and Reay, 1967)

Details of the design, construction and operation of some eccentric rotating mass exciters which have been built are given by Hudson (1962), Shepherd and Reay (1967) and Severn et al (1980). Examples of field application of such exciters to the full-scale testing of highway bridges are briefly described below.

Rotating eccentric mass exciters were used to generate excitation forces during the tests on the Bosphorus suspension bridge (Brownjohn, 1988). The tests had only partial success because the exciters were unable to supply adequate force at frequencies much below 1Hz, which is the range of interest for suspension bridges. During modal testing of the Poinja river bridge, Yugoslavia, Taškov (1988) used two electro-mechanical vibration generators to generate harmonic vibrations in the frequency range 0.5 - 9.0 Hz.

Okauchi et al (1986) successfully conducted forced vibration tests on the Ohnaruto suspension bridge. Excitation of the bridge was by a pair of 200kN vertically acting reciprocating mass exciters operating at a constant amplitude of 140mm. This was sufficient to give reasonably accurate damping estimates. A damping value of 0.53% of critical damping was obtained for the first vertical mode. Ohlsson (1986) conducted swept sine testing on the 366m cable stayed Tjorn bridge, Sweden, with a special type of reciprocating mass exciter. Four vibrational modes were identified in the frequency range 0.4Hz to 1.6Hz.

#### **2.4.2 Electro-hydraulic vibrators**

The electro-hydraulic vibrators can generate higher forces than the other types. The force is generated through the (reciprocating) motion induced by the high-pressure flow of a

liquid. The pressure is provided by one or more pump units. In operation, the system usually consists of a servo-controlled hydraulic actuator which drives an attached mass. The weight of the mass can be varied to obtain varying force magnitudes. The vibrators provide relatively high vibration strokes and allow accurate excitation at different frequencies in bending or torsion. They also have the advantage of being able to apply a static preload and complex waveforms to the test structure. However, the attainable stroke reduces with increasing frequency.

Electro-hydraulic vibrators are less common than the eccentric rotating mass types. Leonard (1974) has described an inertial excitation system, called Energy Input Device, consisting of four masses, each driven by an electro-hydraulic actuator, mounted on a mobile axle. Similar exciters were also used in the tests reported by Galambos and Mayes (1979), Kennedy and Grace (1990), Salane et al (1987), Tsang and Williams (1988) and Williams (1990). The Energy Input Device was used during tests conducted on bridges with individual spans of up to 50m. It was capable of generating sinusoidal forces over the frequency range 1.5Hz to 30Hz at force levels of up to  $\pm 16\text{kN}$ . The actuator used during full-scale tests conducted as part of this research is of the electro-hydraulic type. Details of the design, construction and operation of the actuator are given in Salawu and Williams (1992, 1994b) and chapter six (section 6.2).

Cantiene and Pietrzko (1993) conducted tests on a three span 108m long wooden footbridge to verify design assumptions and check if pedestrian induced vibration was excessive. Excitation of the bridge was by a servo-hydraulic vibrator which was capable of generating a maximum force amplitude of  $\pm 5\text{kN}$  at frequencies  $\geq 2.3\text{Hz}$ . The bridge response was measured in three orthogonal directions at 77 points using accelerometers. The accumulated spectrum over all 231 measured frequency response functions was used to

identify prominent modes. Burst random excitation signal was found to reduce the measurement time and eliminate leakage errors during spectral computations. However, utilization of specialised software and signal conditioning equipment was necessary. Results obtained from the tests showed that the bridge was not susceptible to excessive vibration by walking pedestrians. Similar equipment and procedures were also used by Deger et al (1994) during experimental modal analysis of a prestressed concrete arch bridge.

Forced vibration tests, in addition to fatigue tests, were conducted by Salane et al (1987) on a full-scale in-situ composite three span highway bridge in order to evaluate the effectiveness of using changes in dynamic properties as a means of detecting structural deterioration. A closed-loop electro-hydraulic actuator system was used to generate the excitation forces. Stepped-sine, slow sine sweep and steady-state normal mode testing techniques were utilized. For the stepped-sine tests, the damping values obtained varied from span to span although the range was consistently between 1 and 3 %.

Results of damping measurements on 23 steel and composite bridges (spans between 17m and 213m) were discussed by Eyre and Tilly (1977). The damping was measured from decays of response obtained for the first bending mode though it was acknowledged that higher bending and torsional modes could be significant for bridges having low natural frequencies which coincide with those for the suspension of heavy vehicles. It was found that damping increased with amplitude of vibration and stabilised at an upper level which was about four times higher than the level at small amplitudes. The lower level of damping was associated with the behaviour of the superstructure while the upper damping included contributions from joints and substructure and was more relevant to unduly 'lively' behaviour. A tendency for damping to increase with frequency was also noted. Damping

values for steel, composite and concrete bridges and the intrinsic material values for steel and concrete have been presented by Eyre and Tilly (1977) and Tilly (1977).

Raimer and Pernici (1979) have reported sinusoidal forced vibration tests on a three span pre-stressed concrete bridge. Salane and Baldwin (1990) also conducted steady state sinusoidal tests on a three span highway bridge using an electro-hydraulic actuator. The bridge had a composite deck supported on four steel girders. Three resonant modes - two bending and one torsional - were identified. A modal damping ratio of 0.0134 was obtained for the first bending mode. Servo-hydraulic actuators were also used in the tests conducted by Kroggel (1993) on two road bridges.

### **2.4.3 Impactors**

The simplest means of applying an impact to a structure is by using an instrumented hammer or a suspended mass to deliver blows to the structure. A simple impact device is shown in Figure 2.4. The impulse delivered to the structure can be varied by changing the mass of the impact device. The impact frequency range can also be varied by changing the hammer head type. The impulse function consists of a short duration broad band spectrum. The width of the function determines the frequency content while the height and shape control the energy level of the spectrum (Allemang and Brown, 1988). Impulse testing is susceptible to input noise since the input force is applied over a short period compared to the record length (of the measured response).

Important factors to consider before conducting impact testing are (Raghavendrachar and Aktan, 1992): 1) effect of the level of impact and change in ambient conditions on structural characteristics; and 2) reciprocity between impact and response at alternating

measurement points. These considerations would reveal the suitability, or otherwise, of linear models (for structural identification) on data obtained from impact testing.

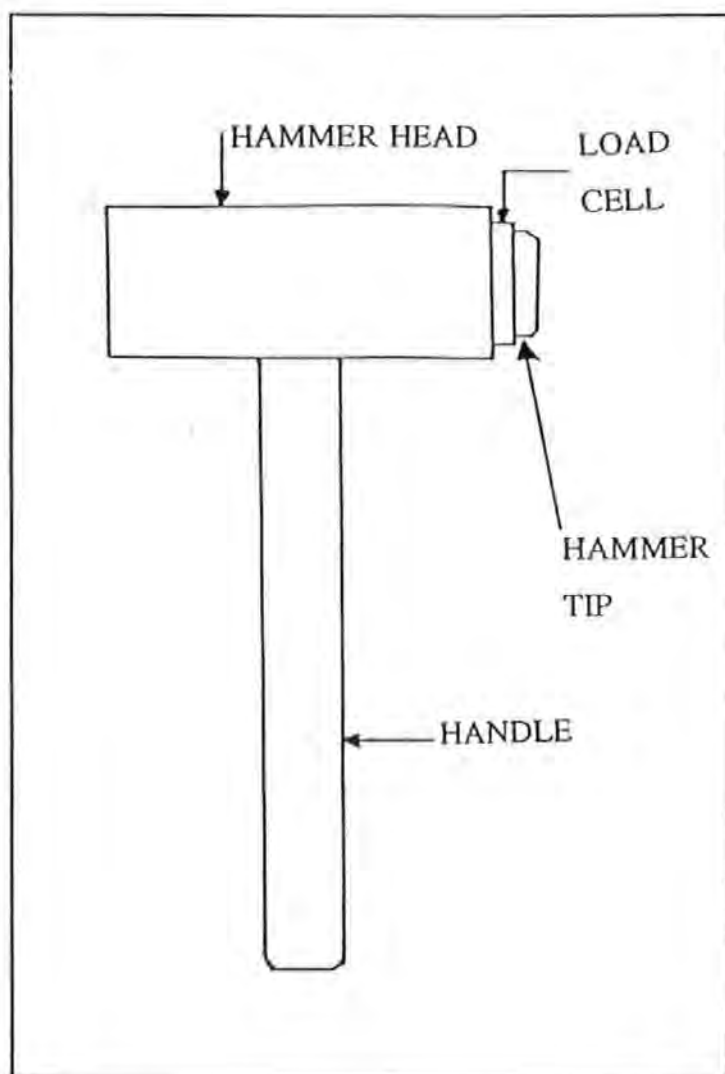


**Figure 2.4 A simple impact device**

Kohoutek and Marshall (1994) used impact testing on three prestressed and reinforced concrete bridges with spans varying from 30m to 100m. Excitation was achieved by dropping a mass (40kg to 70kg depending on size of bridge span) from about 0.5m onto an anvil placed on the bridge deck. A special damping pad was sandwiched between the

mass and the anvil so that the impact frequency content covered the test frequency range. Results from impact tests (66kg dropped from a height of 30cm) were used by Vanhonacker (1994) to validate a finite element model of an 80 years old railway bridge. The validated model was subsequently used to design a strengthening scheme which allowed the bridge to remain in service and accommodate heavy axle load trains running at 80 km/h (compared with 20 km/h previously).

An instrumented hammer (total mass of 23kg) was used during the dynamic tests reported by Green and Cebon (1993). Repeatability of the testing procedure was demonstrated by comparing measurements obtained when the hammer was dropped several times at one position while linearity of the dynamic response was ascertained by comparing measured responses, at a point, due to impact at three different positions on the bridge. Gardner-Morse and Huston (1993) verified linearity of data obtained from impact testing of a cable-stayed footbridge by ascertaining the reciprocity of measured frequency response functions between two measurement points. However, a similar approach was used by Raghavendrachar and Aktan (1992) to indicate nonlinear response and by Imregun and Ågårdh (1994) to confirm repeatability of measurements.

Linearity of the structural system could be assumed in impact testing if the impact level is limited to a certain range (Sun and Hardy, 1992a; 1992b) and the lowest possible level of excitation is used (Ågårdh and Palm, 1992). The estimated damping ratios, from the tests by Green and Cebon, varied from 1.4% to 8.8% of critical damping. Although the authors did not give any reason for the high damping values, they (high damping values) could have been due to high impact energy during excitation. This raises the question of uniformity of 'blows' when using instrumented hammers. During the tests reported by Biswas et al (1990), a soft tipped head was used on the 53.4N hammer employed as the

exciter. This enabled elimination of local damage to the bridge and allowed sufficient bridge response at low frequencies.

Forced vibration tests were conducted (Aktan et al, 1994; Zhang, 1994) on a three span steel-stinger bridge to determine the level of correlation between impact testing and swept-sine testing with a linear mass-inertia exciter. Two modes which were reliably identified by the impact testing could not be identified by swept-sine testing. Although no apparent quality difference was noticed (Aktan et al, 1994) between the two sets of response functions measured, a detailed error analysis (Zhang, 1994) revealed that results from the impact tests were more erroneous.

A 5.4kg instrumented sledge hammer was used by Maguire and Severn (1987) to test four 40 tonne bridge beams. The hammer was reported to have a maximum impact force of 22kN. A cylindrical steel hammer, having a mass of 840kg, was also used as the excitation device during the dynamic tests reported by Lee et al (1987). Despite these published tests, instrumented hammer is not often used on large structures because of the large mass of the latter and the risk of local damage, at the point of contact, to the structure when high force levels are applied.

Other special impact devices have been developed to excite large structures. One of such devices was called a sand drop impactor (Morgan and Oesterle, 1985). It consisted of a weight dropped onto a sand bed that was, in turn, mounted on a load cell. The device has been reported to have successfully excited a number of both steel and concrete structures. More recently, Wood et al (1992) have reported the use of a 'bolt-gun' to excite large structures while Ågårdh (1991; 1994), and Ågårdh and Palm (1992) have reported development and field usage of an impact equipment for exciting concrete bridges. The

main advantages of impact testing are that the test times are short and the instruments required are lightweight and relatively inexpensive.

#### **2.4.4 Other excitation mechanisms**

The other means of forced excitation can generally be classed under transient testing. For these other methods, the input force is not usually measured. They take one of two forms - impulse testing or step relaxation. Excitation by test vehicles driven along the bridge can also be considered as transient. In impulse testing, the impulsive force is applied to a structure, initially at rest, by vehicle impact, vehicle driven over an uneven surface, a dropped weight, rocket impact or controlled jumping of people. The same comments made in the previous sub-section apply to this type of excitation.

In step relaxation testing, excitation is achieved by releasing the structure from a statically deformed position. The initial static deformation is achieved by either loading the structure with a wire or cable (Chasteau, 1973; Eyre, 1976), hydraulic rams (Douglas et al, 1990; Richardson and Douglas, 1987) or by continuous thrust from rocket motors (Selberg, 1966). An example of transient excitation is shown in Figure 2.5. The response of the structure to this form of excitation is strongly dominated by those modes whose deformed shapes best resemble the statically deformed configuration of the structure. Step relaxation is seldom used because it can be mechanically difficult to implement (Carne et al, 1988). However, it is possibly the simplest and most effective method of determining damping (Brownjohn, 1988).

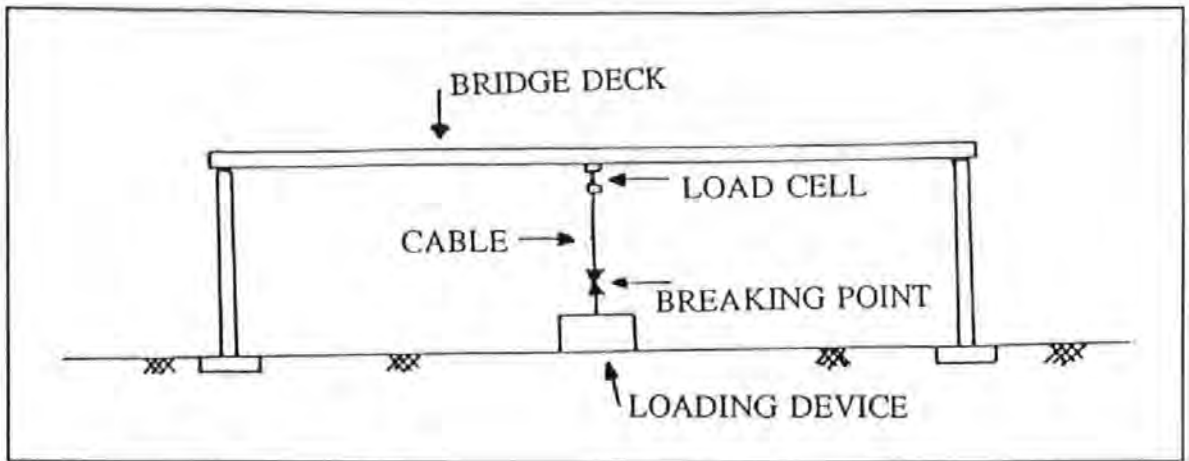


**Figure 2.5 Transient excitation**

The pull-back and quick-release testing method (a form of step relaxation) was used by Douglas and Reid (1982) and Douglas and Richard (1984) to determine the modal parameters of some highway bridges. The dynamic excitations were produced by pulling (using cables) on the bridges with two crawler tractors and simultaneously quick-releasing the loading cables. Marecos et al (1969) had previously used a similar technique on the Tagus bridge. The same method was used in the full-scale tests reported by Richardson and Douglas (1987) to investigate the dynamic response of a 277m long reinforced concrete bridge. However, the initial deformation of the bridge was obtained by using steel rams and hydraulic jacks. Five of the possible six deck acceleration components were measured at each of the 47 bridge deck locations. This allowed the identification of three dimensional mode shapes. The authors used novel presentation methods - power spectral density surfaces and power spectral density contour plots - to display power spectral density curves from different stations on the same plot. Eyre (1976) obtained the dynamic response of the seven span Cleddau bridge by suddenly releasing a 32.7 tonne mass from the centre of the main span.

Douglas et al (1990) have proposed a baseline correction procedure to improve the results

obtained from the normal quick release method. The modified procedure was tested on a series of data obtained during field tests on a two span reinforced concrete box girder bridge. The procedure enhanced the use of the quick release dynamic testing method and also produced detailed static response of the structure as a by-product of the dynamic investigation.

Several full-scale dynamic tests have been conducted in Ontario, Canada, to investigate the effects of traffic and road characteristics on bridge dynamic behaviour. Results from a series of such tests conducted between 1956 and 1971 have been reported by Green (1977). Excitation was by vehicles driven on the bridge. The results indicated that the dynamic deflection can be in excess of values suggested by design specifications. It was found that for superstructures having a (fundamental) longitudinal flexural frequency between 2Hz and 5Hz, the dynamic interaction between vehicle and bridge systems appeared to be present and gave rise to higher dynamic deflections. Values of damping were found to range from 0.64% to 2.39% of critical damping for simple and continuous spans having lengths up to 75m. For structures with a total length in excess of 125m, damping values of 0.64% to 0.95% were found to be representative.

More recently, Billing (1984) has reported dynamic tests on 27 bridges of various configurations, of steel, timber and concrete construction to obtain data to support the Ontario Highway Bridge Design Code (OHBDC) provisions. Excitation of the bridges was by passing trucks and scheduled runs, at known speeds, by test vehicles of various weights. Further details of instrumentation layout, test and data processing procedures adopted are given in Billing (1982). The number of modes found depended upon the particular characteristics of a bridge. Interaction between the vibration modes of the individual spans was also noticed. The damping ratios of the first flexural modes of steel and concrete

bridges were respectively found to be 0.4% - 0.7% and 0.8% - 3.8% of critical damping. These values are consistent with other damping measurements (Cantieni, 1983; Green, 1977; Tilly, 1977).

Williams (1990; 1992a) has reported dynamic tests on the three span Axmouth bridge, which is believed to be the oldest concrete bridge in the U.K. Excitation was by a 7.5 tonne lorry crossing the bridge. A system of three Willmore seismometers were used to monitor vibration levels in three orthogonal directions at eight locations on the bridge. The vibration monitoring was used to assess the effects of piling work on one of the bridge's piers. Modal parameters of the bridge were not given. Proulx et al (1992) also used vehicular-crossing as the source of excitation during dynamic tests on a steel arch bridge. Pressure tubes were used to estimate the total excitation time of the structure and the speed of the test vehicles. Results of the tests were used to estimate the bridge's dynamic amplification factor and dynamic properties. However, accuracy of some of the computed power spectral density curves is doubtful since the frequency resolution was poor and the sampling period shorter than would be expected.

Kohoutek (1993) used a 40kg mass and a 50 tonne truck to excite a five span bridge during full-scale dynamic and modal tests. The test results were correlated with theoretical predictions and used to assess the structural condition of the bridge

## **2.5 Concluding Remarks**

Of the two main types of dynamic testing, ambient vibration testing is easier to conduct since the structural response can be measured while the structure is still in service. Artificial excitation systems, which could sometimes be complex and expensive, are not

required. A disadvantage of the method is that some of the estimated dynamic parameters, especially damping, could be in error since their values may depend on the (uncontrolled) unknown excitation level. Structural response measured under a given operating condition would give a true picture of the behaviour of the structure for that particular service environment. However, use of the model derived from such data may not be reliable in predicting response under a different operating environment. For tests involving normal vehicular traffic as the means of excitation, the natural frequencies of the bridge could be accompanied by some harmonics due to the motion of the vehicles. Despite these shortcomings, the ease and convenience of the method would continue to make it a popular option.

Forced vibration testing produces data from which more accurate system and modal parameters can be obtained especially if the input load is measured. Of the forced vibration test methods, impact testing is the easiest to conduct but probably produces less reliable data compared with tests using rotating mass and electro-hydraulic vibrators. However, the latter types of excitation devices are more difficult to develop. Although the concept of transient testing is quite straightforward, devising and applying suitable transient excitation could be difficult. It is also possible that not all the vibration modes of interest will be sufficiently manifested by transient excitation. Both impact and transient testing have the disadvantage of potentially inducing localized damage on the test structure.

Selection of an appropriate excitation mechanism is one of the main problems encountered in full-scale forced vibration testing of large structures. The system chosen should be robust and be able to generate sufficient force levels while not causing localised damage to the structure. The papers reviewed have illustrated the various types of devices that have been employed. Selection of a particular system will depend on, among other things, type

of structure to be tested, information required from the test and available resources. Factors considered during the development of the excitation system used in the tests reported in chapters seven and eight are discussed in chapter six.

Results from the reported tests indicate that vibration testing is a useful tool for obtaining information on the condition of structural systems. The review has shown that forced vibration testing produces better parameter estimates as compared with ambient testing primarily due to the advantage of being able to relate response to a measurable input. Forced vibration testing was therefore adopted for the full-scale tests conducted in this research. However, ambient testing will continue to be more popular as it is relatively easier to conduct. Most of the reported work were concerned with validating analytical models, characterization of the dynamic behaviour of the test bridges and investigating relationships between vehicular/cyclist/pedestrian traffic (loading) and dynamic response of bridges. Only a few of the published tests dealt with integrity assessment / damage detection despite the potential of using vibration testing for these purposes. For relatively rigid structures, forced vibration testing techniques are more effective for integrity monitoring. Application of vibration testing to integrity assessment of structures is discussed in the next chapter.

## **CHAPTER THREE**

### **A REVIEW OF METHODS OF DAMAGE DETECTION AND INTEGRITY ASSESSMENT USING VIBRATION DATA**

#### **3.1 Introduction**

Nondestructive vibration testing methods of assessing integrity and locating damage in general structural systems are reviewed in this chapter. The methods are grouped according to the parameter used to assess structural condition. Some methods utilizing mathematical error localization schemes are also discussed since these can potentially be applied to detect and locate damaged areas in real structures. Other methods which do not fall into distinct categories are also reviewed. In reviewing the methods, discussions on results from some vibration tests have been included to illustrate the relationships between dynamic parameters and existence of damage in a structure. It should be borne in mind when using dynamic monitoring for integrity assessment that it is stiffness and not strength that is being assessed. Thus, defects causing loss of strength without reduction in stiffness or changes in mass might not be detected. This introductory section discusses the rationale for using vibration monitoring to assess structural integrity.

Vibration monitoring has historically been used to assess structural integrity. The basic principle relies on the fact that dynamic response is a sensitive indicator of the physical integrity of any structure. Early techniques involved use of 'echo methods' in which the object is tapped or sounded and the structural condition assessed from the sound produced. Modern vibration methods of assessment are based on sophisticated extensions of these basic ideas.

As a result of damage, local or global, there would be a reduction in stiffness and a decrease in the free energy stored in the body (DiPasquale et al, 1990). Since dynamic response is governed by the system parameters (stiffness, mass and damping), changes in these parameters would lead to changes in the vibrational response as characterized by the modal parameters (natural frequencies, mode shapes and modal damping values). Due to the fact that each vibration mode has a different energy distribution, any localized damage will affect each mode differently depending on the location and severity of the damage. Modal parameters are also sensitive to the boundary conditions (physical constraints) of the structure.

Results of tests have shown that the size of damage is proportional to the magnitudes of observed changes in identified system parameters (Tsai and Yang, 1988). Although the detection of such changes is relatively easy to achieve, interpretation of the data might require expert knowledge. Results of studies by Rizos et al (1990) have indicated that changes in modal parameters might not be sensitive enough to indicate small structural damage such as those caused by fatigue cracks (Uzgider et al, 1993). The most common types of faults will lead to the following conditions, with respect to frequency and damping, in the structure (Richard and Mannan, 1993):

- \* A decrease in natural frequency combined with an increase in damping of a mode implies that a loss of stiffness, an increase of damping and possibly a decrease in mass has occurred in the structure.
- \* A decrease in natural frequency and a decrease in damping of a mode means that a loss of stiffness and damping, and possibly an increase in mass, occurred in the structure.

Early application of dynamic monitoring for integrity assessment of large structures has

been limited to the 'high tech' industries like nuclear, defence and offshore (Cole, 1992; Vandiver, 1977; Yang et al, 1980). This limitation is probably due to the high quality of data required which would necessitate expensive equipment (Cole, 1992). Extension of the techniques for condition monitoring of general civil engineering structures is continuously receiving attention from researchers and is one of the main objectives of this thesis. First application of vibration monitoring to assess integrity of civil engineering structures was probably in the field of pile integrity testing.

### 3.2 Theoretical Background

A brief consideration of the mathematical representation of the dynamics of a structural system is appropriate before discussing damage detection/location methods. The equations of motion of a vibrating structure are usually derived by applying Newton's second law of motion. For a linear, time-invariant structure, the equations of motion are given by:

$$[M]\{X''(t)\} + [C]\{X'(t)\} + [K]\{X(t)\} = \{F(t)\} \quad (3.1)$$

where  $[M]$ ,  $[K]$  and  $[C]$  are respectively the structural mass, stiffness and (viscous) damping matrices;  $t$  is the time variable;  $\{F(t)\}$  is the vector of externally applied forces;  $\{X(t)\}$ ,  $\{X'(t)\}$  and  $\{X''(t)\}$  are the displacement, velocity and acceleration vectors respectively. Viscous damping has been assumed in Equation (3.1) although other damping mechanisms can be present.  $[C]$  can be regarded as the equivalent viscous damping matrix for the system (Allemang and Brown, 1988; Raghavendrachar and Aktan, 1992). The dynamic model, as represented by Equation (3.1), can be transformed into the frequency domain by applying Fourier transformations. If  $\{X(j\omega)\}$  represents the complex Fourier transform of  $\{X(t)\}$ , denoted by  $\{X(j\omega)\} = FT\{X(t)\}$ , the following relationships exist:

$$\begin{aligned} \{X'(j\omega)\} &= FT\{X'(t)\} = (j\omega)\{X(j\omega)\} \\ \{X''(j\omega)\} &= FT\{X''(t)\} = (j\omega)^2\{X(j\omega)\} = -\omega^2\{X(j\omega)\} \end{aligned} \quad (3.2)$$

where  $\omega$  = frequency in radians per seconds and  $j^2 = -1$ . Equation (3.1) becomes

$$(-[M]\omega^2 + [C](j\omega) + [K])\{X(j\omega)\} = \{F(j\omega)\} \quad (3.3)$$

or

$$\{X(j\omega)\} = [H(j\omega)]\{F(j\omega)\} \quad (3.4)$$

where

$$[H(j\omega)] = \frac{1}{-[M]\omega^2 + [C](j\omega) + [K]} \quad (3.5)$$

$[H(j\omega)]$  is the (displacement) frequency response function (FRF) matrix. Each element  $H_{ik}(j\omega)$  of the matrix is an FRF measurement between two degrees of freedom (DOF) - response measurement location  $i$  and excitation point  $k$  - of the structure.  $H_{ik}(j\omega)$  can be expressed as:

$$H_{ik}(j\omega) = \sum_{r=1}^m \left( \frac{A_{ikr}}{\omega_r^2 - \omega^2 + j2\xi_r\omega\omega_r} \right) \quad (3.6)$$

where

$A_{ikr}$  = modal constant for the  $r$ th mode at point  $i$

$m$  = total number of measured modes

$\omega_r$  = natural frequency (radians/seconds) for the  $r$ th mode

$\xi_r$  = viscous damping ratio for the  $r$ th mode

The first objective of modal testing and analysis is to measure the FRFs of the structure. Curve-fitting Equation (3.6) to the measured values will yield the modal parameters. FRF computation and curve-fitting procedures adopted in this study are discussed in chapter six

(sections 6.4 and 6.5). The system matrices -  $[M]$ ,  $[C]$ ,  $[K]$  - can also be derived from the measured FRFs. There are two main approaches to obtaining the system matrices: 1) using the measured FRF directly by utilizing Equation (3.5); and 2) indirect methods which use the estimated modal parameters. Implementation of an indirect method is discussed in chapter four (sub-section 4.3.2).

Existence of damage in the structure will cause a modification of the system matrices. If  $\Delta$  is taken to represent the change in a given parameter, the FRF matrix  $[H(j\omega)]_D$  of the modified structure is given by:

$$[H(j\omega)]_D = \frac{1}{-[M+\Delta M] \omega^2 + [C+\Delta C] (j\omega) + [K+\Delta K]} \quad (3.7)$$

Curve-fitting response functions given by Equation (3.7) will yield new modal parameters which, depending on the level of damage, will be different from those of the original structure. Mere comparison of the modal parameters could indicate existence of damage. To locate and quantify damage, various methods exploiting the parameter changes exist. Overlay plots of the components of the FRFs of the original and modified structures can also be used to detect and locate damage.

Other approaches, based on system identification and model updating procedures, derive system matrices for the original and modified structures from Equations (3.5) and (3.7). These matrices, with or without the modal parameters, are then used to compute an error identification matrix or index which indicates the damage areas. Some of the available methods for detecting, locating and quantifying structural degradation are reviewed in the next sections.

### **3.3 Methods Based on Measuring Natural Frequency Changes**

Before presenting some of the available methods for detecting damage using natural frequencies, the sensitivity of frequency changes to damage is briefly examined.

#### **3.3.1 Effects of structural damage on natural frequency**

The presence of damage or deterioration in a structure causes changes in the natural frequencies of the structure. The most useful damage location methods are probably those using changes in eigenfrequencies because frequency measurements can be quickly conducted and are often reliable. According to Morgan and Oesterle (1985), abnormal loss of stiffness could be inferred when measured natural frequencies are substantially lower than expected. Frequencies higher than expected are indicative of supports stiffer than expected. It would be necessary for a natural frequency to change by about 5% for damage to be detected with confidence (Creed, 1987). However, significant frequency changes alone do not automatically imply existence of damage since frequency shifts (exceeding 5%) due to changes in ambient conditions have been measured (Aktan et al, 1994) for both concrete and steel bridges within a single day.

At modal nodes, the stress is minimum for the particular mode of vibration. Hence, minimal change in a particular modal frequency could mean that the defect may be close to the modal node. The other modal frequency variations can still be used to determine the magnitude of damage. Results of dynamic tests on 1/7 scale models of simply supported one- and two- cell box girder bridges show a decrease in the fundamental natural frequency with progressive damage (Mirza et al, 1990). Near the ultimate load, the frequency decreased linearly by about 40% and 75% for the one-cell and two-cell bridges

respectively. Other results (Ågårdh, 1991; Haroun et al, 1993; Kawahito, 1974; Kroggel, 1993; Mazurek and DeWolf, 1990, Salane and Baldwin, 1990; Salane et al, 1987; Savage and Hewlett, 1978; Sun and Hardy, 1992a) of dynamic tests on model and structures indicate that changes in resonant frequencies can occur due to support failure, crack propagation, shear failure and overload causing internal damage.

From results of vibration tests on concrete portal frames, Moradalizadeh (1990) reported that the magnitude of frequency reduction is dependent on the position of the defect relative to the mode shape for a particular mode of vibration. Similar observations were reported by Rytter and Kirkegaard (1994) from tests conducted on a 20m high steel mast. Damage at regions of comparatively high stress in the frames (tests by Moradalizadeh) resulted in significant reduction (up to 15%) in the resonant frequencies. Gomes and Silva (1990), Ju and Mimovich (1986) and Salane and Baldwin (1990) also reported increased accuracy of the diagnosis when cracks/damage occurred at sections of high stresses. These findings suggest that detection of damage using frequency measurements might be unreliable when the damage is located at regions of low stresses. Thus, shift in natural frequencies alone might not provide sufficient information for integrity monitoring, unless the failure is in one of the most important load bearing members (Idichandy and Ganapathy, 1990). A theoretical explanation of the relationship between magnitude of frequency changes and extent of damage is given below.

Existence of a crack at a section of a beam is equivalent to a reduction (proportional to the crack's severity) in the second moment of area. This leads to a reduction in the local bending stiffness at the cross-section where it is located. The modified beam can be represented as two beams connected by a torsional spring (which models the crack) with a stiffness dependent on the depth of the crack (Gomes and Silva, 1990). This torsional

spring model was first proposed by Chondras and Dimarogonas (1980). A similar crack model based on the "fracture hinge" concept was proposed by Ju et al (1982) and experimentally verified by Ju and Mimovich (1987). The consequence of reduced local bending stiffness is a lowering of the values of the bending natural frequencies. The natural frequency changes vary proportionally with the square root of the stiffness change, thus underlining the need for relatively large stiffness changes before significant frequency changes can be detected. The reduction (in frequency) becomes more important when the crack is at regions of high curvature for the modes under consideration.

Results from some experimental (Moradalizadeh, 1990; Slařtan and Pietrzko, 1993a) and numerical (Brownjohn, 1988) studies have suggested that the lower vibration modes would probably be best suited for damage detection. However, Begg et al (1976) stated that modes higher than the first should be used in damage detection so as to improve the identification. Alampalli et al (1992), Biswas et al (1990), Cempel et al (1992), Flesch et al (1991), Lieven and Waters (1994) and Mannan and Richardson (1990) have also mentioned the increased sensitivity of the higher modes to local damage. Since these higher modes (those above the 6th mode) are usually unavailable from the results of a full-scale modal survey, their use in damage detection can not be fully justified (Salawu and Williams, 1993a).

### **3.3.2 Damage detection and location using natural frequency changes**

Ju and Mimovich (1986; 1987) used changes in modal frequencies to locate damage occurring at sections of a beam to within 3% of the length. It was found that the accuracy of the damage localization was improved to less than 1% of the length when the built-in end of the experimental beam was represented by a torsional spring. A fundamental

assumption, and limitation, of the method used is that the damage can be represented using the "fracture hinge" concept proposed by Ju et al (1982). Changes in modal frequencies were also used to locate damage in the investigations by Adams et al (1978), Al-Ansary and Azayem (1986), Chondras and Dimarogonas (1980), Gomes and Silva (1990), Gudmundson (1982; 1984) and Springer (1988). The methods used in the investigations are not likely to be applicable to structures other than the simple cases (typically, a simple beam with artificially induced cuts) considered.

The method of Cawley and Adams (1979) uses the sensitivity concept to obtain frequency changes due to stiffness loss. The method is based on the premise that the ratio of frequency changes in two modes is a function of the location of the damage only, if changes in stiffness are independent of frequency. To locate the defect, theoretical frequency shifts, due to damage at selected positions on the structure, were calculated and compared with measured values. A normalized error, which also gave some weight to the crack direction, was calculated at selected sites and used to search for the defective area. The method assumes the damage to be in the form of a hole, which is not always the case, and is unable to locate defects at more than one site. Furthermore, erroneous results are obtained for defects involving creation or alteration of mode shapes and no indication is given as to the accuracy of the predicted damage site. Another drawback of the Cawley and Adams method, and indeed most sensitivity based methods, is the use of considerable computing time subsequent to physical measurement as a consequence of the need to model all possible damage mechanism at various possible sites. Application of the method to damage location in reinforced concrete and steel beams revealed that at least nine modes should be included in the computations if the damage is to be located with any reasonable accuracy (Brownjohn, 1988). Other damage location methods using frequency changes and sensitivity analysis have been proposed (Eggers and Stubbs, 1994; Hearn and Testa, 1991;

Menegetti and Maggiore, 1994; Penny et al, 1993). Accuracy of sensitivity based methods is dependent on the quality of the finite element model (or other theoretical model) used to compute the sensitivities. The methods are most useful for skeletal structures where the damage event affects one significant stiffness component in the structure.

Law et al (1990) have suggested a technique for determining structural stiffness changes and positions of defects from measured changes in resonant frequencies. The technique uses a finite element model of the structure and assumes the structural mass matrix to be unsymmetrical so that a unique identification can be obtained. This assumption does not always hold. Solution of the identification problem involves utilization of a non-linear programming method which requires a weighting matrix and vectors defining upper and lower bounds for the identification factors. Selection of appropriate matrix and vectors would affect the results. It appears that the identification is improved if only certain parts of the structure are included in the formulation. Since prior knowledge of damaged areas is unavailable, determining which part to include might be difficult.

Measurement of natural frequency can be used to estimate the tension in the stay cables of cable-stayed bridges (Gardner-Morse and Huston, 1993). Estimated values of the cable tension significantly lower than design / as-built values would indicate loss of cable tension. A similar approach (though using a different formulation) was adopted by Camomilla et al (1993) to determine the stress levels in the prestressing cables of reinforced concrete stays of the Polcevera viaduct, Genoa, Italy. One main problem with this technique is the fact that deterioration of a rope or cable by corrosion or by breaking of wires will change the rope's cross-section and reduce its strength but may not alter rope tension (Hearn and Testa, 1991). In such circumstances, existence of damage may not be detected by natural frequencies; especially if axial modes are used.

Uzgider et al (1993) have proposed a damage location method which uses measured natural frequencies to identify stiffness parameters. Stiffness parameters and vibration modes which the parameters significantly influence are first selected. The natural frequencies of the selected modes are then used to identify the stiffness parameters. The relative magnitudes of the differences between the identified parameters and prior estimates are used to indicate the presence of structural damage. Success of the method depends on identification of suitable stiffness parameters, accurate definition of base values (prior estimates) of the parameters and values selected for the lower and upper limits of frequency and parameter value variation. The need for a very sophisticated mathematical model of the structure is another limitation of the method.

Zhang et al (1992) proposed a pattern recognition method for detecting structural faults in frame structures. The same approach was also applied to the diagnosis of defects in foundation piles (Zhang et al, 1993). The method is based on the fact that the ratio of the relative change in natural frequency between any two modes is equal to the ratio of the squares of the corresponding strain modal values at the fault. Due to experimental and analysis errors, the equality is only approximate. To account for this, two parameters were defined to control the fault identification. Thus, accuracy of the method is highly dependent on the choice of proper values for the control parameters. Furthermore, the method is only applicable to faults which can be represented as slots.

Two approaches to the integrity assessment of bridges have been proposed by Ward (1984). The first involves monitoring a given bridge, say yearly, to check if there are changes in the dynamic properties with reference to the last/previous measurement(s). The second approach involves comparing the dynamic characteristics of similar structures one of which is known to be in good condition. To account for different ground conditions at various

locations of the bridges, Ward put forward a dimensionless factor - velocity amplification factor - to assess the integrity of the bridges. The velocity amplification factor is defined as the response spectrum of the bridge divided by the spectrum of the ground vibration in the approach to the bridge. Further work would be necessary to assess the factor - or a similar variable - as an identification parameter.

### **3.4 Damage Detection and Location using Mode Shape Data**

Results of studies by Biswas et al (1990), Rubin and Coppelino (1983), Salane and Baldwin (1990), Shahrivar and Bouwkamp (1986), Srinivasan and Kot (1992) and Tang and Leu (1988) have suggested that mode shapes are more sensitive to damage than are natural frequencies since the changes in the mode shape values are much more pronounced (Shepherd and Reay, 1967). In addition, natural frequency changes alone may not identify location of the structural damage (Salawu and Williams, 1994a). This is because cracks associated with similar crack lengths but at two different locations may cause the same amount of frequency change (Pandey et al, 1991). According to Mazurek and DeWolf (1990), mode shapes can be heavily influenced by crack propagation and support failures. The greatest changes occur in the vicinity of the defect, thus offering the opportunity of locating damage. According to Richardson and Mannan (1992), the lower and higher modes can respectively be used to detect and locate structural faults. This is due to the fact that the lower modes are global while the higher modes are more localized to particular regions of the structure. A fault will be located in the vicinity of the anti-nodes of those modes whose poles (frequencies and damping) move the most (Richardson and Mannan, 1993). The sensitivity of modal vectors perpendicular to the predominant modal direction is clearly established for predicting damage in load bearing and highly redundant members (Idichandy and Ganapathy, 1990).

When mode shapes are used for structural assessment, the vibrational modes should be selected such that they provide significant response of the particular members that are being monitored. In general, the changes in mode shapes seem to become more pronounced as the mode number increases (Fox, 1992; Sun and Hardy, 1992b). A distortion of the third vibrational mode shape after damage to reinforced concrete beams was noted by Savage and Hewlett (1978). An important point observed was the development of asymmetry, as damage progressed, of the half wave length between the two nodes in the centre of a simply supported vibrating beam. This observation was useful in pinpointing the damaged area.

Morgan and Oesterle (1985) have described some characteristics of measured mode shapes that can be exploited in evaluating the condition of a bridge. They stated that a condition of local deterioration may be detected if : i) there is a lack of symmetry in a mode shape when symmetry is expected and/or ii) occurrence of two different mode shapes with comparatively close frequencies. A mode shape in which one point participates excessively in the motion could indicate local loss of stiffness. This could be a support or foundation problem if the point concerned is grounded. Jeary and Ellis (1984) have pointed out that mode shapes could indicate onset of increased soil-structure interaction. Mode shapes are more useful than natural frequencies and damping values in detecting damage that leads to creation of new modes. An example of such a case is the creation of new modes due to support failures (Mazurek and DeWolf, 1990).

Chowdhury (1990), while investigating the effects of base support material on the dynamic properties of continuously supported structures, found that the magnitudes of the imaginary parts of FRF increase as the stiffness of the base material reduces. The magnitudes of the imaginary part of the FRF are proportional to the deflection (mode shape) of the structure

at a given frequency of vibration. The mode shape patterns observed were also found to depend on the quality of the support material. These findings suggest that measurement of mode shapes, when properly modified to account for the type of structure, boundary conditions and support type, can be used to identify the support conditions. Crema et al (1985) and Tracy et al (1984) also used mode shapes to detect damage in composite structures.

In analysing results of dynamic tests on a three span highway bridge, Salane and Baldwin (1990) plotted the mode shapes as contours on the bridge deck. Comparison of the contours obtained before and after several fatigue load cycles indicated impending fracture. The technique shows promise as a means of locating structural damage. Analysis of mode shapes measured on a bridge girder was found to be effective in detecting delamination along one side of the girder (Morgan and Oesterle, 1985). Biswas et al (1990), Salane et al (1987), Srinivasan and Kot (1992) also found mode shapes to be good indicators of structural deterioration.

A number of studies have been conducted on the sensitivity of mode shapes, Modal Assurance Criterion (MAC), Coordinate Modal Assurance Criterion (COMAC) and Modal Scale Factor (MSF) to structural changes. The formal definition and mathematical formulation of these parameters are given in chapter four. Also discussed in chapter four is the performance of the methods proposed by Fox (1992), Pandey et al (1991) and Yuen (1985). Application of MAC and COMAC to damage detection and integrity assessment is discussed in chapters four, seven and eight.

The approach adopted by Ko et al (1994) addressed the problem of defining suitable modes when using MAC/COMAC for damage location. The damage is assumed to be at a

particular node and sensitivity analyses are conducted to find the most sensitive modes for a range of damage events. The types of damage considered would obviously place a limitation on the approach. After selecting suitable modes, COMAC values are then computed. If the indicated damage location (with the lowest COMAC value) is the same as the assumed one, then the damage is actually at or close to the assumed position. A new method of determining suitable modes for damage detection and location is presented in chapter four (sub-section 4.2.1) while Salawu (1994?) has discussed the problem of identifying damage sensitive vibration modes.

A modified version of the basic MAC definition was introduced by Fox (1992). The modification, called Node Line MAC, involves using only selected measurement points, which are close to nodes of particular modes, in the MAC computation. The concept is based on the idea that changes in mode shapes will be most noticeable in the vicinity of node points or nodal lines (Wolff and Richardson, 1989). Fox noticed a slight improvement in the identification procedures when the Node Line MAC values were used. It should however be noted that the changes observed are to four significant figures which would be insignificant in practical field tests on full-scale structures.

Lieven and Waters (1994) have recently discussed application of Normalised Cross Orthogonality (NCO), Normalised Difference (NDIF) and Normalised Cross Orthogonality Location (NCOL) to the identification of spatial differences between a finite element model and its corresponding measured modal data. These parameters are similar to MAC and COMAC and can also potentially be used to locate regions of error in a structure.

Despite the foregoing discussions, some authors have suggested that use of mode shapes is not very effective in detecting damage. One of the reasons suggested is the inaccuracy

in estimating mode shapes from measured data. According to Friswell and Penny (1992), a 20% error in a particular element of the mode shape vector would be typical while Raghavendrachar and Aktan (1992) have indicated that the error may be about 30%. Tests by Creed (1987) suggest that measured mode shape ratios are only repeatable to within 35% to 40%. Furthermore, DiPasquale et al (1990) pointed out that, for a given mode, the damaged structure's mode shape is not usually very different from that of the original structure. This view was also reflected in the results of tests (Slařtan and Pietrzko, 1993a) conducted on reinforced concrete T-beams before and after various levels of damage.

According to Hearn and Testa (1991), vibration mode shapes are poor indicators for small damage that does not alter mass. This is a rather curious conclusion since most damage events (involving stiffness reduction) do not lead to significant mass alterations. From numerical evaluation of two structural dynamic identification schemes, Ojalvo (1986) discovered that use of only mode shape data in model error detection resulted in convergence to the wrong answer. If the structure is severely damaged, deciding which modes, from the damaged and undamaged structures, to be paired for damage detection may be difficult (Penny et al, 1993).

### **3.5 Methods Based on Measuring Changes in Damping Values**

Occurrence of damage in a structure would be expected to lead to an increase in damping. Unusually high damping would suggest more energy dissipation mechanism than expected, indicating possibility of cracks in the structure (Morgan and Oesterle, 1985). Similarly, an increase in damping values for similar excitation conditions can be taken to indicate a deterioration in the structure (Jeary and Ellis, 1984). Studies by Tsai and Yang (1988), Yang et al (1983) and Yang et al (1985b) concluded that, for a variety of structures and

loading conditions, damping is generally more sensitive to damage than stiffness. According to Jeary and Ellis (1984), change in damping is a potential indicator of structural changes since the relationship between damping and stiffness suggest that damping changes may indirectly indicate small localised areas of changing stiffness. Damping may be the only indicator of distress when frequencies, as well as mode shapes, are insensitive to damage as in the case of transverse motion of wire ropes (Hearn and Testa, 1991). Considerable changes (up to 80%) in damping values were noticed (Ågårdh, 1991) after shear failure close to the support of a reinforced concrete bridge.

Savage and Hewlett (1978) reported a significant difference (87%) in the damping ratio of two geometrically similar concrete beams but with one prestressed and the other unstressed. The unstressed beam exhibited high damping which was thought to be associated with the presence of micro-cracking along the beam's length. Microscopic movement and resulting friction between solid concrete in the cracked regions probably damped out the response motion to an applied transient. In the stressed beam, the microcracks were effectively closed up by the post-load and hence could not produce friction motion. A general increase in damping values after crack initiation in reinforced concrete beams was reported by Slaštan and Pietrzko (1993a). Results of tests conducted by Kennedy and Grace (1990) on continuous (two spans) bridge models indicated that damping values would increase due to development of transverse cracks in the deck slab near the intermediate pier support.

However, results (Baldwin et al, 1978) from vibration tests during fatigue testing of a full-scale bridge showed that variation in damping ratios was not significant from the viewpoint of structural monitoring. Sun and Hardy (1992a) performed statistical tests of significance on damping estimates, obtained before and after induced damage in a rock structure, with a view to check if there was any significant change in damping as a result of the

modifications. The results from the two statistical tests (F-test and t-test) were not in agreement. The large scatter usually observed in damping estimates would make any statistical test insignificant.

Differences between damping ratios of an undamaged beam and the same beam after strengthening by carbon fibre reinforced plastic laminates were found (Slařtan and Pietrzko, 1993b) to be practically negligible. Some test results (Ågårdh, 1991; Baldwin et al, 1978; Hearn and Testa, 1991; Salane and Baldwin, 1990; Salane et al, 1987) indicate an initial increase in damping before subsequent reduction as damage progressed. Ågårdh and Palm (1992), Alvarez et al (1993), Askegaard and Langsø (1986), Alampalli et al (1992) and Farrar et al (1994) reported a large scatter in the measured damping values from laboratory tests to investigate the effectiveness of damping and frequency measurements in damage detection. The scatter becomes more pronounced when the damping values are low. A change of a factor of two between damping measurements made on the same day was observed by Askegaard and Mossing (1988). According to Shepherd and Reay (1967), the damping mechanism in structures must be better understood before changes in modal damping ratios can be successfully used in damage detection/integrity assessment. Unlike frequency changes which can be associated with highly stressed areas of the structure, damping changes may more properly relate to local motions, or specifically to the potential for increased motion and increased friction as damage loosens connected members (Hearn and Testa, 1991).

From the author's experience, a major factor against the use of measured damping values in integrity assessment is the error involved in estimating damping values especially if ambient testing is used. During modal parameter extraction procedures, the damping values usually have the greatest degree of uncertainty. DiPasquale (1990) and Mazurek and

DeWolf (1990) also concluded that damping values alone can not provide very reliable means of damage detection since quantitative relations between deterioration and the level of damping in structures are not available. Furthermore, there are many methods (Jeary and Ellis, 1984) of estimating damping, each giving dissimilar results, in addition to the different definitions of damping. If damping values are to be used in damage detection, more efforts would be needed to increase the accuracy of data acquisition system, increase the restrictions on the testing environment and improve the quality of parameter extraction routines (Sun and Hardy, 1992a).

### **3.6 Mathematical Model Error Localization Schemes**

As more emphasis is placed on predicting structural behaviour using analytical (usually finite element) models, it becomes more important to validate (update) these models, using test data, before they are used in response predictions. Many model updating methods have been proposed for refining theoretical models. Review papers providing an overview of model refinement techniques have been published (Heylen and Sas, 1987; Ibrahim and Saafan, 1987; Imregun and Visser, 1991). Only some of the methods which have been applied to damage detection and location are reviewed in this section. Theoretical background, implementation and performance evaluation of two model updating based methods are presented in the next chapter.

As a first step, most updating schemes locate regions of errors in the finite element model before the updating proper. If it is assumed that the (analytical) system matrices to be updated (corrected) were obtained from a prior vibration measurement, then the error localization stage can be utilised to detect, locate and quantify damage in a structure from any two measurements of the vibration response. The system matrices are obtained from

measured dynamic response using system identification procedures. Selection of an appropriate system identification algorithm is crucial to the accuracy of the methods. For this approach to be successful, the error introduced by data acquisition and processing should not be large enough to suppress the damage induced deviations in the system matrices. Other factors to be considered in the application of structural identification procedures to damage detection have been investigated by Beck (1991). Link (1990) has discussed the problem of defining bounds for error localization using model updating techniques.

Most of the damage location methods based on model refinement techniques compute an error identification matrix which is used to indicate the damage location. In some cases, the values of the matrix elements can be used to determine the severity of the defect. The basic form of the identification matrix is the stiffness error matrix which represents the difference between the stiffness matrices of the damaged and undamaged structures. The stiffness matrix is used since most damage events will lead to changes in the structure's stiffness. This is probably due to the fact that while very localized defects in a structure produce small, but measurable, changes in the overall dynamic properties, the local stiffness of the structure is significantly reduced at the defect location (Cawley and Adams, 1979; Cawley and Nguyen, 1988). Despite this, Tsai and Yang (1988) proposed a technique which uses ratios between corresponding elements of identified mass matrices of the damaged and undamaged structures. If a location on the test structure is close to a defect, the ratios corresponding to the location will be substantially lower or higher than unit magnitude, thus offering a way of locating the defect.

The locations in the error matrix which have the largest reduction in stiffness give the most likely damage sites. Many of the error matrix methods (Gysin, 1986; He, 1992; Lieven and

Ewins, 1990; Park et al, 1988; Sidhu and Ewins, 1984) use either the basic formulation or modified versions. An evaluation of the performance of a few of the available methods has been presented by Salawu and Williams (1993) and is further discussed in the next chapter while the effect of (data) incompleteness and noise on error matrix calculations has been studied by Lieven and Ewins (1992).

The method proposed by Yang et al (1985a) involves comparison of the diagonal elements of the mass and flexibility matrices before and after damage. It was found that (for cantilever beams), the flexibility does not change significantly for response stations before the damage location while for stations after the damage site, flexibility changes progressively according to the severity of damage and distance from the damage location. A disadvantage of the method is that the full modal matrix is needed to construct the system matrices. In addition, neither is the severity of damage quantified nor multiple damage locations identified.

The approach adopted by Raghavendrachar and Aktan (1992) also uses experimentally determined flexibility matrices but without assuming a mass matrix. Successful application of the method depends on careful consideration of the factors (sub-section 2.4.3) affecting impact testing. The need for many reference points (use of reference points in full-scale tests is discussed in section 7.4), though likely to increase accuracy of the identification, might increase test costs. In addition, about twenty modes are needed to obtain a sufficiently accurate flexibility matrix (Aktan et al, 1994).

Another approach to using error localization methods is to use measured data from the undamaged structure to correct a finite element model of the structure. The system matrices of the corrected model will then represent the undamaged structure. Data from

subsequent tests on the structure are then used to update the correct initial model (model *A*) to obtain a new model (model *B*). The updating is achieved by changing the physical parameters (Young's modulus, member dimensions, density etc) so that the predicted mode shapes and frequencies agree with the measured values. Comparison of the physical parameters of each element of models *A* and *B* (or the system matrices of the two models) will indicate which areas have been affected by damage and to what extent. Application of the technique to damage detection in model trusses has been presented by Doebling et al (1993) and Kaouk and Zimmerman (1993) while Flesch et al (1991) have investigated suitability of the technique for safety evaluation of bridges. The method adopted by Kaouk and Zimmerman includes a minimum rank perturbation algorithm for estimating the extent of damage.

The major limitations of the approach described in the previous paragraph are as follows (Avitable and Li, 1993; Link, 1990): 1) Selection of an appropriate model updating method is crucial; 2) If the wrong parameters are selected for the updating process, incorrect system matrices will result; 3) The mass and stiffness sensitive regions of the structure, for the sets of modes included in the updating process, will always dominate the solution if they are allowed to participate in the process; 4) Accuracy of the error localization depends on the choice of the areas of the model to update and the modes to include; 5) Incompleteness of the measured data would necessitate use of model expansion or reduction techniques to ensure compatibility between the experimental and analytical models. These techniques will introduce further errors; 6) Mismatch of boundary conditions between analytical and experimental models; and 7) Measurement and modelling errors. Zhang (1994) has suggested that an error analysis of the modal data should be conducted before they are used in system identification/model updating. Since such an analysis would involve conducting more than one series of tests (and ideally with different excitation/testing techniques) on

the reference structure, resource constraints would limit any widespread practical application.

### **3.7 Other Damage Location Methods**

There are other damage location and quantification methods which do not fall into the categories already described. Most of these methods use the FRFs directly to either compute a damage indication parameter or develop patterns to be used in damage diagnosis. The simplest methods are probably those that involve overlay plots of magnitudes and squares of the real and imaginary parts of the FRF (Biswas et al, 1990; Richardson and Mannan, 1993; Salawu and Williams, 1994?). Baumgärtner and Waubke (1993) have also suggested use of banded spectra plots in which the FRFs obtained from long term dynamic monitoring are plotted as histograms and the relative shifts in amplitude used to assess stress levels in the structure. These plots could indicate existence of degradation and which modes are most affected. The sensitivity of the plots largely depends on the severity of the damage and the accuracy of FRF measurement. A similar approach but with the added advantage of damage location was proposed by Afolabi (1987). The approach is based on the premise that the minima in FRF plots for points on a structure do not change for points at which damage has occurred, but that the further a point lies from a damage site, the greater the number of shifted minima.

A signal subspace correlation (SSC) index for detecting structural changes was proposed by Cherng and Abdelhamid (1993). The method utilizes impulse response functions (IRF). For a single mode, the frequency domain equivalent of the index is the drop of the FRF peak as frequency changes. For a multi-degree of freedom system, the SSC index indicates the change in the most sensitive mode. The method proposed by Stubbs and Osegueda

(1990a; 1990b) involves determining damage location and severity from expressions relating variations in stiffnesses of structural elements to changes in modal stiffnesses. The approach is limited to structural elements (such as beams, plates and shells) and requires predefining the damage locations.

Application of neural networks (Caudill and Butler, 1992) to damage detection has been investigated by some researchers (Kudva et al, 1992; Rytter and Kirkegaard, 1994; Worden et al, 1993; Wu et al, 1992). The rationale is based on the fact that fault location can be considered as a process of distinguishing between data from the original structure from that of the damaged structure. The neural network has to be trained by feeding it sets of modal parameter changes along with the mass, stiffness and damping changes that caused them (Richardson and Mannan, 1993). The network, in turn, computes a set of internal weights that allows it to predict mass, stiffness and damping changes that caused the modal parameter changes. After training the network, it can be used to predict the location and extent of defects that caused measured modal parameter changes. The major drawback is the significant amount of computation involved in training the network (at least 100 000 changes are needed to train a network - Mannan et al, 1994). Furthermore, the accuracy is limited by the number and type of damage cases built into the network. If experimental data are used to train the network, the quality of the data must be very good.

Perturbation analysis is sometimes conducted as an alternative to repeating the full dynamic analysis in order to compute changes in modal parameters due to localized damage. Although most sensitivity based methods utilize natural frequencies and mode shapes, it is sometimes more convenient to use the sensitivities of FRFs directly. Sensitivity based methods using changes in FRF characteristics have been proposed (Brandon, 1987; He, 1993; Law et al, 1991; 1992). However, methods utilizing response functions might be

inappropriate if the FRFs contain a substantial amount of noise (Imregun and Ågårdh, 1994).

Application of signature analysis to condition assessment of bridge structures has been studied by Samman and Biswas (1994a; 1994b). The measured FRFs are used as signatures. The signatures are first processed by applying a "smoother" (a form of low-pass digital filter) which reduces their peakedness without destroying their characteristic appearance. The "smoother" also reduces/removes noise in/from the signals. Different types of signal recognition tools are then applied to detect differences between any series of signatures. The techniques can be used to identify presence of damage before damage location schemes are used to indicate affected areas. They can therefore serve as condition monitoring tools. The procedures were used to detect the presence of simulated cracks in a model bridge. Limited success was obtained in detecting damage in a full-scale highway bridge.

Armstrong et al (1993) have reported application of a dynamic stiffness technique to integrity assesment of masonry arches. The approach, which is based on earlier studies by Davis and Dunn (1974) and Sibbald (1988), involves utilization of the displacement FRF values at low (close to 0.0Hz) frequencies. However, use of FRF values at low frequencies is unreliable since measurements at the low frequency range are more susceptible to errors. In fact, the low frequency components are sometimes attenuated during field testing of large civil engineering structures.

One approach that is also applicable to the problem of structural assessment (damage detection/location) is 'reverse' structural modification. The usual structural modification techniques (Snyder, 1985; Jones and Iberle, 1986) seek to find the optimum changes in a

structure necessary to achieve desired dynamic properties. A reversal of this procedure would be to find positions (and magnitudes) of structural modifications that would cause observed changes in the structure's dynamic properties. Application of this reverse approach to detect, locate and quantify damage is rare. It would involve creating a reference database of possible modification (damage) sites corresponding with known parameter changes. The accuracy of structural modification methods are affected by truncation errors - only an incomplete set of all the possible vibration modes are usually measured. Ulm (1986) has studied the accuracy of structural modification relative to errors and deficiencies of typical modal data while a procedure to predict error bounds for results from structural modification has been proposed by Braun and Ram (1990).

### **3.8 Factors To Consider**

Some factors to consider when using vibration testing for integrity assessment are discussed in this section. For successful utilization of vibration data in assessing structural condition, measurements should be taken at points where all the modes (in the frequency range of interest) are well represented. The simplest way of achieving this is to conduct a theoretical vibration analysis of the structure prior to testing. The best positions would be those points where the sum of the magnitudes of the mode shape vectors are maximized. Models for selecting the best excitation (Kientzy et al, 1989) and measurement (Penny et al, 1992; Shah and Udawadia, 1978) locations have been proposed while Larson et al (1994) have presented a comparative study of several pre-modal test planning techniques. A few simple procedures that may also be applicable to test planning can be found in Bolton (1994). Schütze et al (1994) have described an expert system for vibration test planning.

For effective utilization of dynamic testing as a diagnostic tool, it is necessary to

understand the effects of deterioration and defects on the dynamic characteristics of structural systems. For example, long span bridges are not likely to show measurable changes in dynamic properties if local damage is sustained (Brownjohn, 1988). In addition, dynamic characteristics are sensitive to changes in support conditions that may have little structural consequence. Responses measured at boundaries (abutment, piers and other support types) could also yield erroneous results (Zhang, 1994). It is also important that the effects of environmental factors, such as temperature and humidity, on changes in dynamic characteristics be either small or predictable (Askegaard and Mossing, 1988). Al-Ansary and Azayem (1986) have pointed out the need for 'sufficient' number of frequency variations before defects can be adequately located. According to Tang and Leu (1989), it would be necessary to detect changes in natural frequencies in the order of 0.01Hz for safety inspection of bridges. However, this is probably only applicable to long span suspension bridges.

Quantitative relationships between changes in dynamic parameters and environmental factors are very rare. The many variables involved will make assigning numerical factors difficult. An investigation into this issue has been reported by Askegaard and Mossing (1988) who showed that the relative change in the magnitude of a well defined natural frequency of an undamaged structure is little influenced by changes in temperature, humidity etc if measurements to be compared are made at the same time of the year. Their results (Figures 3.1 and 3.2) showed that changes in natural frequencies during short term tests were insignificant while the fluctuation observed over a two year period were much less than those occurring in deteriorated structures (Askegaard and Langsø, 1986). Further discussions of the effects of temperature on the resonant frequencies of structures can be found in Adams and Coppendale (1976). The fluctuations in damping values (Figures 3.1 and 3.2) are much larger and have been discussed in section 3.5.

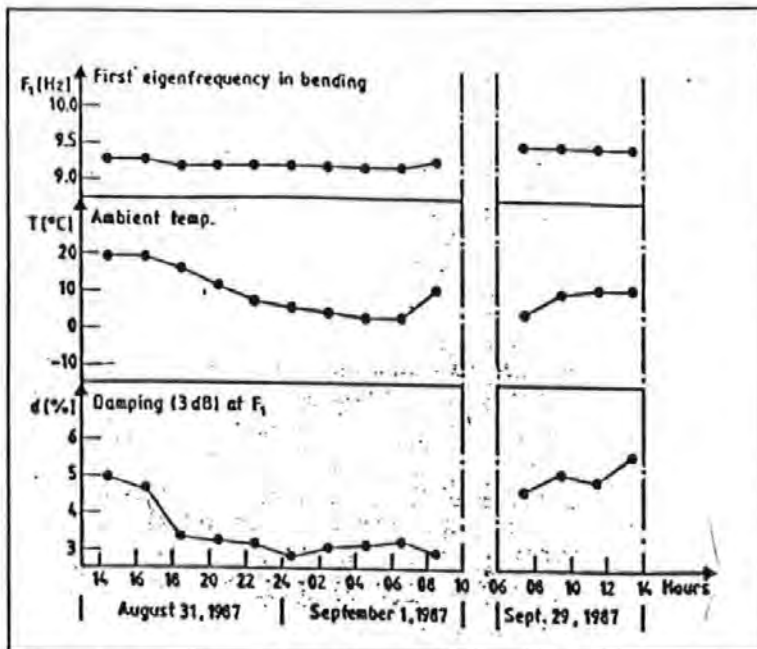


Figure 3.1 Changes in frequency, damping and temperature in short term-tests (Askegaard and Mousing, 1988)

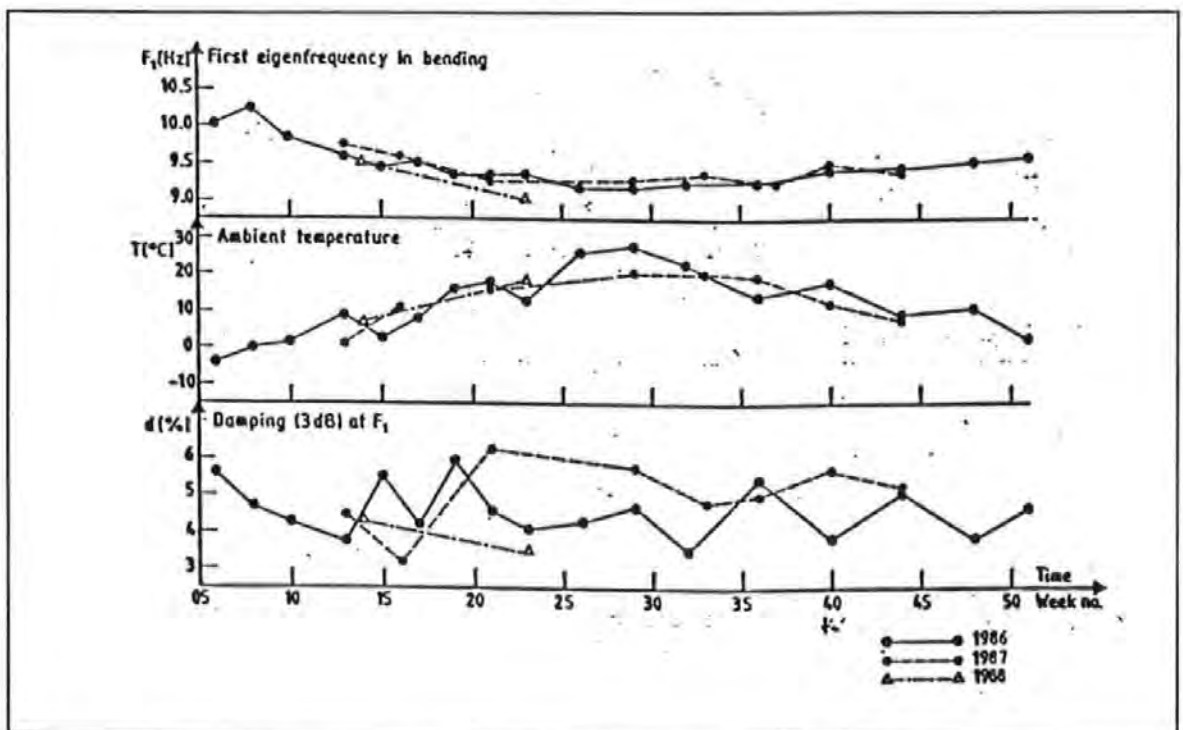


Figure 3.2 Long-term changes in frequency, damping and temperature (Askegaard and Mousing, 1988)

From an analysis of the effect of ambient conditions on the dynamic response of four prestressed concrete bridge decks, Purkiss et al (1997a; 1997b) concluded that the most significant variable affecting measured responses is the soffit temperature of the bridge deck. The other variables investigated were the site's air temperature and humidity; mean upper deck temperature; local temperature variation; mean local humidity; mean air pressure; and mean rainfall on the day preceding the test. The results show a gradual decrease in natural frequency with increasing soffit temperature. The authors used the normalized frequency-temperature gradient to analyze variation in dynamic response with soffit temperatures. A procedure for calculating the normalized frequency-temperature gradient was proposed. The variation in temperature was not related with time. The relationships observed would not undermine using vibration data for assessment as long as measurements are taken at similar periods and ambient conditions are similar.

Other factors to consider are the consistency and reliability of the testing procedures. Alampalli et al (1992) have noted that previous investigations paid little attention to the random effect of environment and test equipment on test results. They also pointed out that the sensitivity of a dynamic monitoring system is limited, at least, by the observed random variation due to environmental influence and instrumentation accuracy. Other researchers (Aktan et al, 1994; Fox, 1992; Kroggel, 1993) have also mentioned these factors. To account for these limitations, Alampalli et al (1992) suggested development of criteria based on statistical concepts to establish windows for warning triggering. Use of trigger windows would be synonymous with the concept of mechanical signature analysis employed in the mechanical and nuclear industries for assessing integrity of machinery and products. Some researchers (Aktan et al, 1994) have questioned the reliability of modal parameters as integrity indices and have suggested other indices, also derived from the measured dynamic response, for condition assessment.

One potential problem with the use of mode shapes in integrity assessment is the possibility of changes in the dynamic condition of the bridge during the course of a test programme. During a full-scale bridge test, Richardson and Douglas (1987) noticed changes in the dynamic response of the bridge as a day's testing progressed with the bridge returning to its original state overnight. This phenomenon could prevent the complete identification of some mode shapes. However, an approach similar to that adopted by Purkiss et al (1997b) - mentioned earlier - may be used to account for the variation in the dynamic response.

A limitation of structural assessment using vibration testing is the need to conduct at least two series of tests - one on the pristine structure and another after a period of time. In most cases, the (measured) dynamic parameters of the as-built structure are unavailable and assessment engineers require information on the current state of the structure. To circumvent this limitation, Alocco et al (1993) have suggested two methods for assessing the integrity of prestressed bridges using results from one series of tests. In principle, the methods should be applicable to any type of bridge. At least two or three tests would be necessary to determine the frequency and damping ratio of the first mode. The first test will be on the structure without any load while the others will be after adding different levels of uniformly distributed imposed loads. The main disadvantage of the technique is the requirement to apply large imposed loads especially for large structures where the practicability and cost could be prohibitive.

### **3.9 Conclusions**

A review of methods of damage detection using vibration data has shown that the approach is potentially useful for routine integrity assessment of structures. Of the dynamic parameters, damping values seem to be the least appropriate, despite the sensitivity of

damping values to damage, because of the large scatter in reported experimentally determined values. Methods using natural frequencies and mode shapes are more attractive since they can identify the occurrence, and to some extent, locate and quantify damage. However, many of the proposed methods require either a theoretical model of damage or a set of sensitivity values to be computed before physical measurements. Perturbation/sensitivity analysis methods could be very slow if matrices are large especially if a complete eigensolution is required for each iteration. To be truly realistic, the methods would require consideration of all possible damage events at various locations on the structure. Consequently, the computations that would be required for large civil engineering structures could be prohibitive. These methods are thus limited in application to specific structural geometries and the type of damage model assumed. In addition, utilization of a theoretical damage model could introduce uncertainties into the results. Methods that rely only on measured data without any prior theoretical assumptions would be more appropriate to large civil engineering structures.

Damage detection using system identification and model updating schemes is limited by the accuracy of the system identification algorithm used. Many system identification methods have been proposed but none is completely satisfactory since there is no unique solution to the problem of obtaining a set of system matrices, from a set of incomplete measured data, that would realistically model the structure. In addition, model updating tends to spread the effect of damage around the structure (as represented by the system matrices), making damage localization difficult.

Integrity assessment of civil engineering structures using vibration data would require a method which uses only test data from the first few modes and is based on simple assumptions about the behaviour of the structure. In the next chapter, the effectiveness of

some of the more promising methods reviewed in this chapter are evaluated. This would enable development of a scheme, taking account of the limitations of the methods assessed, for integrity assessment.

# CHAPTER FOUR

## EVALUATION OF SOME DAMAGE LOCATION METHODS

### 4.1 Introduction

The review in the last chapter has revealed the existence of a significant number of methods for detecting, locating and quantifying damage. Each method has its advantages and limitations so that selection of a particular method would require some knowledge of its performance in locating damage in the type of structure under consideration. Evaluation of existing methods is desirable so that important merits and drawbacks of these methods can be emphasised. This would aid in directing future research towards more productive areas. For these reasons, the relative effectiveness of some damage location methods is considered in this chapter. The more promising methods out of those reviewed in chapter three were selected. Both theoretical and experimental data were used in the studies.

Simple configurations (a cantilever beam for the theoretical model and a simply supported steel beam for the experimental structure) whose behaviour could be easily understood were used. In addition to evaluating the methods, it was intended to investigate which factors are most influential in damage detection and location. The number of damage cases that can be considered is unlimited. Therefore, the cases selected were chosen to reflect the more common damage situations and facilitate reasonable comparison of the performance of the methods tested. Details of the methods evaluated, numerical simulations, experiments conducted and results obtained are given.

Figure 4.1 shows a generalized section of a structure represented with beam elements. This

figure would be referred to while explaining how results from some of the methods are interpreted. The discussions in this chapter assume a background knowledge of matrix algebra.

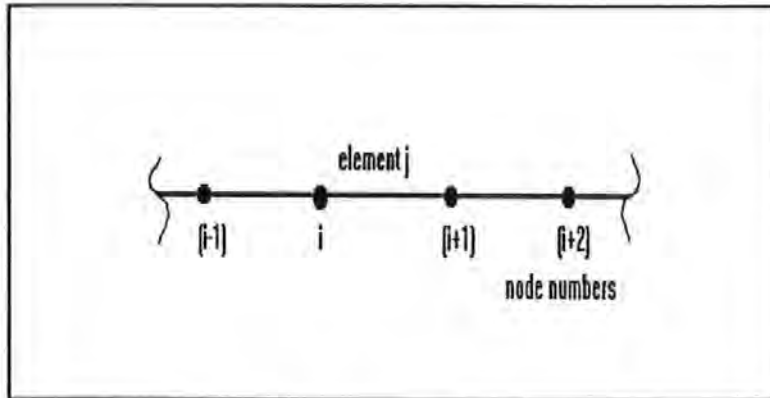


Figure 4.1 Section of a general structure

## 4.2 Methods Utilizing Modal Data

### 4.2.1 MAC, COMAC and MSV

The two most commonly used methods to compare two sets of vibration mode shapes are the Modal Assurance Criterion (MAC) and the Coordinate Modal Assurance Criterion (COMAC). The criteria are applicable to any two sets of vibration data - measured/measured, theoretical/theoretical and theoretical/measured. MAC indicates correlation between mode shapes while COMAC indicates the correlation between the mode shapes at a selected measurement point on the structure (Pandey et al, 1991). If the two sets of data are from the damaged and undamaged structures, MAC can be used to indicate the modes most sensitive to damage while COMAC could indicate possible damage locations. The MAC between the  $q$ th mode of the first data set  $A$  and the  $r$ th mode of the second data set  $B$  is defined as (Allemang and Brown, 1983):

$$MAC(\{\phi_A\}_q, \{\phi_B\}_r) = \frac{|\{\phi_A\}_q^T \{\phi_B\}_r|^2}{(\{\phi_A\}_q^T \{\phi_A\}_q \{\phi_B\}_r^T \{\phi_B\}_r)} \quad (4.1)$$

where  $\{\phi_A\}_q =$  mode shape vector for mode  $q$  of data set  $A$

$\{\phi_B\}_r =$  mode shape vector for mode  $r$  of data set  $B$

A MAC value close to 1 indicates that the two modes are well correlated while a value close to 0 is indicative of uncorrelated modes.

To compute the COMAC values, correlated modes from the two sets  $A$  and  $B$  are paired.

If  $i =$  measurement location,  $L =$  total number of correlated mode pairs and  $(\phi_A)_i =$  element of mode shape vector for set  $A$  in correlated mode pair 1, then the COMAC for measurement location  $i$  is defined as (Lieven and Ewins, 1988):

$$COMAC(i) = \frac{[\sum (\phi_A)_i (\phi_B)_i]^2}{\sum (\phi_A)_i^2 \sum (\phi_B)_i^2} \quad (4.2)$$

where the summation is from  $1 = 1$  to  $L$ . A COMAC value close to 1 indicates good correlation, at the selected location, between the two data sets.

A new function, called Modal Sensitivity Value (MSV), for identifying damage sensitive modes is proposed here. If  $(\phi_{Ar}) =$  element of the  $r$ th mode shape vector at measurement point  $i$  for data set  $A$  and  $\lambda_{Ar} =$  eigenvalue of mode  $r$  for data set  $A$ , MSV for mode  $r$  is defined as:

$$MSV(\{\phi_A\}_r, \{\phi_B\}_r) = \left| \frac{\frac{\sum (\phi_{Br})^2)^{0.5}}{\lambda_{Br}} - \frac{\sum (\phi_{Ar})^2)^{0.5}}{\lambda_{Ar}}}{\frac{\sum (\phi_{Ar})^2)^{0.5}}{\lambda_{Ar}}} \right| \quad (4.3)$$

where the summation is from 1 to n (number of measurement points).  $\{\sum(\phi_{Ar})^2\}^{0.5}$  is the Euclidean norm of the rth mode shape vector of data set A and represents the distance of the vector from the origin in  $\mathbf{R}^n$ .  $\mathbf{R}^n$  denotes the set of all n-dimensional column vectors with real number coefficients and  $\{\phi_A\}_r, \{\phi_B\}_r \in \mathbf{R}^n$ . Assuming data set B to be from the damaged structure, existence of damage will cause  $\{\sum(\phi_{Br})^2\}^{0.5}$  to be greater or less than  $\{\sum(\phi_{Ar})^2\}^{0.5}$ . Only the magnitude of the change is considered since damage identification is the sole intention. Since  $\{\sum(\phi_{Ar})^2\}^{0.5}$  is unchanged, occurrence of damage can be inferred from the magnitudes of MSV. The MSV for all modes (for a particular damage case) are normalised such that the mode showing least correlation, thus most affected by damage, has a MSV value of 100. In Equations (4.1) to (4.3), the modes have been assumed to be real.

#### 4.2.2 Eigenparameter method

The eigenparameter method uses the changes in the eigenvectors to locate damage in beam-like structures. It is based on the existence of a systematic change in the fundamental mode shape with respect to the damage location. The eigenparameter  $\{U\}_r$  for mode r is defined (Yuen, 1986) as the vector difference between the damaged and undamaged case of the mass orthonormalised eigenvector divided by the corresponding eigenvalue and is mathematically expressed as:

$$\{U\}_r = \left( \frac{\{\phi_D\}_r}{\lambda_{Dr}} - \frac{\{\phi_O\}_r}{\lambda_{Or}} \right) \times 10^6 \quad (4.4)$$

Where

$$\lambda_{Dr} = \text{rth eigenvalue of damaged structure}$$

$\lambda_{0r}$  = rth eigenvalue of undamaged structure

$\{\phi_D\}_r$  = rth eigenvector of damaged structure

$\{\phi_0\}_r$  = rth eigenvector of undamaged structure

The  $10^6$  factor is merely to increase the values of the elements of the eigenparameter vector since normalization by the eigenvalues could lead to very small values. Only the fundamental mode ( $r = 1$ ) is used since the higher modes require functions more complex than the eigenvalues for the eigenvector normalization (Yuen, 1985).

Characteristics of the plot of  $\{U\}_r$  against the measurement points are used to infer the damage position. For simply supported beams, change in slope of the plots will occur at the damage position while the magnitude of  $\{U\}_r$  will increase with increasing degree of damage. For cantilever beams, the value of  $\{U\}_r$  will be negligible for positions between the fixed end and the damage location. Beyond that,  $\{U\}_r$  is expected to exhibit a linear characteristic against the distance from the damage location. The slope of the linear portion increases with the severity of the damage. Figure 4.2 illustrates the characteristics of the eigenparameter plots for the case of damage in element  $j$  of Figure 4.1.

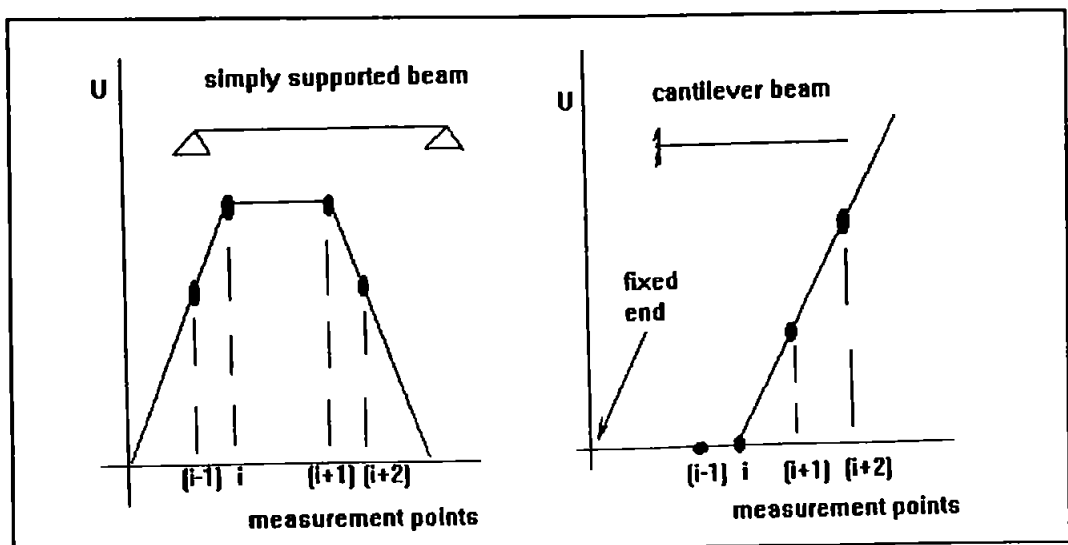


**Figure 4.2 Eigenparameter plots**

### 4.2.3 Curvature mode shape method

Existence of a crack or damage at any section of a structure reduces the stiffness (as represented by EI where E and I are respectively the modulus of elasticity and the second moment of the cross-sectional area) at the crack location. The reduction in EI leads to an increase in the magnitude of the curvature  $v''$  at the section as given by the relation  $v'' = M / (EI)$  where M is the bending moment at the section. Since the changes in the curvatures are local and depend on the extent of reduction in (EI), the curvature changes can be used to detect, locate and quantify damage. The absolute difference in the curvature mode shapes between the damaged and undamaged structure is expected to show a maximum at the damaged region. In addition, the maximum difference increases with increasing degree of reduction in the stiffness of the damaged zone (Pandey et al, 1991). The curvatures are computed from the displacement mode shapes using a central difference approximation (Pandey et al, 1991):

$$(v_{ir}'') = \frac{(\phi_{(i+1)r}) - 2(\phi_{ir}) + (\phi_{(i-1)r})}{h^2} \quad (4.5)$$

where h is the length of each beam element,  $(v_{ir}'')$  and  $(\phi_{ir})$  are respectively elements of the curvature and displacement mode shapes for mode r at measurement point i. In implementing the method, h was taken as the average of the lengths of the elements on either side of i while an element length was regarded as being the distance between two consecutive measurement points.

#### 4.2.4 Mode shape relative difference method

In this method, graphical comparison of displacement mode shapes is used to indicate the damage position. The parameter used is the relative difference  $\{RD\}$  between the scaled mode shapes and is defined as (Fox, 1992):

$$\{RD\}_r = \frac{\{\phi_{O'}\}_r - \{\phi_{D'}\}_r}{\{\phi_{O'}\}_r} \quad (4.6)$$

The method relies on the fact that the largest differences in mode shapes occur within the vicinity of the nodes. A plot of  $\{RD\}$  against the measurement positions would show a definite trend with distinct discontinuity at the defect position and significant peaks in the region of the nodes. The modes most affected by the damage are more likely to show the patterns sought for in the  $\{RD\}$  plots.

### 4.3 Methods Based on Model Updating Procedures

#### 4.3.1 Matrix cursor method

The matrix cursor method (Brown, 1988) is based on vector space theory and seeks to locate the error region by identifying all the degrees of freedom associated with the element in error. Much of the background vector space theory (Milne, 1980) has been omitted from this discussion. The case of stiffness error only (unchanged mass) is first considered. An approximation  $[\delta_s]$  to the stiffness error matrix  $[\Delta K]$  is defined as:

$$[\delta_s] = [K^H] - [K_O] \quad (4.7)$$

where  $[K_O]$  is the stiffness matrix of the undamaged structure and  $[K^H]$  is an 'hybrid' form of the stiffness matrix.  $[K^H]$  is given by (Brown, 1987):

$$[K^H] = [M_O] [\Psi_D] [\lambda_D] [\Psi_D]^T [M_O] - [K_O] [\Psi_D] [\Psi_D]^T [M_O] - [M_O] [\Psi_D] [\Psi_D]^T [K_O] + [K_O] + [M_O] [\Psi_D] [\Psi_D]^T [K_O] [\Psi_D] [\Psi_D]^T [M_O] \quad (4.8)$$

where  $[M_O]$  = mass matrix of undamaged structure  
 $[\Psi_D]$  = mode shape matrix of undamaged structure  
 $[\lambda_D]$  = eigenvalue matrix of damaged structure

Another approximation  $[\epsilon_s]$  to  $[\Delta K]$  can be defined as

$$[\epsilon_s] = [M_O] [\Psi_D] [\lambda_D] [\Psi_D]^T [M_O] - [M_O] [\Psi_D] [\Psi_D]^T [K_O] [\Psi_D] [\Psi_D]^T [M_O] \quad (4.9)$$

The best approximation  $[\alpha_s]$  to  $[\Delta K]$  will be an average of the two previous versions.

Thus,

$$[\alpha_s] = 0.5 ([\delta_s] + [\epsilon_s]) = 0.5 (2 [M_O] [\Psi_D] [\lambda_D] [\Psi_D]^T [M_O] - [M_O] [\Psi_D] [\Psi_D]^T [K_O] - [K_O] [\Psi_D] [\Psi_D]^T [M_O]) \quad (4.10)$$

Using vector space representation,  $[\alpha_s]$  can be defined as:

$$[\alpha_s] = 0.5 ([P]^T [\Delta K] + [\Delta K] [P]) \quad (4.11)$$

where  $[P]$  is a matrix projection operator expressed as:

$$[P] = [\Psi_D] ([\Psi_D]^T [M_O] [\Psi_D])^{-1} [\Psi_D]^T [M_O] \quad (4.12)$$

and

$$[P]^T = [M_O] [\Psi_D] ([\Psi_D]^T [M_O] [\Psi_D])^{-1} [\Psi_D]^T \quad (4.13)$$

For any zero row of  $[\Delta K]$ ,  $([\Delta K][P]) = 0$  since  $[0]^T [\Psi_D] [\Psi_D]^T [M_O] = [0]^T$  and for any zero column of  $[\Delta K]$ ,  $([P]^T [\Delta K]) = 0$  since  $[M_O] [\Psi_D] [\Psi_D]^T [0] = [0]$ . This implies that only non-zero values of  $[\Delta K]$  will contain non-zero values in the error identification matrix  $[\alpha_s]$ .

For the case of mass error only, the same procedure is applied to obtain

$$[\alpha_M] = 0.5 (-2 [M_O] [\Psi_D] [\lambda_D] [\Psi_D]^T [M_O] + [K_D] [\Psi_D] [\Psi_D]^T [M_O] + [M_O] [\Psi_D] [\Psi_D]^T [K_O]) \quad (4.14)$$

where  $[\alpha_M]$  is the mass error matrix. Comparison of Equations (4.10) and (4.14) shows that  $[\alpha_s] = -[\alpha_M]$ . Therefore, a general expression for the error location matrix, which identifies either mass or stiffness (or both) errors, can be established. Equation (4.10) will be taken as this expression. In order to use this method, it is necessary to compute the system

matrices ( $[K_o]$ ,  $[M_o]$  and  $[K_D]$ ) from the measured data. The system identification method adopted is described in sub-section 4.3.2.

In practice, the rows and columns (of the identification matrix) associated with the error will contain elements whose values are much greater than other elements in the matrix. The process is illustrated by using the structure in Figure 4.1. Assuming damage in element  $j$ , the matrix cursors are shown in Figure 4.3. The damage location is identified by the coordinates corresponding to elements on the leading diagonal with comparatively large values. In general, there will be  $u$  error locations ( $u \geq 2$ ) leading to  $u^2$  intersections with  $(u^2 - u)$  of them not on the leading diagonal. If the matrix in Figure 4.3 is represented by a three-dimensional histogram, the height of the bars corresponding to the damage positions will have the highest values.

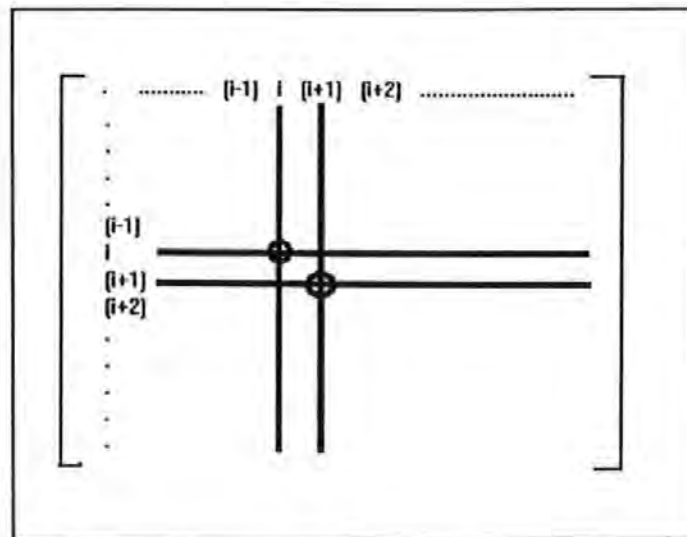


Figure 4.3 Matrix cursor example

### 4.3.2 Identification of system matrices

The equation of motion for a multi-degree of freedom system in the physical space is given by Equation (3.1). A number of methods exists for estimating the system matrices ( $[M]$ ,  $[C]$  and  $[K]$ ) from measured vibration data. These methods are either direct (using the measured FRF directly) or indirect (using modal parameters obtained from curve-fitting the FRF). The method implemented here is an indirect method and computes the system matrices using the orthogonality properties of vibrating systems. The technique (Luk, 1987) is applicable to general systems - both complete ( $n = m$ ) and truncated ( $n > m$ ) where  $n$  and  $m$  are respectively the number of measured degrees of freedom (DOF) and modes. The experimental DOF of a physical structure can be defined by the direction and location at which the measurement transducers for acquiring data are attached. A truncated system is usually obtained from experimental testing since the structure will typically have an almost infinite number of DOF and vibration modes and only a few of these can be measured.

By assuming proportional damping and using the transformation  $\{X\} = [\Psi]\{\phi\}$ , Equation (3.1) can be decoupled to yield

$$[m]\{\phi''\} + [c]\{\phi'\} + [k]\{\phi\} = [\Psi]^T\{F(t)\} \quad (4.15)$$

where

$$\begin{aligned} [c] &= [\Psi]^T [C] [\Psi] \\ [k] &= [\Psi]^T [K] [\Psi] \\ [m] &= [\Psi]^T [M] [\Psi] \end{aligned}$$

(4.16)

$[c]$ ,  $[k]$  and  $[m]$  are the diagonal modal viscous damping, mass and stiffness matrices, respectively, obtained during modal parameter extraction while  $\{\phi\}$ ,  $\{\dot{\phi}'\}$  and  $\{\ddot{\phi}''\}$  are, respectively, the normal displacement (mode shape), velocity and acceleration vectors.  $[\Psi]$  is the mode shape matrix.

For a complete system, the physical matrices can be obtained from Equation (4.16) by pre- and post-multiplying by the appropriate inverses to get

$$\begin{aligned} [C] &= ([\Psi]^T)^{-1} [c] [\Psi]^{-1} \\ [K] &= ([\Psi]^T)^{-1} [k] [\Psi]^{-1} \\ [M] &= ([\Psi]^T)^{-1} [m] [\Psi]^{-1} \end{aligned}$$

(4.17)

All the matrices in Equation (4.17) are of order  $n \times n$ . However, the data obtained from experimental testing usually describe a truncated system. A truncated system leads to a non-square modal matrix  $[\Psi]$  thereby making the ordinary matrix inverse inapplicable. A special type of inverse, called pseudo-inverse, is necessary. The pseudo-inverse is a generalised inverse that can deal with a non-square or a square but singular matrix. By using the pseudo-inverses, Equation (4.18) can be written (for a general system) as:

$$\begin{aligned} [C] &= ([\Psi]^T)^+ [c] [\Psi]^+ \\ [K] &= ([\Psi]^T)^+ [k] [\Psi]^+ \\ [M] &= ([\Psi]^T)^+ [m] [\Psi]^+ \end{aligned}$$

(4.18)

In Equation (4.18),  $[C]$ ,  $[K]$  and  $[M]$  are of order  $n \times n$ ,  $[c]$ ,  $[k]$  and  $[m]$  are of order  $m \times m$ ,  $[\Psi]$  is of order  $n \times m$  and  $^+$  denotes a pseudo-inverse.

### 4.3.3 Stiffness error matrix method

The basic formulation for the stiffness error matrix between the undamaged  $[K_0]$  and damaged  $[K_D]$  structures is  $[\Delta K] = [K_D] - [K_0]$ . The error location can be identified as those degrees of freedom (DOF) corresponding to non-zero elements of  $[\Delta K]$  since all other DOF not affected by the damage will have zero stiffness changes. In reality, the elements of  $[\Delta K]$  corresponding to the damage location should have much larger values as compared to the others. The simplest way to evaluate  $[\Delta K]$  would be by obtaining the matrices  $[K_0]$  and  $[K_D]$  using a method such as that described in the last sub-section. However, this direct approach leads to poor damage identification (Salawu and Williams, 1993; Park et al, 1988). To improve the sensitivity of  $[\Delta K]$  to stiffness errors, many modified versions of the direct approach have been suggested. The version implemented here was proposed by Lieven and Ewins (1990) and uses the pseudo-flexibility matrix  $[K^+]^{-1}$  defined as follows:

$$[K^+]^{-1} = [\Psi] [\lambda]^{-1} [\Psi]^T \quad (4.19)$$

where  $[K^+]$ ,  $[\Psi]$  and  $[\lambda]$  are respectively the pseudo-stiffness, mode shape and eigenvalue matrices.  $[K^+]$  is then obtained by finding the psuedo-inverse of  $[K^+]^{-1}$  using Singular Value Decomposition (SVD). Thus,

$$[K^+] = [ [K^+]^{-1} ]^{-1} \quad (4.20)$$

Substituting Equations (4.19) and (4.20) in the expression for  $[\Delta K]$  yields:

$$[\Delta K] = ([\Psi_D] [\lambda_D]^{-1} [\Psi_D]^T)^{-1} - ([\Psi_O] [\lambda_O]^{-1} [\Psi_O]^T)^{-1} \quad (4.21)$$

where the subscripts D and O respectively refer to the damaged and undamaged structures.

#### 4.4 Cantilever Beam

Figure 4.4 shows the cantilever beam model used to generate the theoretical data. The beam was modelled with six 0.5m uniform beam elements. Each node has two translational DOF in the X and Y directions. Values of the geometrical and material properties used are shown in the figure. An eigenvalue analysis was conducted to determine the natural frequencies and mode shapes of the first six bending modes. Since flexural modes were considered, only displacements in the Y direction were used in evaluating the methods.

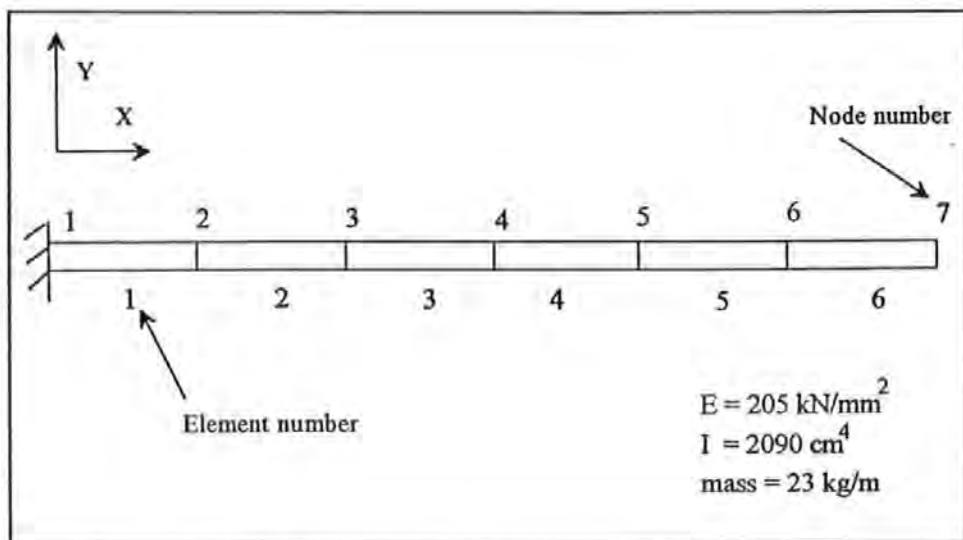


Figure 4.4 Cantilever beam model

#### 4.4.1 Damage simulation

Damage was simulated by reducing the modulus of elasticity  $E$  for selected elements. The degree of damage is proportional to the extent of reduction. As characteristics of each mode of vibration would be affected only by modifications to the stiffness of the relevant degrees of freedom, the introduction of a reduced modulus of elasticity as the damage representation could be interpreted as equivalent to a biased reduction in the values of the elements of the stiffness matrix for the relevant DOF (Yuen, 1985). This implies that only damage affecting the structural stiffness was considered. This is a convenient way of modelling damage since minor modifications to the analysis input file are necessary. The damage representation simulates practical vibration monitoring problems in which the location and size of the damage are both unknown, thereby making detailed theoretical modelling of damage unjustifiable.

The damage cases considered were:

- |        |   |  |
|--------|---|--|
| Case 1 | = | No damage  |
| Case 2 | = | 50% reduction in global $E$                                    |
| Case 3 | = | 50% reduction in $E$ of element 3                              |
| Case 4 | = | 50% reduction in $E$ of elements 3 and 5                       |
| Case 5 | = | 80% and 50% reduction in $E$ of elements 3 and 5 respectively. |

Damage case 2 was meant to test the ability of the methods in detecting damage that affects the whole structure in more or less a uniform manner. Previous researchers have ignored this important case. Case 3 is the damage situation usually studied and represents damage at a single location. Cases 4 and 5 were designed to investigate possibility of detecting multiple damage locations. For each damage case, the eigenvalues and

eigenvectors of the beam were calculated for the first six modes. The calculated modal parameters were used to synthesize FRFs at each node.

#### **4.4.2 Results from the analysis**

Table 4.1 shows the natural frequencies for the six modes. It can be seen (from the table) that damage case 2 has the largest frequency reduction for all modes. The magnitude of the change (as a percentage of the undamaged frequencies) for case 2 is the same for all modes due to the nature of the damage. For each mode, the severity of the damage (as measured by the reduction in frequency) decreases according to the progression case 2 → case 5 → case 4 → case 3. This is as expected. The magnitudes of the frequency reduction show that the simulated damage cases are severe.

### **4.5 Experimental Steel Beam**

#### **4.5.1 Experimental arrangement**

The experimental set-up for the beam tests is shown in Figure 4.5. The test beam was an I-section (UB 203 x 102 x 23 kg/m) steel beam. The beam was excited by an electromagnetic vibrator while the dynamic response in the vertical direction was measured at eight locations using accelerometers. The instrumentation used and data processing techniques adopted are described in chapter six. A periodic random signal was used as the excitation signal. The tests were conducted within the frequency range 0 - 250 Hz which was sufficient to cover the first three bending modes. An HP9122 computer was used to control the test and acquire FRF data via an HP3582A dual channel spectrum analyzer. The FRFs were subsequently transferred to an OPUS PCSX 386SX computer for further

analysis.

**Table 4.1 Natural frequencies of the cantilever beam**

Mode number	Frequency (Hz)				
	Case 1	Case 2	Case 3	Case 4	Case 5
1	26.405	18.671 (-29.3)*	24.781 (-6.2)	24.676 (-6.5)	21.160 (-19.9)
2	151.668	107.246 (-29.3)	137.876 (-9.1)	132.062 (-12.9)	114.226 (-24.7)
3	380.022	268.716 (-29.3)	360.371 (-5.2)	325.786 (-14.3)	293.862 (-22.7)
4	654.857	463.054 (-29.3)	614.795 (-6.1)	566.314 (-13.5)	493.911 (-24.58)
5	938.683	663.749 (-29.3)	879.969 (-6.3)	812.043 (-13.5)	770.522 (-17.9)
6	1165.42	824.079 (-29.3)	1086.30 (-6.8)	977.582 (-16.1)	872.741 (-25.1)

\* % change in frequency from case 1

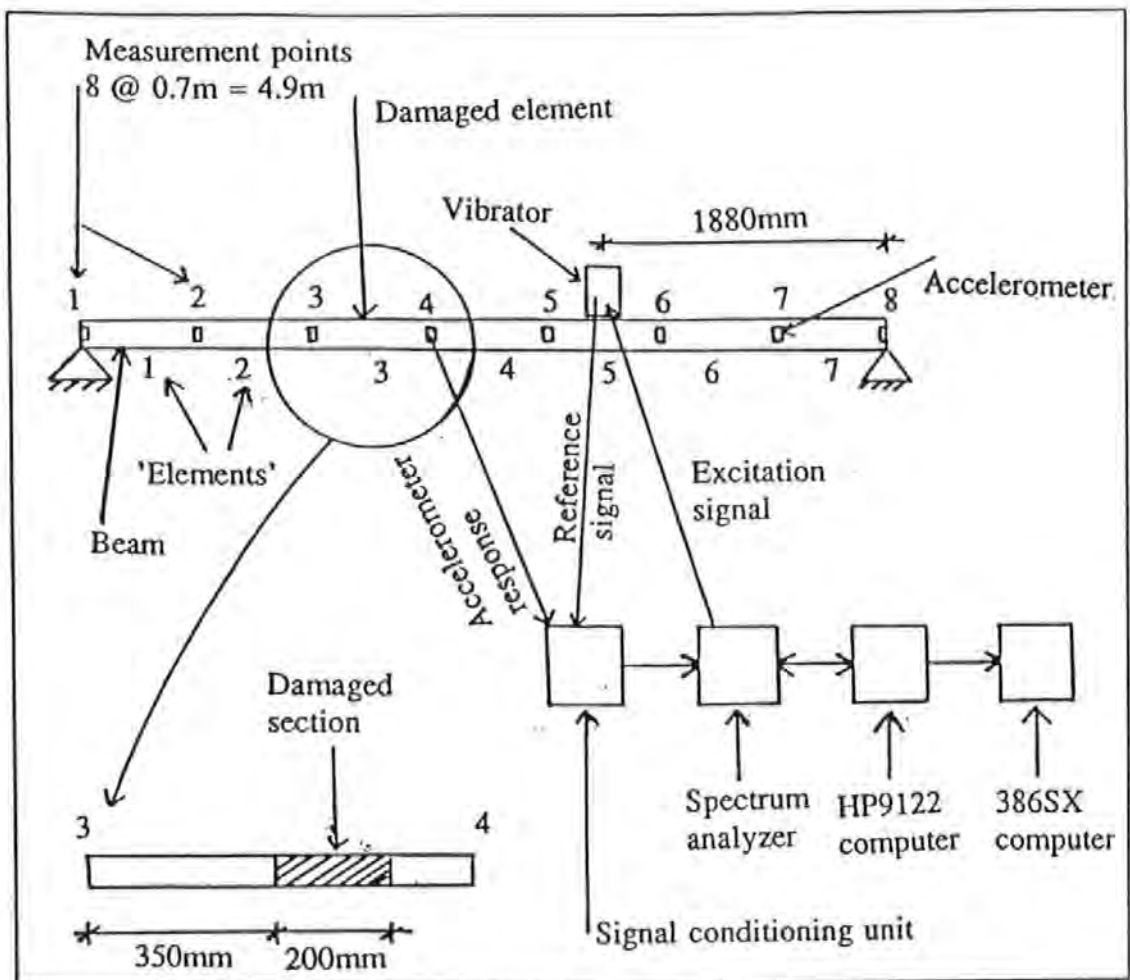


**Figure 4.5 Experimental arrangement for beam tests**

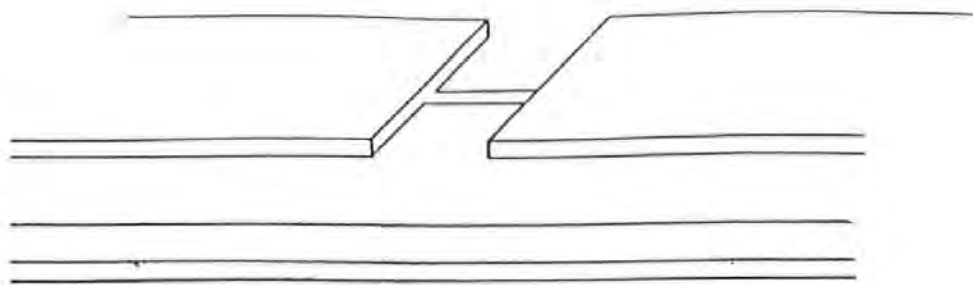
#### 4.5.2 Damage cases

The damaged section is shown in Figure 4.5 while sketches of the damage cases are shown in Figure 4.6. Four damage cases were considered. These were:

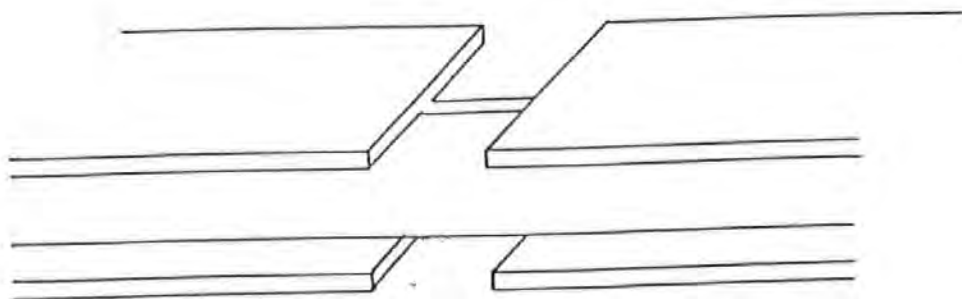
- Case I = Undamaged beam
- Case II = Removal of top flange at the damage location
- Case III = Case II plus removal of bottom flange at the damage location
- Case IV = Case III plus removal of half web at the damage location

The damage cases were selected so that the effects of relatively mild (case II) and severe (cases III and IV) damage could be investigated. One other factor was the need for the

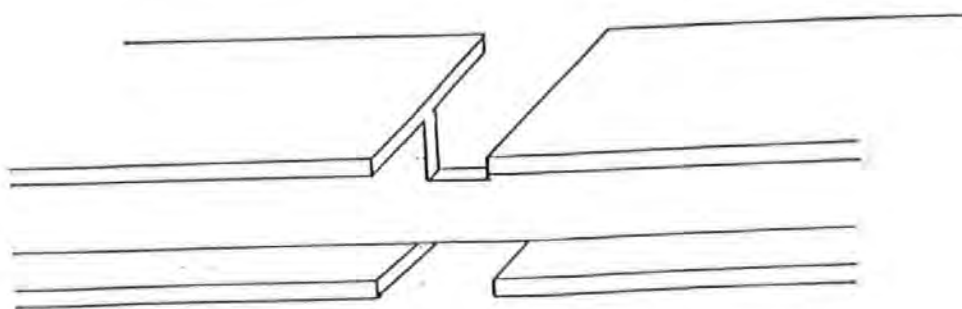
damage site to have small participation (i.e. close to a node) in at least one of the measured modes. This was meant to give an indication of the effects of damage location on the sensitivity (to damage) of the modes. Thus, the damage site was located close to a node of mode 3.



Damage case II



Damage case III



Damage case IV

**Figure 4.6 Diagramatic representation of induced damage - steel beam**

### 4.5.3 Test results

The natural frequencies and viscous damping ratios obtained from the tests are shown in Tables 4.2 and 4.3. There is a reduction in frequency with increasing level of damage except for mode 3 (cases II and III). Using the natural frequency changes alone, it would appear that modes 1 and 2 are more affected by the damage. The pattern of the frequency changes suggests that the damage is close to positions of maximum displacement of modes 1 and 2 but near a node of mode 3. This observation can be useful for preliminary damage site identification.

**Table 4.2 Natural frequencies obtained from beam tests**

Mode number	Frequency (Hz) for Damage Case ....			
	Case I	Case II	Case III	Case IV
1	22.98	22.53 (-2.0)*	20.42 (-11.14)	15.12 (-34.20)
2	94.49	90.47 (-4.3)	88.62 (-6.2)	74.14 (-21.5)
3	207.8	208.83 (0.5)	208.67 (0.4)	194.75 (-6.3)

\* % change from case I

The damping values increase with increasing degree of damage. The only exception is in mode 2 where the values decrease after an initial increase. Trends similar to those observed were reported by Baldwin et al (1978), Salane and Baldwin (1990) and Salane et al (1987). The mode shapes are shown in Figure 4.7. The differences in the mode

shape amplitudes indicate existence of damage. The damage location can be inferred from mode 2 where the nodal point has changed and the largest differences exist at measurement point 3 (closest to damage site). The modal amplitudes increase with increasing level of damage but, suprisingly, modal amplitude values from the undamaged structure are generally larger than those from the damaged structure.

**Table 4.3 Viscous damping ratios from beam tests**

Mode number	Viscous damping ratio			
	Damage Cases			
	Case I	Case II	Case III	Case IV
1	0.00480	0.00696	0.00721	0.00923
2	0.00417	0.00777	0.00702	0.00600
3	0.00575	0.00625	0.00879	0.01040

#### 4.6 Performance of the Methods

##### 4.6.1 Methods based on modal data

###### 4.6.1.1 Cantilever beam

Table 4.4 shows elements on the leading diagonal of the MAC matrix and MSV values for the different damage cases. A MAC value of 1.0 indicates good correlation (which implies no damage present) between the damaged and undamaged mode shapes for the modes concerned. For case 2 with the largest amount of damage, the MAC values for all modes are 1.0. MAC is unable to indicate the presence of damage in case 2 because, due to the nature of the simulated damage, the mode shapes are identical. However, MSV values of 100 for all modes in case 2 correctly indicate that damage is present and all modes are equally sensitive to the damage type. For cases 3 to 5, only modes 5 and 6 (and mode 4

for cases 4 and 5) have MAC values significantly less than 1.0.

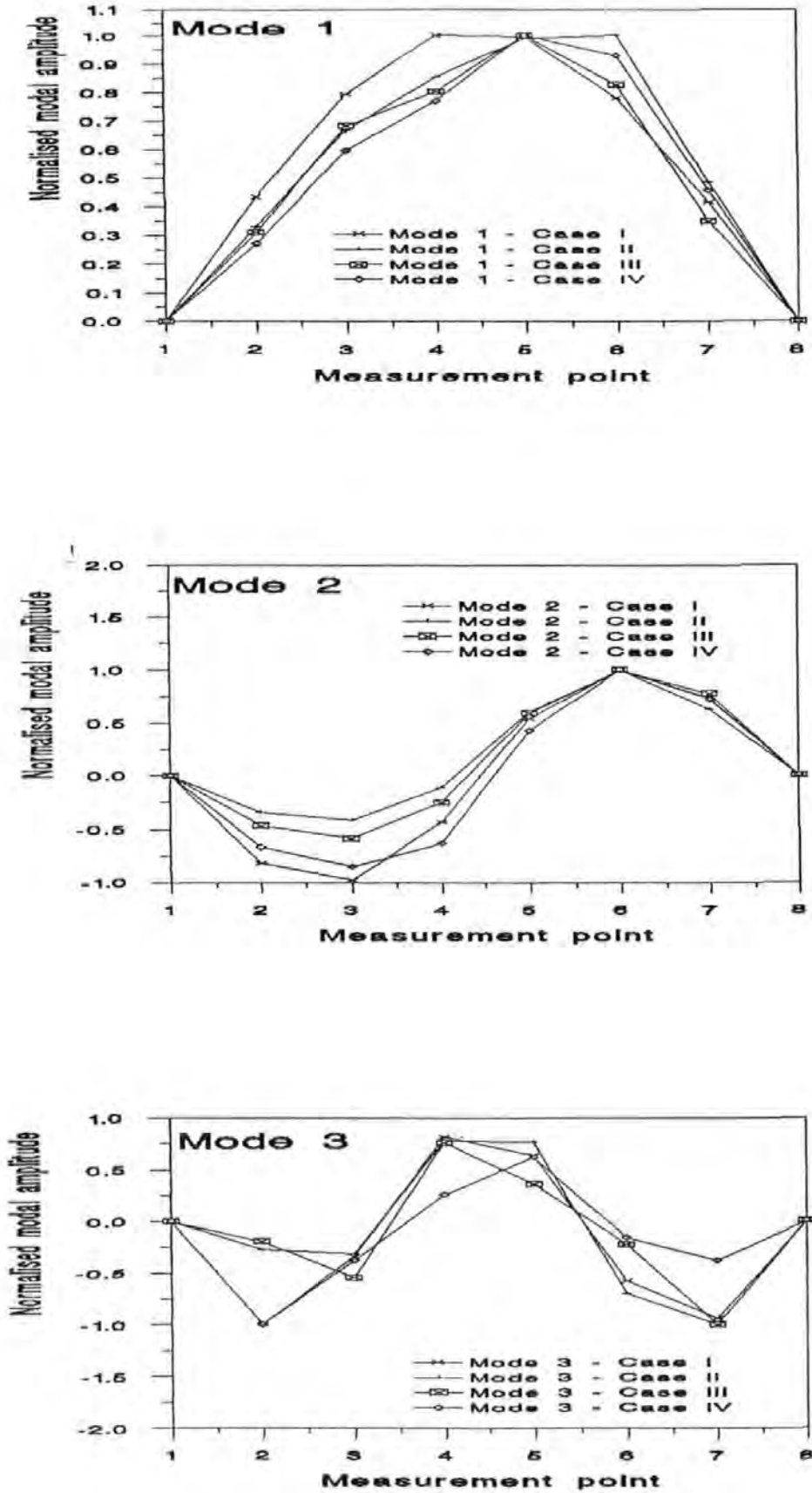


Figure 4.7 Mode shapes for steel beam

**Table 4.4 MAC and MSV for the cantilever beam\***

Mode	Case 2		Case 3		Case 4		Case 5	
	MAC	MSV	MAC	MSV	MAC	MSV	MAC	MSV
1	1.0	100	1.0	63.05	1.0	45.29	1.00	72.41
2	1.0	100	1.0	72.60	1.0	87.10	0.99	79.35
3	1.0	100	0.99	46.12	0.99	100.0	0.98	77.71
4	1.0	100	0.99	72.01	0.96	92.98	0.90	98.09
5	1.0	100	0.94	25.12	0.94	85.24	0.94	36.35
6	1.0	100	0.95	100.0	0.96	94.79	0.95	100.0

\* Case 1 as reference

The MSV values show varying degrees of sensitivity to damage (cases 3 - 5) by the modes. The effectiveness of MSV in suggesting damage sensitive modes is compared against that of natural frequency changes in Figure 4.8. In the figure, the magnitudes of natural frequency reductions (see Table 4.1) have been normalised such that the largest reduction has a value of 100. This allows easy comparison with MSV values. Apart from case 2, Figure 4.8 shows that the two parameters indicate slightly different modes as being most sensitive to damage. This might be expected since MSV uses mode shape data in addition to frequency values and would therefore indicate modes that are sensitive to both global and local damage. The results have shown MSV to be a useful indicator of sensitive modes and performing better than MAC as regards damage detection.

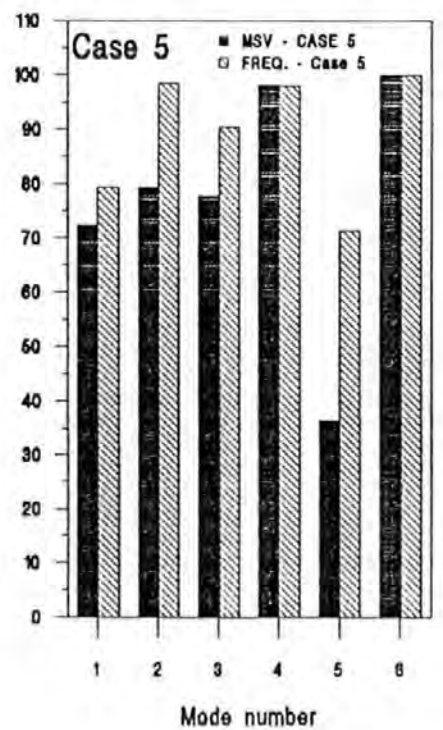
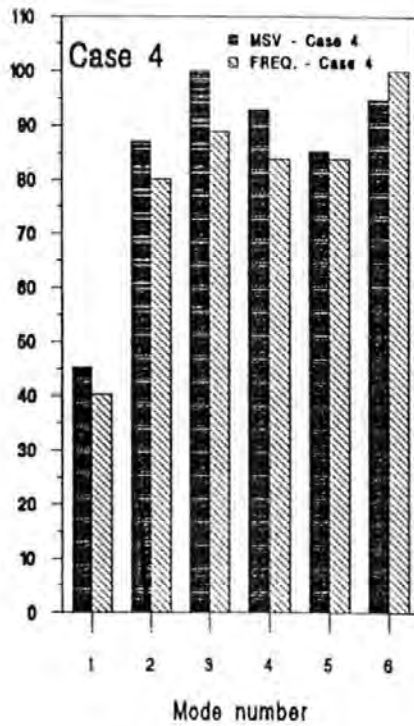
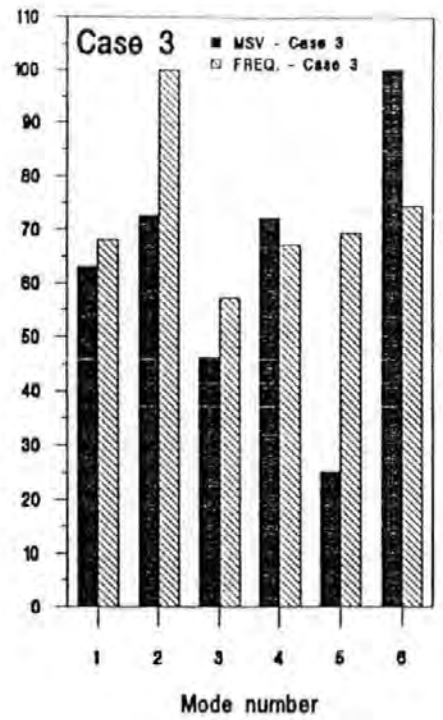
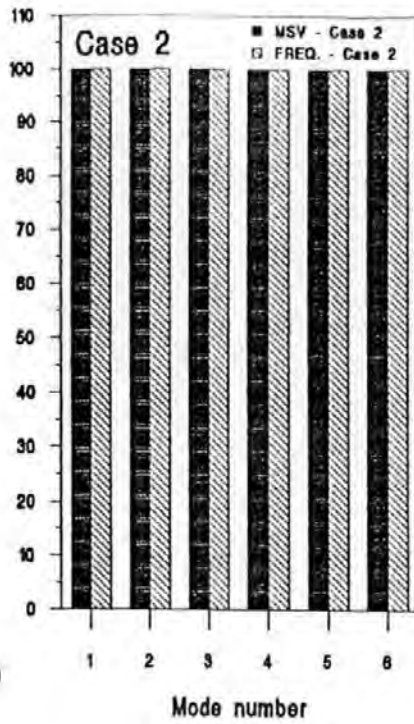


**Figure 4.8 Identification of sensitive modes using MSV and frequency changes - cantilever beam**

MAC, MSV and frequency changes can only detect damage. The other methods described in section 4.2 will be used for damage location. Table 4.5 shows COMAC values for the cantilever beam. The larger the difference of a COMAC value from unity, the more the possibility of the corresponding point being a damage site. COMAC values are unable to detect damage case 2 since the damage is not limited to a portion of the beam. For cases 3 - 5, the COMAC values are much lower than 1 but it is difficult to identify the damaged area from the information. The damage cases have been described in sub-section 4.4.1.

**Table 4.5 COMAC values for the cantilever beam\***

Node number	COMAC for Damage Case ....			
	Case 2	Case 3	Case 4	Case 5
1	1.00	1.00	1.00	1.00
2	1.00	0.05	0.96	0.49
3	1.00	0.14	0.88	0.32
4	1.00	0.62	0.73	0.14
5	1.00	0.26	0.41	0.00
6	1.00	0.01	0.10	0.05
7	1.00	0.09	0.30	0.10

\* Case 1 as reference

The eigenparameter plots for the damage cases are shown in Figure 4.9. If no damage is present, the eigenparameter plot should be flat as shown by the plot for case 1. Existence of damage in case 2 is detected while the damage in element 3 (between nodes 3 and 4)

is correctly identified for cases 3 - 5. However, element 5, also damaged in cases 4 and 5, is not identified. The method has therefore been unable to identify multiple damage locations. The slope of the plot is expected to increase with the severity of damage. This is demonstrated in Figure 4.9 with the plot for case 5 having a steeper slope than those for cases 3 and 4. The difference in the degree of damage between cases 3 and 4 is not revealed while case 5 is shown to be, incorrectly, slightly more severe than case 2.

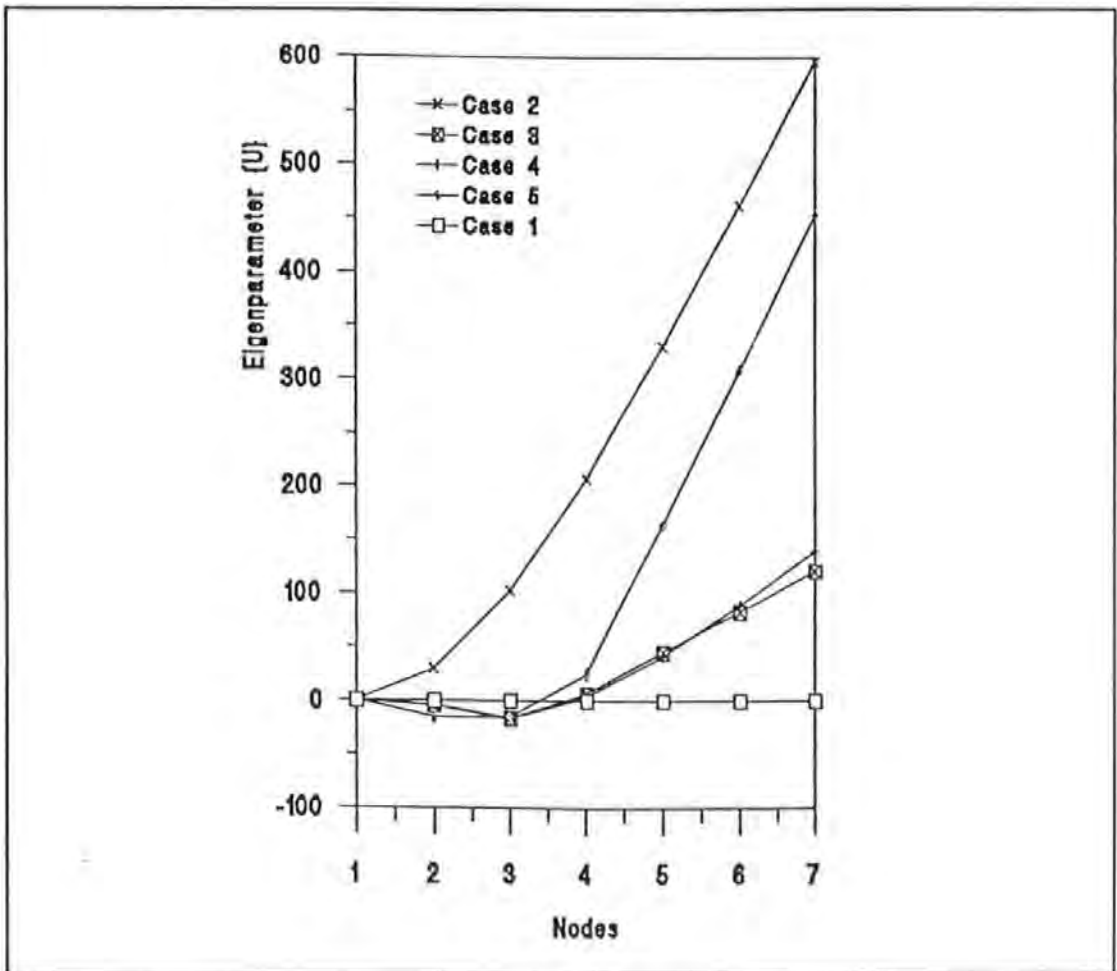


Figure 4.9 Eigenparameter plots for all damage cases - cantilever beam

Plots of absolute difference in curvature mode shapes is shown in Figure 4.10. The damage in element 3 is indicated by all modes though the location is not distinct for mode 6. Only modes 3 and 5 clearly indicate existence of damage in element 5. As for the degree of damage, only modes 1, 5 and 6 show the difference in the severity of the damage cases. None of the modes show existence of damage case 2.

Damage case 2 was also not identified by the relative difference in mode shape plots (Figure 4.11). The distinct discontinuity expected at the damage location is obvious (damage in element 3) for modes 1, 3, 4 and 5. Damage in element 5 (multiple damage locations) was not identified. The plots in Figure 4.10 and 4.11 further demonstrate the fact that sensitivity of a particular mode depends on the damage type and that identification of the appropriate modes could be crucial for successful damage location.

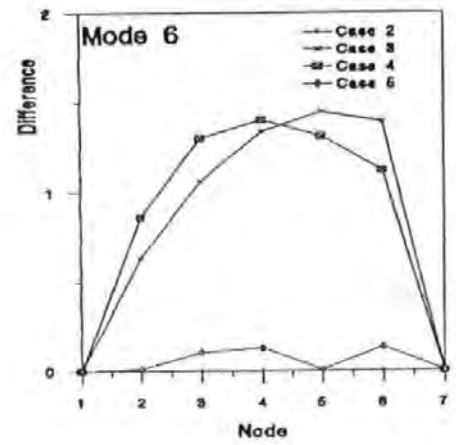
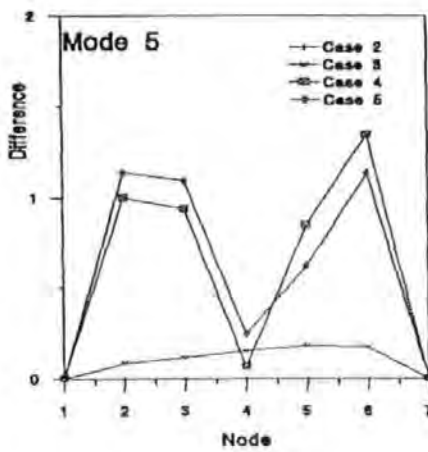
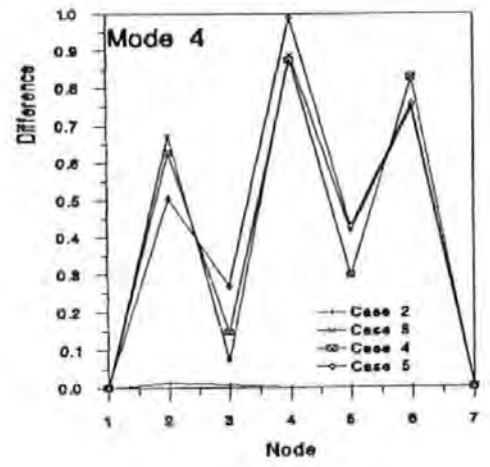
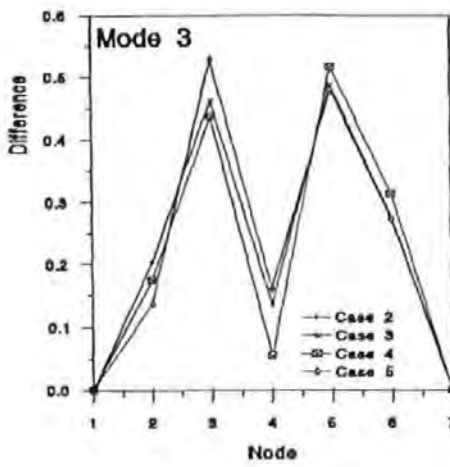
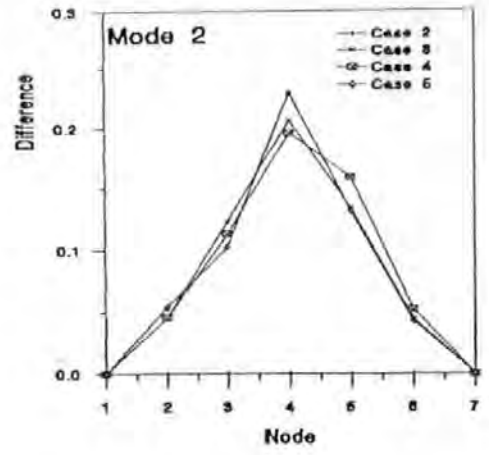
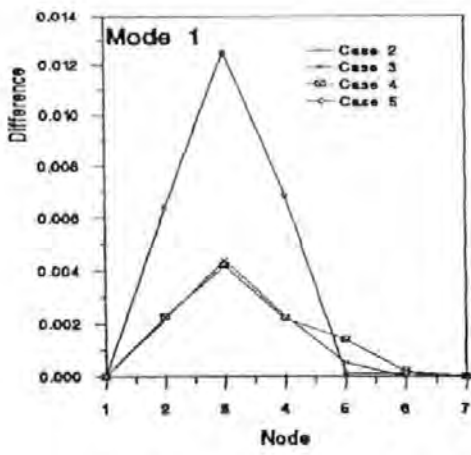
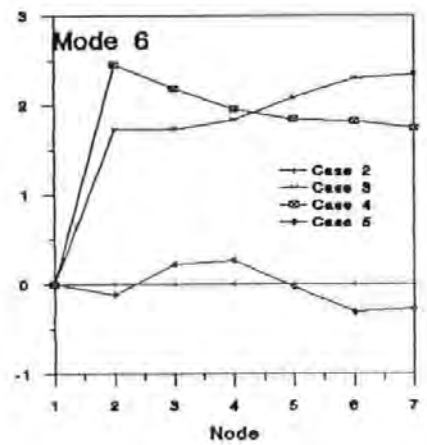
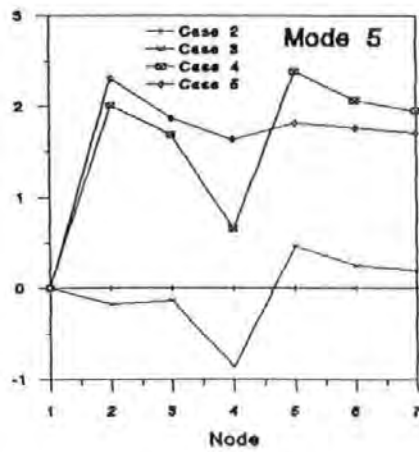
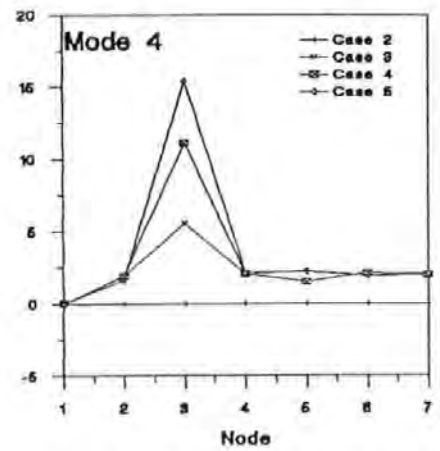
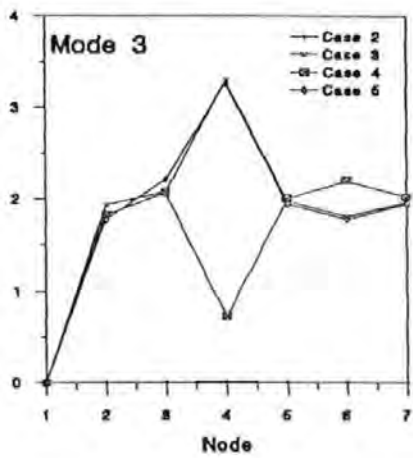
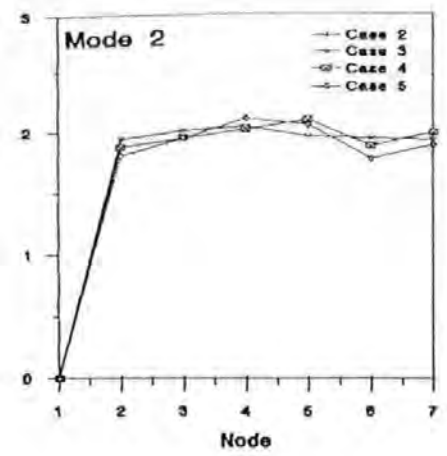
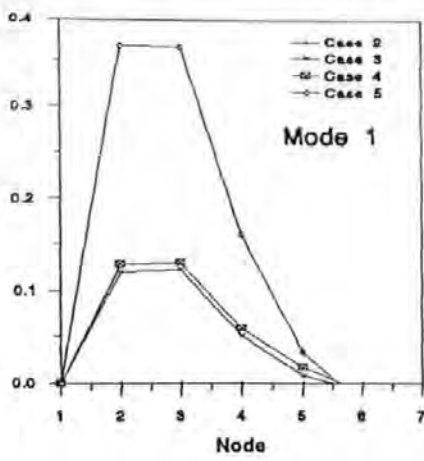


Figure 4.10 Absolute difference in curvature mode shapes - cantilever beam



**Figure 4.11** Plots of relative difference in displacement mode shapes - cantilever beam

#### 4.6.1.2 Steel beam

Elements on the leading diagonal of the MAC matrix and MSV values for the steel beam are shown in Table 4.6. Both MAC and MSV indicate existence of damage in all cases (damage cases described in sub-section 4.5.2). The relative sensitivity of the modes to damage as suggested by both criteria is similar. It is interesting to note that although the frequency reductions (Table 4.2) for mode 3 are the least, the mode has been indicated by MAC and MSV as being the most sensitive for cases III and IV. This is due to the poor correlation of mode shapes (Figure 4.7) for this mode. COMAC values are shown in Table 4.7 with those corresponding to the affected points underlined. Existence of damage in element 3 is indicated especially for cases II and IV.

Figure 4.12 shows the displacement eigenparameter curves. The curves correctly show that the damage is located around point 3 and that case IV is the most severe. However, the difference between the extent of damage in cases II and III could not be indicated. The absolute difference in curvature mode shapes are shown in Figure 4.13. Only mode 1 (damage cases II and IV) correctly indicates the damage location. Evidence of any difference in the severity of the damage cases can not be seen in the plots. Relative difference in displacement mode shapes are shown in Figure 4.14. The distinct discontinuity expected at the damage location is only evident in mode 2 - but at element 5. The other modes do not show any discernible trend that can be used to locate the damage.

**Table 4.6 MAC and MSV for steel beam\***

Mode	Case II		Case III		Case IV	
	MAC	MSV	MAC	MSV	MAC	MSV
1	0.97	3.20	0.99	14.12	0.96	56.23
2	0.85	100.0	0.93	55.98	0.98	50.80
3	0.83	44.20	0.74	100.0	0.79	100.0

\* Case I as reference

**Table 4.7 COMAC values for steel beam\***

Measurement location	COMAC		
	Case II	Case III	Case IV
1	1.00	1.00	1.00
2	0.92	0.99	0.83
3	<u>0.89</u>	<u>0.97</u>	<u>0.90</u>
4	<u>0.92</u>	<u>0.99</u>	<u>0.80</u>
5	1.00	1.00	1.00
6	0.99	1.00	0.99
7	0.98	0.99	0.98
8	1.00	1.00	1.00

\* Case I as reference

The geometrical symmetry of the beam (elements 3 and 5 are symmetrical) probably affected the results from both the curvature mode shape and relative difference in mode shapes method. This would explain why element 5 (for example, curvature mode shape method: damage case IV, modes 2 and 3; see Figure 4.13) was identified in some cases. On the whole, the performance of the two methods is unsatisfactory when compared to results obtained from the cantilever beam.

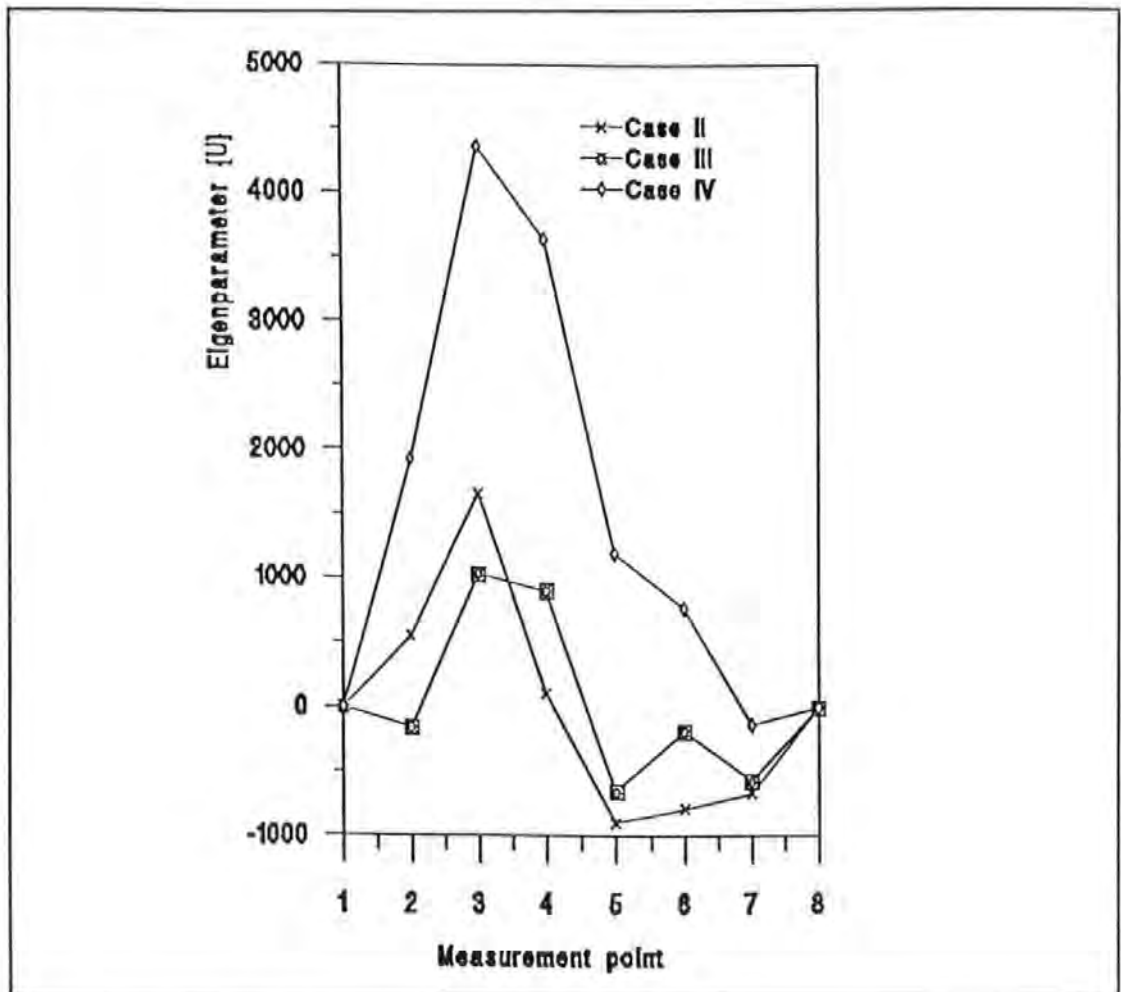


Figure 4.12 Displacement eigenparameter plot for steel beam

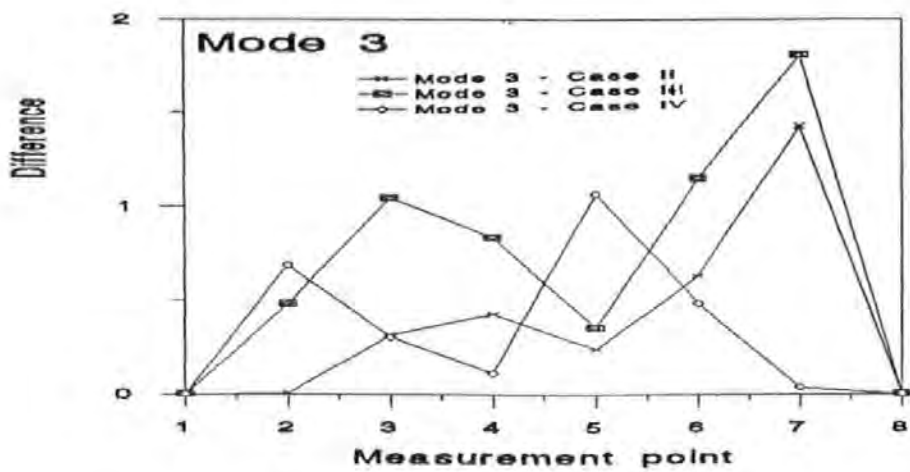
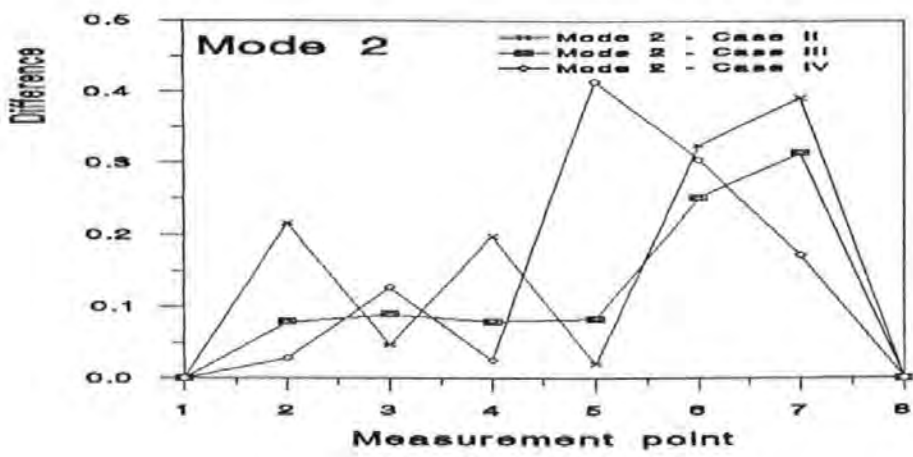
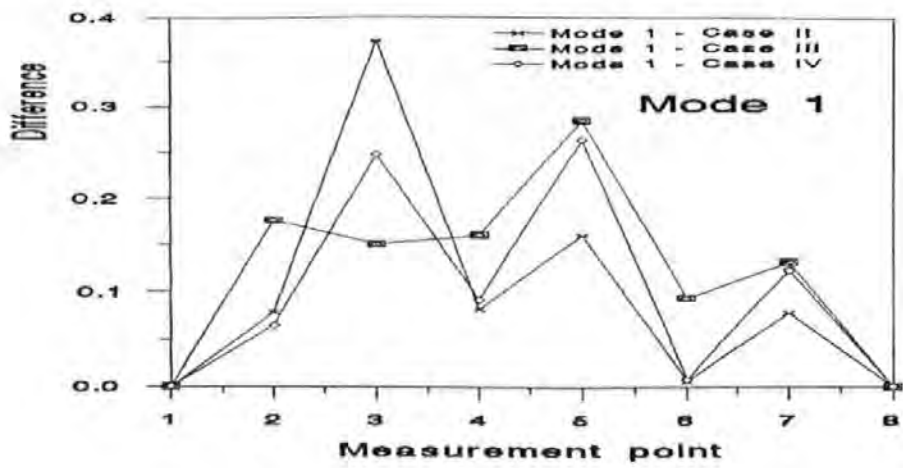


Figure 4.13 Absolute difference in curvature mode shapes - steel beam

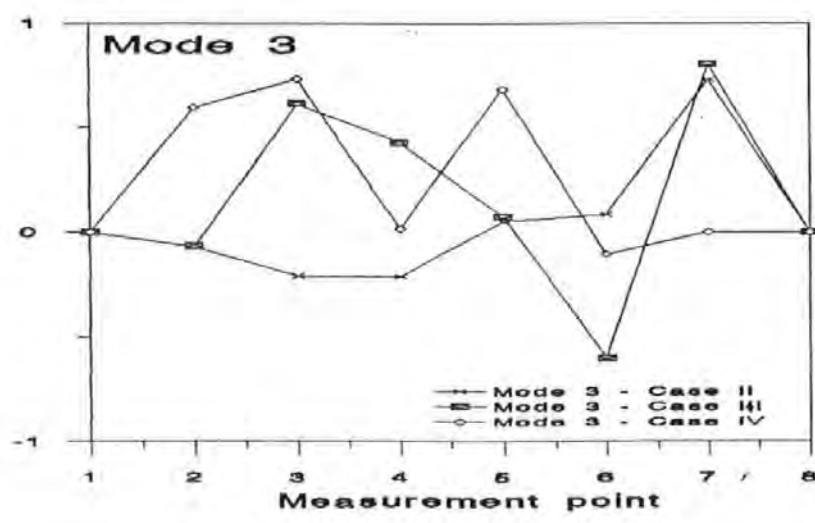
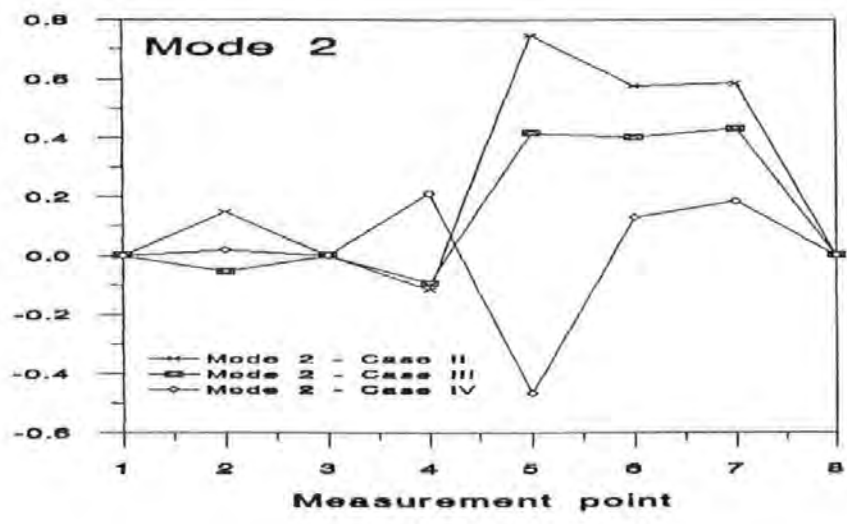
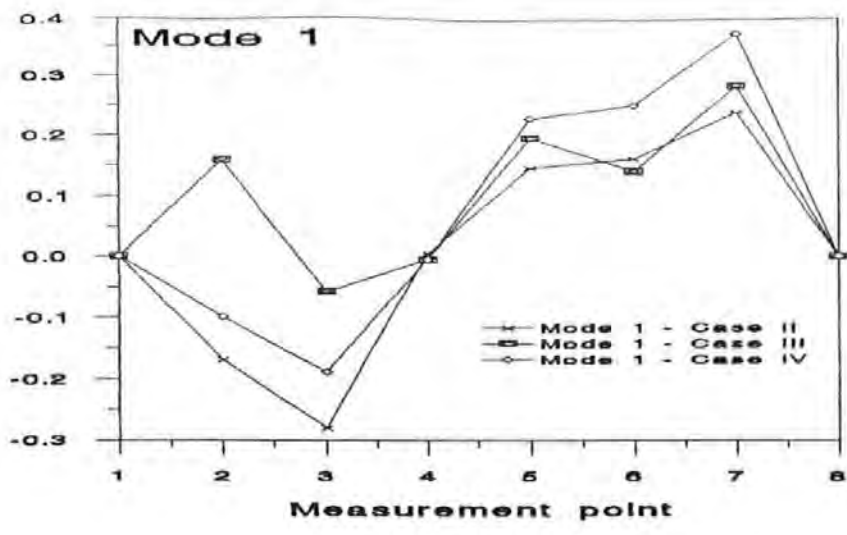


Figure 4.14 Relative difference in displacement mode shapes - steel beam

#### 4.6.2 Model updating methods

The system matrices identified using Equation (4.18) will depend on the particular FRF (hence measurement point) from which the diagonal modal matrices  $[c]$ ,  $[k]$  and  $[m]$  were obtained. Previous studies (Salawu and Williams, 1993) have shown that if the identified system matrices are merely to be used in obtaining the error matrix, it is only necessary to use the FRFs at the same point for different damage cases. Thus, points 2 and 4 were respectively used for the cantilever and steel beams. For the cantilever beam, a unit force was assumed to be applied at point 2.

To demonstrate ability of the system identification method to reproduce measured parameters, the original FRF at point 5 (undamaged cantilever beam) was compared with that regenerated using the identified matrices. This comparison is shown in Figure 4.15. As mentioned earlier, the regenerated curve at point 5 in Figure 4.15 was obtained using modal parameters from point 2. The high degree of correlation of the curves shows the ability of the method to correctly reproduce measured (simulated in this case) data.

In computing the damage identification matrices, the physical connectivity of the measurement points was enforced. For example, since point  $i$  in Figure 4.1 can only be physically connected to points  $(i-1)$  and  $(i+1)$ , all entries in column  $i$  and row  $i$  for other points - 1 to  $(i-2)$  and  $(i+2)$  to  $n$  ( $n$  = total number of points) - were ascribed the minimum value in the matrices.

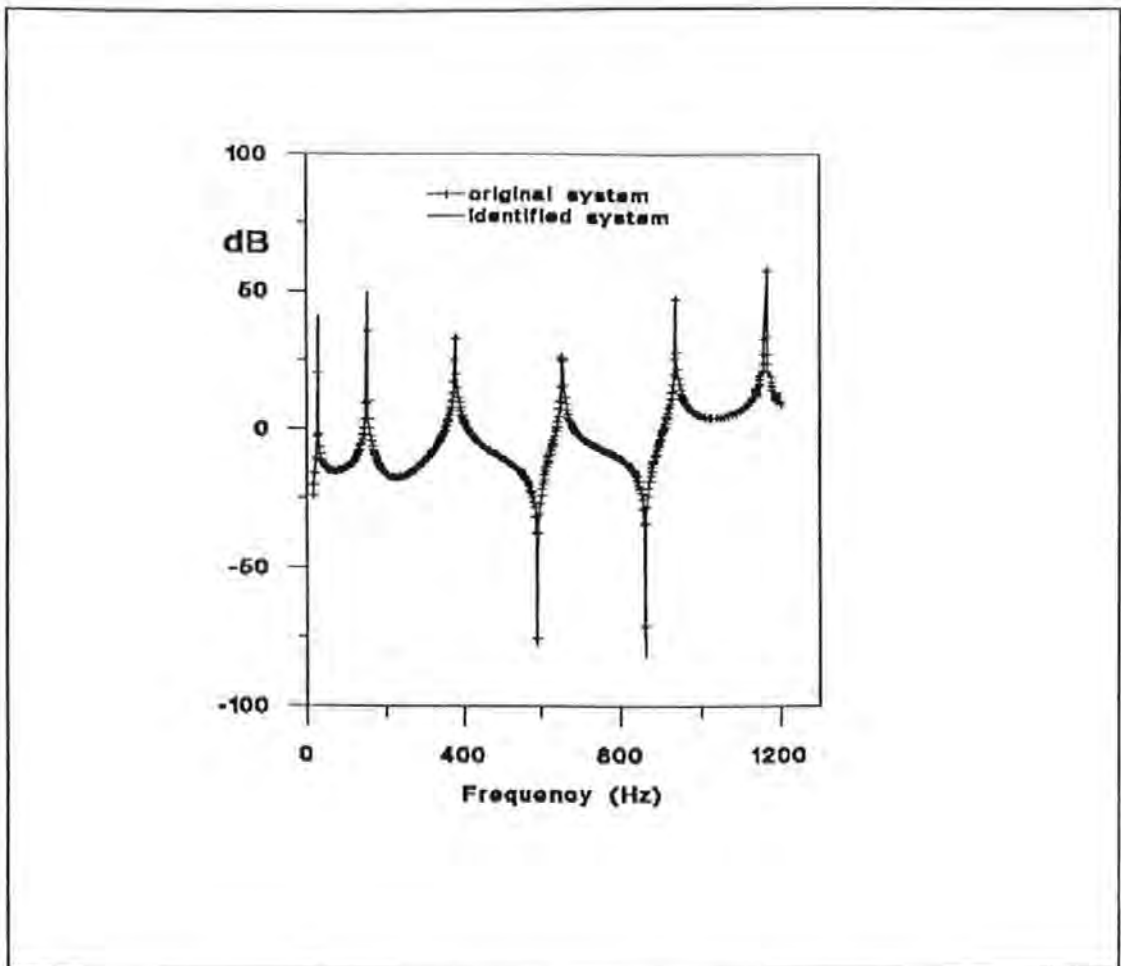


**Figure 4.15 Comparison of FRFs from original and identified system matrices of cantilever beam**

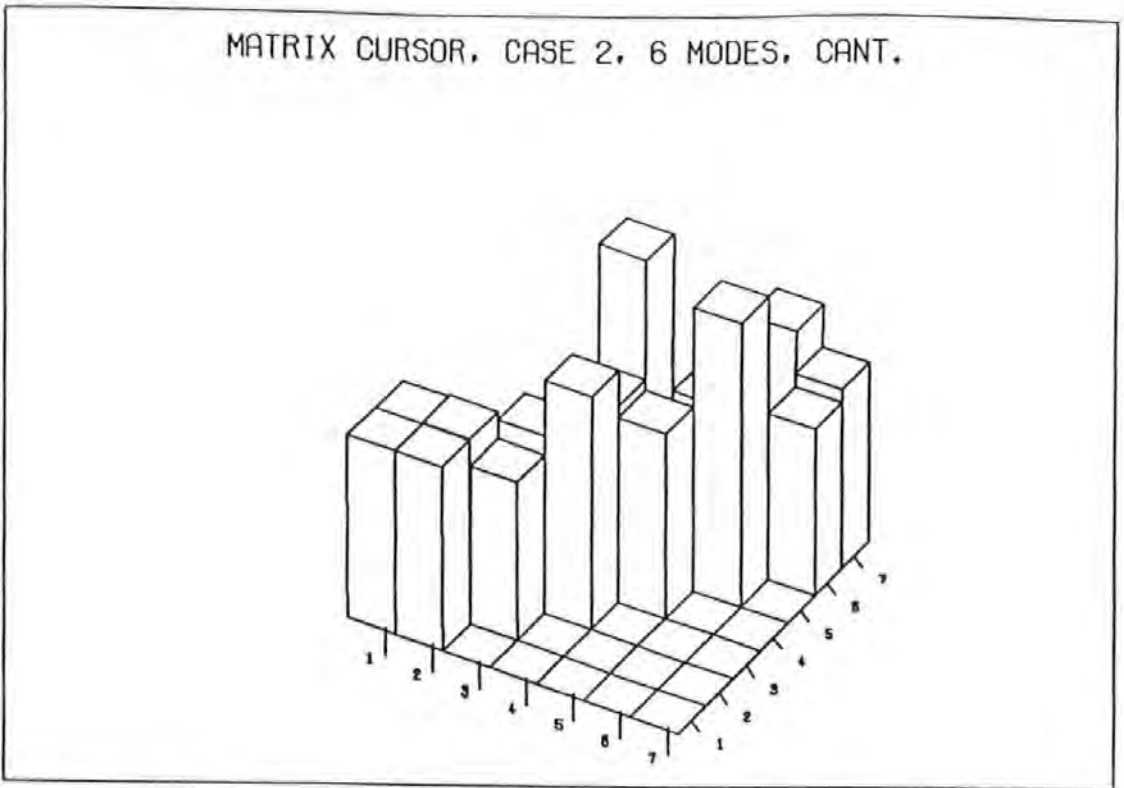
#### 4.6.2.1 Cantilever beam

Since the stiffness reduction in damage case 2 affects all elements equally, the elements of the stiffness error matrix would be expected to have the same values. Figure 4.16 shows 3-dimensional plots of the error location matrix, using all six modes, for damage case 2. The expected shape (all bars of equal height) is not displayed. The axes annotation in Figures 4.16 and subsequent figures refers to the node (measurement point for the steel beam) numbers. For other damage cases, the height of the bars corresponding to nodes associated with the damaged elements should be larger than the rest. Furthermore, since the damage location for cases 4 and 5 are the same, the error plots for the two cases should

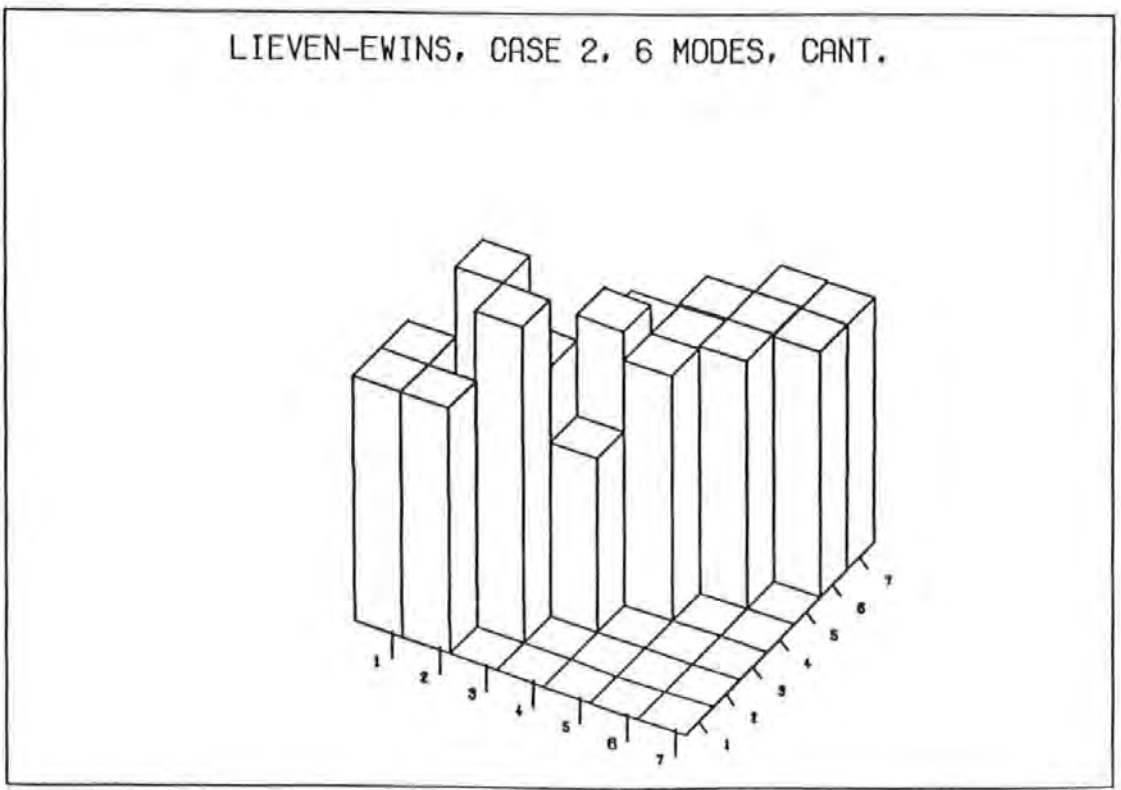
be similar. The plot for case 5 should show slightly larger values at nodes connected to element 3. This trend is shown in Figures 4.17 and 4.18. Existence of damage in elements 3 and 5 (cases 4 and 5) is indicated by the matrix cursor (Figure 4.17) while the stiffness error matrix method (Figure 4.18) is only able to identify damage in element 3 for case 5. Figure 4.18 also incorrectly identifies node 2 has been affected by damage.

Effects of number and type of modes used on the identification process was investigated using damage case 3. For each method, three situations were considered: 1) all six modes; 2) first three modes; and 3) three most affected modes (2, 4 and 6) as indicated by MSV and frequency reductions (Figure 4.8). Figure 4.19 shows plots obtained from the matrix cursor method for the three situations. Only Figure 4.19a (6 modes) gives an indication of the damage location. Figures 4.19a and 4.17a-b are identical. Thus, damage in element 3 controls the identification as regards the matrix cursor method. This observation highlights a potential problem with many model updating methods - the error identification is most likely to be governed by any defect located in a stiffness sensitive region of the modes included in the updating process.

The stiffness error matrix method was able to identify the damage location for all three situations (Figure 4.20). The best identification was achieved in situations 1 (all six modes) and 2 (first three modes). Utilizing the most sensitive three modes did not substantially improve the identification.



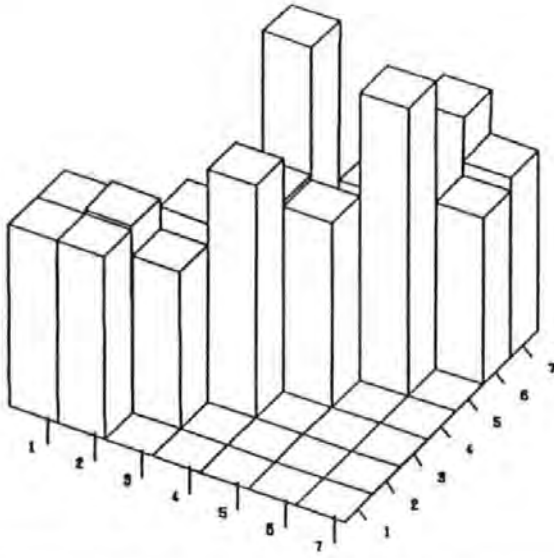
(a) Matrix cursor method



(b) Stiffness error matrix method

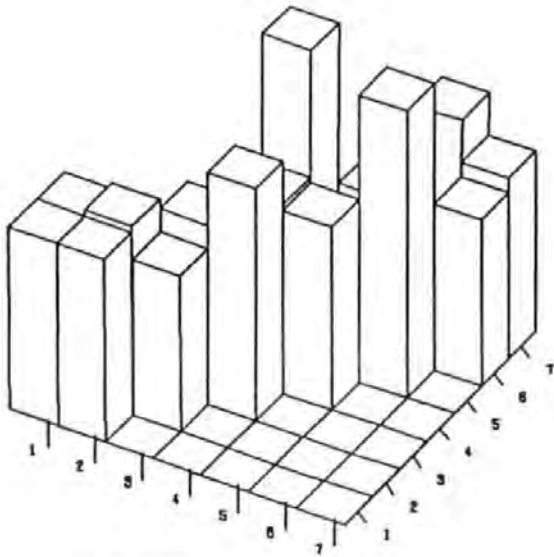
Figure 4.16 Damage location plots for cantilever beam using all six modes: case 2

MATRIX CURSOR, CASE 4, 6 MODES, CANT.



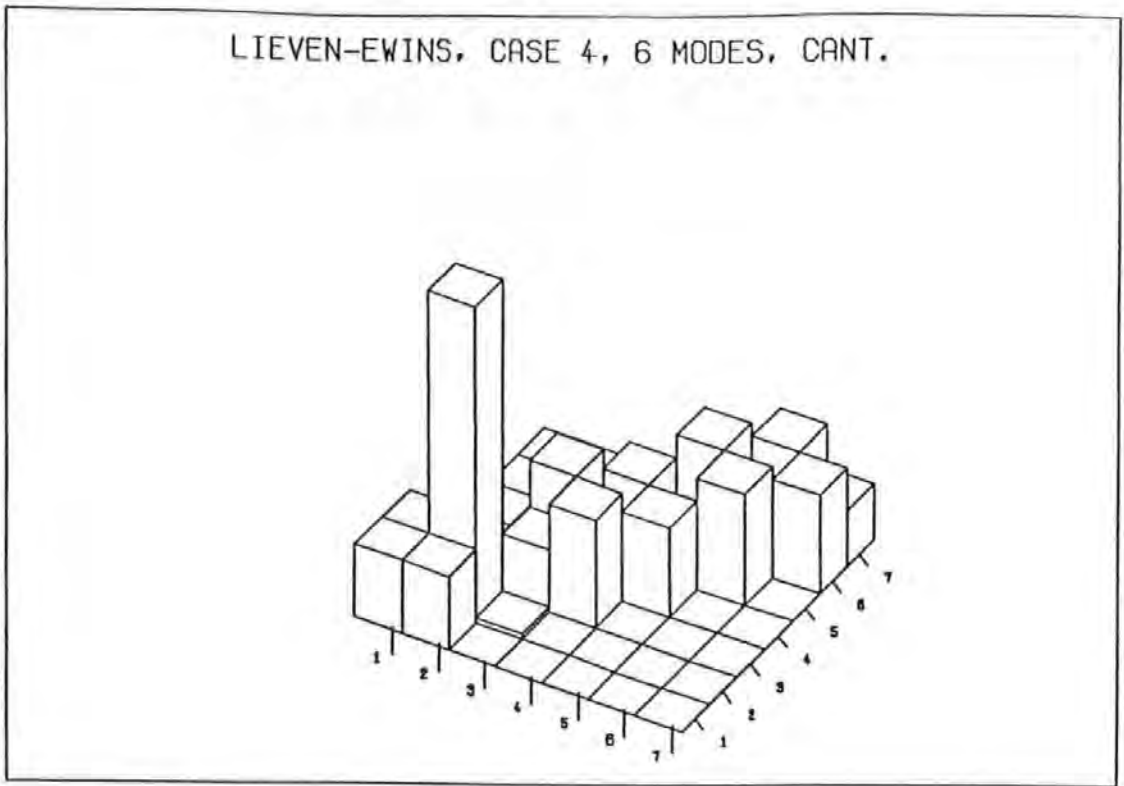
(a) Case 4

MATRIX CURSOR, CASE 5, 6 MODES, CANT.

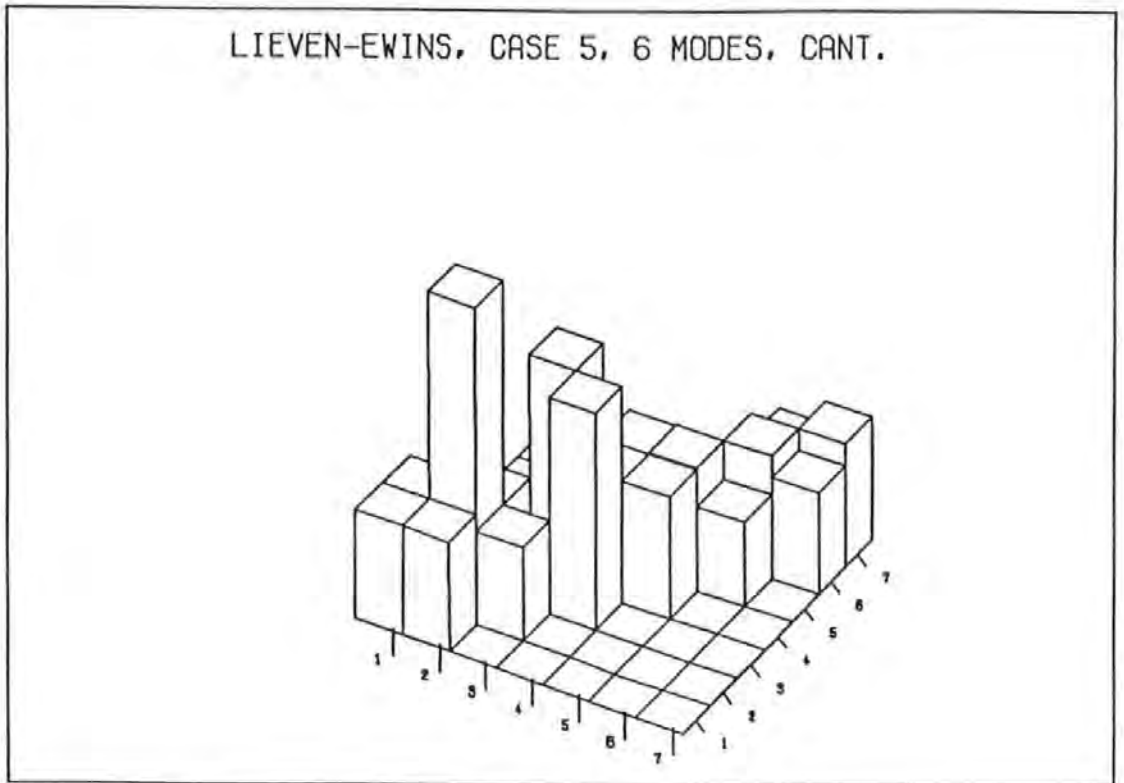


(b) Case 5

**Figure 4.17 Damage location plots for cantilever beam using the matrix cursor method with six modes**

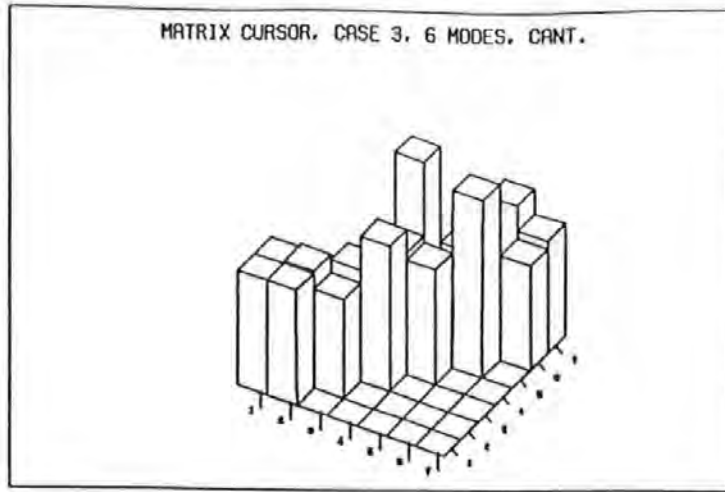


(a) Case 4

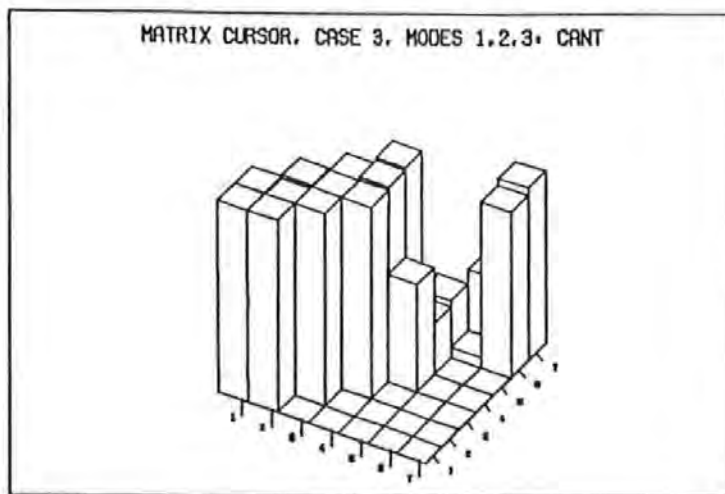


(b) Case 5

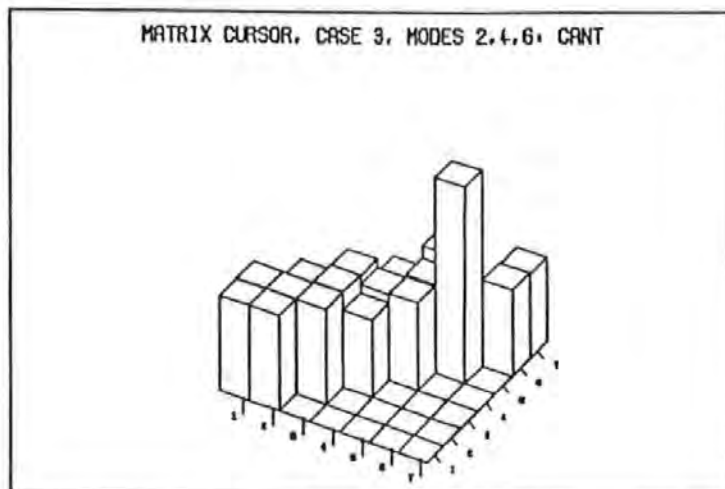
**Figure 4.18** Damage location plots for cantilever beam using stiffness error matrix method with six modes



(a) All six modes

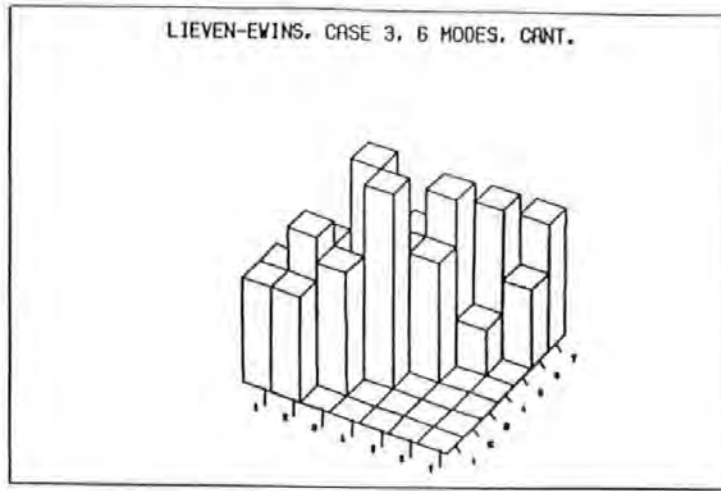


(b) Modes 1, 2 and 3

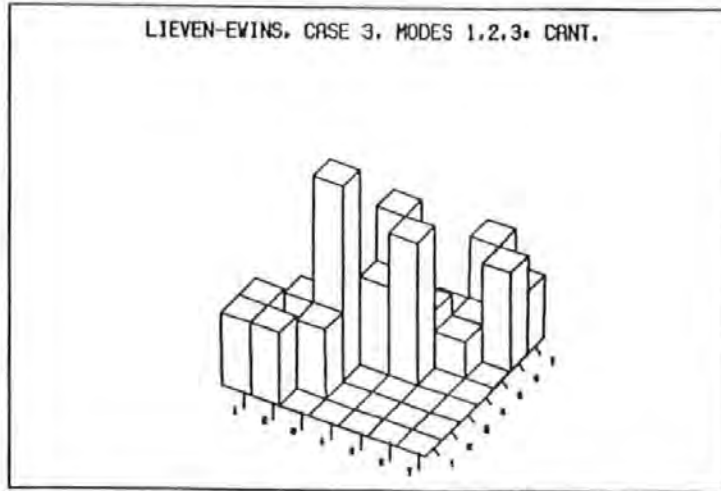


(c) Modes 2, 4 and 6

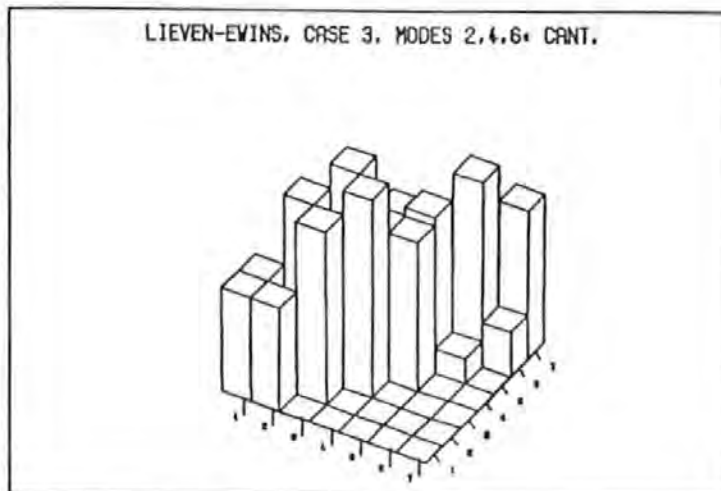
**Figure 4.19 Damage location plots for cantilever beam using the matrix cursor method: case 3**



(a) All six modes



(b) Modes 1, 2 and 3



(c) Modes 2, 4 and 6

**Figure 4.20 Damage location plots for cantilever beam using stiffness error matrix method: case 3**

#### 4.6.2.2 Steel beam

The identification plots obtained using the matrix cursor method were identical for all damage cases. Although similarity between the plots will be expected since all the cases relate to the same location, effects of increasing degree of deterioration should be reflected. The typical plot, shown in Figure 4.21, does not unambiguously reveal the damage location. The damage location was identified with the stiffness error matrix method (Figure 4.22). The figure indicates that the effects of the damage on points not directly connected to the damaged zone increased with increasing level of damage. This is a logical trend. Identification of element 5 as being damaged in Figure 4.22c is a result of the symmetrical nature of the beam.

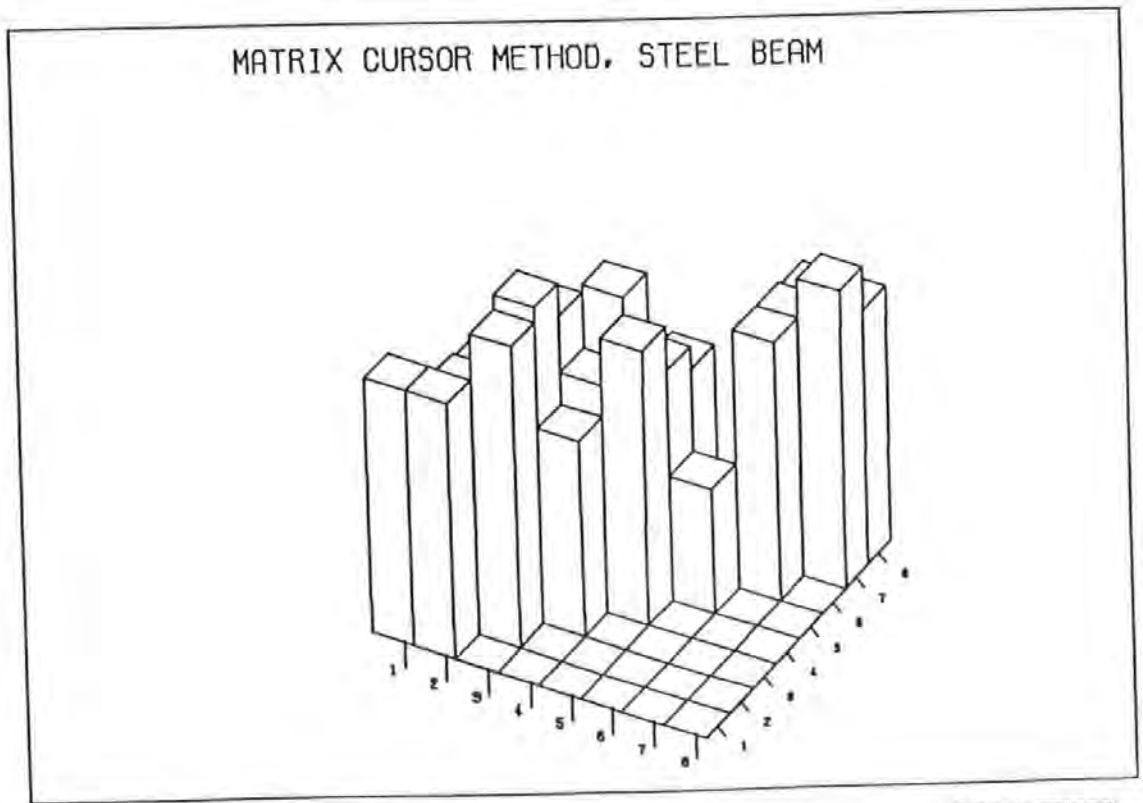
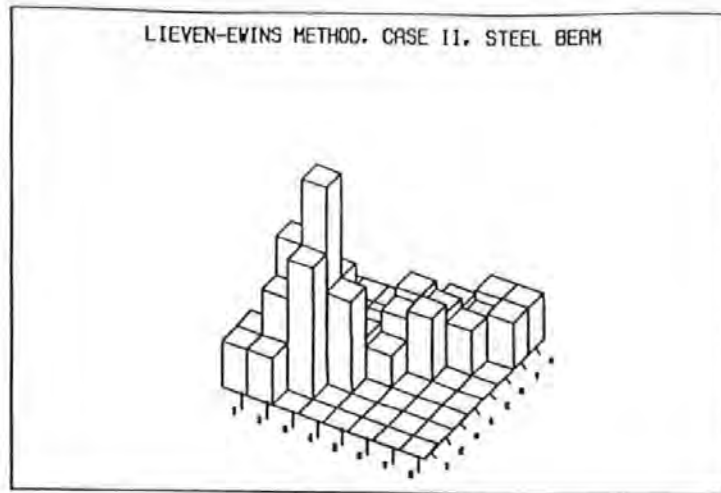


**Figure 4.21** Damage identification plot for steel beam using matrix cursor method



(a) Case II



(b) Case III



(c) Case IV

**Figure 4.22 Damage location plots for steel beam using stiffness error matrix method**

The results show that the version of the stiffness error matrix implemented is more effective than the matrix cursor method in damage location. All the three modes were used in obtaining the plots in Figures 4.21 and 4.22.

#### 4.7 Conclusions

Results of the studies reported in this chapter have revealed the relationships between damage in a structure and the various parameters used to characterize the structure's dynamic response. As would be expected, existence of damage leads to a reduction in frequency and an increase in the viscous damping ratios. A reduction, after an initial increase, in the damping ratio of the second mode occurred for the steel beam. The usefulness of a new function (MSV) proposed by the author for identifying damage sensitive modes was demonstrated.

Although MAC and COMAC showed sensitivity to damage, they were unable to clearly indicate the damage location in the cantilever beam. However, damage in the experimental steel beam was correctly located by COMAC values while a better (as compared to the simulated data) indication of the damage was given by MAC. All the modal data based methods identified, to an extent, the damaged area in the case of single damage location. Performance of the curvature mode shape and mode shape relative difference methods on experimental data was poor. The most important factor in using these two methods is determining which modes to use since only some of the modes correctly identified and located the damage. The proposed function MSV should be useful for this task. Detection of multiple damage sites is generally difficult, if not impossible, for most damage location schemes. Only the curvature mode shape method was able to give an indication of simulated multiple damage locations. The modal data based methods, apart from COMAC,

## CHAPTER FIVE

### THE INTEGRITY INDEX DAMAGE LOCATION METHOD

#### 5.1 Introduction

Discussions in the last two chapters suggest that damage location/integrity assessment of civil engineering structures using vibration data requires a robust method based on only test data and simple assumptions about the behaviour of the structure. To improve the damage location process, it would be necessary to utilize only the damage sensitive modes. Another factor to consider is the applicability of the method to any structural form and damage case. Attainment of these properties would make the method suitable to all engineering structures. Most of the methods available do not possess these attributes mainly because they were developed for specific structural and damage types.

Results of the studies in chapter four show that both natural frequencies and the appropriate mode shapes should be used in order to locate the damage site(s) with reasonable accuracy. Since each mode shows a different response to the presence of damage, use of weighting factors to magnify the response of the most affected modes would be expected to improve the damage location process. The development, implementation and evaluation of a new damage detection and location method, called Integrity Index Damage Location Method, are described in this chapter. The proposed method uses measured natural frequencies and mode shapes in conjunction with weighting factors appropriate to the type of structure considered. The method is applicable to any structure and any damage type that affects the integrity/stiffness of the structure. Performance of the method is evaluated using both

simulated and experimental data.

## 5.2 Development and Implementation

### 5.2.1 Global Integrity Index

The first case considered is that of determining whether there has been a change in the structural integrity. The change could be either a reduction (e.g. presence of damage) or an increase (e.g. due to strengthening and repair) in the global structural stiffness. A parameter GI (Global Integrity Index) is defined to represent the structural integrity. GI has the following properties:

$GI = f(\omega)$	;	$\omega =$ natural frequency in radians/seconds
$GI < 1$	;	loss of integrity
$GI = 1$	;	no loss of integrity (unmodified structure)
$GI > 1$	;	gain in integrity

A linear combination of the ratios of the damaged structure's frequencies to the undamaged structure's frequencies is used to represent the function  $f(\omega)$ . Thus,

$$f(\omega) = \sum [a_r (\omega_{Dr} / \omega_{Or})] = GI \quad (5.1)$$

where the subscripts D and O respectively refer to the damaged and undamaged structures; and r refers to the mode number.  $a_r$  is the weighting factor for mode r.

Equation (5.1) is a general expression to assess the integrity of any engineering structure. Since only natural frequencies are used, only one measurement point is sufficient. Three questions need to be addressed before Equation (5.1) can be implemented. These are: 1)

how many modes to include; 2) which modes to include; and 3) what values of  $a_r$  should be used. Since the method is meant for general application, the answers to the questions might, in a few cases, be dependent on the structural system.

The number of modes to include will generally be dependent on the number ( $m$ ) of measured modes. It is suggested that at least three modes be included. In all the examples presented later, only three modes were used. If  $m > 3$ , the second question - which modes to include - arises. Some researchers have suggested that the lower modes are most affected by damage while others (researchers) maintain that the higher modes are most sensitive to damage (chapter three). The approach adopted here is to use the three most (damage) sensitive modes as indicated by the function MSV defined in chapter four (sub-section 4.2.1). Alternatively, MAC (sub-section 4.2.1) can also be used to select the modes to be included.

As stated earlier, the values of  $a_r$  could be structure dependent. Maguire (1992) suggested that the first three modes dominate the dynamic response of large civil engineering structures and that the effective participation can be assigned as : mode 1 - 70%; mode 2 - 20%; other modes - 10%. As regards integrity assessment/damage detection (and location), it would be assumed that the three modes selected using MSV (or MAC) will dominate the response. Thus, the values of  $a_r$  are chosen such that the most sensitive mode has  $a_r = 0.7$  while  $a_r$  for the least sensitive mode is 0.1. The  $a_r$  values 0.7, 0.2 and 0.1 were used in all the examples described in this chapter.

### 5.2.2 Local Integrity Indices

GI (Equation 5.1) will only indicate loss or gain of integrity. It is however still necessary to locate the defective areas so that appropriate remedial actions can be taken. In addition, due to its global nature, GI might not be very sensitive to highly localized defects. New indices, called Local Integrity Indices (LI), will be used to detect localized defects and locate damage areas. The requirement to locate damage sites necessitates inclusion of mode shapes in the formulation for the local indices.  $LI_i$  represents the local integrity at measurement point  $i$  and has the following properties:

$$\begin{aligned} LI_i &= f(\omega, [\Psi]); & [\Psi] & \text{is the mode shape matrix} \\ |LI_i - 1| &= 0; & & \text{no loss of integrity at point } i \\ |LI_i - 1| &> 0; & & \text{loss of integrity at point } i \end{aligned}$$

Changes in the local stiffness would cause the modal amplitudes to either increase or decrease at the point concerned. The direction of the change is immaterial because only the location is needed. Furthermore, GI would have indicated the nature of the change. Therefore, ratios of the squares of the modal amplitudes are used to compute  $LI_i$  while the absolute difference of  $LI_i$  from unity is used to infer the damage site.  $LI_i$  is given by;

$$LI_i = \sum [a_r (\omega_{Dr} / \omega_{Or}) ( (\phi_{Dir})^2 / (\phi_{Oir})^2 )] \quad (5.2)$$

where  $(\phi_{Dir})$  and  $(\phi_{Oir})$  are respectively elements of the  $r$ th mode shape vector at measurement point  $i$  for the damaged and undamaged structures. The values of  $a_r$  and the number and type of modes to include have been discussed in sub-section 5.2.1. Existence of damage in a practical structure would invariably lead to  $|LI_i - 1| > 0$  for all  $i$ . However, values of  $|LI_i - 1|$  for points most likely to be the damage locations would be much greater than those for other points.

To identify single damage locations,  $|LI_i - 1|$  values from all points are normalised such that the point with the largest value (hence, the most likely damage site) has a value of 100. The values at other points will indicate to what extent the points have been affected by the damage. If multiple damage locations are suspected, the process is repeated without the previously identified point(s).

Equations (5.1) and (5.2) are simple expressions that can be easily implemented. They do not require extensive computer time and memory. If the modes to be used and the weighting factors have been previously determined, GI and  $LI_i$  can be evaluated using a desk calculator. A simplified flowchart of the Fortran program written to calculate GI and  $LI_i$  is shown in Figure 5.1. Figure 5.1 only illustrates the procedure for identifying single damage sites.

### **5.3 Evaluation of the Method using Simulated Data**

Performance of the Integrity Index method on numerical data was studied using a cantilever beam and an eight degrees of freedom (8-DOF) mass-spring (no damping) system. The system represented any structure and was designed to test the general applicability of the method. The numerical data were error free thereby facilitating investigation of effects of simulated deterioration only. Influence of errors from testing and data analysis procedures was considered by using experimental data obtained from laboratory testing. This is discussed in section 5.4.

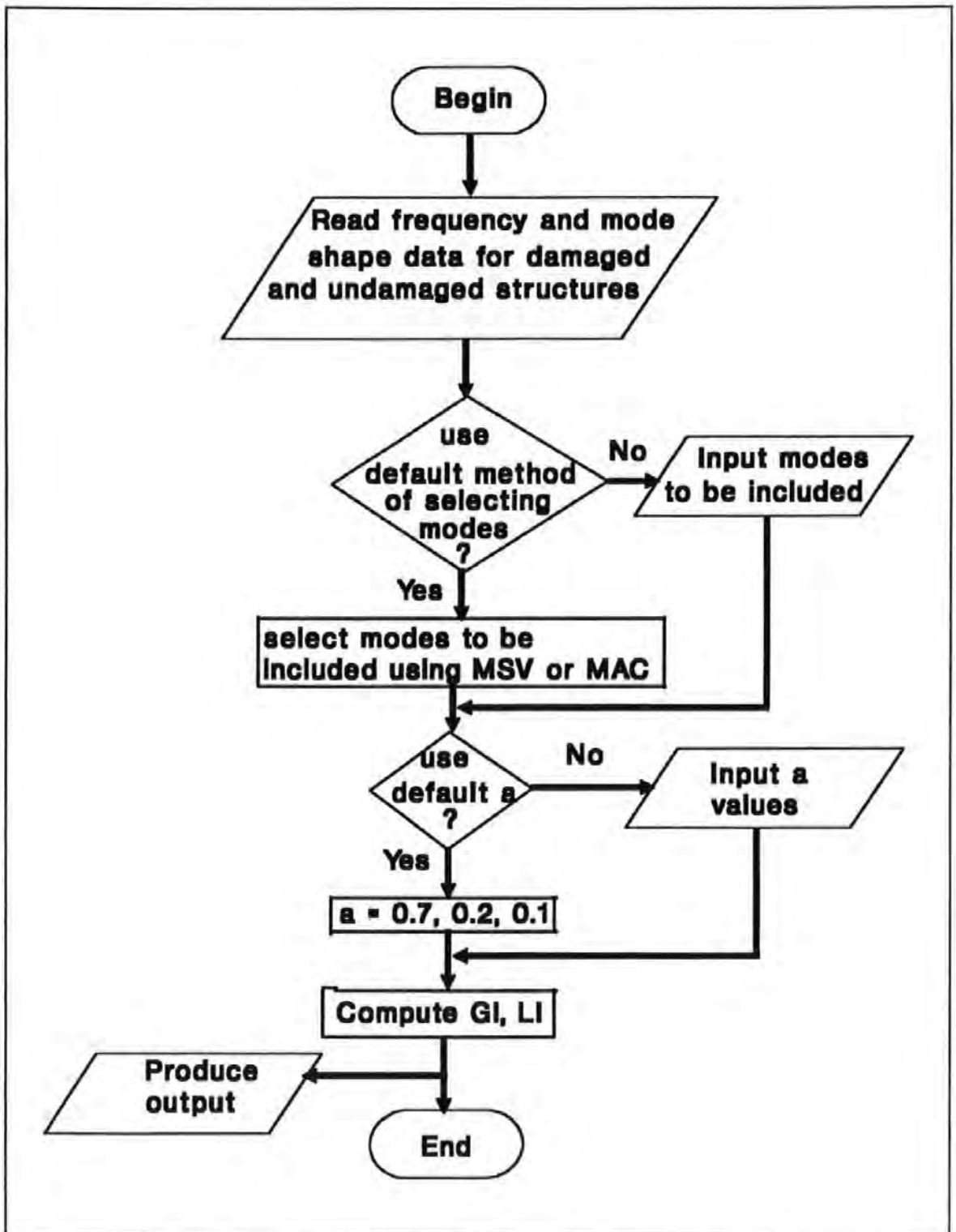


Figure 5.1 Flowchart for identifying damage locations using the Integrity Index Method

### 5.3.1 Cantilever beam

Details of the model used, damage simulations and results from the analysis have been presented in section 4.4. Results of damage detection and location using the Integrity Index method are shown in Tables 5.1 and 5.2. From Table 5.1, it can be seen that the Global Integrity Index (GI) reveals existence of damage and correctly indicates the relative severity (see sub-section 4.4.1) of the simulated damage cases. While the methods evaluated in chapter four were unable to indicate existence or/and severity of damage case 2, GI values show that case 2 is the worst situation. Results of damage location using Local Integrity Indices (LI) are shown in Table 5.2. The damage site for case 2 is identified as being the whole beam while element 3 (nodes 3 and 4 have the largest LI in Table 5.2) is indicated as being damaged in damage case 3.

**Table 5.1 Global Integrity Indices for cantilever beam**

Damage case	Global Integrity Index
Case 2	0.71
Case 3	0.94
Case 4	0.86
Case 5	0.77

**Table 5.2 Local Integrity Indices for cantilever beam**

Node	Case 2	Case 3	Case 4	Case 5
1	100	3.3	5.6	2.7
2	100	4.8	77.6	16.9
3	100	26.4	100	100
4	100	100	41.9	19.4
5	100	2.9	81.3	19.6
6	100	13.1	75.5	17.5
7	100	7.7	71.8	18.2

Cases 4 and 5 represent multiple (two) damage locations. Element 3 is still identified as damaged while element 5 (which is also damaged) has the next largest LI for both cases. If the multiple damage location procedure described earlier is applied (by eliminating node 3 during a second identification process), element 5 will be shown as being damaged. Even without utilizing the second stage identification, the relative values of the LI shown in Table 5.2 indicate to what extent each node has been affected by damage. This information shows that there is a wider spread of damage (double location) in case 4 than in cases 3 and 5. Although case 5 also has double damage locations, the higher severity of the defect in element 3 is more prominent. Nonetheless, the LI values for nodes 5 and 6 (hence element 5) in case 5 are larger than for case 3 thereby showing effects of the double damage sites.

### 5.3.2 Eight degrees of freedom (8-DOF) mass-spring system

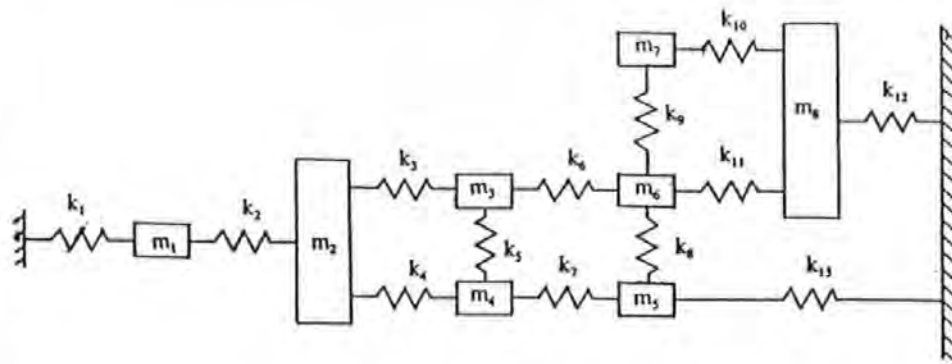
The 8-DOF system, representing any general structure, is shown in Figure 5.2. For the case of no external forces (free vibration) and no damping, the equations of motion of the system are given by:

$$[M] \{X''(t)\} + [K] \{X(t)\} = \{0\} \quad (5.3)$$

where

$[K]$	=	system stiffness matrix
$[M]$	=	system mass matrix
$\{X(t)\}$	=	physical coordinate displacement vector
$\{X(t)''\}$	=	physical coordinate acceleration vector
$t$	=	time variable

The mass and stiffness matrices are given in Figure 5.2. The generalised eigenvalue problem in Equation (5.3) was solved to obtain the system's eigenvalues and eigenvectors. These are shown in Figures 5.3 and 5.4 where column  $r$  contains the  $r$ th eigenvalue and eigenvector respectively.



$$\begin{aligned}
 k_1 = k_2 = \dots = k_{13} &= 1000 \text{ N/m} \\
 m_1 &= 1 \text{ kg}; \quad m_2 = 3 \text{ kg}; \quad m_3 = m_4 = m_7 = 2 \text{ kg} \\
 m_5 = m_6 &= 1.5 \text{ kg}; \quad m_8 = 3.5 \text{ kg}
 \end{aligned}$$

$$[M] = \begin{bmatrix}
 m_1 & 0 & 0 & 0 & 0 & 0 & 0 & 0 \\
 0 & m_2 & 0 & 0 & 0 & 0 & 0 & 0 \\
 0 & 0 & m_3 & 0 & 0 & 0 & 0 & 0 \\
 0 & 0 & 0 & m_4 & 0 & 0 & 0 & 0 \\
 0 & 0 & 0 & 0 & m_5 & 0 & 0 & 0 \\
 0 & 0 & 0 & 0 & 0 & m_6 & 0 & 0 \\
 0 & 0 & 0 & 0 & 0 & 0 & m_7 & 0 \\
 0 & 0 & 0 & 0 & 0 & 0 & 0 & m_8
 \end{bmatrix}$$

$$[K] = \begin{bmatrix}
 k_1 + k_2 & -k_2 & 0 & 0 & 0 & 0 & 0 & 0 \\
 -k_2 & k_2 + k_3 + k_4 & -k_3 & -k_4 & 0 & 0 & 0 & 0 \\
 0 & -k_3 & k_3 + k_5 + k_6 & -k_5 & 0 & -k_6 & 0 & 0 \\
 0 & -k_4 & -k_5 & k_4 + k_5 + k_7 & -k_7 & 0 & 0 & 0 \\
 0 & 0 & 0 & -k_7 & k_7 + k_8 + k_{13} & -k_8 & 0 & 0 \\
 0 & 0 & -k_6 & 0 & -k_8 & k_6 + k_8 + k_9 + k_{11} & -k_9 & -k_{11} \\
 0 & 0 & 0 & 0 & 0 & -k_9 & k_9 + k_{10} & -k_{10} \\
 0 & 0 & 0 & 0 & 0 & -k_{11} & -k_{10} & k_{10} + k_{11} + k_{12}
 \end{bmatrix}$$

Figure 5.2 8-DOF system

134.294	0	0	0	0	0	0	0
0	379.419	0	0	0	0	0	0
0	0	1128.08	0	0	0	0	0
0	0	0	1306.12	0	0	0	0
0	0	0	0	1707.25	0	0	0
0	0	0	0	0	2078.61	0	0
0	0	0	0	0	0	2348.86	0
0	0	0	0	0	0	0	3441.19

**Figure 5.3 Eigenvalues [(rad/sec.)<sup>2</sup>] of 8-DOF system**

-.2178	-.2648	-.4998	-.1256	.2512	.5305	-.8723	.0080
-.4064	-.4292	-.4358	-.0874	.0735	-.0417	.3043	-.0116
-.4306	-.2269	.2590	.0474	-.7331	.0883	-.1085	.2591
-.4071	-.3073	.4083	.1588	.3258	-.4839	-.2506	-.1822
-.2750	-.0326	.4805	.1016	.5245	.5134	.2297	.4600
-.3625	.2280	.2202	-.0531	-.0955	.4234	.1305	-.8122
-.3786	.5665	-.0150	-.8005	.0588	-.1686	-.0421	.1514
-.2929	.4752	-.2163	.5432	.0123	-.0596	-.0169	.0731

**Figure 5.4 Eigenvectors of 8-DOF system**

The 'damage' cases considered were:

Case k<sub>1</sub> : k<sub>1</sub> = 2000 N/m

Case k<sub>7</sub> : k<sub>7</sub> = 500 N/m

Case m<sub>3</sub> : m<sub>3</sub> = 0.5 kg

Cases k<sub>1</sub> and k<sub>7</sub> were expected to respectively increase and decrease the global stiffness while case m<sub>3</sub> represented a mass error. Using the magnitude of the changes made to the system as a damage indication parameter, cases m<sub>3</sub> and k<sub>7</sub> are respectively the most and least severe. The natural frequencies for the damaged and undamaged cases are shown in Table 5.3. In case m<sub>3</sub>, the total mass is reduced (constant stiffness) thereby leading to an increase in frequency since frequency is inversely proportional to mass. The frequency changes (given, as a percentage, in parentheses in Table 5.3) are small (except mode 8,

case m\_3) when compared to those of the cantilever beam (Table 4.1). This situation was meant to test performance of the method on defects causing small changes in frequency. The natural frequency changes do not clearly indicate the relative severity of the damage cases.

**Table 5.3 Natural frequencies of 8-DOF system for different damage cases**

Mode	Natural frequency (Hz)			
	Undamaged	Case k_1	Case k_7	Case m_3
1	1.844	1.934 (4.8)*	1.803 (-2.2)	1.966 (6.6)
2	3.100	3.176 (2.5)	3.012 (-2.8)	3.152 (1.7)
3	5.346	5.518 (3.2)	5.339 (-0.1)	5.426 (1.5)
4	5.752	5.765 (0.2)	5.748 (-0.1)	5.754 (0.03)
5	6.576	6.607 (0.5)	6.393 (-2.8)	7.239 (10.1)
6	7.256	7.350 (1.3)	6.667 (-8.1)	7.658 (5.5)
7	7.713	8.956 (16.1)	7.651 (-0.8)	8.675 (12.5)
8	9.336	9.336 (0.0)	9.205 (-1.4)	12.98 (39.1)

\*Change in frequency, in percentage, from undamaged state

The GI values are given in Table 5.4. The values in the table reflect the relative extent of the simulated damage cases. Case k\_1 is shown to have increased the overall integrity as would be expected. The structural integrity is also shown to have been improved due to damage case m\_3 since the mass was reduced while stiffness remained constant. In practical situations, defects involving significant mass reductions, as simulated here, would be visually obvious. In almost all cases, stiffness errors are the main concern and the performance of the method as regards this is satisfactory. Damage events involving both mass and stiffness reductions are further considered in section 5.4.

Results of the damage location are shown in Table 5.5. The damage sites for cases k\_1

and k\_7 are identified. For case m\_3, DOF 2 was incorrectly identified although DOF 3, which is the damage site, has the next largest value. Incorrect identification of the mass error location is not regarded as a limitation of the method since mass reductions would usually involve stiffness changes, to which the method is very sensitive. The identification for case m\_3 is still reasonably satisfactory since one out of the two DOF strongly suggested is the actual damage site.

**Table 5.4 Global Integrity Indices for 8-DOF system**

Damage case	Global Integrity Index
Case k_1	1.13
Case k_7	0.93
Case m_3	1.31

**Table 5.5 Local Integrity Indices for 8-DOF system**

DOF	Case k_1	Case k_7	Case m_3
1	100	4.7	8.1
2	64.8	3.1	100
3	54.0	23.9	85.6
4	49.6	82.9	2.9
5	46.0	100	1.5
6	34.0	10	36.2
7	82.8	34.3	14.7
8	33.3	71.5	25.9

## **5.4 Evaluation of the Method Using Experimental Data**

### **5.4.1 Simply supported steel beam**

Experimental data from tests conducted on the steel beam described in section 4.5 were used to evaluate the method. The experimental procedure, damage cases considered and test results have been presented in section 4.5. The damage cases involved both mass and stiffness loss and were induced in 'element' three (Figure 4.5) of the beam. The data include both experimental error and inaccuracies introduced during modal parameter extraction and thus represent a realistic test for the method. The last statement is also true for the data used in sub-section 5.4.2.

The Global Integrity Indices are shown in Table 5.6 while Table 5.7 shows the Local Integrity Indices. The values in Table 5.6 indicate the correct progression of the severity of the damage (see also sub-section 4.5.2) while the damage location is correctly identified in Table 5.7. From the values in Table 5.6, it can be seen that removal of half the web and the two flanges is a more severe form of damage than removal of both flanges alone. In addition, losing one or both flanges seem to produce the same level of integrity loss. The correct identification of the relative extent and location of damage shows that the method is sensitive to both mass and stiffness errors when both occur simultaneously.

**Table 5.6 Global Integrity Indices for steel beam**

Damage case	Global Integrity Index
Case II	0.95
Case III	0.94
Case IV	0.71

**Table 5.7 Local Integrity Indices for steel beam**

Location	Case II	Case III	Case IV
1	6.6	8.5	14.8
2	89.8	89.9	27.4
3	93.4	100	100
4	100	94.4	94
5	15.6	14.2	73.8
6	8.9	5.3	3.3
7	23.0	3.8	28.9
8	6.6	8.5	14.0

#### 5.4.2 3-storey frame model structure

Experimental data obtained by Beck (1991) from impact tests on a 3-storey frame structure (Figure 5.5) were also used to further evaluate performance of the method. The frame was made from aluminium with each member having a length, width and thickness of 254.0mm, 25.4mm and 3.175mm respectively. The beam and column elements were connected by aluminium elbows. The undamaged state referred to the frame just after assembly. Damage was simulated by replacing member M3 by a vinyl member thereby reducing the

stiffness of M3 by about 80%. Further details of the experimental setup, procedures and results are given on pages 91-93 and 100-102 of Beck (1991).

The modal parameters for the first three modes of the structure are shown in Table 5.8 while results from the identification are shown in Table 5.9. A value of 0.91 for the Global Integrity Index strongly suggests presence of damage. The results correctly indicate the damage location to be between coordinates U1 and U2 (coordinates with the largest indices in Table 5.9) i.e. member M3. The MSV for modes 1, 2 and 3 are respectively 59.4, 100.0 and 9.71.

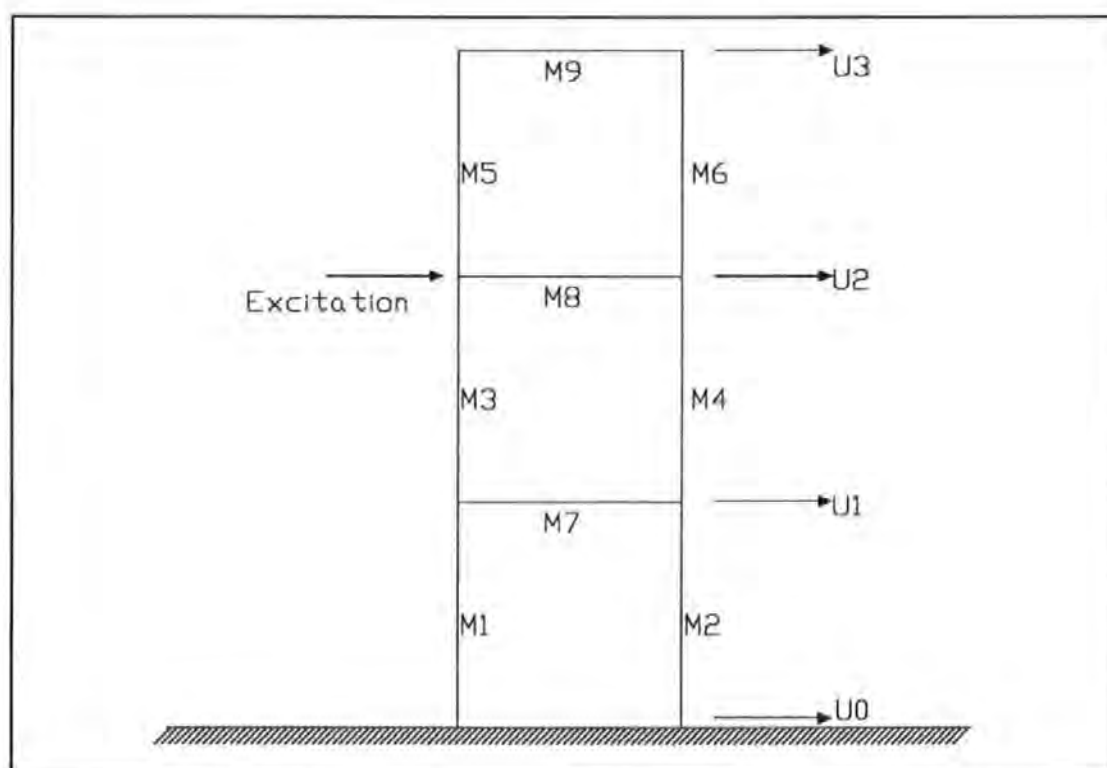


**Figure 5.5 Elevation of the model structure (after Beck, 1991)**

**Table 5.8 Modal parameters of 3-storey model structure\***

		Mode 1	Mode 2	Mode 3
<b>Undamaged structure</b>	Natural frequency (Hz)	8.986	28.63	48.00
	Damping ratio	0.0083	0.0046	0.0045
	Eigenvector			
	U0	0.00	0.00	0.00
	U1	0.308	-0.719	1.30
	U2	0.610	-0.291	-1.21
	U3	1.00	1.00	1.00
<hr/>				
<b>Damaged structure</b>	Natural frequency (Hz)	7.601	27.04	38.06
	Damping ratio	0.0149	0.0083	0.0101
	Eigenvector			
	U0	0.00	0.00	0.00
	U1	0.236	-1.358	0.595
	U2	0.769	-0.242	-1.023
	U3	1.00	1.00	1.00

\* (After Table 5.9 in Beck, 1991)

**Table 5.9 Global and Local Integrity Indices for 3-storey model structure**

Coordinate	Local Integrity Index
U0	6.1
U1	100.0
U2	14.7
U3	6.1
Global Integrity Index = 0.91	

### 5.5 Conclusions

The Integrity Index method has been shown to be satisfactory in predicting loss or gain in structural integrity and also indicating areas affected by damage/defects. The method performed satisfactorily on both simulated and measured data and, unlike most other methods, is applicable to any structure. An indication of the severity of the damage is also given. If only structural integrity is to be assessed, only one measurement point is needed to compute the Global Integrity Index. To locate damage sites, more measurement points would be required to reasonably define the mode shapes and localize the affected areas. The number of points to be used will depend on the degree of refinement desired.

A practical approach using the method would be to first evaluate the Global Integrity Index. If loss of integrity is suggested, measurements can then be taken at a few widely spaced points. More measurements would then be taken close to those points suggested by the Local Integrity Indices as being affected by damage. This approach will zoom-in on the affected areas and optimize test resources.

## CHAPTER SIX

### TEST EQUIPMENT AND ANALYSIS PROCEDURES

#### 6.1 Introduction

The equipment used during full-scale (chapters seven and eight) and laboratory (chapter four) tests conducted, and the data analysis techniques adopted for the measured data, are described in this chapter. The basic stages involved in forced vibration testing have been shown in Figure 2.1. The particular instrumentation layout employed during the full-scale tests is shown in Figure 6.1. The experimental approach utilized is briefly described in the next paragraph with reference to the figure.

The test procedure involved feeding excitation signals (usually generated by a spectrum analyzer) to the vibrator control unit. The unit was adjusted until the vibrator generated optimum excitation energy to allow measurable response of the test structure. The structural response was measured by accelerometers while a load cell incorporated within the vibrator allowed measurement of the input load. Signals from the accelerometers and load cell were conditioned, to improve signal quality, using the signal conditioning unit. Oscilloscopes were used to monitor recorded signals. Selected portions of the signals were recorded on ultraviolet paper using the oscillograph. Limited real time analysis was conducted on the spectrum analyzer to monitor test progress, signal quality and obtain initial estimates of natural frequencies. An analogue tape recorder was used to record the signals for detailed analysis off-site. Details of the equipment shown in Figure 6.1 and data analysis procedures are given in the following sections.

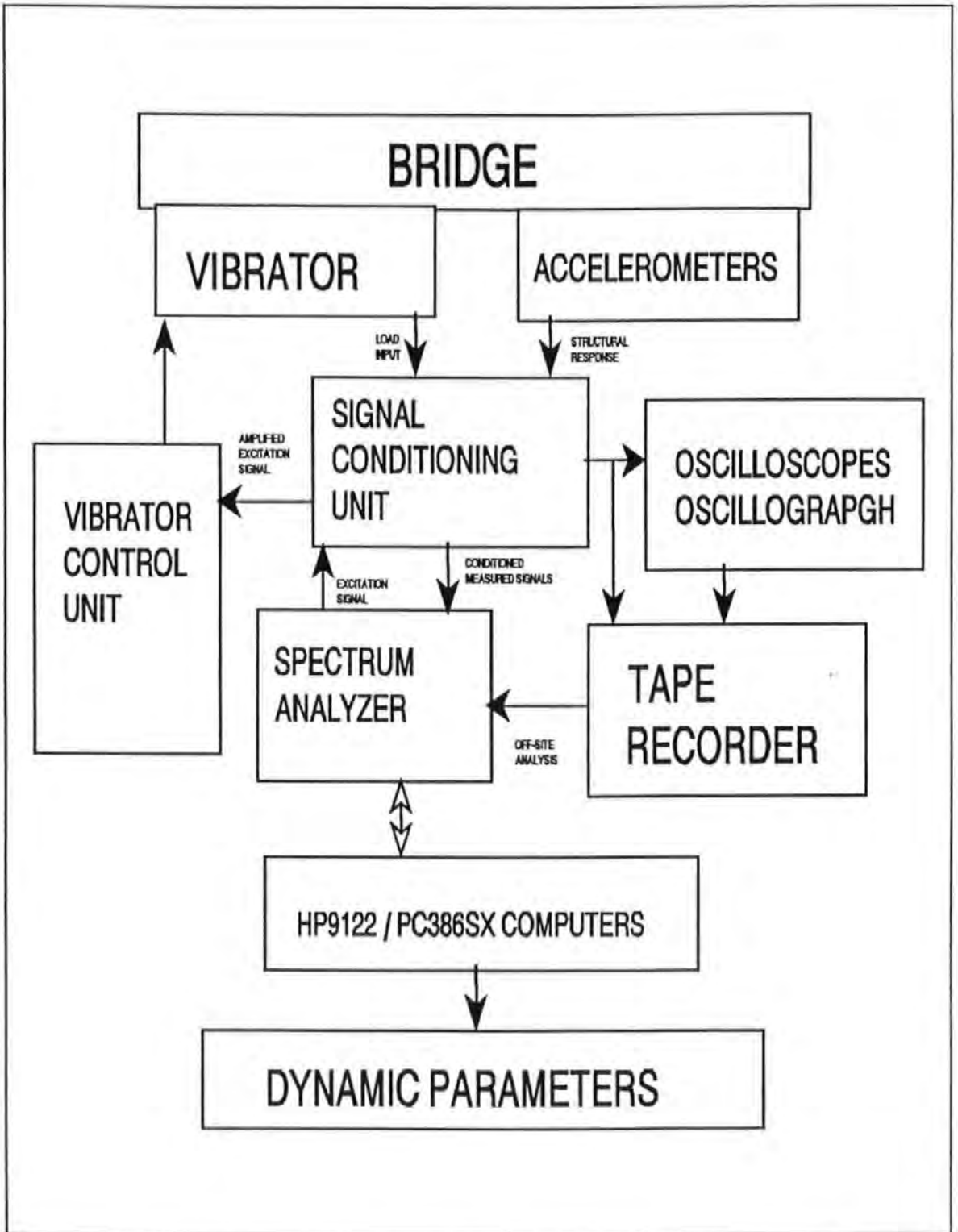


Figure 6.1 Instrumentation layout for dynamic tests

## **6.2 An Excitation System for Full-Scale Testing**

As mentioned in chapter two, selection of an appropriate excitation mechanism is one of the main problems encountered in full-scale forced vibration testing of large structures. The system chosen should be able to generate sufficient force levels while not causing localised damage on the test structure. Portability and ease of operation on site are other factors to consider.

An excitation system incorporating an existing hydraulic jack and pumps was developed to generate artificial excitation during full-scale tests. The system is optimised for testing structures which deflect most readily in the vertical direction, for example, highway bridges and long span floors. While the system might not be an ideal one, it is the best compromise after due consideration of existing equipment, available resources and service requirements. Development of the system has been reported in the literature (Salawu and Williams, 1992; 1994b). Components and operating characteristics of the system are described below.

### **6.2.1 Description of System**

A block diagram of the excitation system is shown in Figure 6.2. The excitation signal is either generated by an external source or the vibrator control unit. The unit controls the level of excitation signal and operation of the vibrator and pumps. Any form of excitation signal can be input to the system. Figure 6.3 shows part of the excitation system on location with the test frame, within which the jack, load cell and 'dead' masses are housed, on the left. The pump unit is in the middle of the figure while the electronic control unit is on the right. The output from the stroke and load transducers within the vibrator are

passed to the control unit.

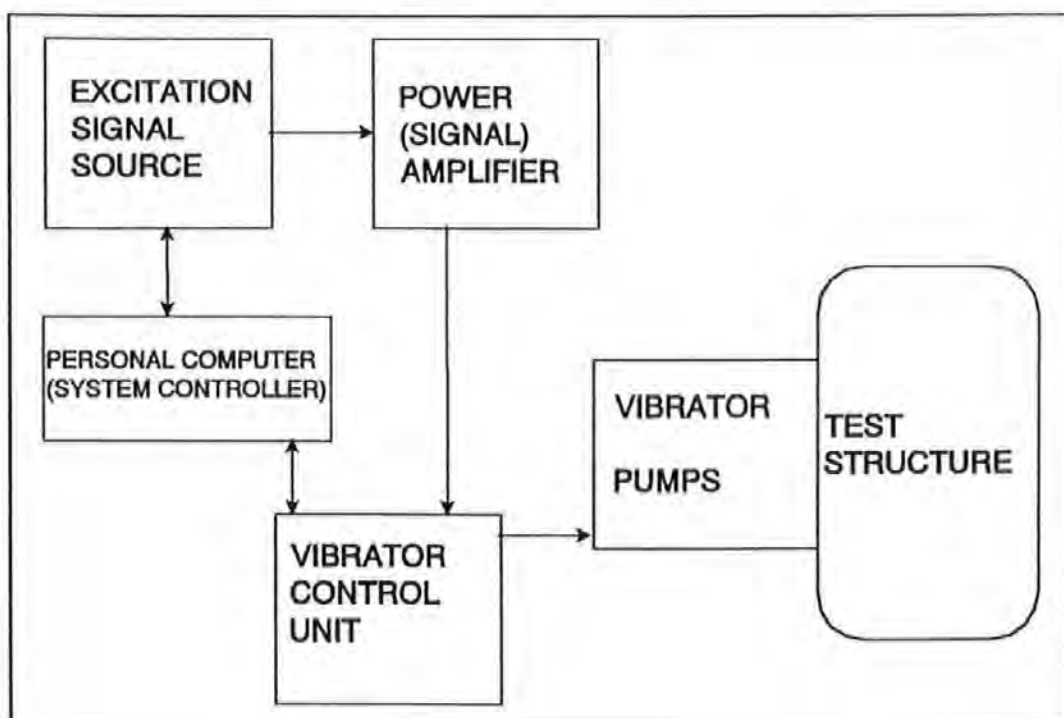


**Figure 6.2 Block diagram of excitation system**

The vibrator (shown in Figure 6.4) consists of a test frame, hydraulic jack, weights ('dead' masses) and load and stroke transducers. The total mass of the vibrator (excluding weights) is about 500kg. A computer is included within the system to control signal generation and acquire outputs from the transducers via the control unit. The test controller in Figure 2.1 can also act as the excitation system controller. An HP9122 computer and an HP3582A spectrum analyser were jointly used as the excitation system controller (see also Figure 6.1).

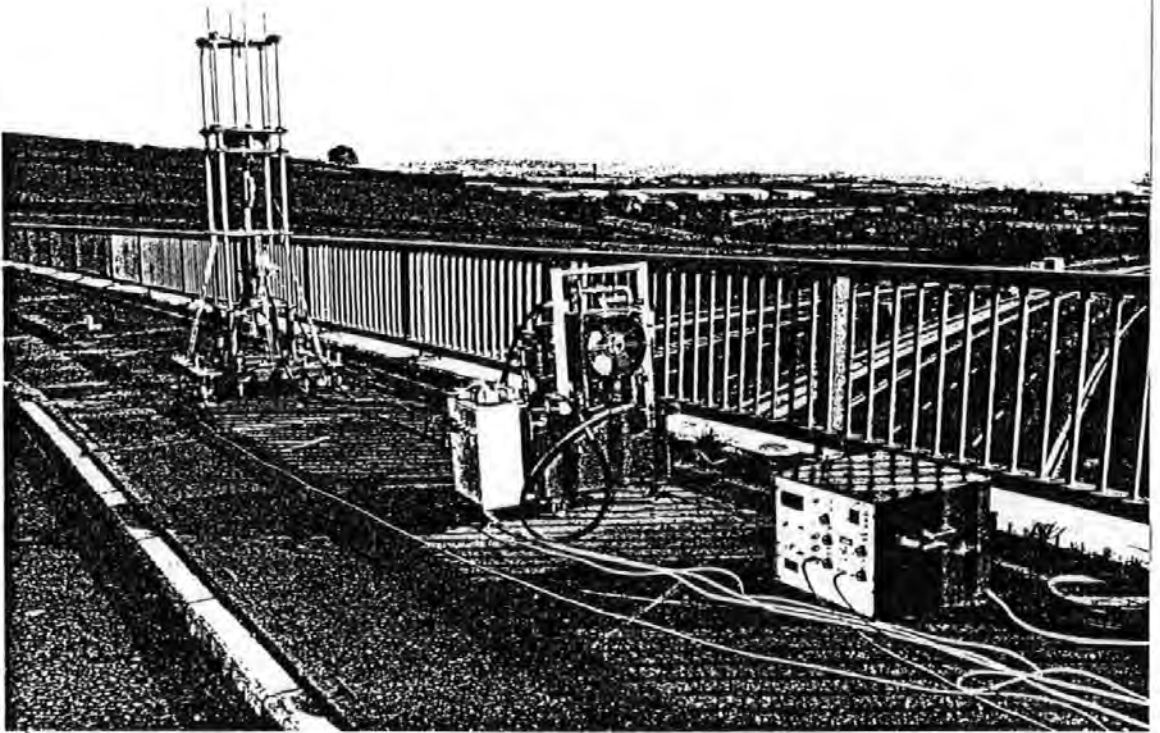
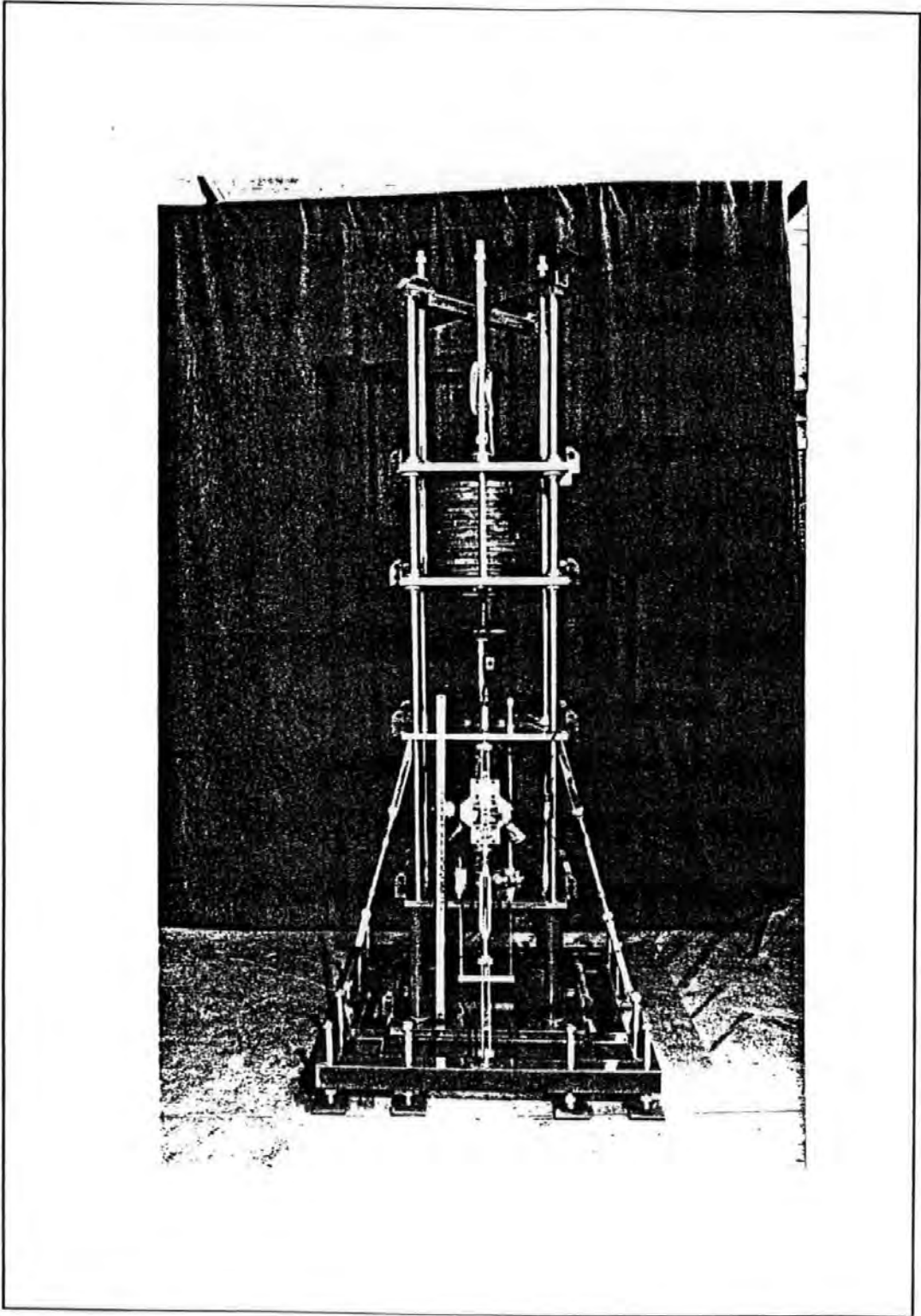


Figure 6.3 Excitation system on location



**Figure 6.4** The electro-hydraulic vibrator used in full-scale tests

## **6.2.2 Excitation signal generation**

### **6.2.2.1 Signal source**

An excitation signal generator enables generation of signals with known amplitudes and phase at desired frequencies for controlled excitation of the structure. The random noise source of the HP3582A spectrum analyzer and the signal generator on the vibrator electronic control unit were used for excitation signal generation. The spectrum analyzer noise source has variable signal levels. The maximum level (corresponding to about 6.2V peak-to-peak) was always used. The input attenuator on the vibrator control unit was used to control the level of signal generated by the unit or any external signal fed into it.

### **6.2.2.2 Signal types**

The main requirement of the excitation is that it has frequency content at the frequencies of the vibration modes of the structure. An excitation signal or function is defined by a mathematical relation and used as the input to the excitation mechanism. Three types of signals were used - sinusoidal, pure random and periodic random. The sinusoidal signal was used in a slow sine sweep test conducted at the beginning of each (field) test series so that predominant modes within the test frequency range could be identified. The signal was generated by the control unit of the vibrator. Sine testing is slow and also has the potential disadvantage of driving the structure into the non-linear range. In addition, the excitation energy at resonance could be excessive. For these reasons, sinusoidal tests were only conducted once, for each test series, to give an indication of the vibration modes.

Random signals generated by the spectrum analyzer were used in detailed tests. The noise

source produces a broadband periodic pseudo random signal. A random signal attenuates nonlinear response of the structure and allows more even distribution of the input energy over the frequency range of interest. Random vibration tests take a relatively short time to conduct. The random signal could be either periodic or pure random. If the signal is periodic, the period is automatically adjusted so that one period covers one span setting (frequency band) and the spectral analysis is not affected by the periodicity. Leakage errors (sub-section 6.4.2) are also avoided by using a periodic random signal. However, the frequency resolution and analysis bandwidth are fixed and constrained by the analyzer settings. These limitations do not apply to data obtained from pure random excitation. Thus, response data from pure random testing can be analysed with other analysis systems in order to eliminate some of the constraints of the spectrum analyzer. However, since the signal is not periodic, a weighting function (window) has to be applied.

### **6.2.3 Hydraulic jack and pumps**

The jack incorporated in the vibrator is a Dartec uni-axial servo-hydraulic jack supplied with two pumps and an electronic control unit. The jack can generate static or dynamic load in any given direction and has a frequency bandwidth of 0.001 to 100Hz. To generate the dynamic load in a specified direction, a suitable test frame (rig) incorporating a weight carrying system and its coupling to the jack has to be built. The frame and weight carrying system used are discussed in the next two sub-sections. The electronic control unit of the jack also controls the vibrator. The dynamic capacity of the jack is  $\pm 5\text{kN}$  while the total stroke is 300mm. A brief description of the characteristics of the jack is given below to serve as background knowledge before discussing performance characteristics (sub-section 6.2.6) of the system.

The jack is double-acting and driven by pressurised oil supplied from the two pumps. Flow of oil between the jack and pumps is controlled by an electronic servo-controlled valve (3.8 l/min capacity) mounted on the jack. The attainable stroke and frequency are limited by the piston (within the jack) velocity and oil flow rate. The jack will be unable to follow the input excitation signal if the velocities demanded are in excess of the capabilities of the jack or the flow demanded exceeds the output of the pumps. The maximum velocity is governed by the maximum flow rate of oil through the valve while the stroke amplitude attainable at any frequency is limited by the maximum piston velocity. The pressure supplied by the pumps is top-limited to 3000psi . Therefore, if the mass attached to the jack ram is too large, then oil pressure will be inadequate to provide a sufficient force magnitude to accelerate the mass as required.

#### 6.2.4 The test frame/rig

A test frame was designed to enable the jack exert dynamic forces in a vertical direction. A number of factors had to be considered in the design of the frame. Full-scale testing of civil engineering structures requires that equipment be portable, robust and relatively quick to operate on site. These requirements often lead to conflicting requirements of portability and rigidity of the test frame. The main factors considered were:

- \* **Robustness** - This translated to minimum height and maximum width to provide a rigid frame. However, the minimum/maximum stroke amplitude desired will often place a limitation on the minimum height that can be used. Although a height/width ratio of between 1 and 2 would be desirable, the maximum width of the area (for example, kerbs/footpath on highway bridges) on which the frame would stand controls the frame's width.

- \* **Symmetry** - As much as possible, there should be symmetry throughout the rig to prevent undesirable load components. It is equally important to ensure perfect alignment of the centre of the moving 'dead' masses with the jack's ram. Undue misalignment will cause damage to the leak proof seals between the cylinder of the ram and the jack's jacket.
  
- \* **Portability** - Ease of transporting to and assembling on site also plays a major role in selecting a suitable frame. This would require the frame to be in easy-to-handle components. However, rigidity must not be sacrificed.

A schematic diagram of the configuration adopted for the test frame is shown in Figure 6.5. Based on symmetry considerations, it was decided to use four corner supports each 2.16m long. The supports were made from galvanised steel and are held at intervals by steel plates through which they pass. Each of the plates is 500mm square except the base plate FT1 which is 640mm square. The base-frame is composed of 70mm X 70mm hollow square sections (to further reduce weight) and is 1000mm square in plan. Four nylon plain bearing medium duty castors were attached to the underside of the base-frame to ease transportation of the test frame from one location, on a structure, to another.

The jack (cylindrical shape) was bolted at each end to plates FT2 and FT3 which are screwed into the corner supports passing through them. Four tensioners, one on each side of the frame, attached between the mid-point of each side of FT3 and the base-frame serve to provide rigidity for the frame. The frame is very portable in that each part is separate and the whole unit can be assembled on site. On the average, it takes between 45 and 60 minutes to assemble the vibrator unit.

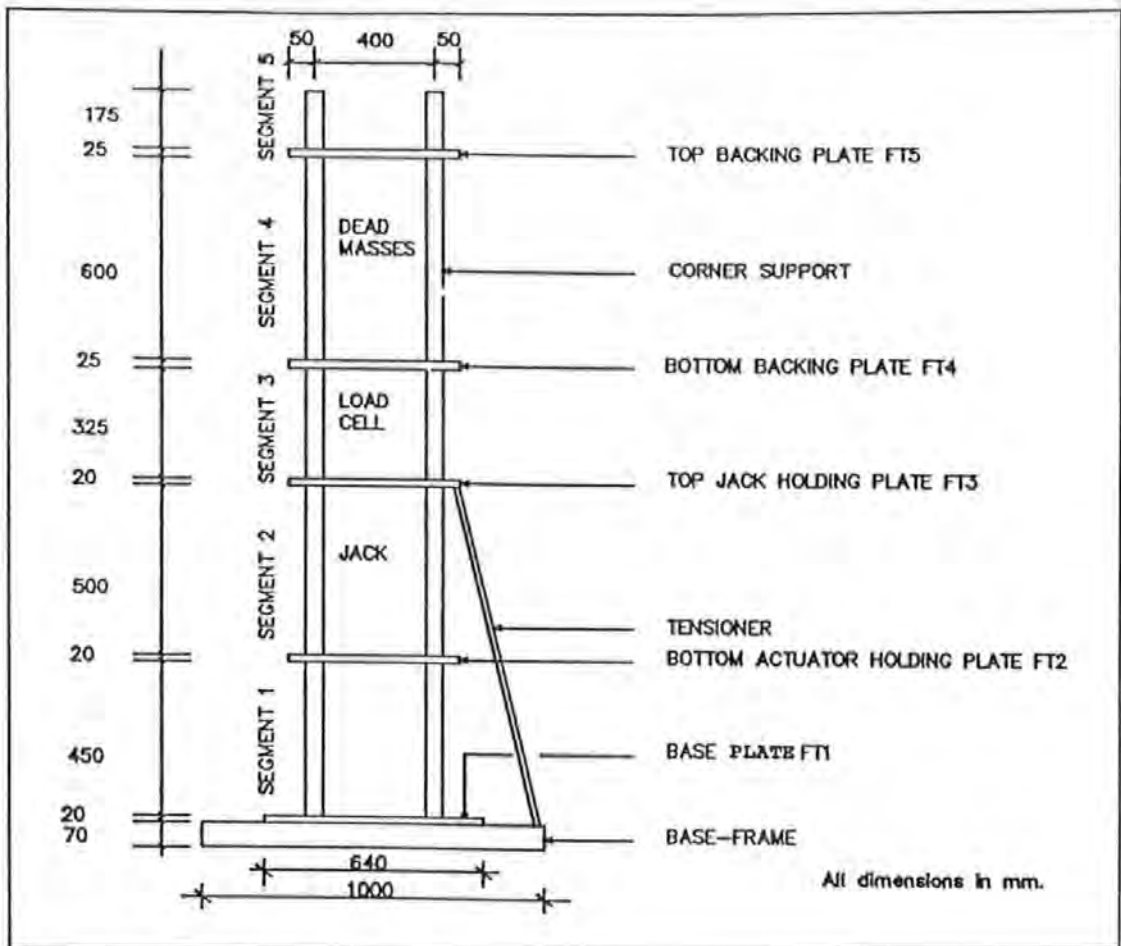


Figure 6.5 Side view of the test frame

### 6.2.5 Weight carrying system

Different configurations were considered for the weight carrying system (segment 4 in Figure 6.5). One involved bolting (another option was welding) four guide shafts onto the corner supports. The weights would then rest on a flat square plate with four open ball bushings at each corner. The idea was for the plate and masses to slide up and down the guide shafts. This configuration was rejected because of the possibility of grit in the open bushings and fatigue stresses likely to be developed at the connections between the shafts and corner supports.

Eventually, a weight carrying system consisting of two square backing plates, with the

(circular) 'dead' masses between them, rigidly clamped together with four studs - one on each side of the plates - was adopted. The plates have bored closed bearings (at each corner) through which the corner supports of the test frame pass. This configuration eliminates the need for any connection and also improves symmetry. The total weight is also reduced since the corner supports double as guide shafts. A sketch of this system is shown in Figure 6.6.

Steel was chosen over lead as the material to be used in making the 'dead' masses. This was meant to give a fine finish, accurate dimensions and mass - thereby improving overall symmetry and alignment. However, steel is lighter than lead so that more units are required to achieve the same mass. This directly translated into an increase in the overall height. Each 'dead' mass is 20mm thick with a diameter of 350mm and weighs approximately 15kg. The mass of the backing plates are always included in the value of the total moving mass.

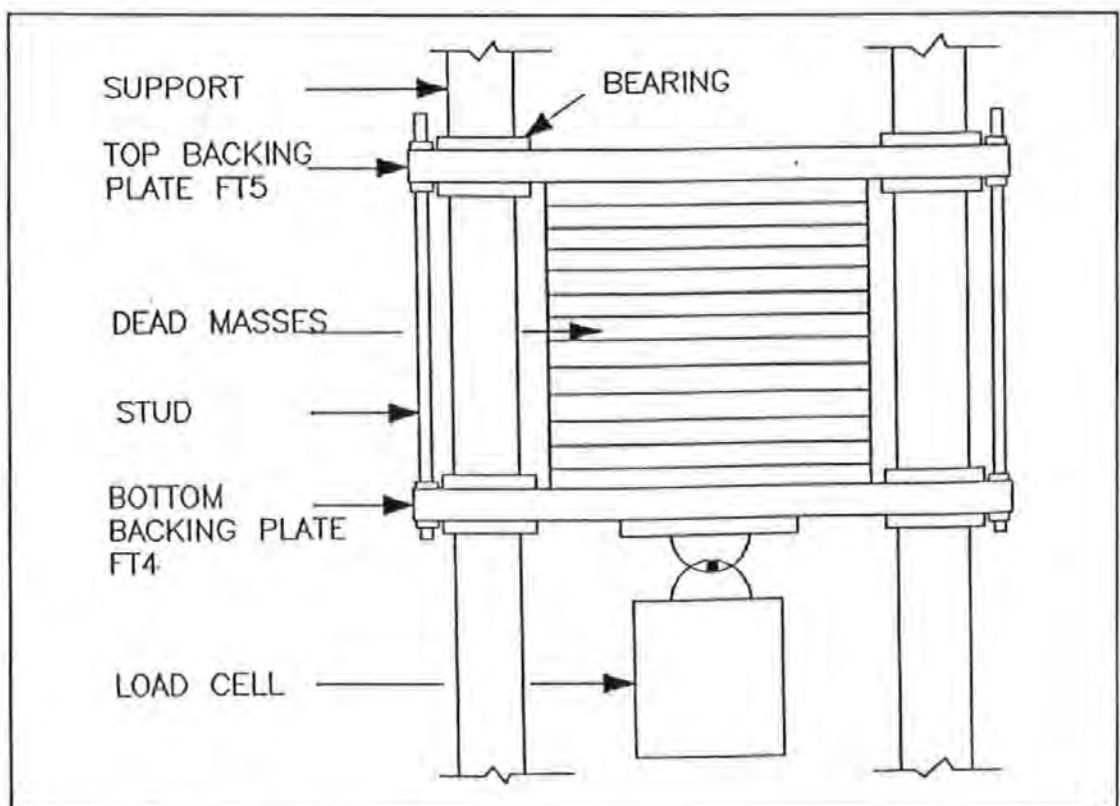


**Figure 6.6 Weight carrying system**

### 6.2.6 Performance characteristics

In operation, the test frame is supported on adjustable feet (attached to the base-frame) so that the centre line of the frame remains truly vertical at all times irrespective of the terrain of the test structure's surface. The frame is placed on the structure and not bolted or glued - the self weight is sufficient to ensure that full contact is maintained with the test structure during testing. A series of tests was conducted to obtain characteristics of the vibrator with respect to input voltage (of the driving signal), stroke amplitude, load generated, operating frequencies and total moving mass. The experimental set-up for the investigations is shown in Figure 6.7. Two types of excitation signals were used during the exercise - sinusoidal and periodic random within the frequency range of 0 - 25 Hz. Full details of the tests and results obtained are presented in Salawu and Williams (1992). The main performance characteristics will be briefly described here.

During the tests, the vibrator was under stroke command i.e. for a given frequency (or frequency span) and a fixed value of the total moving mass, the input stroke was varied. Variation of the stroke level was achieved by attenuating the excitation signal levels using a multi-turn potentiometer (command attenuator) on the vibrator control unit. The stroke amplitude for a given voltage level of the input signal and a known value of the command attenuator is given by  $AM = 0.3(IV)(CA)$  where AM is the peak to peak (or zero to peak) amplitude in mm, IV is the peak to peak (or zero to peak) input voltage in Volts and CA is the setting of the command attenuator in percentage.

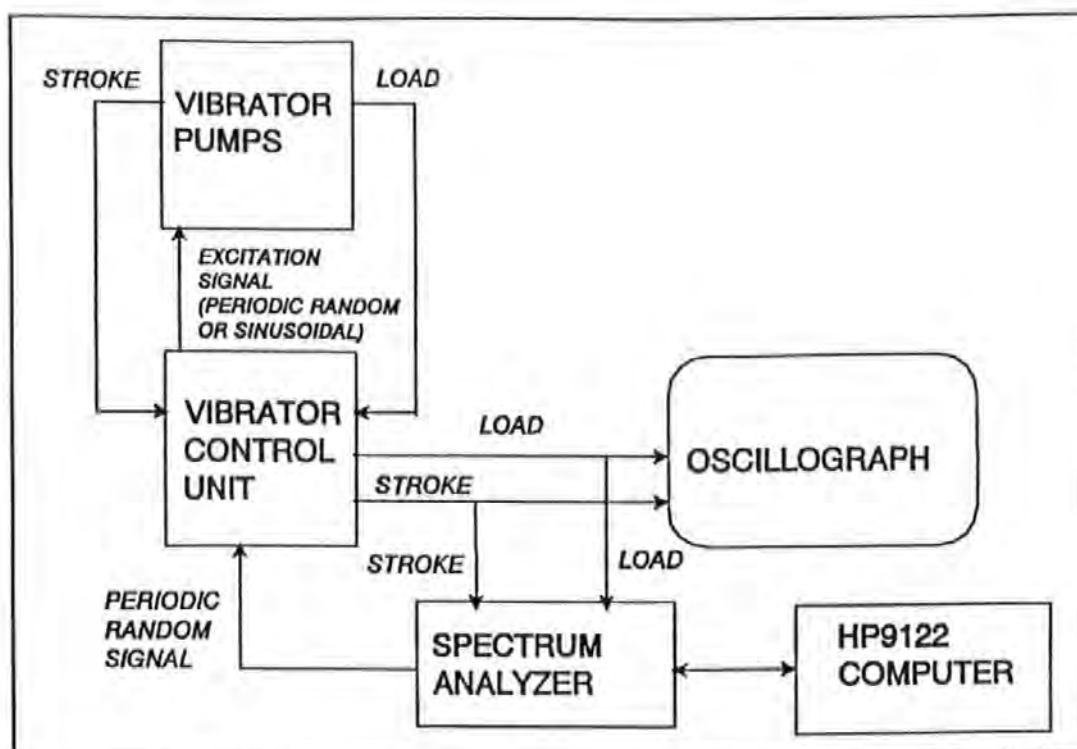


**Figure 6.7** Block diagram of experimental set-up to determine characteristics of vibrator

The relatively high slenderness of the test frame makes it susceptible to swaying and shaking at high frequencies. Even though the vibrator might be producing desired load levels, its performance could be unsatisfactory if the test frame has significant vibratory motion within the frequency range of interest. For the values of total moving mass investigated (113.05 to 258.05kg), vibration of the test frame occurred between 2.5Hz and 3.0Hz and at frequencies greater than 30Hz. The higher frequency vibration only occurs if the input signal voltage level is very high (within 20% of the  $\pm 10V$  DC maximum input command signal level). A premise inferred from the lower frequency vibration was that a natural frequency of the whole system (for the configurations considered) is probably between 2.5 to 3.0Hz.

### 6.2.6.1 Correlation between input signal, load response and stroke response

The periodic random signal was mainly used to investigate the correlation between the input signal and the vibrator response. The degree of association between the input signal and the load/stroke response was measured with the coherence function (sub-section 6.4.3). A value of 1.0 for the coherence function indicates good correlation at that frequency. There is good correlation between the excitation signal and the response signal from the load cell except at low frequencies ( $< 1.5\text{Hz}$ ) and low input signal levels. The second case can be eliminated by reducing the degree of attenuation at the vibrator control unit. There is a slight phase difference between the two signals for frequencies below 5Hz. Typical curves illustrating the characteristics are shown in Figures 6.8 and 6.9. There is also good correlation between the stroke amplitude response and the input signal (Figure 6.10).

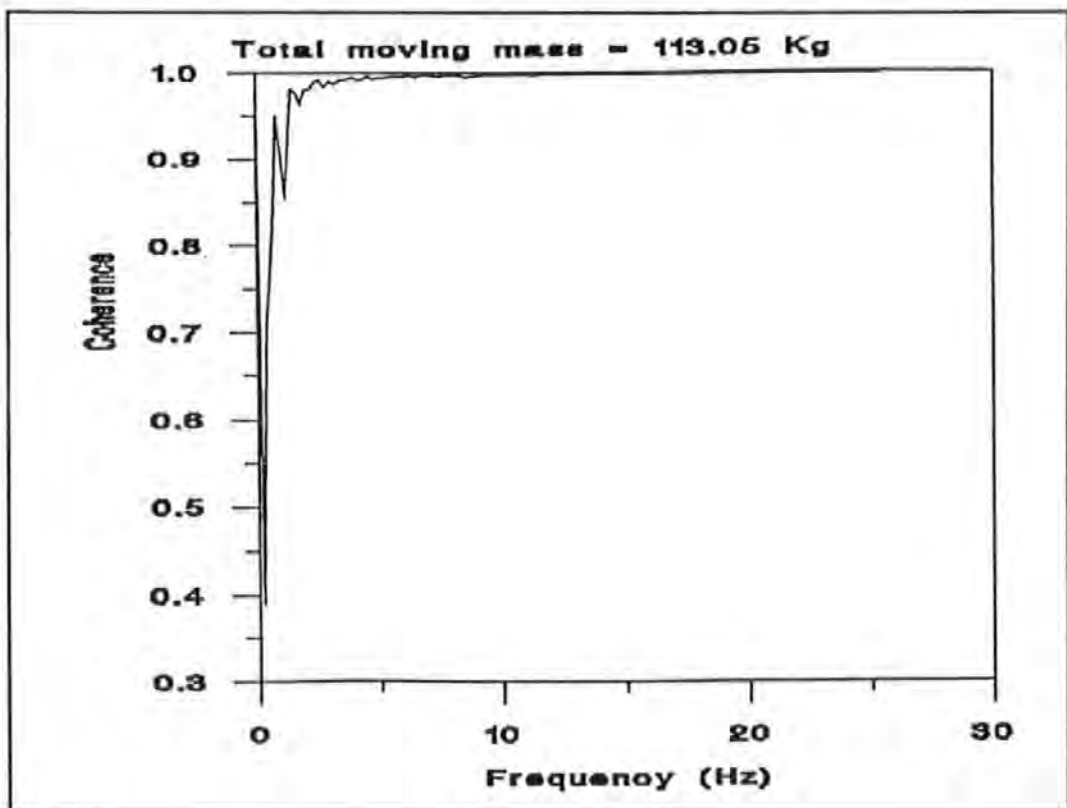


Figure 6.8 Coherence function between excitation signal and response from load cell

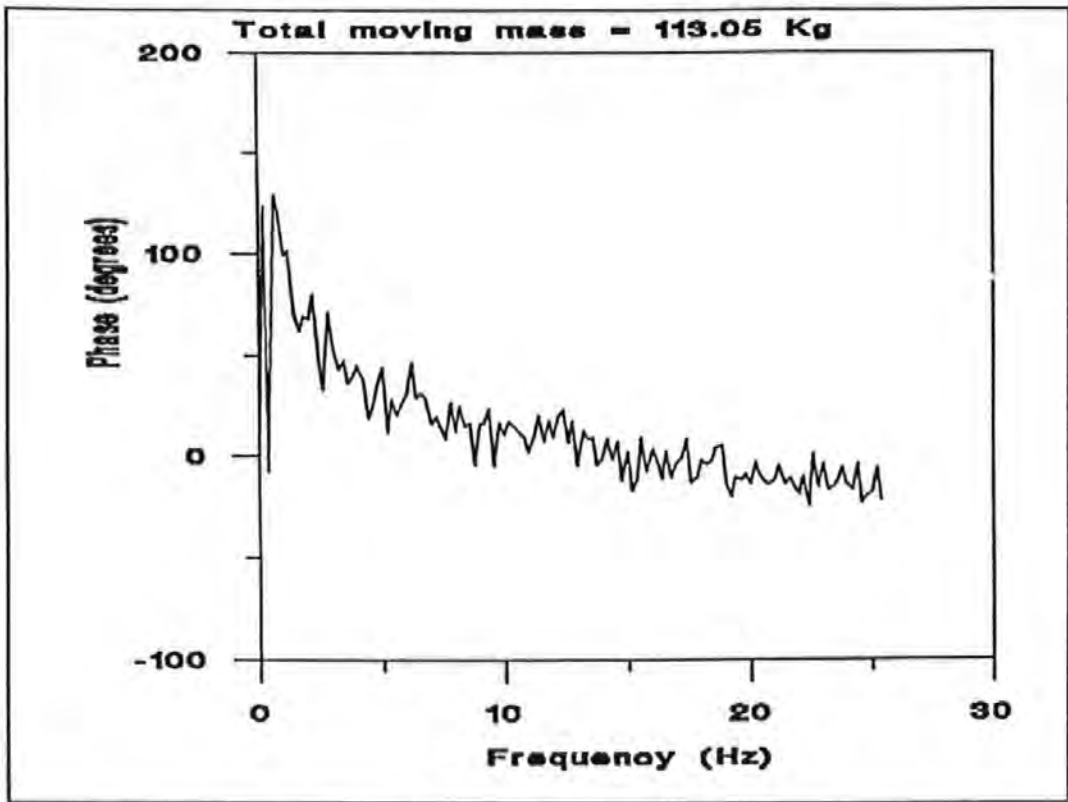


Figure 6.9 Phase of signal from load cell relative to the excitation signal

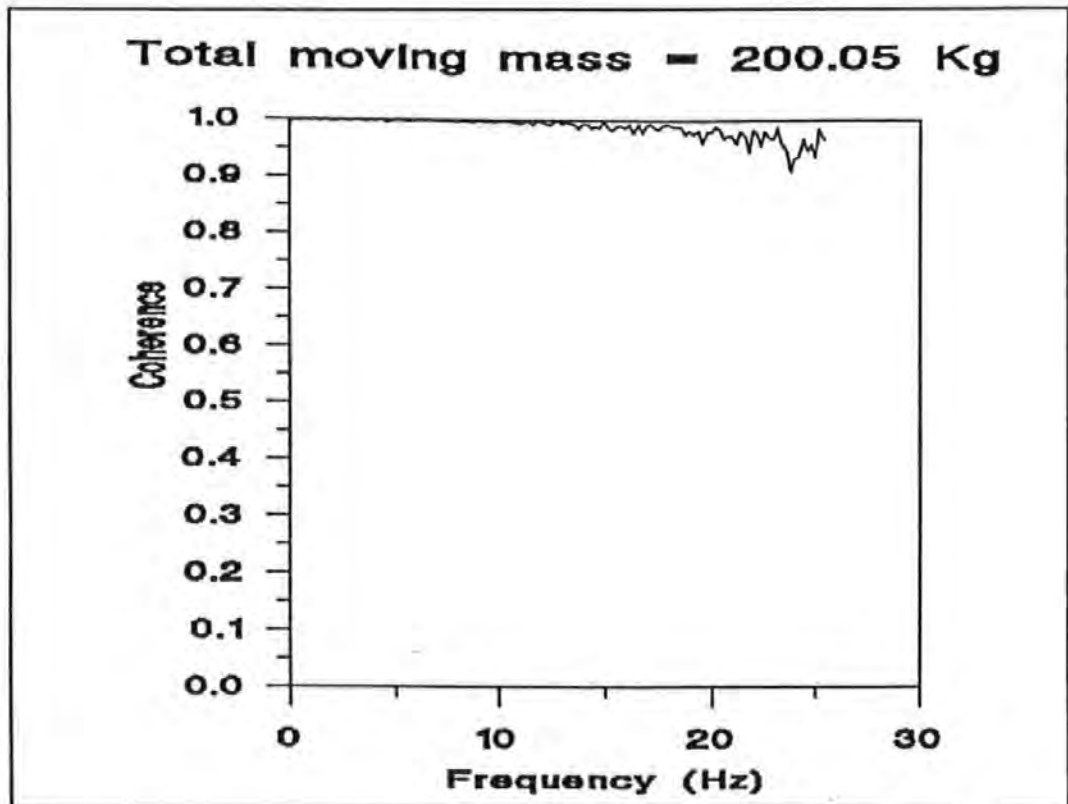


Figure 6.10 Coherence function between excitation signal and stroke amplitude

### 6.2.6.2 Characteristics of the load generated

Generally, there is an increase, up to a limiting value, in the load generated with increasing values of the input (signal) voltage and total moving mass. For a given input signal level, the magnitude of the load peaks (at a value depending on the total moving mass) at about 4Hz and remains constant (Figure 6.11). This flat load spectrum is part of the characteristics required of the system.

Determining the relationships between the load transferred into the structure and the load output from the built-in load cell would require comparing response from load cell(s) located between the rig and a test structure with the response from the built-in load cell. One possible problem with this approach is the need for the load cell(s) to support the weight of the rig while still being able to detect relatively small dynamic load variations. Suitable load cells were not available and an alternative scheme involving attachment of two motion transducers (accelerometers) to an isolated platform (test structure) supporting the vibrator was adopted.

The relatively high correlation (Figure 6.12) between the responses from the motion transducers and the built-in load cell indicates that the structure's motion was caused by the vibrator. The actual load transferred into the test structure is directly proportional to the measured load (by the built-in load cell) as long as the test frame is stable and remains rigidly in contact with the structure while the dead masses, backing plates, and the jack's ram are the only moving parts. This is usually the situation except at high frequencies and high input signal levels (as previously mentioned) when the top part of the rig starts shaking as a result of its relatively high slenderness. The constant of proportionality between the load experienced by the structure and the measured load does not affect

accuracy of identified dynamic parameters of the test structure.

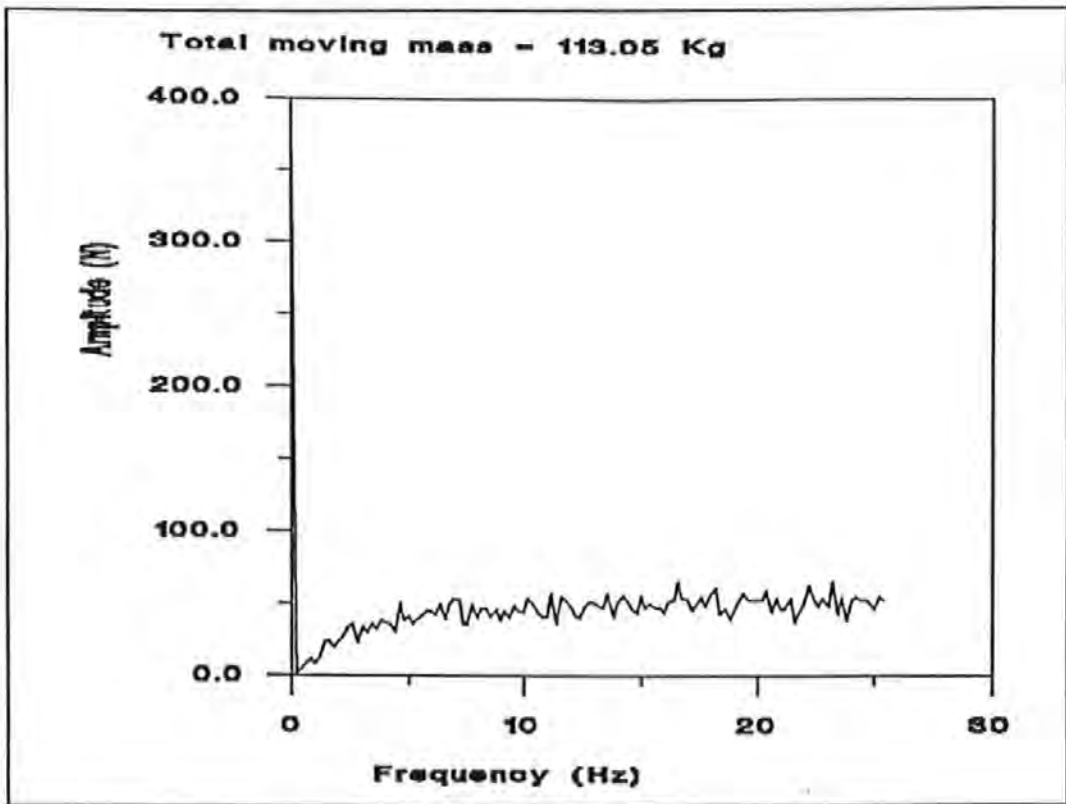


**Figure 6.11 Sample amplitude response of the load generated**

With the relationships between level of load generated, frequency, input signal level and total moving mass determined, the number of moving 'dead' masses that would give the highest load level was then investigated. The optimum number of 'dead' masses was found to be six, corresponding to a total moving mass of 200.05kg.

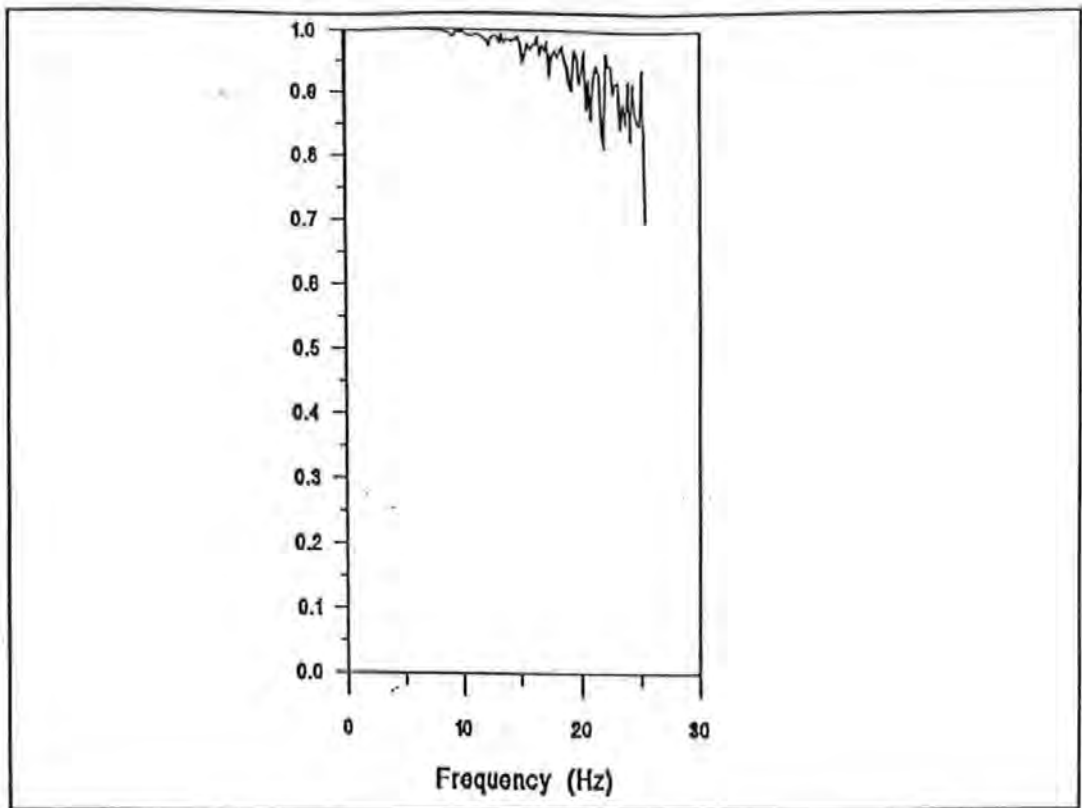


**Figure 6.12 Coherence function between transducer (accelerometer) and input load**

### 6.2.6.3 Characteristics of the stroke response

As would be expected from an electro-hydraulic vibrator, the stroke amplitude decreases with increasing frequency and increases with increasing excitation signal level. The amplitude becomes very low at frequencies above 10Hz (Figure 6.13). This behaviour is repeated irrespective of the total moving mass. The increase in amplitude with increasing input signal level peaks at a value which depends on the input voltage range and settings on the signal attenuator of the control unit. The optimum attenuator setting depends on the structure under test. The stroke amplitude spectra (Salawu and Williams, 1992) show that the attainable amplitude decreases under load. This loss of amplitude increases with total moving mass and total available stroke.

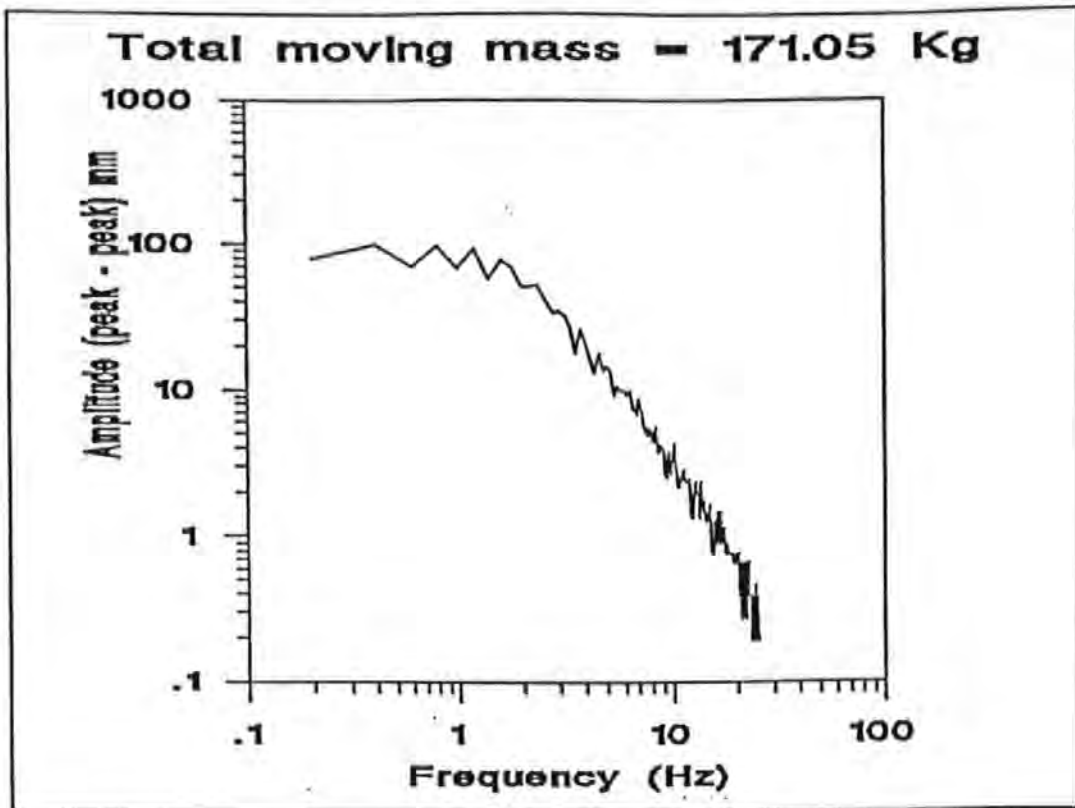


Figure 6.13 Auto-spectrum of stroke

### 6.3 Data Acquisition and Recording System

#### 6.3.1 Response transducers

Measurement devices are required to monitor the input to and response of a structure under forced vibration testing. The input is usually the excitation force while the responses of interest are the displacement, velocity and acceleration. Acceleration is currently the accepted method of measuring modal response and was the parameter measured. The input load was measured by the load cell incorporated within the vibrator while four accelerometers were used to measure the structural response.

The accelerometers are Schaevitz (LS Series) linear servo accelerometers capable of

measuring acceleration as low as  $10^{-6}$  g. The LS series are solid state, dc, closed-loop, force-balance accelerometers with accuracy, stability and reliability several orders of magnitude greater than open-loop types. The main sources of inaccuracy in the open-loop types, the mechanical spring and the displacement-to-voltage transducer, are eliminated. Each accelerometer has a seismic mass which is kept static by a small control system and the current necessary to maintain this position is monitored. This current is proportional to the acceleration experienced by the seismic mass.

The accelerometers were connected to the signal conditioning units by screened cables which deliver electrical power to them as well as transmitting the output signal to the signal conditioning units. Before and after each series of tests, the accelerometers were statically calibrated to ascertain consistency in sensitivity. The calibration procedure is further discussed in sub-section 6.6.1.

### **6.3.2 Signal conditioning equipment**

Signal conditioning refers to those processes that include a number of ancillary operations applied to the transducer output signals in order to obtain a useful electrical signal that can be transmitted or recorded. The signal conditioning equipment used consists of two units designed and built in-house. The first is an integrated unit consisting of six channels of offset units, amplifiers (with variable gains:  $\times 5$ ,  $\times 10$ ,  $\times 20$ ,  $\times 50$   $\times 100$ ) and low-pass analogue filters with cut-off frequencies at 15Hz and 60Hz. This unit also powers the accelerometers. The second unit is a filter 'box' containing six channels of low-pass analogue filters with cut-off frequencies at 10Hz, 20Hz, 30Hz, 40Hz, 50Hz and 60Hz.

The amplifiers were used to boost weak signals from the accelerometers and to amplify any

external excitation signal before 'feeding' it into the vibrator control unit. The filters were used to attenuate extraneous high frequency signals. Those on the second unit were also used as anti-aliasing filters for the PC based data acquisition system.

### **6.3.3 Signal monitoring and recording equipment**

Response of the structure, as test progressed, was monitored with oscilloscopes. A reference accelerometer was permanently connected to one oscilloscope channel. Signal outputs from the other accelerometers, load cell and excitation signal generator were also monitored in turn. This allowed detection of errors (such as loose cable connections) or any unexpected behaviour. The approach adopted was to monitor the signals being recorded on tape to ensure that the correct data is stored. An oscillograph was used to obtain hard copies, on ultra-violet paper, of selected portions of the measured signals. All the accelerometers and load cell were connected to the oscillograph.

Since complete real-time analysis was not possible, the conditioned analogue signals were recorded for further processing off-site. The recording was done on magnetic tapes using a RACAL Store 7 tape recorder in the frequency modulation (FM) mode. An advantage of FM recording is that it can record down to dc since a dc signal is simply represented by a constant deviation of the carrier signal. The tape recorder has seven tracks for recording in addition to a voice channel which allowed documentation of tests. The recording speed can be chosen to match the test frequency bandwidth. Other facilities such as flutter compensation are also provided.

#### **6.3.4 PC based data acquisition system**

This system consists of a 386 personal computer connected to a chassis housing one multi-channel analogue input module and a 12-bit analogue-to-digital converter with a maximum throughput in excess of 50000 samples/second and a calibrated input range of  $\pm 10$ Volts. The analogue input module has sixteen input channels and twenty programmable input ranges. WINDSPEED data logging software was used to control the data acquisition. The analogue-to-digital converter preconditions and scales the input signals. Both hardware and software were supplied by Biodata Ltd.

Using this system resulted in huge computer memory requirements to store the digitized time history data. Since a dedicated computer with sufficient hard disk size was not available, this system was laboratory based and only used on selected parts of the measured data. The signals recorded on tape were played back into the system after the tests.

#### **6.4 Analysis of Vibration Data**

Structural vibration response is usually measured as a time history record of amplitude versus time. The time history record is then subjected to data processing operations to extract 'refined' data for subsequent analysis. Early signal processing techniques were based on analogue methods. Introduction of the fast Fourier transform (FFT) and rapid development of efficient and affordable microprocessors resulted in a preference for digital processing methods. The signals are first converted to digital data using analogue-to-digital conversion (ADC) procedures. Mitchell (1985) has traced the development of the signal processing industry. In analysing random structural vibration data, the structure is usually assumed to be linear, time-invariant, stable, observable and physically realizable (Allemang

and Brown, 1988; Bendant and Piersol, 1986). Assumption of linearity of the structure is a good practical approximation as long as the amplitude of the force input remains small (Yar and Hammond, 1987).

#### 6.4.1 Discrete Fourier transform

In digital processing of random data, the Fourier series is used as an accurate way to approximate the discretized data. The Fourier series is based on the theory that any periodic signal may be evaluated as a combination of a number of sinusoidal signals with harmonically related frequencies. The discrete Fourier transform (DFT) is used as an approximate means of evaluating the coefficients of a Fourier series representing a finite time segment of data. The FFT is a specialised and very fast means of conducting a DFT and is used to estimate the frequency response function (FRF) from experimental data. Details of digital processing and DFT can be found in Bendant and Piersol, (1980), Bendant and Piersol, (1986), Bracewell (1978), Castro (1989), Curtis, (1988) and Newland (1975). Only basic and important stages of the process are highlighted in this and the next sub-section.

The complex Fourier transform  $U(jf)$  of  $u(t)$  is given by

$$U(jf) = \int_{-\infty}^{\infty} u(t) e^{-j2\pi ft} dt \quad (6.1)$$

where  $u(t)$  is the time history of a process  $u$ .  $f$  and  $t$  are the frequency (in Hz) and time variables respectively. The FFT only operates on a function with a non-negative independent variable and exists within finite limits of a stationary process. Thus, only a finite range of Equation (6.1) is of interest. Equation (6.1) then becomes

$$U(jf) = \int_0^T u(t) e^{-j2\pi ft} dt \quad (6.2)$$

where  $T$  is the record length of  $u(t)$ .

In digital processing, the function  $u(t)$  to be transformed only exists as  $u_n$  ( $n=0, N-1$ ) at  $N$  discrete values equally spaced in the time domain. The DFT then becomes

$$U(jf_k) = \Delta t \sum_{n=0}^{N-1} u_n e^{-j \frac{2\pi kn}{N}} ; k = 0, 1, 2, \dots, N-1 \quad (6.3)$$

$\Delta t$  is the sampling interval and  $(1/\Delta t)$  is the sampling rate (frequency). Equation (6.3) gives the spectrum values  $U_k = U(jf_k)$  at  $N$  discrete frequencies ( $k\Delta f$ ) where  $\Delta f = 1/T$  is the frequency resolution. The Fourier coefficients obtained using DFT are only unique for the first  $N/2$  values. Hence, the maximum frequency that can be sampled, called Nyquist frequency  $f_{\text{NYQ}}$ , occurs when  $k = N/2$  i.e.  $f_{\text{NYQ}} = (N\Delta f)/2 = N/2T = 1/(2\Delta t)$ .

To enhance the quality of the FRF (especially with random excitation) computed using FFT, ensemble averaging is used. The time history record of total length  $T_T$  is divided into  $b$  data blocks each of record length  $T$  ( $= T_T/b$ ) as shown in Figure 6.14. Each block is assumed periodic (with period  $T$  and base frequency  $1/T$ ) and digitized into  $N$  discrete values at equal intervals  $\Delta t$ . Before further data processing, statistical analyses to remove spurious trends and ascertain data quality are performed on each block. The discretized data is Fourier transformed into the frequency domain as described above.

The process illustrated in Figure 6.14 is sequential averaging i.e. the spectrum of consecutive blocks are added and the average spectrum computed. In practice, it is often better to use overlap averaging (Ewins, 1984) as shown in Figure 6.15. In this case, the

transform is performed as soon as possible using the most recent  $2N$  data values even though some of these may have been used in the previous transform. This approach leads to a better estimate of the average spectrum. The accuracy of a single spectral estimate increases with the square root of the number of averages (Brownjohn et al, 1987). However, excessive averaging could lead to a reduction in frequency resolution since  $T_T$  is constant.

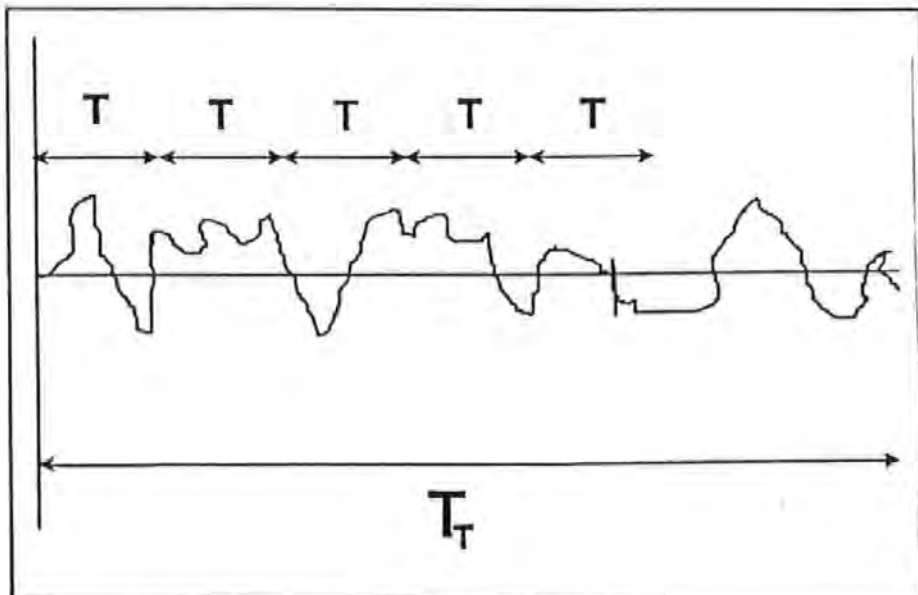


Figure 6.14 Partitioning of time history

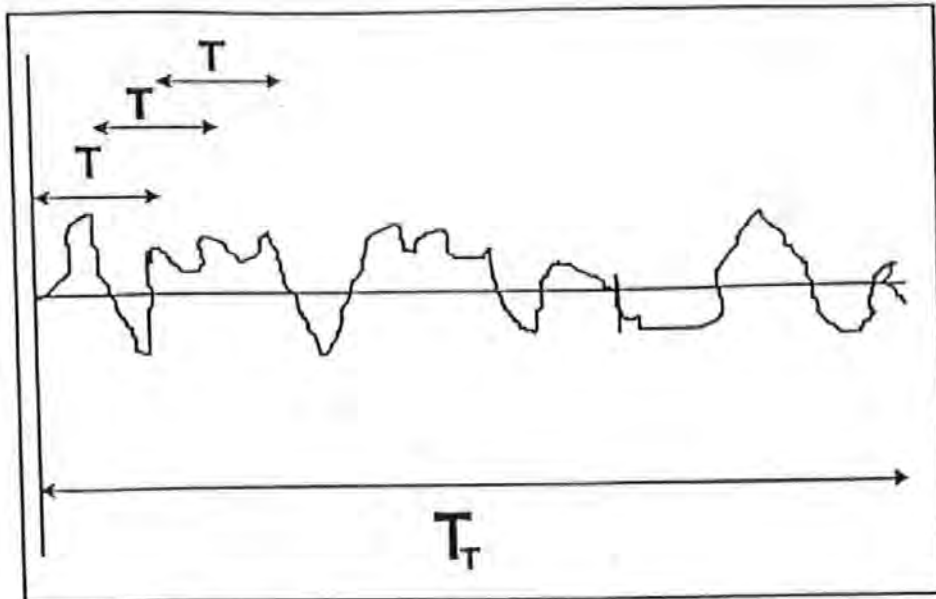


Figure 6.15 Overlapp averaging

#### 6.4.2 Signal processing errors

The limitation on maximum frequency content and the implied periodicity within the record length (or of each data block) introduce errors in the DFT process. Consequently, any quantity derived from the DFT will also be susceptible to these errors. An appreciation of these factors is necessary to avoid erroneous results. Brief details of the main errors introduced by digital signal processing are described below.

##### (a) Quantization errors

Quantization errors arise as a result of transforming the original analogue time history record into a digital signal having a number of distinct levels. Let an analogue signal  $u(t)$  be quantized with a step size  $\Delta u_n$  and  $u_n$  be the nearest quantising level to an instantaneous amplitude in  $u(t)$ . Then, all amplitudes, in the original signal, within the range  $(u_n - \Delta u_n/2)$  to  $(u_n + \Delta u_n/2)$  will be referred to the nearest level ( $u_n$ ) during analogue to digital conversion (ADC). If the quantization is done properly i.e. choosing suitable  $\Delta u_n$ , the true levels of the original signal will be well approximated. To reduce quantization errors and

improve resolution, it should be ensured that the time history occupies as much of the quantizing levels as possible. This entails setting suitable sensitivity levels on the signal analysis equipment.

### **(b) Aliasing**

Aliasing is an error introduced by the ADC procedure in digital processing and occurs if an inappropriate sampling rate is used in the digitization process preceding digital Fourier analysis. Redundant data results if the sampling interval is too short while a large sampling interval leads to confusion between low and high frequency components in the original data. As a result of aliasing, all frequencies higher than  $f_{\text{NYQ}}$  will appear folded (aliased) below  $f_{\text{NYQ}}$  in the Fourier spectrum.

For any frequency  $f$  ( $0 \leq f \leq f_{\text{NYQ}}$ ), the higher frequencies aliased with  $f$  are given by  $(2nf_{\text{NYQ}} \pm f)$ , where  $n$  is an integer. This condition distorts the spectrum in the region of the Nyquist frequency and leads to a confusion between low and high frequency components of the original data. Aliasing is prevented by using analogue low-pass filters (anti-aliasing filters) before ADC to remove portions of the original signal with frequencies above  $f_{\text{NYQ}}$ . To ensure that all frequencies above  $f_{\text{NYQ}}$  are rejected, it is usually necessary to set the filter cut-off frequency to about 60% - 80% of  $f_{\text{NYQ}}$  depending on the sharpness of the filter.

### **(c) Leakage**

The DFT necessarily assumes the input signal to be periodic in the data window of length  $T$  seconds. However, this is not usually true for real data such as those obtained from pure random excitation. This leads to the problem of leakage in which the power in a single frequency component leaks into adjacent frequency bands of the spectrum. The physical

limitation of taking measurements within a finite time period can also lead to leakage. Leakage error leads to distortion in the Fourier spectrum by broadening peaks and causing appearance of side lobes. The coherence at resonant frequencies is also reduced (Olsen, 1986). For a signal truly periodic in the time window, leakage does not occur.

Leakage is minimized by multiplying each data block, before FFT, by a weighting (window) function which forces the data to appear periodic within the time window by assigning low weights to the end values. The analysed signal is therefore a product of the original signal and the weighting function. It is necessary to scale up the windowed data due to a reduction in energy content as a result of windowing. Various window functions are available (deSilva, 1986) and choice of a suitable function depends on the signal type.

#### **(d) Poor frequency resolution**

Another problem encountered in digital processing via DFT is that of inadequate frequency resolution. This is particularly important for lightly damped structures and at regions of resonance. Inadequate frequency resolution implies that there are not sufficient spectral lines to accurately define the spectrum at areas of interest and can give rise to low coherence and bias errors. This is primarily due to a limited number of available discrete data points and the need to take measurements within a limited time length. The problem of inadequate frequency resolution is usually solved by zoom processing techniques in which the available spectral lines are concentrated within a narrow frequency range (Ewins, 1984).

### 6.4.3 Frequency response function calculation

Various parameters characterizing structural vibration signals are estimated using the FFT. In the frequency domain, the parameters of interest are the auto-spectrum, cross-spectrum and frequency response function (FRF). A simple single input-output system to illustrate FRF computation is shown in Figure 6.16.

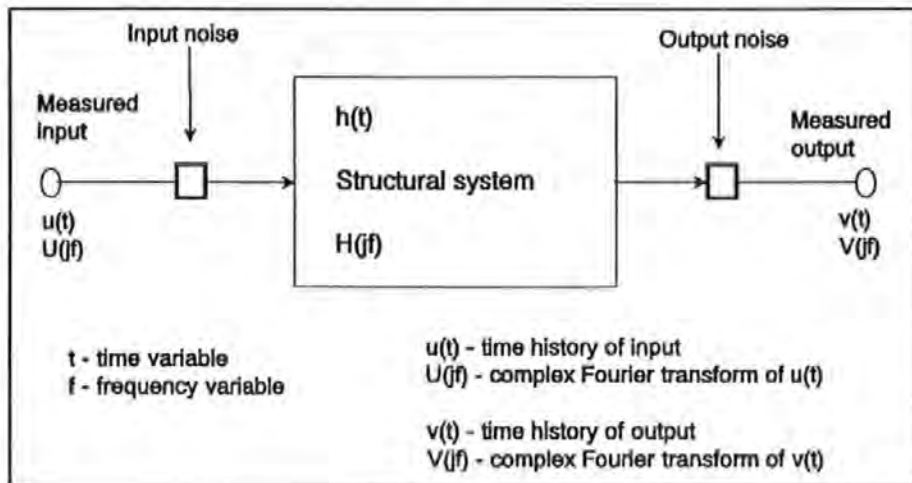


Figure 6.16 Single input-output system

The one-sided auto-spectral density function of the input  $G_{uu}(f)$  and output  $G_{vv}(f)$  are given by

$$\begin{aligned} G_{uu}(f) &= U^*(jf) U(jf) \\ G_{vv}(f) &= V^*(jf) V(jf) \end{aligned} \quad (6.4)$$

where  $U^*(jf)$  is the complex conjugate of  $U(jf)$ . The cross-spectrum between the input and output is a description of the common correlated frequency composition in each signal and is defined as

$$G_{uv}(jf) = U^*(jf) V(jf) \quad (6.5)$$

The FRF  $H_1(jf)$  is computed from complex ratios of the average cross-spectrum of the input (excitation) and response to the average auto-spectrum of the input and is expressed as

$$H_1(jf) = \frac{G_{uv}(jf)}{G_{uu}(f)} = \frac{U^*(jf) V(jf)}{U^*(jf) U(jf)} = \frac{V(jf)}{U(jf)} \quad (6.6)$$

Equation (6.6) is the most common method of estimating the FRF. If sufficient averaging is used, all the uncorrelated noise disappears from  $G_{uv}(jf)$  thereby enhancing  $H_1(jf)$ . Input noise could lead to contamination of the input auto-spectrum  $G_{uu}(f)$ , leading to FRF estimation lower than normal. This is particularly crucial at resonances where the true input auto-spectrum is low so that effect of measurement noise on  $G_{uu}(f)$  becomes significant.

To alleviate this problem, an alternate method of estimating the FRF has been proposed (Mitchell, 1982). The method computes the FRF using the estimator  $H_2(jf)$  defined as

$$H_2(jf) = \frac{G_{vv}(f)}{G_{uv}(jf)} \quad (6.7)$$

$H_2(jf)$  is contaminated by noise in the output. Since the system output is high around resonance (leading to insignificant output noise), Equation (6.7) gives a better estimate of the FRF in the resonance region (Mitchell, 1985). Some FFT systems use Equations (6.6) and (6.7) to respectively compute the FRF in regions of low magnitudes (anti-resonances) and high magnitudes (resonances).

An indication of the quality of data is given by the coherence function  $\gamma_{uv}^2(f)$ . The coherence function can be interpreted as the fractional part of the mean square value at the output that is contributed by the input at the frequency of interest (Bendat and Piersol,

1986).  $\gamma_{uv}^2(f)$  is given by

$$\gamma_{uv}^2(f) = \frac{|G_{uv}(jf)|^2}{G_{uu}(f) G_{vv}(jf)} \quad (6.8)$$

The coherence function varies between 0 and 1. It is 1 when  $u(t)$  and  $v(t)$  are not contaminated with noise.  $\gamma_{uv}^2(f)$  lower than 1 is indicative of, among other things, presence of measurement errors and possible system non-linearities. It should however be noted that coherence will not detect cross talk (within the analysis equipment) which arises when the input signal is much larger than the output signal (Mitchell, 1985).

#### 6.4.4 Signal analysis equipment

The HP3582A spectrum analyzer (Hewlett-Packard, 1979) was mainly used to compute FRFs. The analyzer is a FFT based digital instrument with dual measurement channels. It uses the H<sub>1</sub> FRF estimator, has four (two in both frequency and time domain) averaging types and zooming facilities. The frequency domain averaging are similar to those described in sub-section 6.4.1. For the overlap averaging, the latest spectrum is weighted by 1/4 and added to the previous average (weighted by 3/4) such that the Nth spectrum before the current one is given the weight  $(1/4)(3/4)^N$ .

The analyzer has built-in signal input sensitivity selectors, analogue-to-digital converters, anti-aliasing filters and three window functions. It also has 256 and 128 spectral display points for single and dual channel, respectively, operation. This fixes the frequency resolution for a given frequency band (sub-section 6.4.1). Operation of the analyzer can be remotely controlled with a computer using an HP-IB interface. An HP9122 computer was used for this purpose and to also retrieve the FRF data from the analyzer's memory

buffer. The FRFs were subsequently transferred to an OPUS 386SX PC, using the utility program LIFUTIL (Hewlett-Packard, 1990), for further analysis to extract dynamic parameters.

FRFs of selected parts of the data were also computed using two commercial data analysis software packages - ADEPT (Roberts, 1990) and FAMOS (IMC, 1989). ADEPT is a suite of programs for acquiring and analysing time series data while FAMOS is a general purpose signal analysis software that operates in MS-Windows. As a result of the general nature of FAMOS, a macro (called sequence) was written to implement the  $H_1$  FRF estimator using sequential averaging procedures. The softwares were used in conjunction with the PC based data acquisition system. Using these programs allows easy access (as compared to the spectrum analyzer) to the time history data (in digital form) and affords the opportunity to vary the frequency resolution. Preliminary analyses were conducted to ensure that the three methods (HP3528, ADEPT and FAMOS) produce similar results.

## **6.5 Modal Parameter Extraction**

A variety of methods for analyzing vibration response data in order to extract modal parameters is in existence. The methods range from simple single mode techniques to complex and sophisticated multi-mode algorithms. Some of the algorithms only differ in the numerical implementation of a basic mathematical model. The best method to use depends on the particular application since there is no exact method - all methods being approximations. Modal extraction can be conducted in either the frequency domain or in the time domain. Hybrid methods also exist (Li, 1986). Methods that operate in the frequency domain (using FRF) are more common. Only frequency domain modal identification is considered. Detail review of modal parameter extraction methods can be

found in Budiwantoro and Jezequel (1990), Ewins (1984) and Rades (1985).

Frequency domain modal identification is based on fitting a mathematical expression of the FRF to the measured data. Assuming real modes, the expression for the displacement FRF (receptance) is given by

$$H_{ik}(j\omega) = \sum_{z=1}^m \left( \frac{A_{ikz}}{\omega_z^2 - \omega^2 + j2\xi_z\omega\omega_z} \right) \quad (6.9)$$

where	$H_{ik}(j\omega) =$	FRF measured at point $i$ for excitation at point $k$
	$A_{ikz} =$	modal constant for the $z$ th mode at point $i$
	$m =$	total number of measured modes
	$\omega =$	frequency (radians/seconds) variable
	$\omega_z =$	natural frequency for the $z$ th mode
	$\xi_z =$	viscous damping ratio for the $z$ th mode

Multi-degree-of-freedom (MDOF) methods utilize Equation (6.9) by performing a simultaneous fit of all resonance peaks of interest in the measured FRF. Thus, modal parameters of several modes within the analysis frequency band are simultaneously obtained. MDOF techniques are useful for systems with high modal density or high damping. Most of the MDOF methods account for effect of out-of-band modes by using either additional residual terms in Equation (6.9) or extra modes in the identification model. Many of the MDOF algorithms are quite complex and there is a tendency to use softwares based on them as 'black boxes' with the user having no feel for what is happening.

Single-degree-of-freedom (SDOF) methods require more user interaction. The user has

control over, among other things, the choice of points to be used in the fitting process. The procedure is slower and less automatic as compared with MDOF identification. However, of more importance is the fact that a better understanding of the structural dynamic behaviour and physical interpretation of the process is achieved. In SDOF identification, each resonance peak (mode) in the FRF is independently fitted. The basic assumption of the approach is that in the vicinity of resonance, the mode with the nearest natural frequency dominates the response.

Equation (6.9) can be rewritten as

$$H_{ik}(j\omega) = \frac{A_{ikr}}{\omega_r^2 - \omega^2 + j2\xi_r\omega\omega_r} + \sum_{z=1, \neq r}^m \left( \frac{A_{ikz}}{\omega_z^2 - \omega^2 + j2\xi_z\omega\omega_z} \right) \quad (6.10)$$

where  $r$  is the current mode number. SDOF methods assume that the second term in Equation (6.10) is negligible around each resonance  $r$ . Thus, the FRF (around each mode) is simply represented by

$$H_{ik}(j\omega) = \frac{A_{ikr}}{\omega_r^2 - \omega^2 + j2\xi_r\omega\omega_r} \quad (6.11)$$

Data points within the resonance region in the FRF plot are then fitted to Equation (6.11) to obtain the modal parameters for the current mode. Equation (6.11) represents a circle in the Nyquist plane and this characteristic is exploited in the circle-fit analysis. The three SDOF methods implemented are described below.

### 6.5.1 Inverse Method

This method is an alternative to the common circle-fit method and uses the fact that a function which generates a circle when plotted in the Nyquist (complex) plane will, when plotted as a reciprocal, trace out a straight line (Ewins, 1984). Development of the method has been described by Maia (1990). The inverse of the receptance around mode  $r$  is given by

$$\begin{aligned} \frac{1}{H_{ik}(j\omega)} &= \frac{\omega_r^2 - \omega^2 + j2\xi_r\omega_r\omega}{A_{ikr}} \\ &= \frac{\omega_r^2 - \omega^2}{A_{ikr}} + j\frac{2\xi_r\omega_r\omega}{A_{ikr}} \end{aligned} \quad (6.12)$$

Writing  $H_{ik}(j\omega)$  as  $H_{ik}$  for simplicity, Equation (6.12) can be separated into real  $\text{Re}(1/H_{ik})$  and imaginary  $\text{Im}(1/H_{ik})$  parts to yield

$$\frac{1}{H_{ik}} = \text{Re}\left(\frac{1}{H_{ik}}\right) + j\text{Im}\left(\frac{1}{H_{ik}}\right) \quad (6.13)$$

$$\text{Re}\left(\frac{1}{H_{ik}}\right) = -\frac{1}{A_{ikr}}\omega^2 + \frac{\omega_r^2}{A_{ikr}} \quad (6.14)$$

$$\text{Im}\left(\frac{1}{H_{ik}}\right) = \frac{2\xi_r\omega_r\omega}{A_{ikr}} \quad (6.15)$$

Equation (6.14) represents a straight line in  $\omega^2$  while Equation (6.15) represents a straight line in  $\omega$ . Plots of these expressions are shown in Figure 6.17. Considering Equation (6.14) and Figure 6.17a, the intercept of  $\text{Re}(1/H_{ik})$  with the horizontal axis gives the value of  $\omega_r$  while  $A_{ikr}$  is given by the reciprocal of the slope. With  $\omega_r$  and  $A_{ikr}$  known,  $\xi_r$  can be determined from the slope of  $\text{Im}(1/H_{ik})$ . The method is suitable for systems with relatively

well separated real (which has been implicitly assumed in the analysis) modes.

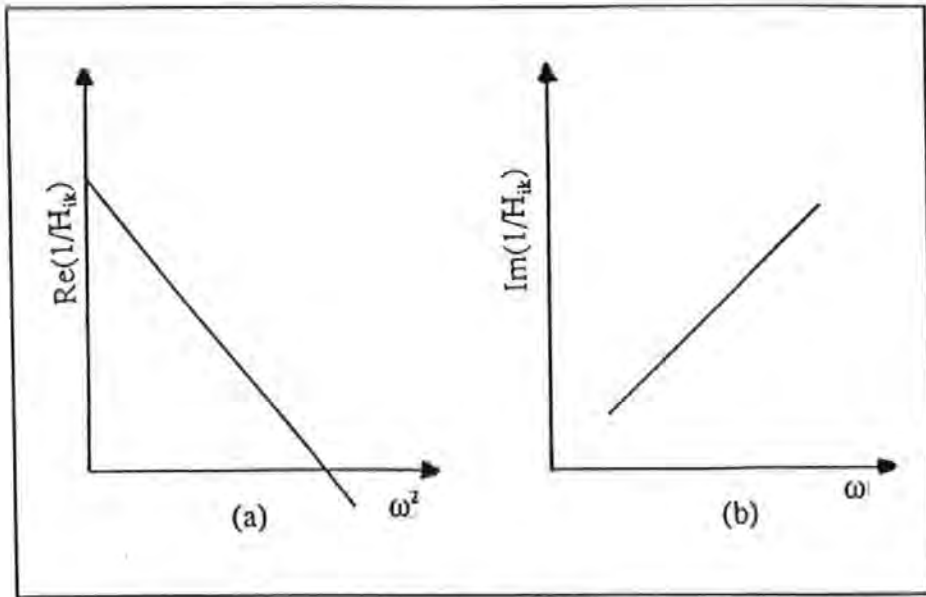


Figure 6.17 Real and imaginary parts of receptance

### 6.5.2 Direct least squares (DLS) method

This method was proposed by Tsang and Williams (1990) and belongs to the family of direct least squares methods. Development of the method starts with the frequency domain representation of the equation of motion as:

$$[K] - \omega^2 [M] + j\omega [C] = \frac{\{F(j\omega)\}}{\{X(j\omega)\}} = \frac{1}{[H(j\omega)]} \quad (6.16)$$

where  $[K]$ ,  $[M]$  and  $[C]$  are respectively the stiffness, mass and damping matrices; and  $\{X(j\omega)\}$  and  $\{F(j\omega)\}$  are respectively the complex Fourier transforms of the displacement response and force vectors.  $[H(j\omega)]$  is the FRF matrix. Each element  $H_{ik}(j\omega)$  of  $[H(j\omega)]$  represents the FRF measured at  $i$  for excitation at  $k$ . Considering these two ( $i$  and  $k$ ) DOF and using Equation (6.13), it follows that

$$\begin{pmatrix} 1 & -\omega^2 & 0 \\ 0 & 0 & \omega \end{pmatrix} \begin{pmatrix} k' \\ m' \\ c' \end{pmatrix} = \begin{pmatrix} \operatorname{Re}\left(\frac{1}{H_{ik}}\right) \\ \operatorname{Im}\left(\frac{1}{H_{ik}}\right) \end{pmatrix} \quad (6.17)$$

where

$$k' = \frac{k_r}{(\phi_{ir})(\phi_{kr})} ; m' = \frac{m_r}{(\phi_{ir})(\phi_{kr})} ; c' = \frac{c_r}{(\phi_{ir})(\phi_{kr})} \quad (6.18)$$

$k_r$ ,  $m_r$  and  $c_r$  are respectively the modal stiffness, mass and damping for mode  $r$ , while  $(\phi_{ir})$  is the element of the  $r$ th mode shape at point  $i$ . Equation (6.17) exists at each forcing frequency  $\omega$ . For  $N$  such frequencies, a total of  $N$  sets of equations can be formulated. The  $N$  frequencies are chosen within the resonance region. Combining the  $N$  equations, the following expression is obtained

$$\begin{pmatrix} N & -\sum_{n=1}^N \omega_n^2 & 0 \\ -\sum_{n=1}^N \omega_n^2 & \sum_{n=1}^N \omega_n^4 & 0 \\ 0 & 0 & \sum_{n=1}^N \omega_n^2 \end{pmatrix} \begin{pmatrix} k' \\ m' \\ c' \end{pmatrix} = \begin{pmatrix} \sum_{n=1}^N \operatorname{Re}\left(\frac{1}{H_{ik}}\right)_n \\ -\sum_{n=1}^N \omega_n^2 \operatorname{Re}\left(\frac{1}{H_{ik}}\right)_n \\ \sum_{n=1}^N \omega_n \operatorname{Im}\left(\frac{1}{H_{ik}}\right)_n \end{pmatrix} \quad (6.19)$$

Equation (6.19) is solved for  $k'$ ,  $m'$  and  $c'$  and the modal parameters obtained using the following expressions:

$$\omega_r^2 = \frac{k'}{m'} ; \xi_r = \frac{c'}{2\sqrt{m'k'}} ; A_{ikr} = \frac{1}{m'} \quad (6.20)$$

The DLS method is only applicable to systems with real modes.

### 6.5.3 Improved amplitude fitting (IAF) method

The IAF method (Rinawi and Clough, 1992) is an improvement of the SDOF amplitude fitting algorithm proposed by Clough et al (1987) and Mau and Wang (1989). At a given

forcing frequency  $\omega$ , the amplitude (magnitude) of the receptance, within the vicinity of mode  $r$ , is given by

$$|H_{ik}| = \frac{|A_{ikr}|}{\sqrt{(\omega_r^2 - \omega^2)^2 + (2\omega_r \xi_r \omega)^2}} \quad (6.21)$$

$$Q = \frac{P_r}{D}$$

where  $Q = |H_{ik}|$  and  $P_r$  (called modal participation factor) represents the magnitude of the modal constant. Equation (6.21) can also be written, after scaling by  $Q$ , as:

$$Q^3 D^2 - Q P_r^2 = 0 \quad (6.22)$$

Substituting  $D$  from Equation (6.21) into Equation (6.22) yields

$$Q^3 x_1 + Q^3 \omega^2 x_2 - Q x_3 = -Q^3 \omega^4 \quad (6.23)$$

where

$$\begin{aligned} x_1 &= \omega_r^4 \\ x_2 &= 4\xi_r^2 \omega_r^2 - 2\omega_r^2 \\ x_3 &= P_r^2 \end{aligned} \quad (6.24)$$

For a set of  $N$  frequencies around the resonance region, Equation (6.23) becomes

$$\begin{vmatrix} \sum_{n=1}^N Q_n^6 & \sum_{n=1}^N Q_n^6 \omega_n^2 & -\sum_{n=1}^N Q_n^4 \\ \sum_{n=1}^N Q_n^6 \omega_n^2 & \sum_{n=1}^N Q_n^6 \omega_n^4 & -\sum_{n=1}^N Q_n^4 \omega_n^2 \\ -\sum_{n=1}^N Q_n^4 & -\sum_{n=1}^N Q_n^4 \omega_n^2 & \sum_{n=1}^N Q_n^2 \end{vmatrix} \begin{Bmatrix} x_1 \\ x_2 \\ x_3 \end{Bmatrix} = \begin{Bmatrix} -\sum_{n=1}^N Q_n^6 \omega_n^4 \\ -\sum_{n=1}^N Q_n^6 \omega_n^6 \\ \sum_{n=1}^N Q_n^4 \omega_n^4 \end{Bmatrix} \quad (6.25)$$

The modal parameters can be obtained from the solution of Equation (6.25) using the following relations:

$$\begin{aligned}
 \omega_r &= x_1^{1/4} \\
 \xi_r &= \sqrt{\frac{x_2}{4\omega_r^2} + \frac{1}{2}} \\
 P_r &= \sqrt{x_3}
 \end{aligned}
 \tag{6.26}$$

#### 6.5.4 Implementation of the methods

The three methods described above all use receptance whereas inertance (acceleration FRF) is usually measured. Thus, the first step was to convert the measured inertance to receptance. Mixed language (C and Fortran) computer programs were written to implement the methods. Program TXT\_FRF was written for the IAF method while both the DLS and inverse methods were implemented in program SALMOD\_D. A post-processor MODPLOT was written to process results from SALMOD\_D so that the results can be viewed in various display formats. TXT\_FRF has its own results display modules which can also be used to graphically display FRFs. In the programs, options are available to remove the effects of other modes on the mode being analysed.

The methods as originally proposed do not account for the effects of modes outside the analysis frequency band. To accommodate effects of out-of-band modes, a procedure was adopted for the IAF method. The procedure adopted was to select two frequency points (one at either end of the analysis frequency range) to act as pivots. The error between the measured and regenerated FRFs is then minimized, using the pivots as origins, in a least squares sense. The fitting process when using the IAF method was also made iterative (the IAF algorithm as proposed by Rinawi and Clough (1992) is a non-iterative method). Thus, the IAF method was mostly used to analyse the measured data.

It should also be noted that the IAF method only gives the magnitude of the modal

constant. A simple approach was adopted to determine the phase. The phase of the modal constant was taken as the phase difference between the FRFs measured at the point in question and at a reference point on the structure. The modal constant was considered as positive or negative if the phase angle was between  $\pm 20^\circ$  of  $0^\circ$  or  $180^\circ$  respectively. Any other value of the phase angle indicates a complex mode. The flowchart of the module used to implement the IAF method, as modified here, is shown in Figure 6.18.

## **6.6 Repeatability and Accuracy of Results from Test System**

The degree of accuracy and repeatability of any measurement system has to be ascertained so that the level of reliability of the data obtained from the system can be determined. In this research, the systems of interest consist of the measurement transducers, signal conditioning, recording and processing equipment and the data analysis techniques adopted. The transducers, signal conditioning and recording equipment are the ones most likely to be affected by changes in environmental factors, especially temperature. To reduce this, all equipment (except of course the vibrator and pumps) were kept in a van during full-scale tests.

The load cell within the vibrator is stable within environmental fluctuations and has been pre-calibrated at 1V to 0.5kN. This factor was constant throughout the research period. The consistency of the accelerometers, signal conditioning and recording equipment was checked by calibrating them before and after each test series. Effect of temperature on their performance was also investigated and is discussed in sub-section 6.6.1.

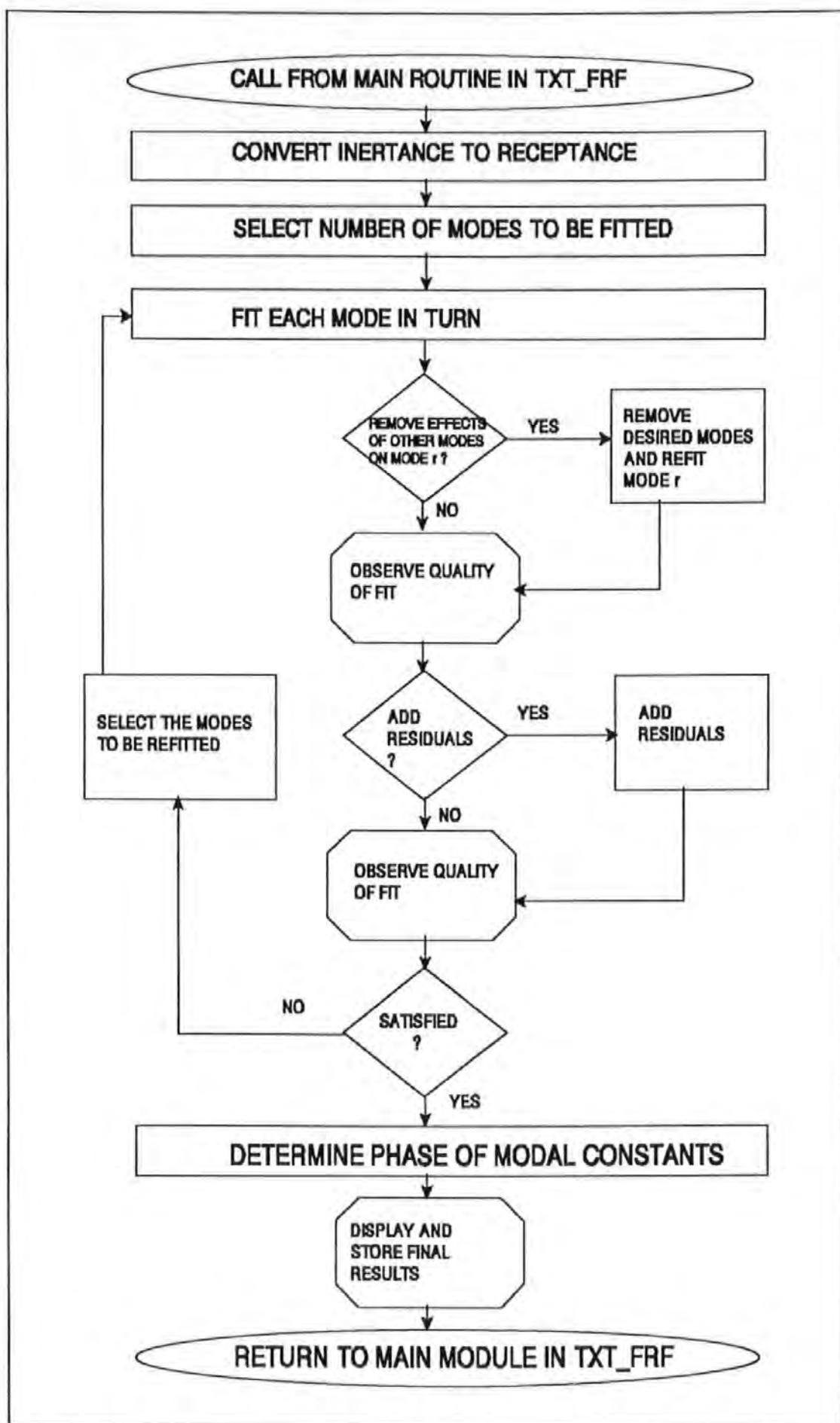


Figure 6.18 Flow chart of the module used to implement the modified IAF method

It is difficult, if not impossible, to quantify effects of random environmental factors and other experimental errors on the dynamic response of a prototype structure. Therefore, it is important to ascertain that the test and analysis systems are not significantly affected by changes in these factors. This would enable true changes in the structural response to be differentiated from errors introduced by the test configuration. Specifically, observed changes must be greater than inherent uncertainty of the test system. To investigate the reliability and consistency of the combined measurement and analysis systems, tests were conducted on a simply supported beam between 1992 and 1993. Results from the tests are reported in sub-section 6.6.2.

#### **6.6.1 Effect of temperature on signal acquisition and recording equipment**

The effect of temperature on the accelerometers, signal conditioning units and tape recorder was investigated in a temperature controlled room. The approach adopted was to measure the calibration factor for the whole system at various temperatures. The temperatures investigated were 10°C, 20°C, 25°C and 30°C. These values were felt to reasonably represent the likely temperature variation to be met on site. During all tests, the relative humidity was maintained at 52%. Only static calibration was done. The results also provided the factors necessary to convert voltage outputs to physical units.

The experimental set up is shown in Figure 6.19. The accelerometer was mounted on a Jones-Shipman universal vice type UX8238-41 which acted as the 'sine table'. The vice allowed inclination, with respect to the vertical, of the accelerometers at any desired angle. The angles were varied from 0° to 90° at 10° intervals in two opposing directions as shown in Figure 6.20. For an inclination angle of  $\pm\theta$ , the input acceleration is  $\pm g\sin\theta$  where  $g$  is the gravitational acceleration.

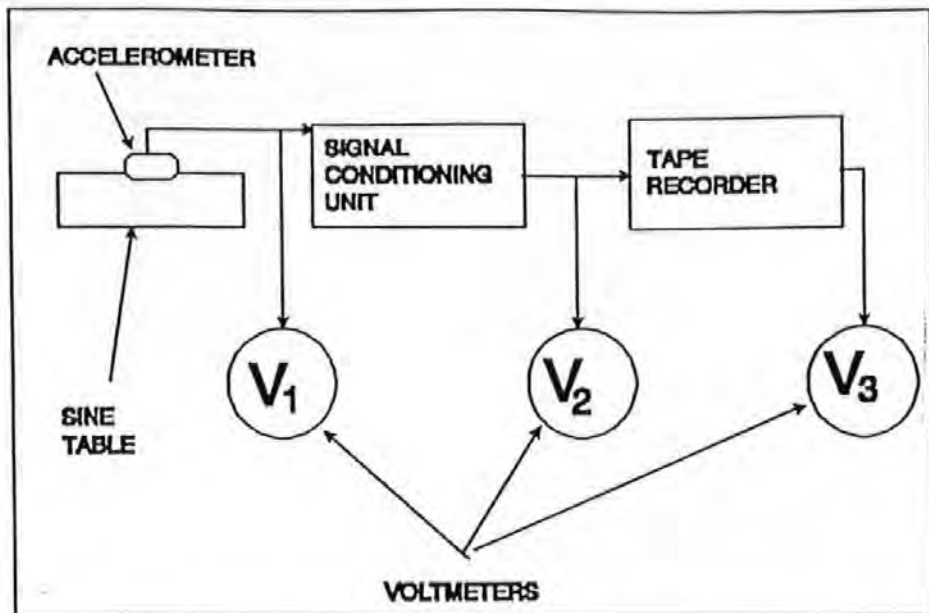


Figure 6.19 Experimental set-up for signal acquisition system calibration

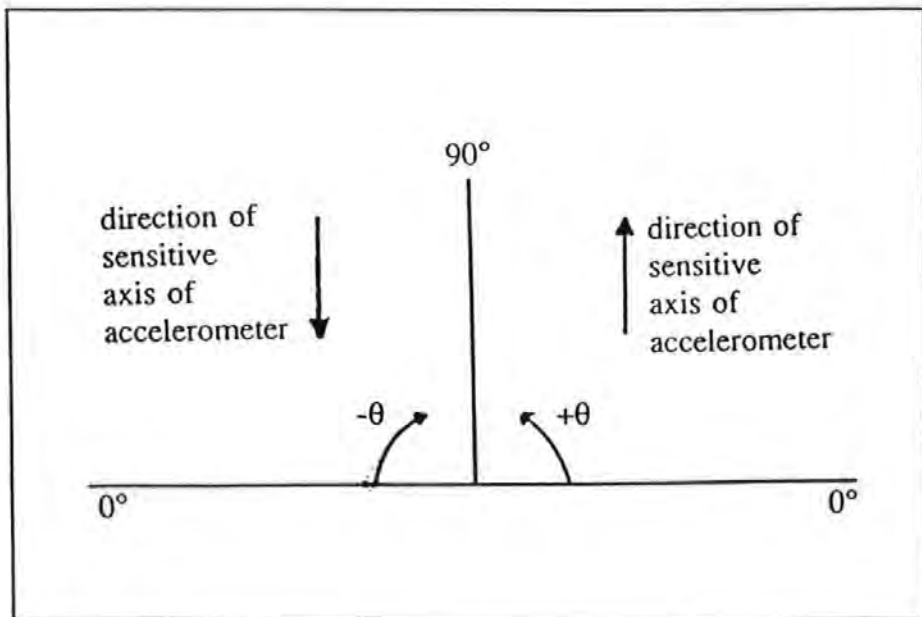


Figure 6.20 Inclination of accelerometers

For each inclination angle, it was intended to measure the output signal level at three points using voltmeters  $V_1$ ,  $V_2$  and  $V_3$  (Figure 6.19). This was meant to allow simultaneous calibration of the system and the component units. However, because of the two way flow of electrical power and signal between the accelerometers and signal conditioning unit,  $V_1$  was not used. Trial tests indicated that the readings from  $V_2$  and  $V_3$  were very similar (less than 1% difference). Thus, only values from  $V_3$  are reported here. In addition, it is only the calibration at  $V_3$  that is really required since the system's global sensitivity is desired. Readings were taken when the tape recorder was recording and when it was not. Both conditions gave the same readings.

Each accelerometer was calibrated on a specific channel on the signal conditioning unit and tape recorder. The same accelerometer-channel match was maintained during all calibration, laboratory and field tests. The calibration factors (Table 6.1) were obtained from the slopes of the least squares lines fitting plots of  $V_3$  against acceleration. From Table 6.1, it can be seen that the system calibration does not significantly fluctuate with temperature. This fact, coupled with the consistency of the factors obtained before and after each test series, demonstrate the stability and accuracy of the signal acquisition system. The results in Table 6.1 were obtained from the first calibration exercise before any full-scale tests. Subsequent calibrations were conducted at 20°C.

**Table 6.1 System calibration factors**

ASC	CSCU	CTR	Calibration factors (Volts/g)			
			10°C	20°C	25°C	30°C
6230	1	1	2.021	2.017	2.026	2.023
1653	2	2	1.670	1.662	1.667	1.656
1652	3	4	1.651	1.649	1.641	1.646
1658	4	5	1.679	1.682	1.700	1.680

ASC - Accelerometer serial number

CSCU - Channel on signal conditioning unit

CTR - Channel on tape recorder

### 6.6.2 Effect of random environmental factors

Twenty tests were conducted over a one year period on an I-section simply supported steel beam to determine consistency and reliability of the measurement and analysis procedures.

The tests were intended to simulate realistic conditions. Thus, the data collected included effects of temperature and humidity fluctuations, noise as a result of vibrations in the surroundings, any signal processing errors, human errors and other experimental errors.

This meant that accuracy of modal parameters obtained by curve-fitting would also be affected since the imperfect data will affect the curve-fitting process.

The tests were conducted in an open space structures laboratory and the experimental arrangement is shown in Figure 6.21. Periodic random excitation in the range 0 - 250 Hz was used. The beam's response was measured at eight locations using the accelerometers and recorded on magnetic tape. The excitation was by an electromagnetic vibrator placed

on the beam. The output from an accelerometer mounted on a metal block placed on top of the vibrator served as the reference signal. The test procedure has been described in sub-section 4.5.1. The IAF method was used for curve-fitting. Similar test and analysis procedures were adopted for each test.

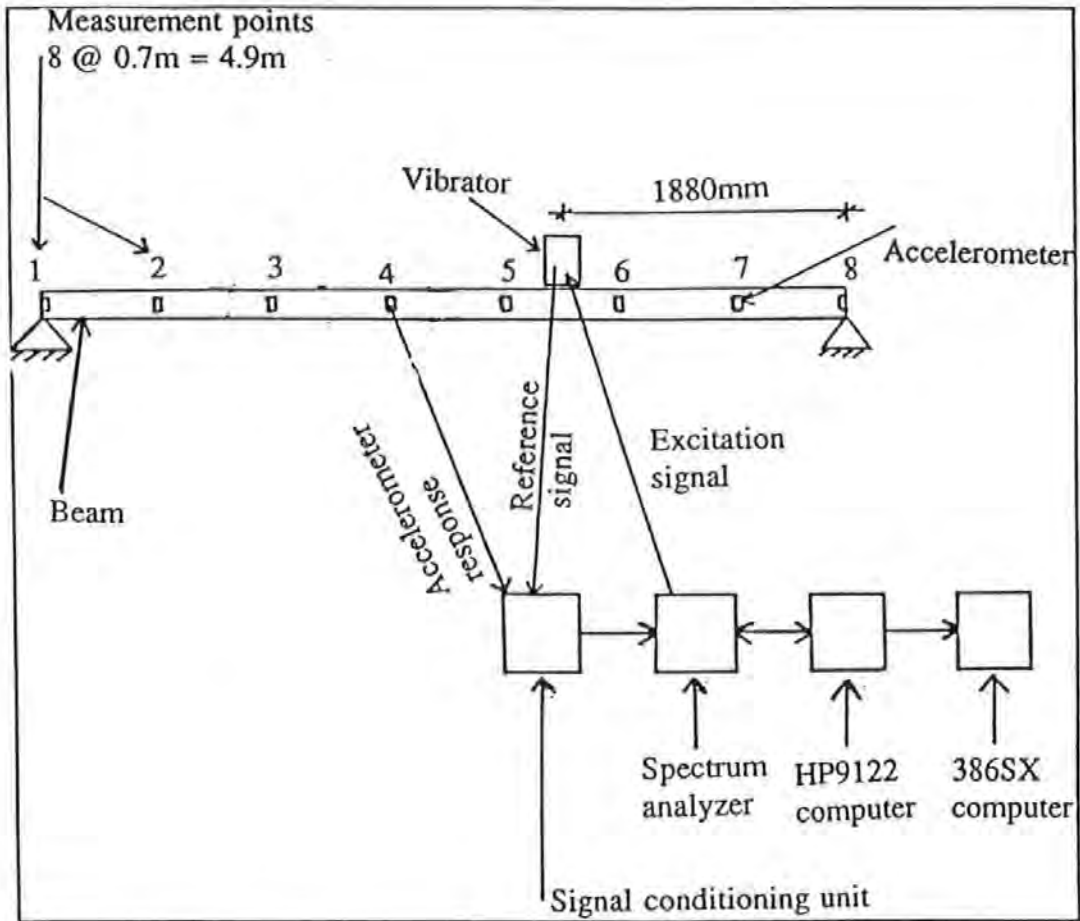


**Figure 6.21 Set-up of tests to investigate effect of random experimental errors on test and analysis techniques**

Tables 6.2 and 6.3 show the natural frequencies and modal viscous damping values obtained. The mean, standard deviation (STD) and covariance COV (standard deviation divided by mean) are also shown in the tables. STD indicates absolute dispersion while COV is a measure of relative dispersion. The values entered for LDF in the tables represent the percentage difference between the largest and lowest values for each mode. The Modal Assurance Criterion MAC (chapter four) was used to investigate the consistency of measured mode shapes. Values of the diagonal elements of the MAC matrix are shown in Table 6.4. In calculating the MAC values, results from a free vibration analysis of the beam was used as reference.

Consistency of the extracted modal parameters is reasonably high (as indicated by low COV) with the natural frequency variations being the lowest. In addition, visual inspection of the mode shapes did not reveal any significant changes. The relatively high (4% - 19.3%) values of percentage differences (LDF) in damping ratios are not uncommon and further demonstrate the difficulty in using changes in damping values as an integrity assessment parameter. The low values of the damping ratios will magnify percentage differences between them even though the covariance is reasonably low (less than 6%).

**Table 6.2 Repeatability of results: comparison of natural frequencies (Hz)**

Date	Mode 1	Mode 2	Mode 3
20-5-92	23.0	94.42	207.93
21-5-92	23.18	93.99	207.77
22-5-92	23.43	93.96	208.00
27-5-92	22.93	94.50	207.76
29-3-93	22.80	94.70	207.67
30-3-93	22.95	94.60	207.83
31-3-93	22.92	94.50	207.67
1-4-93	22.87	94.02	208.00
2-4-93	22.92	94.60	207.33
5-4-93	22.98	94.72	207.83
6-4-93	22.97	94.67	207.67
8-4-93	22.95	94.7	207.80
15-4-93	22.96	94.67	207.84
16-4-93	22.98	97.70	208.00
19-4-93	22.97	94.70	207.91
20-4-93	22.89	94.33	207.89
21-4-93	23.0	94.21	208.00
22-4-93	22.98	94.50	207.50
23-4-93	23.0	94.62	207.72
26-4-93	22.97	94.72	207.93
<b>LDF (%)</b>	2.8	0.8	0.2
<b>mean (Hz)</b>	22.98	94.49	207.80
<b>STD (Hz)</b>	0.13	0.255	0.176
<b>COV</b>	0.0055	0.0027	0.0008

LDF = % difference between largest and lowest values for each mode

STD = Standard deviation

COV = Covariance = STD ÷ mean

**Table 6.3 Repeatability of results: comparison of modal damping values (% of critical damping)**

Date	Mode 1	Mode 2	Mode 3
20-5-92	0.483	0.423	0.564
21-5-92	0.474	0.426	0.662
22-5-92	0.481	0.417	0.568
27-5-92	0.485	0.425	0.555
29-3-93	0.470	0.427	0.569
30-3-93	0.479	0.413	0.559
31-3-93	0.483	0.408	0.561
1-4-93	0.477	0.415	0.556
2-4-93	0.480	0.422	0.591
5-4-93	0.489	0.413	0.570
6-4-93	0.471	0.406	0.563
8-4-93	0.485	0.416	0.569
15-4-93	0.480	0.420	0.565
16-4-93	0.479	0.404	0.560
19-4-93	0.483	0.400	0.566
20-4-93	0.478	0.431	0.570
21-4-93	0.472	0.425	0.560
22-4-93	0.481	0.405	0.556
23-4-93	0.479	0.430	0.568
26-4-93	0.483	0.422	0.662
<b>LDF (%)</b>	4.0	7.5	19.3
<b>mean</b>	0.480	0.417	0.575
<b>STD</b>	0.005	0.009	0.031
<b>COV</b>	0.010	0.022	0.053

LDF = % difference between largest and lowest values for each mode

STD = Standard deviation

COV = Covariance = STD ÷ mean

**Table 6.4 Repeatability of results: comparison of MAC values**

Date	Mode 1	Mode 2	Mode 3
20-5-92	0.91	0.93	0.94
21-5-92	0.97	0.92	0.99
22-5-92	0.99	1.00	0.90
27-5-92	1.00	0.94	0.98
29-3-93	0.98	0.96	0.97
30-3-93	0.99	0.99	0.99
31-3-93	0.96	0.99	1.00
1-4-93	0.95	0.98	0.95
2-4-93	0.97	0.97	0.96
5-4-93	1.00	0.96	1.00
6-4-93	0.92	0.95	0.99
8-4-93	0.93	0.94	0.97
15-4-93	0.97	0.97	0.98
16-4-93	0.96	0.93	0.99
19-4-93	1.00	0.92	0.99
20-4-93	0.99	0.99	0.90
21-4-93	0.99	0.93	0.92
22-4-93	0.91	1.00	0.91
23-4-93	0.93	1.00	0.97
26-4-93	0.96	0.97	1.00
<b>LDF (%)</b>	9	8	10
<b>mean</b>	0.96	0.96	0.97
<b>STD</b>	0.03	0.03	0.03
<b>COV</b>	0.031	0.029	0.035

LDF = % difference between largest and lowest values for each mode

STD = Standard deviation

COV = Covariance = STD ÷ mean

### Consistency of 'stiffness' estimates

To further increase confidence in the procedures, the modulus of elasticity  $E$  (taken here to represent stiffness since the sectional modulus is constant) obtained from each modal frequency should be very close.

For a simply supported beam in bending vibration, the natural frequencies are given by:

$$f_r = \frac{r^2 \pi}{2l^2} \sqrt{\frac{EI}{M}} ; r = 1, 2, \dots \quad (6.27)$$

- where  $f_r$  = natural frequency (Hz) for mode  $r$   
 $I$  = second moment of area of section  
 $l$  = length of beam  
 $M$  = mass per unit length of the beam

Since the geometrical and material properties of the beam were unchanged, Equation (6.27) can be rewritten as

$$f_r = r^2 W \sqrt{E} \quad (6.28)$$

where

$$W = \frac{\pi}{2l^2} \sqrt{\frac{I}{M}} \quad (6.29)$$

The modulus of elasticity is therefore given by (from Equation 6.28):

$$E = \frac{f_r^2}{r^4 W^2} \quad (6.30)$$

Since  $W$  is a constant, an "effective modulus of elasticity"  $E'$  can be defined as

$$E' = \frac{f_r^2}{r^4} \quad (6.31)$$

Using the mean frequency values from Table 6.2 in Equation (6.31), the values in Table 6.5 are obtained. The  $E'$  values are close, as should be expected for repeatable results, with a maximum difference of 5.5%.

**Table 6.5 Identified values of effective modulus of elasticity**

	Mode 1	Mode 2	Mode 3
Frequency (Hz)	22.98	94.49	207.80
$E'$ (Hz <sup>2</sup> )	528.08	558.02	533.10

## 6.7 Conclusions

An excitation system, developed in the course of the research programme, suitable for inducing vertical excitation of horizontal structures has been described. Factors to be considered in designing such systems for full-scale dynamic testing were discussed. The observed behaviour (with respect to relationships between attainable stroke, load and operating frequencies) of the system is generally in accordance with expected characteristics of an hydraulic vibrator. The load output has a flat amplitude spectrum while the phase difference between excitation signal and load response is minimal except at frequencies below 5Hz. The best operating frequency bandwidth is 5 to 25Hz. Within this range, the vibrator produces stable output signals and does not generate unwanted motion.

Details of the equipment and procedures adopted for obtaining and analysing data during tests conducted as part of the research project were given in the chapter. The results presented indicate that the accuracy, reliability and consistency of the measurement and analysis equipment and procedures are satisfactory. In particular, the covariance, from 20 tests conducted over a one year period, of measured natural frequencies and damping ratios of a steel beam were respectively in the range 0.1% to 0.6% and 1.0% to 5.3%.

## CHAPTER SEVEN

### FULL-SCALE TESTING OF DEEP LANE BRIDGE

#### 7.1 Introduction

Experimental results from condition monitoring of full-scale bridges using forced vibration testing are few. Some of the reasons for these have been discussed in chapter two. In this (and the next) chapter, results from dynamic tests conducted on two full-scale highway bridges are presented. The aims of the tests were to investigate the effectiveness of forced vibration testing as: 1) an integrity monitoring tool; and 2) a viable means of validating theoretical structural models of civil engineering structures.

Results from experimental and theoretical modal analysis of Deep Lane bridge, Plymouth, are discussed in this chapter. The bridge was chosen because some structural repairs were to be carried out on it. Thus, an opportunity arose to investigate any correlation that may exist between the repair works and changes in the dynamic characteristics of the bridge. This was meant to study the performance of forced vibration testing as an integrity assessment method. The forced vibration tests were conducted before and after the repairs. Details of the bridge, repair works, test and analysis procedures and results obtained are presented in subsequent sections of the chapter.

#### 7.2 Description of Bridge

Deep Lane bridge (Figure 7.1) is an insitu reinforced concrete structure located in Plympton, near Plymouth, South West England. The bridge was designed and built in the

late 1960s and early 1970s. It carries a single two lane carriageway a total distance of 104m over the A38 trunk road and its slip roads. Figure 7.2 shows the basic dimensions of the structure. The bridge deck supports are noted (Figure 7.2) A to G consecutively from north to south. The deck's width is constant at 13.7m while the spans vary from approximately 12.4m to 20.5m. The total number of spans is six.

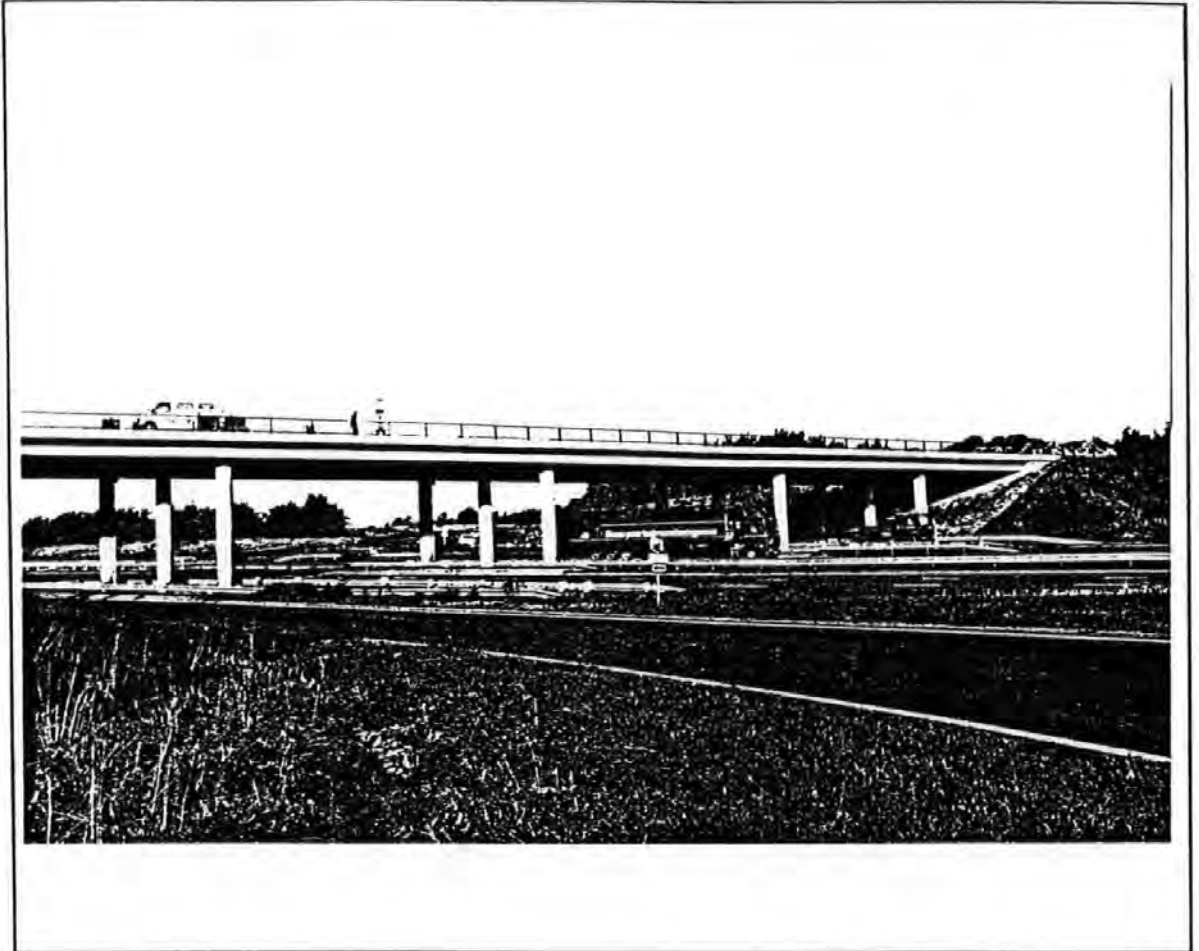


**Figure 7.1** Photograph showing Deep Lane bridge



The deck is continuous and of voided slab construction except at the supports where it is of solid section to improve shear capacity. Each circular void in the deck is 610mm in diameter. The deck slab is supported by spill through type abutments at each end and at five intermediate points by groups of three circular columns. The height of the columns varies from approximately 5.3m to 7.1m.

At abutment A, the deck is supported on a fixed bearing comprising a continuous rubber bearing strip 100mm X 12mm thick and 20mm diameter dowel bars at 300mm centres providing longitudinal and lateral restraint. It is supported on sliding bearings at abutment G and at each inner support. One bearing is provided at each column and eleven at abutment G. Each bearing is of PSC Tetron type and consists of a stainless steel faced top plate sliding against a PTFE pad bonded to a similar bottom plate. An expansion joint is provided at abutment G. The foundations to the abutments and intermediate column supports are reinforced concrete spread footings.

### **7.3 The Repair Scheme**

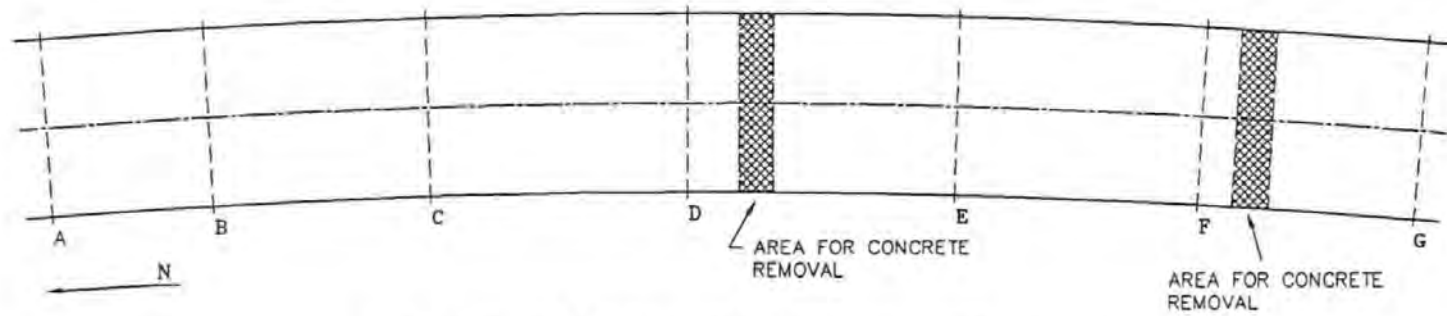
Strengthening measures were designed for spans DE and FG after a structural assessment of the bridge (Mott MacDonald, 1990; 1991). The measures were designed to make good the shortfall in longitudinal flexural capacity to resist hogging moments and mainly consisted of addition of top reinforcement to the deck in the areas of shortfall. Figure 7.3a shows a plan of the bridge indicating the repair locations. The repair involved extending the top (main) reinforcement bars within the hatched regions in spans DE and FG. Each repair zone has a width of 1.65m.

The exact locations of the repairs are shown in Figure 7.3b. The concrete within the

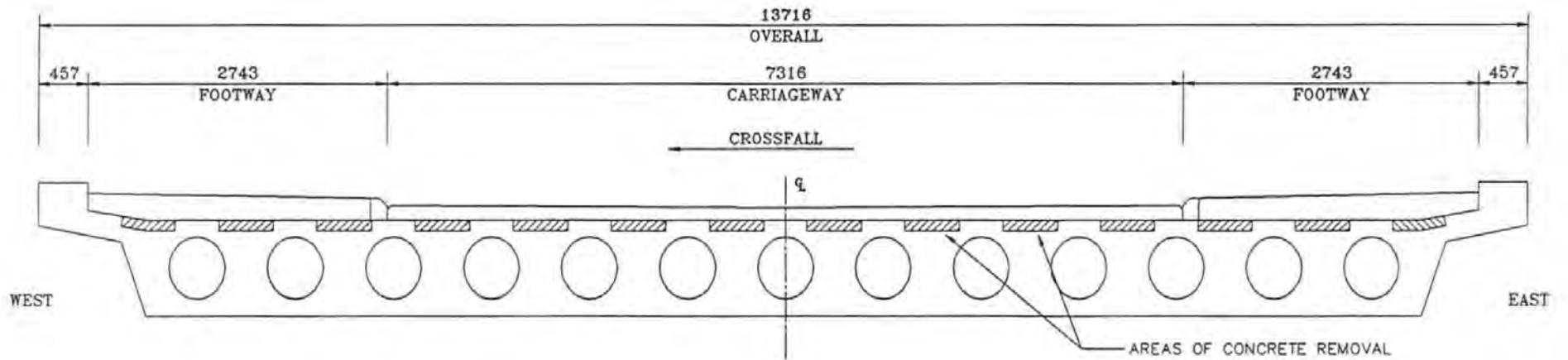
hatched areas in Figure 7.3b was removed by waterjetting. Within the exposed sections, new main reinforcement were then fixed to the existing ones with couplers. Where necessary, the transverse reinforcement and links were modified to permit fixing the new reinforcement. The old concrete surfaces were treated with proprietary grout before being re-concreted with proprietary concrete. The repair works were sequenced so that the bridge was neither closed to traffic nor subjected to undue stresses throughout the construction period.

#### **7.4 Full-Scale Testing**

Two series of full-scale tests were conducted on the bridge. The equipment, experimental and data analysis procedures adopted for each test series were the same. A frequency range of 0 - 25Hz was chosen for the tests so that the first few modes could be observed. The first series of tests was conducted on the 14th and 15th of October, 1992 while the second series was carried out on May 25th and 26th, 1993. Only brief details of the test and analysis methods are discussed in the following sub-sections. Full details of the procedures used have been presented in chapter six.



(a) Plan of bridge showing repaired zones



(b) Cross-section showing exact locations of repairs

Figure 7.3 Location of the repairs

#### **7.4.1 Equipment**

The instrumentation layout adopted during the tests is shown in Figure 6.1. The equipment used were an electro-hydraulic vibrator, four accelerometers, signal conditioning devices, signal transmission cables, an oscilloscope, an oscillograph, a spectrum analyzer and a FM tape recorder. Details of these equipment have been given in the previous chapter (sections 6.2 and 6.3).

#### **7.4.2 Measurement locations**

The main criteria for selecting the measurement points were the need to adequately identify the first five to seven modes and monitor changes in the dynamic response of the spans around the repair zones. Due to resource limitations, it was decided to monitor only three of the six spans. Of the two spans (DE and FG - Figure 7.3a) containing the repair zones, DE is longer and would be more responsive to dynamic excitation. Thus, span DE and the two adjacent spans CD and EF were chosen in order to monitor the effects of the repairs.

The dynamic response of the bridge was measured at 54 points (27 locations on either side of the bridge deck) on spans CD, DE and EF. Figure 7.4 shows the measurement locations. Of the 54 locations, only points 11, 38 and 39 were within the repair zone on span DE. Although Figure 7.4 has been drawn 'square' to illustrate the measurement positions, it should be noted that the bridge is slightly curved in plan. The relative locations of the accelerometers with respect to the deck cross-section and pier locations are shown in Figure 7.2.

Throughout the testing period for each series of tests, one accelerometer was stationed

permanently at a reference point noted REF in Figure 7.4. The other three accelerometers were moved from point to point until all the measurement locations were covered. Measurement at four locations (three "new" points and the reference point) constituted a test. The vibrator was located on the eastside footway at a distance 8.5m from E in span DE.

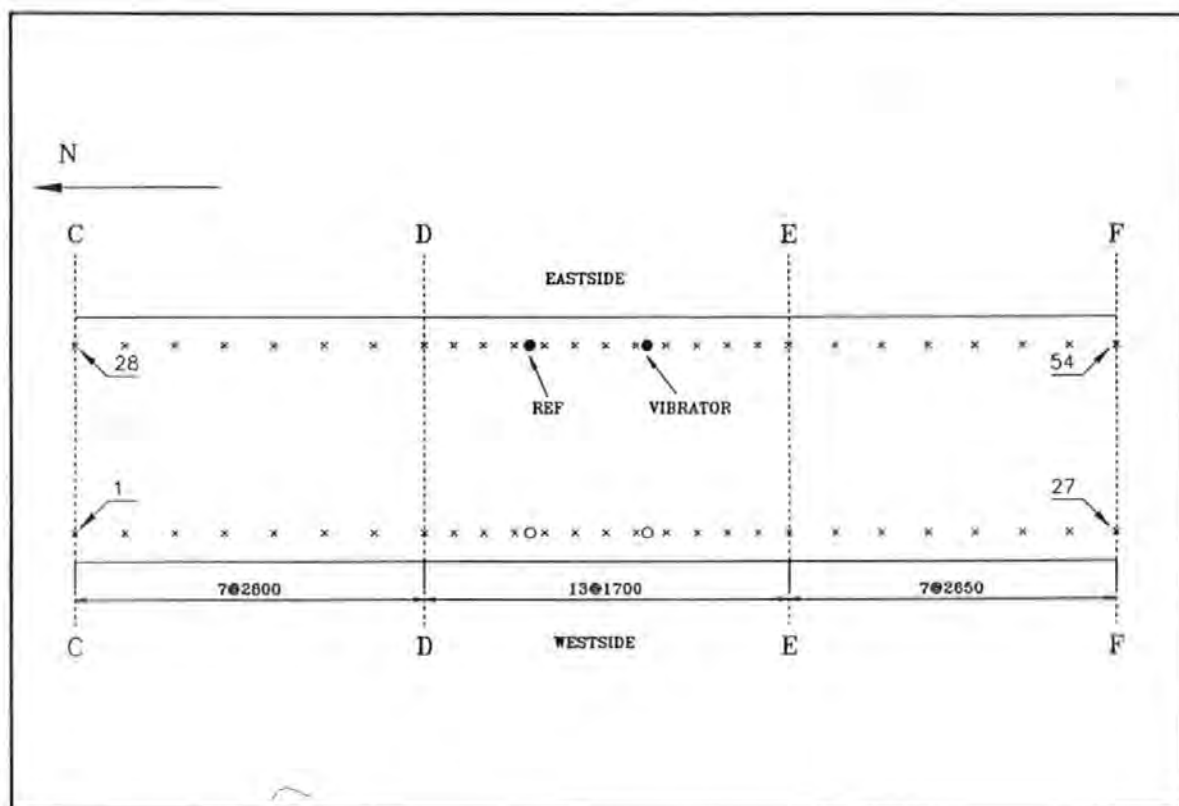
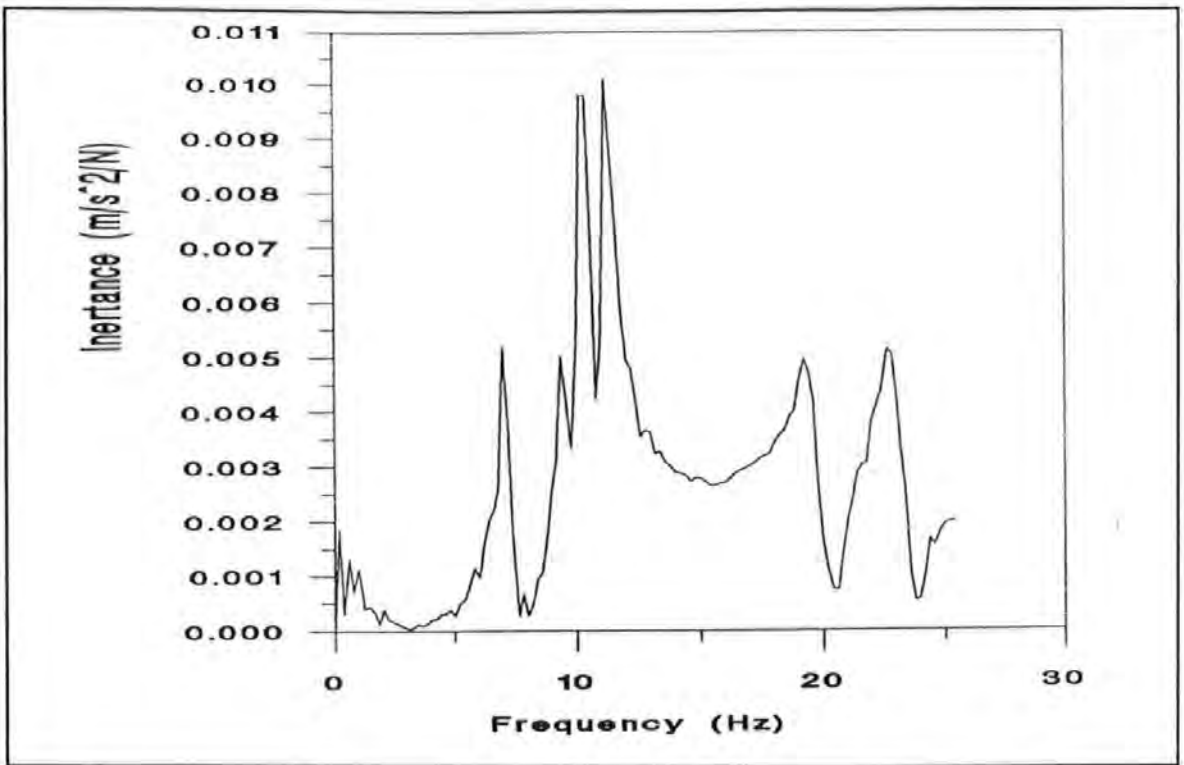


Figure 7.4 Measurement locations (dimensions in mm)

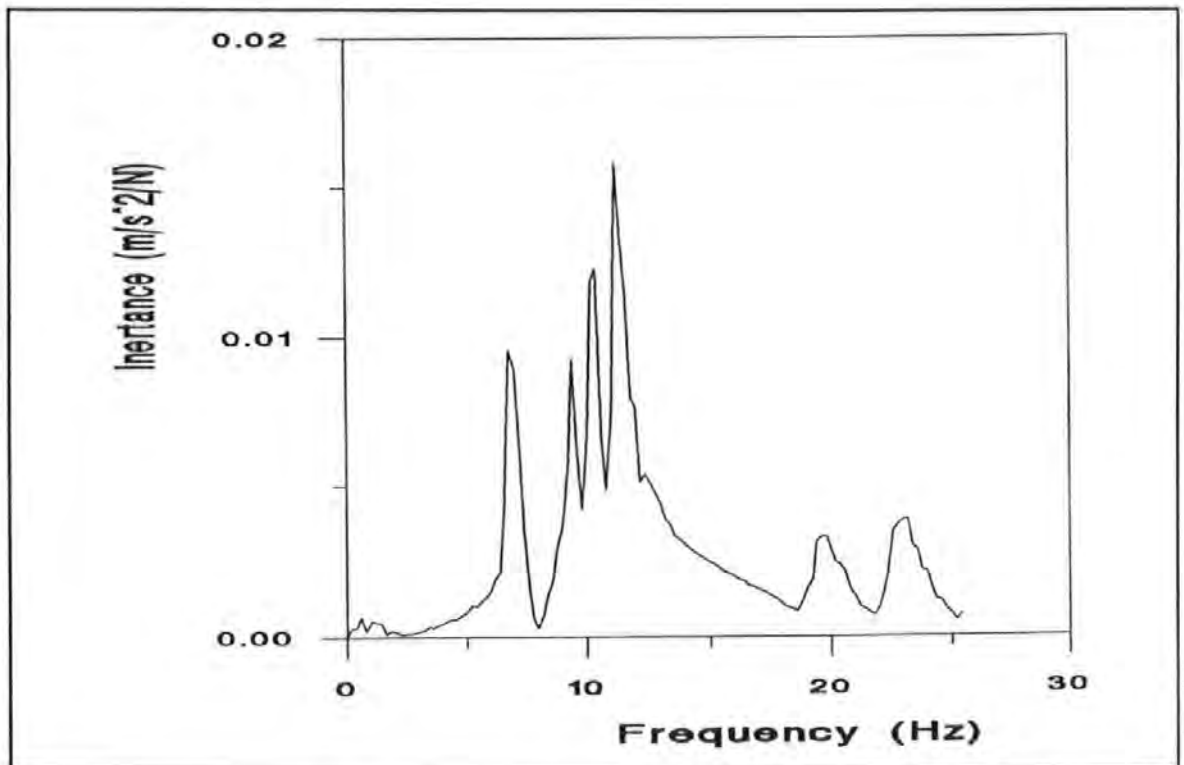
### 7.4.3 Test procedure

For each test, the motion of the bridge deck resulting from forced excitation (by the electro-hydraulic vibrator) was "picked-up" by the accelerometers. The signal outputs from the accelerometers were conditioned and recorded on magnetic tape for detailed analysis off-site. The recorded signals were monitored using the oscilloscope and oscillograph. Limited real time analysis was conducted using a HP3582A dual channel spectrum analyzer.

At the start of each test series, a sine sweep test was conducted so that predominant modes within the chosen frequency range could be identified. To achieve this, the frequency response functions (FRFs) between the input sinusoidal load and the bridge's response at selected points were computed with the spectrum analyzer. Sample FRFs obtained from points 37 and 43 (see Figure 7.4) are shown in Figure 7.5. The natural frequencies of the vibration modes occur at frequency values corresponding to the peaks in the FRF plots. Subsequently, a periodic-random signal was used as the excitation signal. Reasons for the choice of signals have been discussed in section 6.2.



(a) Point 37



(b) Point 43

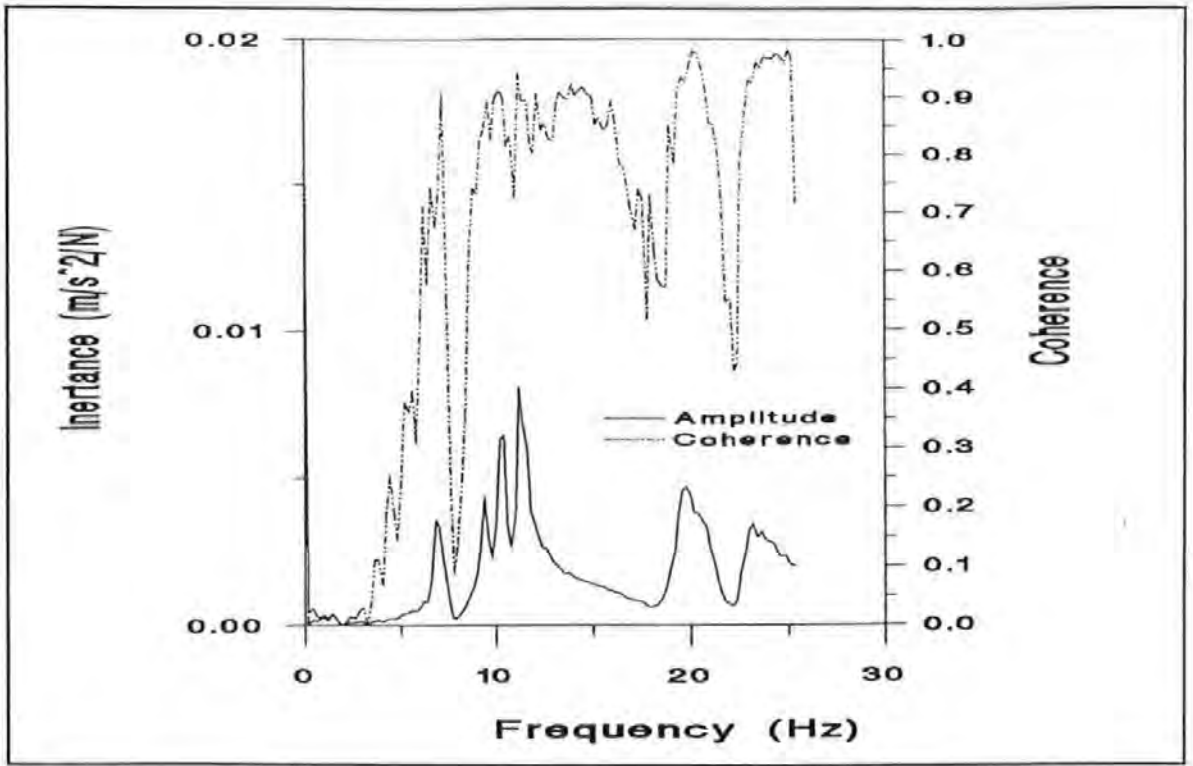
**Figure 7.5 FRFs from sine sweep test**

#### 7.4.4 Data analysis

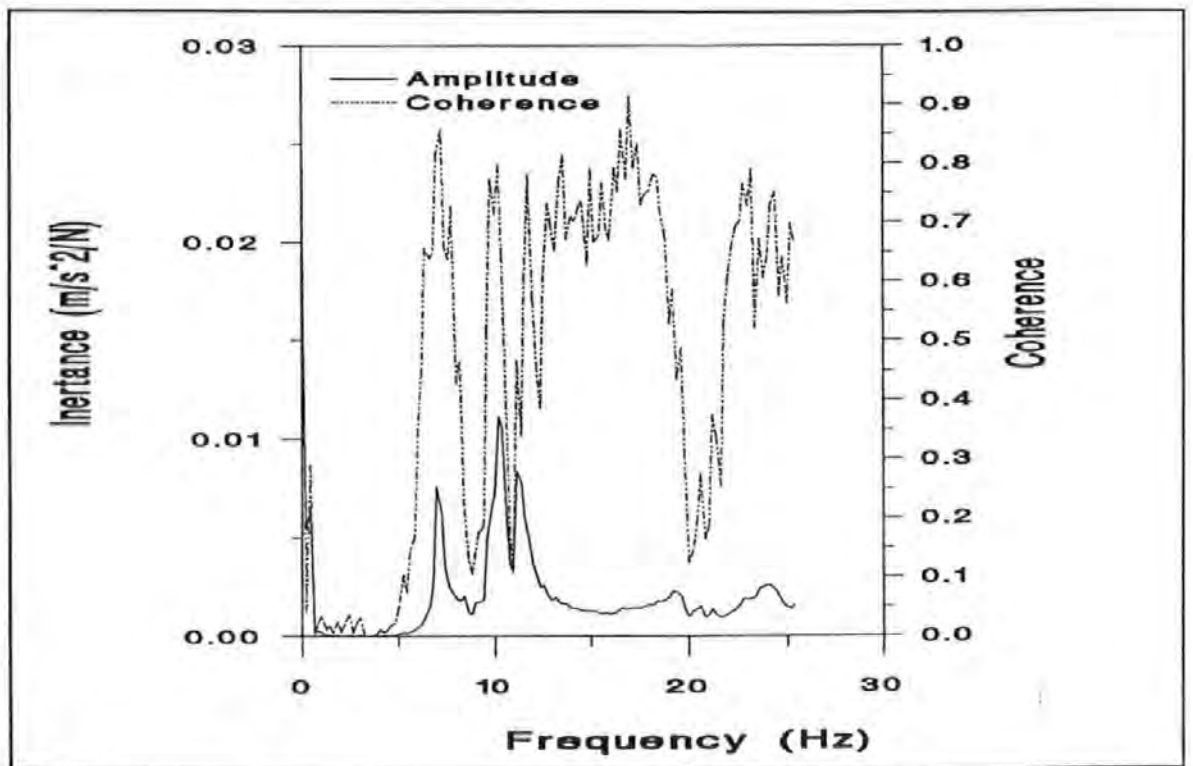
After the tests, the recorded signals were played back in the laboratory and, for each series, a total of 54 FRFs (one input and 54 outputs in the vertical direction) computed within the frequency range 0 - 25Hz using the spectrum analyzer. Details of FRF computation have been presented in the previous chapter (sub-section 6.4.3).

The coherence function was used to assess the quality of measured data. Typical plots of the coherence function are shown in Figures 7.6 and 7.7. The FRF amplitude and coherence have been plotted on the same space to illustrate variation of coherence with location of the modes. The figures show good coherence around each resonance.

The FRF data were transferred to computer disks and subsequent analysis conducted on a personal computer. The modal parameters were extracted using the enhanced version of the improved amplitude fitting method as implemented in the modal analysis program TXT\_FRF described in sub-section 6.5.4. To assess accuracy of the parameter extraction process, each FRF was regenerated using the estimated parameters. Typical curve-fits are shown in Figures 7.8 - 7.11.

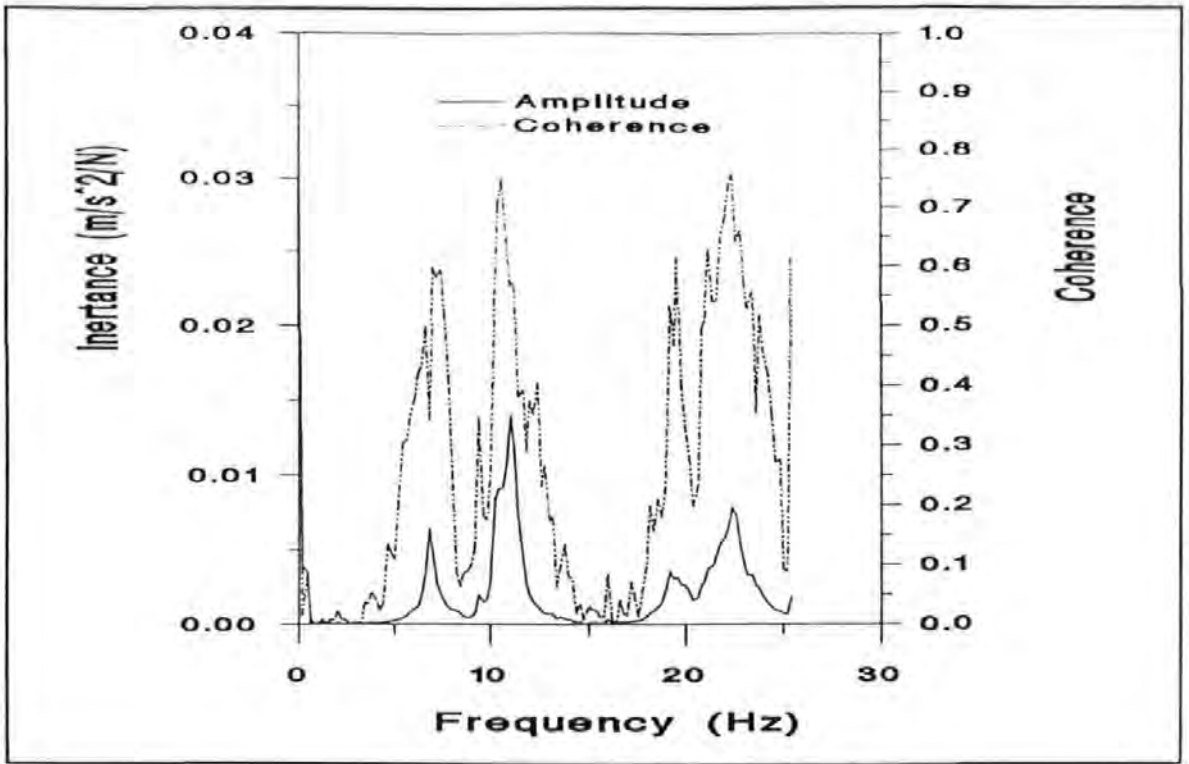


(a) Point 46

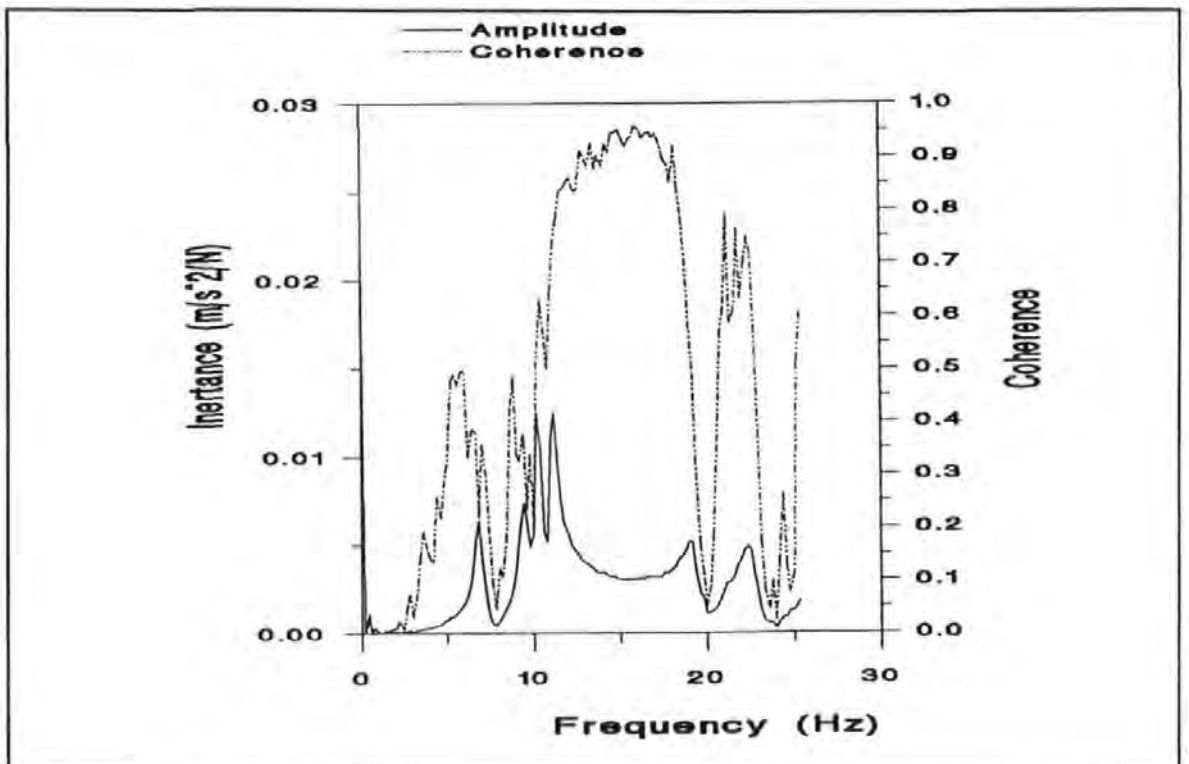


(b) Point 16

Figure 7.6 Typical plots of FRF amplitude and coherence from tests before the repairs



(a) Point 6



(b) Point 50

Figure 7.7 Typical plots of FRF amplitude and coherence from tests after the repairs

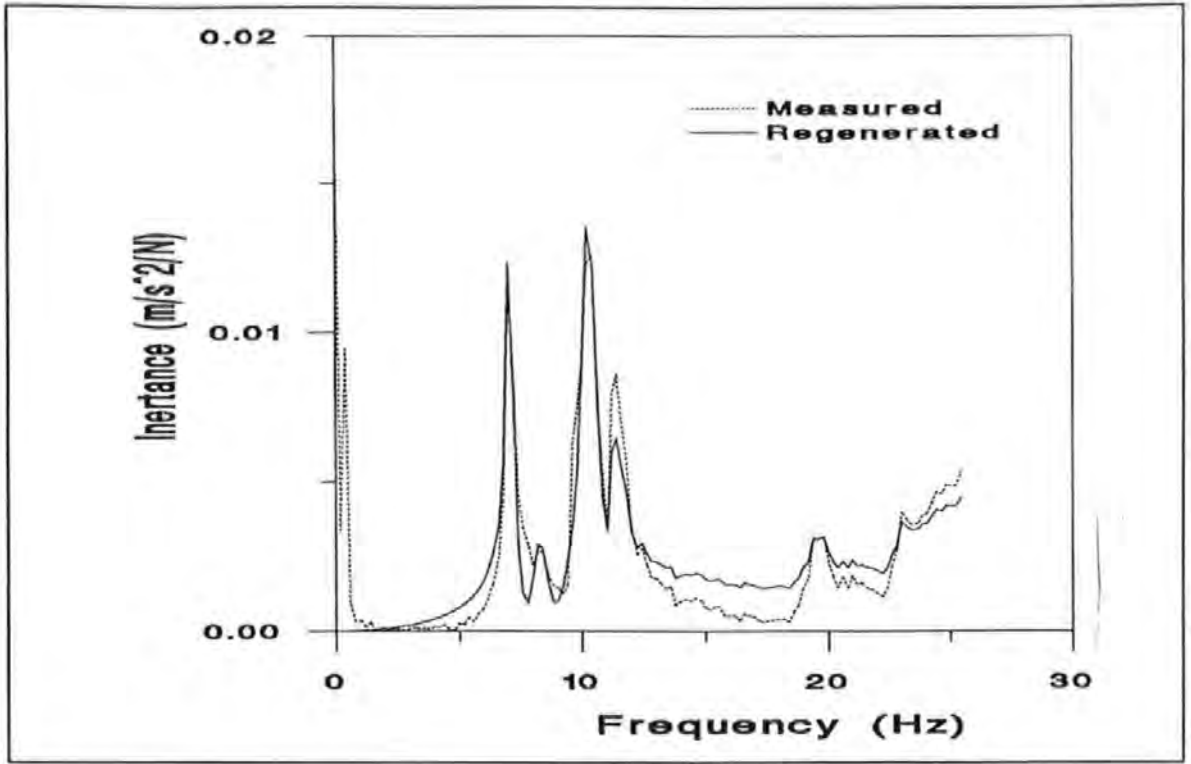


Figure 7.8 Example of curve-fit - point 11 : before repairs

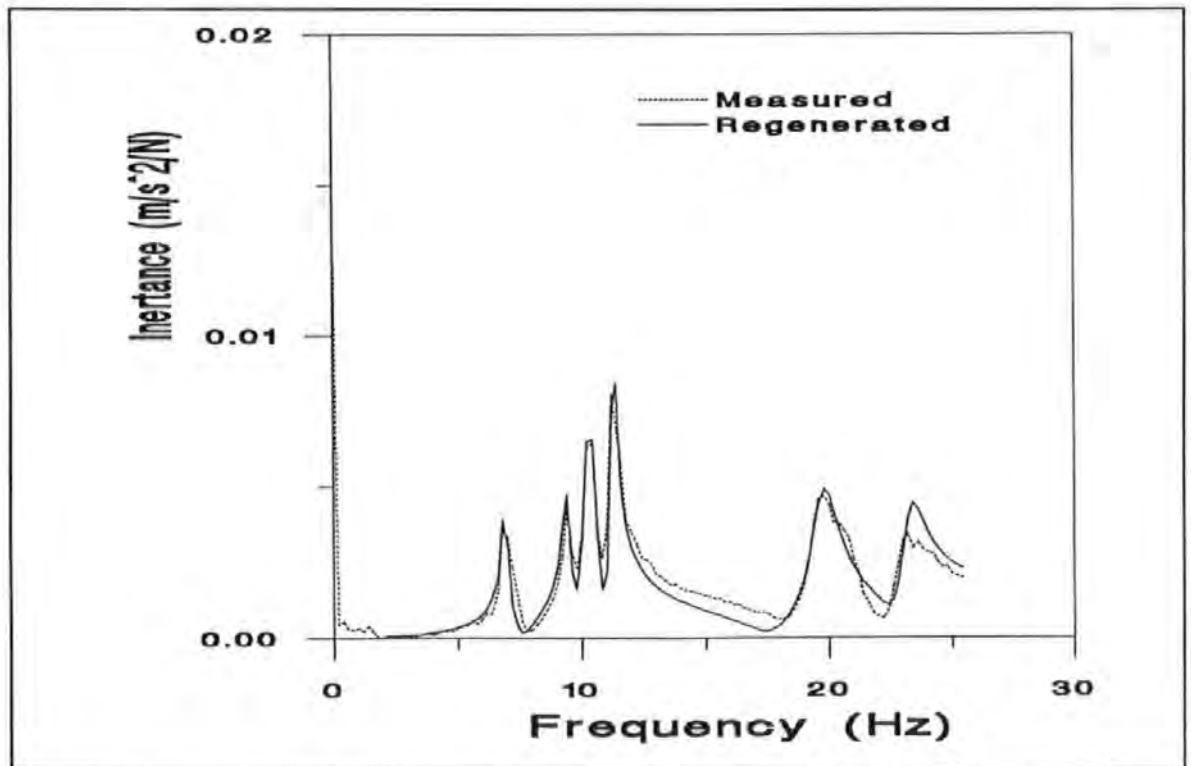


Figure 7.9 Example of curve-fit - point 46 : before repairs

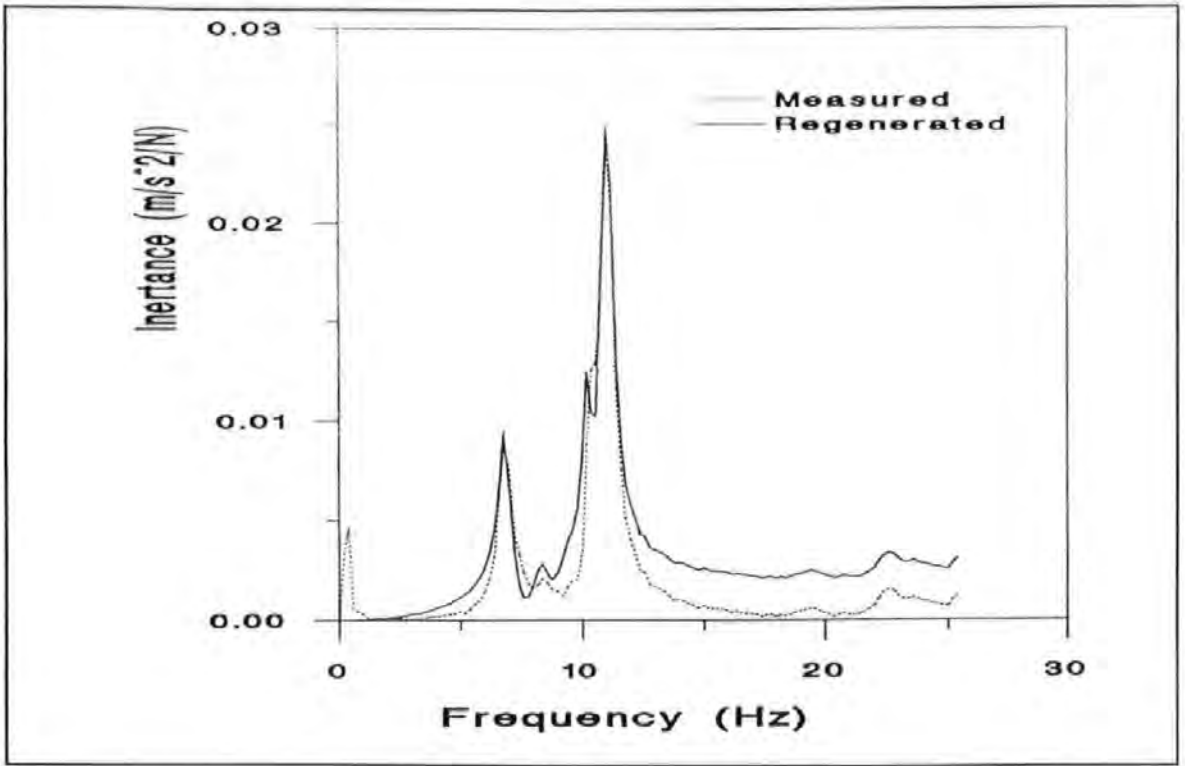


Figure 7.10 Example of curve-fit - point 4 : after repairs

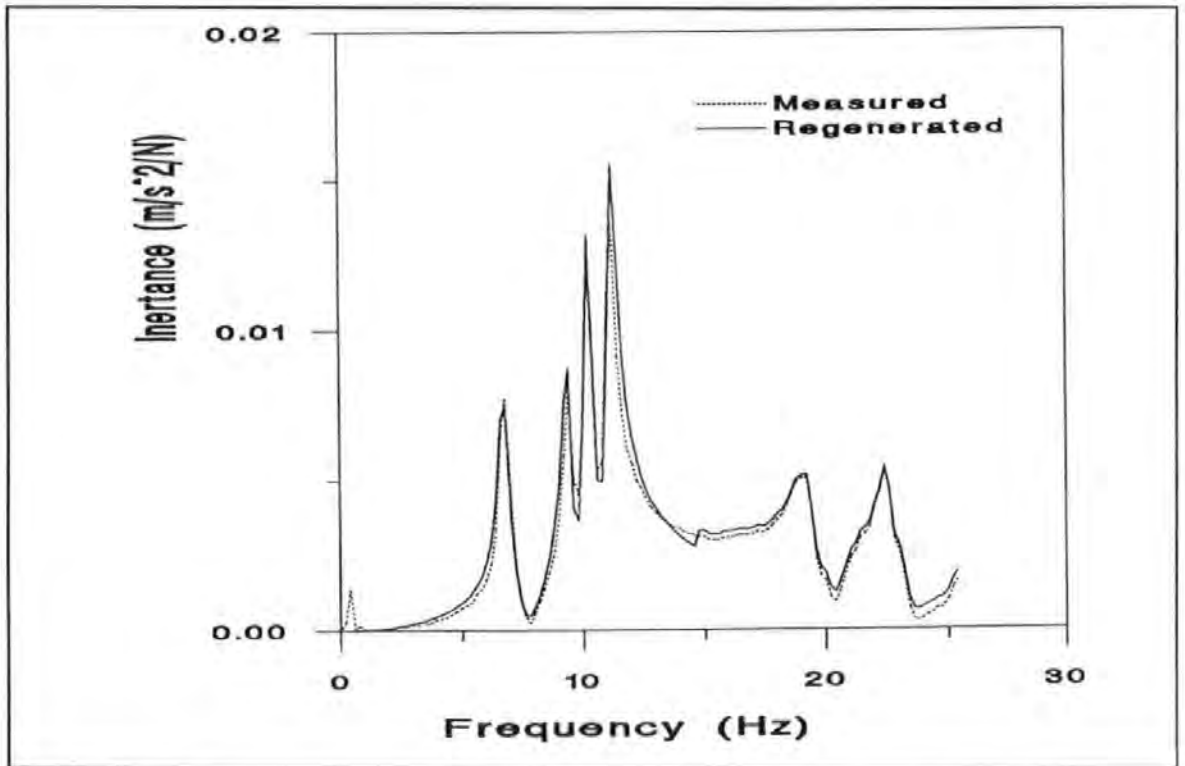
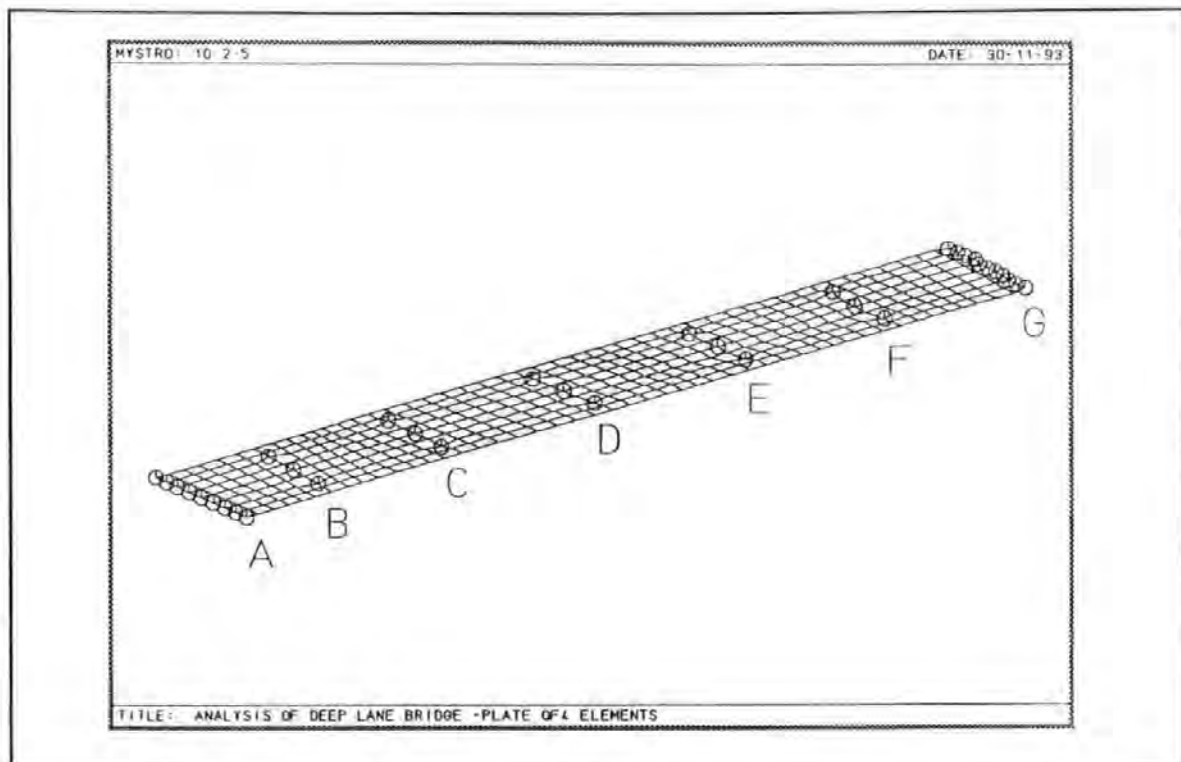


Figure 7.11 Example of curve-fit - reference point, test 8 : after repairs

## 7.5 Theoretical Vibration Analysis

A linear-elastic free vibration analysis of the structure was performed using the finite element (FE) program LUSAS (FEA, 1990). The analysis was performed on a model which represented the bridge's condition before the repairs. The deck slab was modelled as a series of 2-dimensional plate elements (Figure 7.12). All the six spans of the bridge were included in the model without making any symmetry assumptions. Each element has three degrees of freedom (DOF) - one translation (vertical) and two rotations (about the transverse and longitudinal axes) - at each node. 376 quadrilateral and two triangular thin plate elements were used. The finite element nodes were chosen to either lie at the small solid section between two voided segments or at the mid-point (or third points for longer segments) of a voided segment. The total number of nodes was 434. The substructure was not included in the model.

At each support node, the DOF in the vertical and rotation about the longitudinal axis directions were fully restrained while the third DOF was unrestrained. Although the bearings have a small rotational capacity (Mott MacDonald, 1990; 1991), the value of this capacity is unknown. When the supports were represented as sprung and support stiffness values estimated, the results obtained from the analysis were inconsistent. Furthermore, the bearing manufacturers were unable to supply stiffness values, in any DOF, for the bearings. Therefore, fixed or free conditions were used at the support nodes. Although the bearings at abutment G were supposed to allow longitudinal movement, satisfactory results were only obtained by fully restraining the longitudinal DOF at this support. Thus, only free rotation was allowed at each abutment. Accurate representation of the as-built boundary conditions is usually generally difficult when modelling these types of structures.



**Figure 7.12 Finite element model of Deep Lane bridge**

To obtain realistic predictions, the inertia and material properties used in the model should very closely mirror the values for the existing structure. The inertia of the plain concrete section is usually used for the reinforced section if it can be shown (as is usually assumed) that the effects of steel reinforcement and concrete cracking compensate each other and may therefore be ignored (Lee et al, 1987 and Wills, 1977). However, a statistical analysis of inertia data from 82 bridges have shown that steel reinforcement and the asphalt layer each has a relative participation of about 6% in the global inertia (Hassan et al, 1993). Thus, the concept of effective inertia can be used. The effective inertia of the deck was taken to be the inertia of the plain concrete section (primary inertia) modified to account for steel reinforcement and other "stiffening elements".

The bridge is constructed of concrete class 4500 $\frac{3}{4}$  which corresponds to a characteristic cube strength of 31N/mm<sup>2</sup> at 28 days. The corresponding (28 days) static modulus of

elasticity  $E_{c,28}$  varies from  $20\text{kN/mm}^2$  to  $32\text{kN/mm}^2$  (Mosley and Bungey, 1990). An average value of  $26\text{kN/mm}^2$  was adopted. Accurately estimating the modulus of elasticity is difficult. Not only are code formulae for estimating  $E_{c,28}$  sometimes inaccurate (Baalbaki et al, 1992), the modulus of elasticity is time and strain dependent. The dynamic modulus of elasticity  $E_d$  ( $E_d = (E_c+19) / 1.25$ , where  $E_c$  and  $E_d$  are respectively the static and dynamic moduli at a specified age) was used since previous results (Lee et al, 1987) suggest that better agreement between theoretical and experimental results is achieved if the dynamic modulus is adopted. Strength enhancement due to the age of the concrete was allowed for up to five years. The poisson ratio and density of reinforced concrete were respectively taken as 0.2 and  $2446\text{ kg/m}^3$  respectively.

The FE program used did not have a structural optimisation module. Therefore, a simple interactive routine was developed, external to the FE program, that improves the analytical model by updating given model input parameters until the differences between (analytical and experimental) targeted result parameters are minimised. The elasticity modulus and effective inertia were the input variables while the natural frequencies were the result parameters selected. Further details of the analytical modelling are given in Salawu et al (1994).

## **7.6 Experimental Results and Comparison with Theoretical Results**

The number of vibration modes obtainable from a finite element analysis is only limited by the number of DOF of the model. The first fifteen vertical modes were computed. Generally, the number of measured modes of such a structure will be less than that predicted. Seven experimental modes were identified from the measured data. Since the analytical model represented the original structure, only data from tests before the repairs

are considered in this section.

Pairing of modes from the analytical and experimental sets was done using mode shapes as described later. Since the response of only three out of the six spans was measured, analytical modes in which the unmeasured spans dominate were omitted during mode pairing.

Table 7.1 shows a comparison of analytical and experimental natural frequencies. The chronological mode order of the experimental set has been adopted in Table 7.1 and will be used in subsequent discussions. The table shows reasonable agreement between the calculated and measured frequencies. The one major exception is mode 4. The average error in frequency (excluding mode 4) is 6.4%. The probable reasons for the relatively large difference between the predicted and measured frequency for mode 4 are the possible inadequate modelling of the support conditions and the low sophistication of the correlation procedure. Though realistic modelling of the boundary conditions is necessary to achieve good results, accurate representation of support conditions of built structures is often difficult (Baumgärtner and Waubke, 1993; Doll, 1994; Hoff and Natke, 1989; Pabst and Hagedorn, 1994; Ventura et al, 1994).

Full structural details of the bridge were not available until after completion of the tests. This meant that the measurement locations and position of the vibrator were chosen without guidance from a pre-test analysis. The main implication of this was that the measured points were not fully coincidental with the analytical nodes. Therefore, modal comparison using Modal Assurance Criterion (MAC) and Coordinate Modal Assurance Criterion (COMAC) - described in sub-section 4.2.1 - could not be fully justified. Thus, mode pairing was by visual inspection and overlay plots of the two sets of mode shapes. Only

nodes (of the analytical model) on the same line as the measurement points and on the measured spans were used. Figure 7.13 shows overlay plots of corresponding experimental and (reduced) theoretical mode shapes. The degree of correlation is reasonably good.

**Table 7.1 Comparison of analytical and experimental frequencies of Deep Lane bridge**

Mode	Natural Frequency (Hz)		
	Experimental	Analytical	Error (%)
1	7.0	6.7 <sup>a</sup>	-4.3
2	8.4	8.0 <sup>b</sup>	-4.8
3	9.5	9.5 <sup>c</sup>	0
4	10.4	14.9 <sup>d</sup>	43.3
5	11.4	12.7 <sup>e</sup>	11.4
6	19.3	20.2 <sup>f</sup>	4.7
7	22.7	21.2 <sup>g</sup>	-6.6

a = Analytical mode 1

b = Analytical mode 2

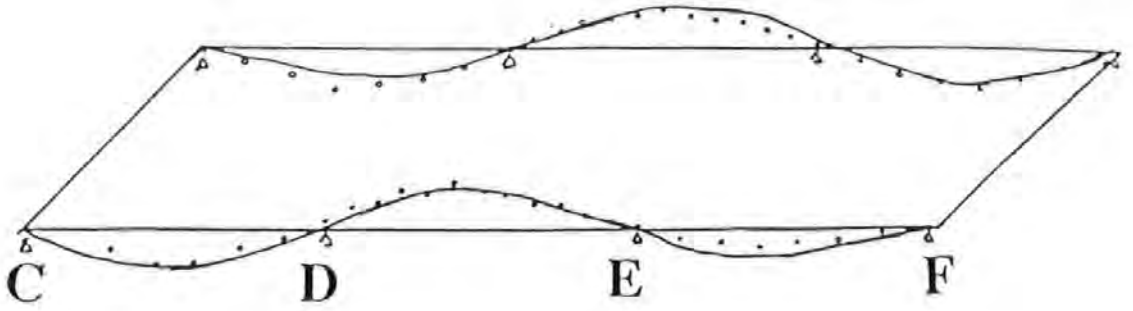
c = Analytical mode 3

d = Analytical mode 8

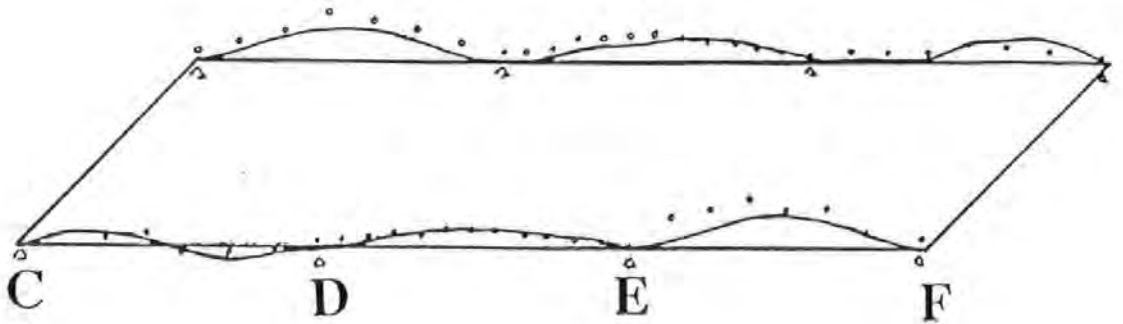
e = Analytical mode 6

f = Analytical mode 11

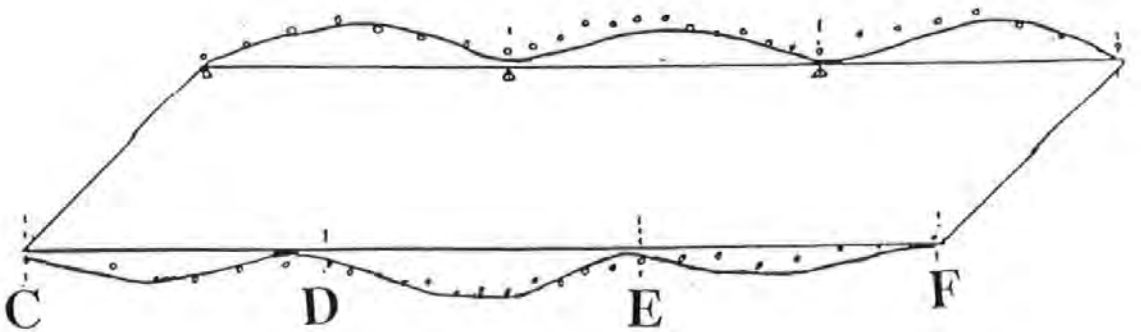
g = Analytical mode 12



(a) Mode 1: ○○○○ Experimental (7.0 Hz)  
 — Analytical (6.7 Hz)

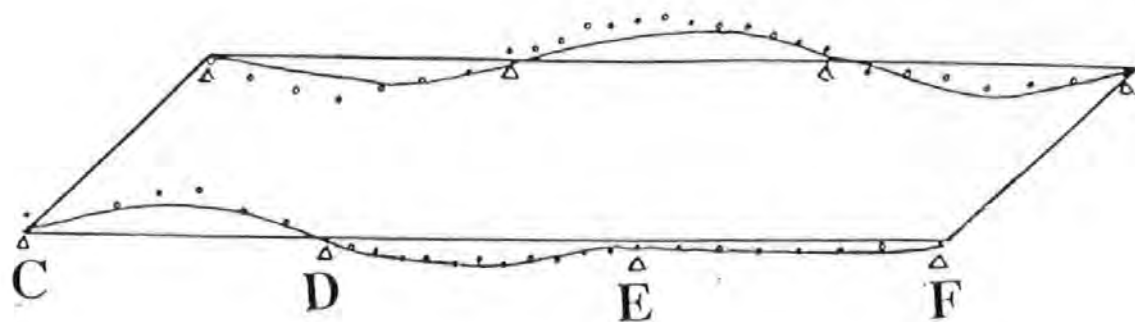


(b) Mode 3: ○○○○ Experimental (9.5 Hz)  
 — Analytical (9.5 Hz)

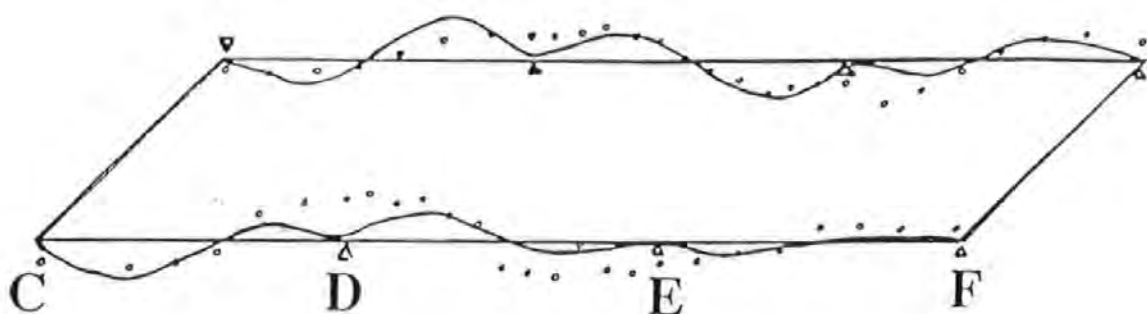


(c) Mode 4: ○○○○ Experimental (10.4 Hz)  
 — Analytical (14.9 Hz)

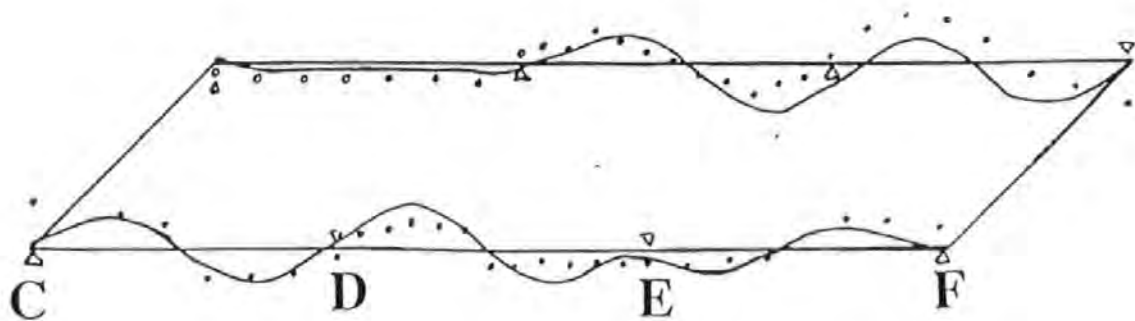
**Figure 7.13 Comparison of experimental and analytical mode shapes**



(d) Mode 5: ○○○○ Experimental (11.4 Hz)  
 — Analytical (12.7 Hz)



(e) Mode 6: ○○○○ Experimental (19.3 Hz)  
 — Analytical (20.2 Hz)



(f) Mode 7: ○○○○ Experimental (22.7 Hz)  
 — Analytical (21.2 Hz)

Figure 7.13 Comparison of experimental and analytical mode shapes (continued)

Modes 1 and 6 respectively represent the first and second pure bending modes while mode 4 is the first torsional mode. The other modes involve both pure bending and torsion. In the third vibration mode, spans DE and EF are in bending while CD is in torsion. Spans CD and DE are in torsion while EF is in bending for mode 5. Mode 7 is similar to mode 3 except that spans DE and EF are in second bending (EF in torsional bending). Modes 1, 4 and 6 are symmetrical modes.

It should be noted that the measurement points on the support lines (C, D, E and F) were not actually on the piers (Figure 7.2). This explains why elements of the mode shape matrix corresponding to these points are relatively large for some modes. The mode shape for mode 2 was not fully experimentally identified because the vibrator was inadvertently placed close to a node of this mode. Thus, mode 2 has been omitted from Figure 7.13.

## **7.7 Discussion of Experimental Results**

In this section, results obtained from the two series of tests are presented and discussed. The two result sets are compared using the non-parametric and parametric variables described in chapters four and five. The progression (in the evaluation of results) from sub-section 7.7.1 to 7.7.4 is akin to stages that could be adopted in an integrity assessment scheme using vibration testing.

Before the test results are evaluated, it is necessary to check the level of consistency of measured data before differences in them can be exploited. The reliability and consistency of the test and analysis procedures adopted in this research were discussed in chapter six. As a check on the repeatability and consistency of the measured field data, the response at the reference point was measured for each test of each series. Figures 7.14 and 7.15

show typical FRFs measured at the reference point. As should be expected, the curves (for each series) are almost identical. The degree of sparsity, as measured by the covariance (sub-section 6.6.2), of identified natural frequencies and damping values is presented in sub-section 7.7.2

Other factors to consider are the effects of changes in environmental conditions (such as temperature and humidity) on the dynamic response of the bridge. Comparison of the environmental variables during the test periods is presented in the appendix (Tables A.1 to A.4 and Figure A.1). The wind speeds were similar while the temperature and relative humidity were higher during the second series of tests. Quantitative information on the direct relationships between changes in environmental variables and changes in a structure's dynamic properties are rare. Experimental results (Askegaard and Langsø, 1986) indicate that variation in natural frequency due to ambient variables is negligible when compared to the frequency changes observed in deteriorated structures. The values of the changes in temperature and relative humidity (during the two tests periods) are not large enough to cause significant changes in dynamic parameters. As discussed in chapter three (sections 3.3 and 3.9), frequency changes not greater than 5% can be attributed to fluctuations in environmental conditions and other sources of error.

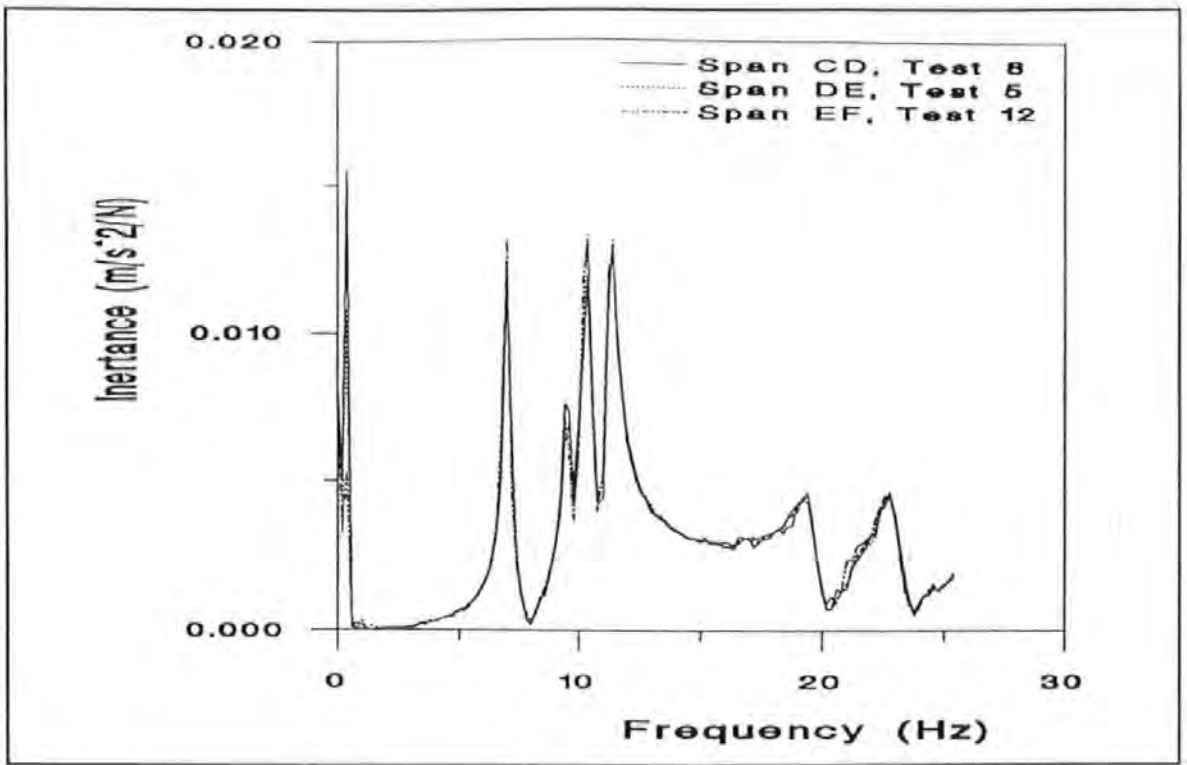
As opposed to frequency, temperature variations could lead to modifications of the damping values since the variations may cause changes in length and curvature of the bridge which in turn could influence support conditions and thereby damping (Askegaard and Mossing, 1988). In addition to temperature, windspeed and relative humidity also influence humidity transport in the bridge deck and may thereby also change damping (Swamy and Rigby, 1971). The possibility of damping changes due to environmental factors coupled with the scatter in reported measured values (chapter three) could make exploitation of damping

changes difficult.

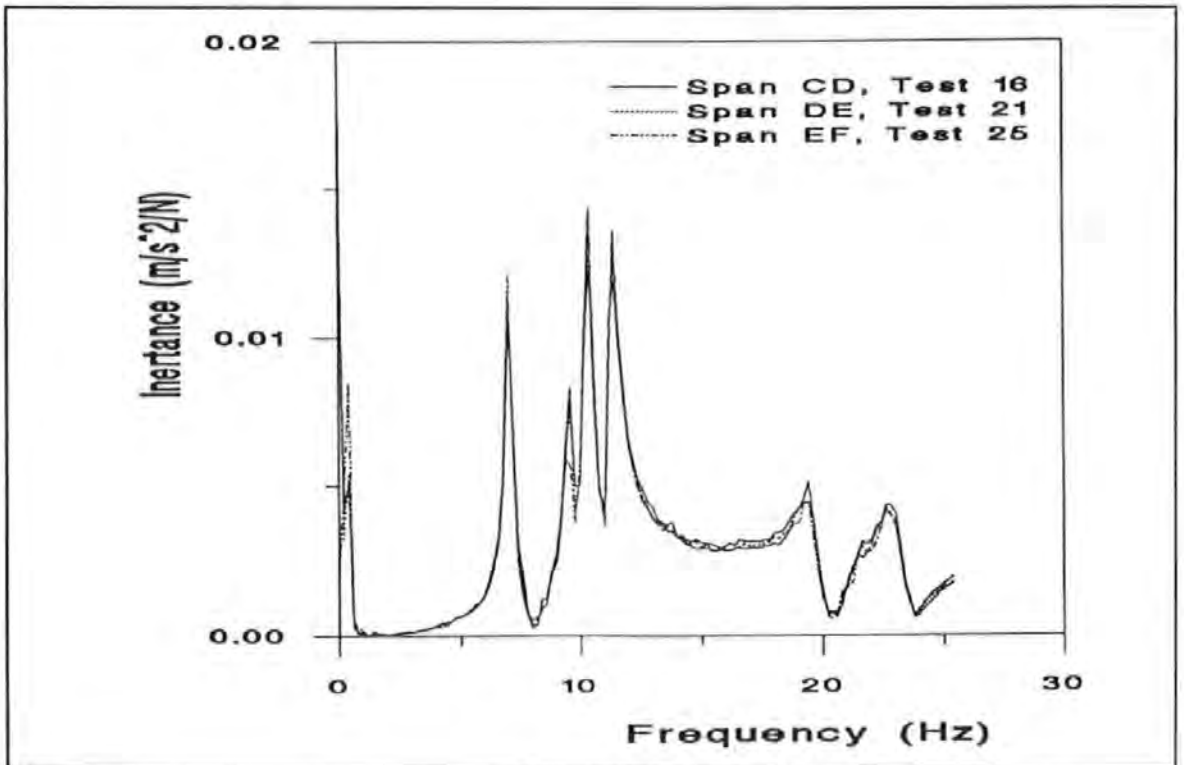
### 7.7.1 Frequency response function (FRF)

For each test series, the FRF measured at the reference point, and from points on the eastern and western sides of the bridge were added and each resulting function normalized with respect to the largest value. Figure 7.16 shows a comparison of the magnitudes of the FRF before and after repairs. From the figure, it can be seen that changes in the cumulative response functions are detectable thus giving an indication that there has been a change in the bridge's condition. It should be noted that the reference point lies within the repair zone in span DE.

Biswas et al (1990) and Richardson and Mannan (1993) suggested that the sum of the imaginary part of the FRF shows the differences best. Normalised cumulative curves of the squares of the imaginary part before and after repairs are shown in Figure 7.17. For completeness and comparison, the normalised cumulative curves of the squares of the real part are shown in Figure 7.18. The plots also show detectable differences between the two states of the bridge. Plots of the squares of the real part appear to give the best indication of the differences. Although the curves in Figures 7.16 - 7.18 indicate existence of some modification, quantifying the differences is difficult. Further comparison of the modal parameters would be necessary to determine which state is "stiffer" and which locations were modified.

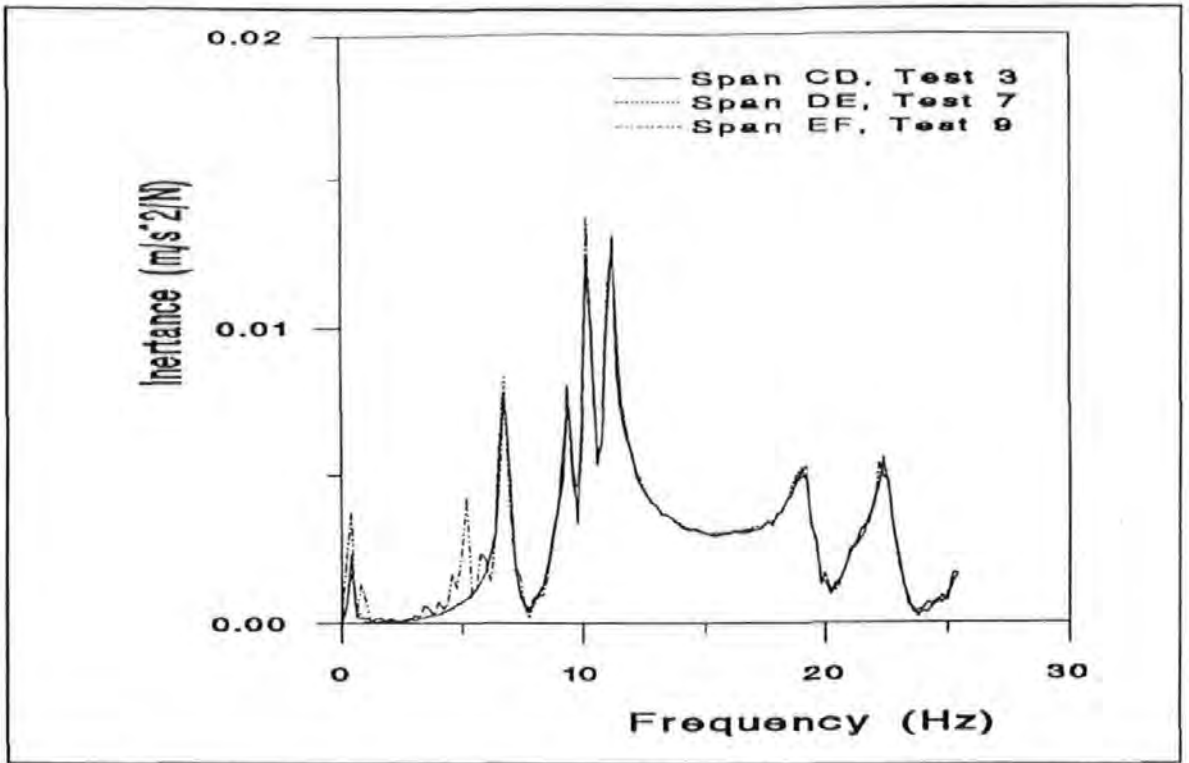


(a) East side

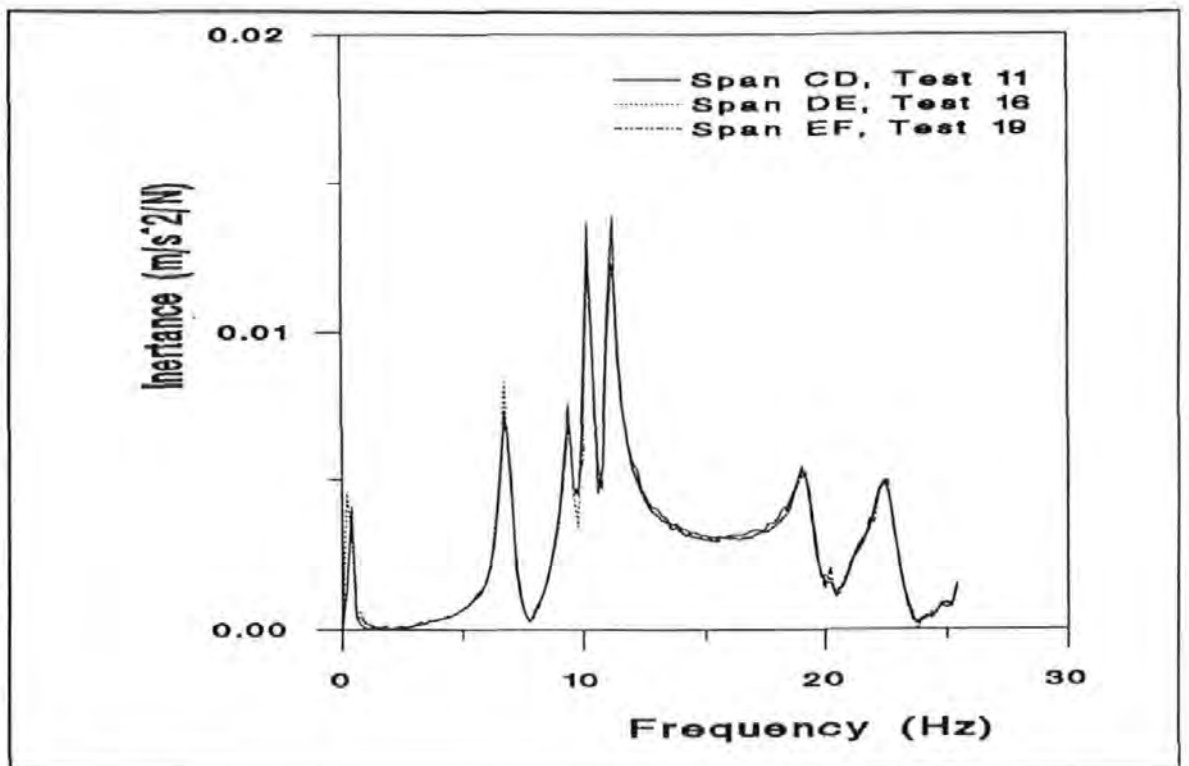


(b) West side

Figure 7.14 FRFs measured at the reference point before the repairs

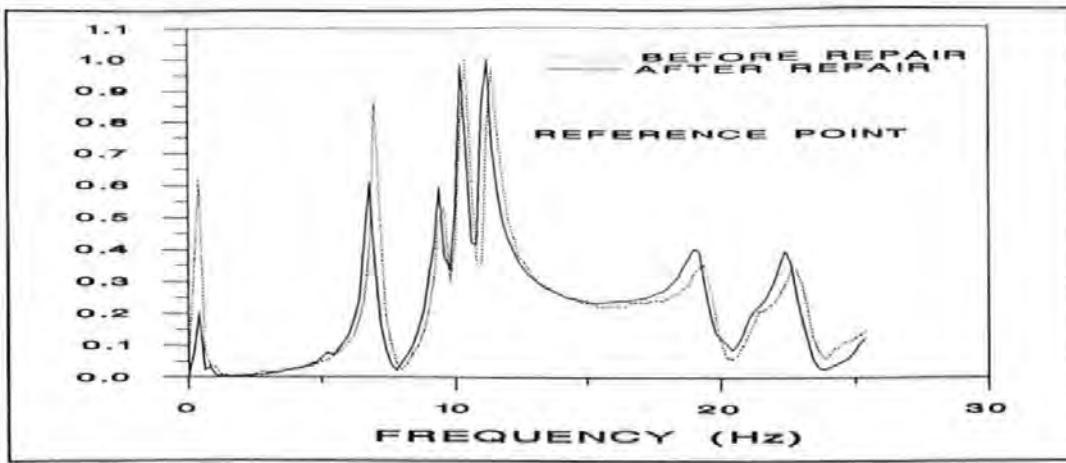


(a) East side

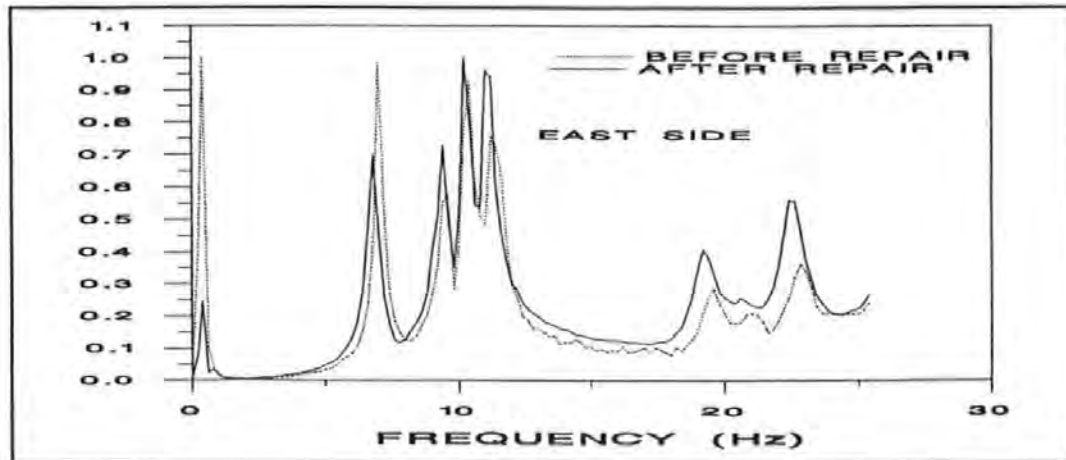


(b) West side

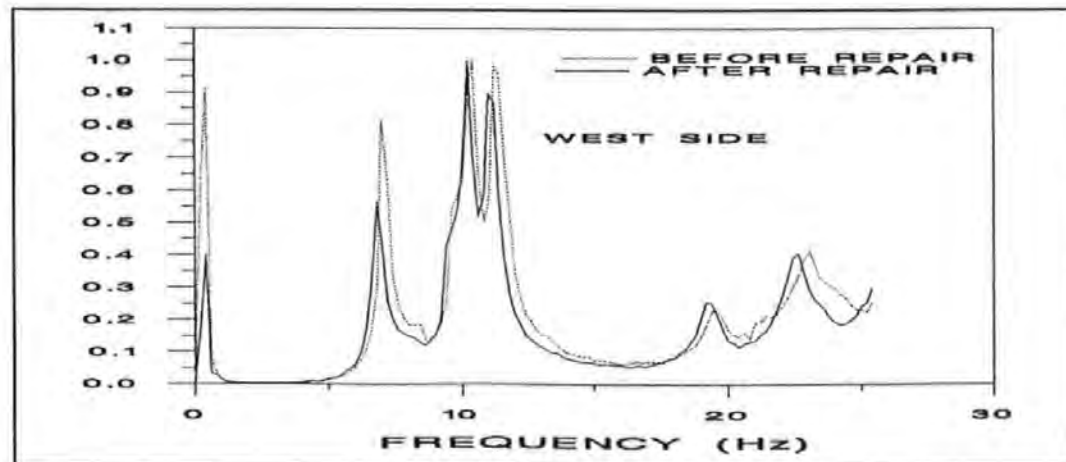
Figure 7.15 FRFs measured at the reference point after the repairs



(a) Measurements from the reference point

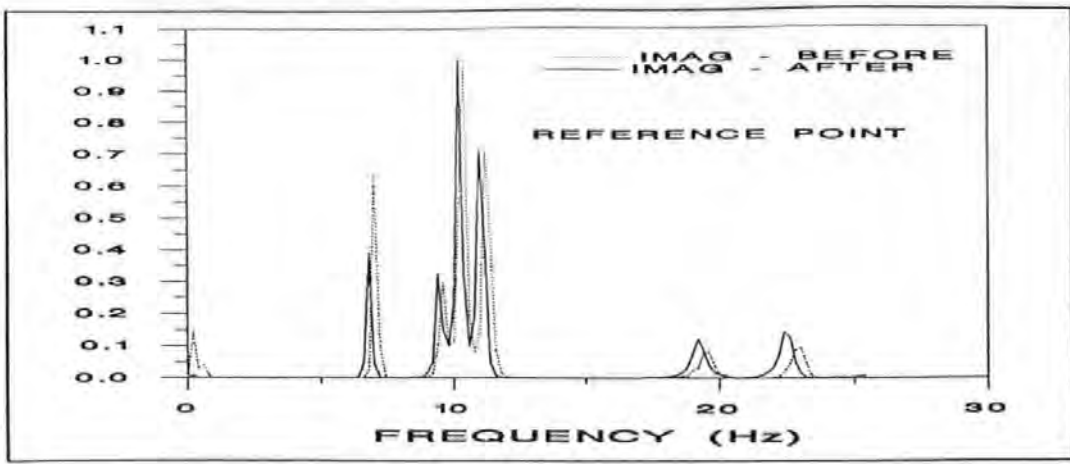


(b) Measurements from the east side

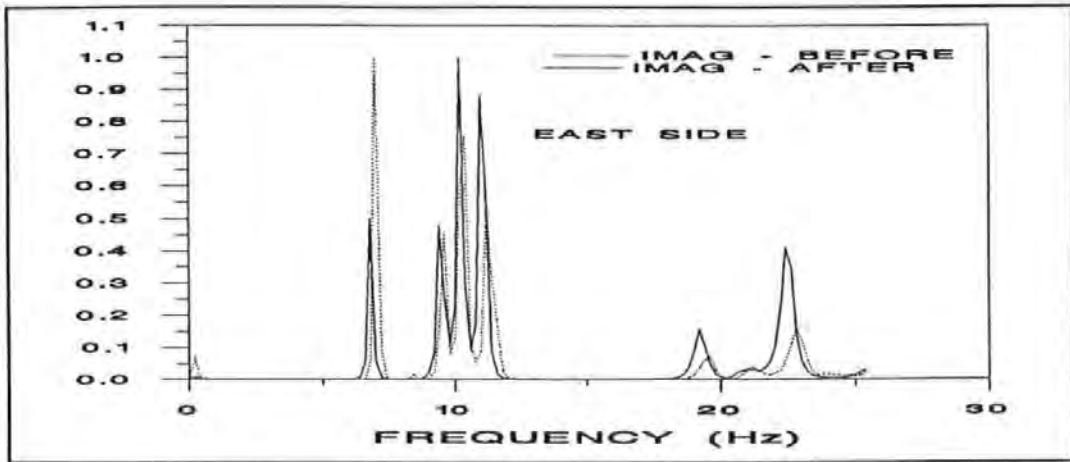


(c) Measurements from the west side

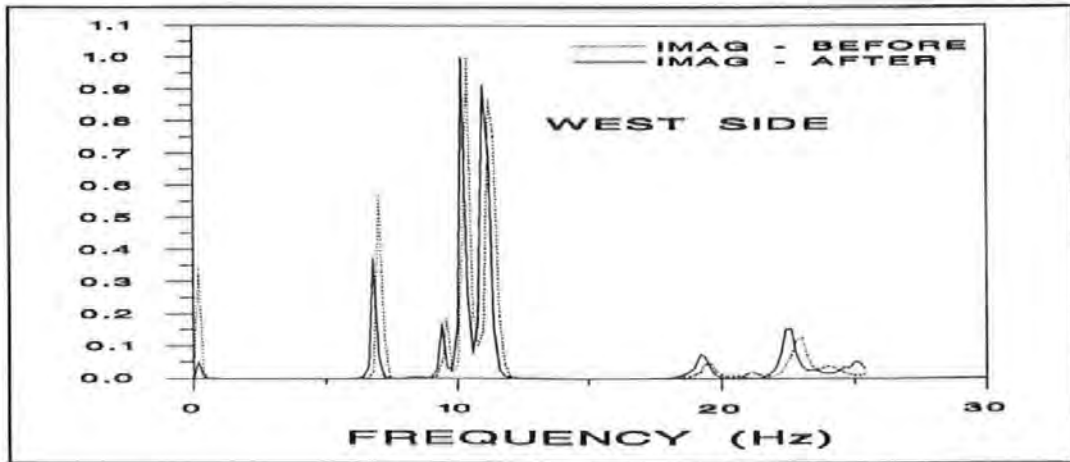
Figure 7.16 Comparison of the magnitudes of FRF : Deep Lane bridge



(a) Measurements from the reference point

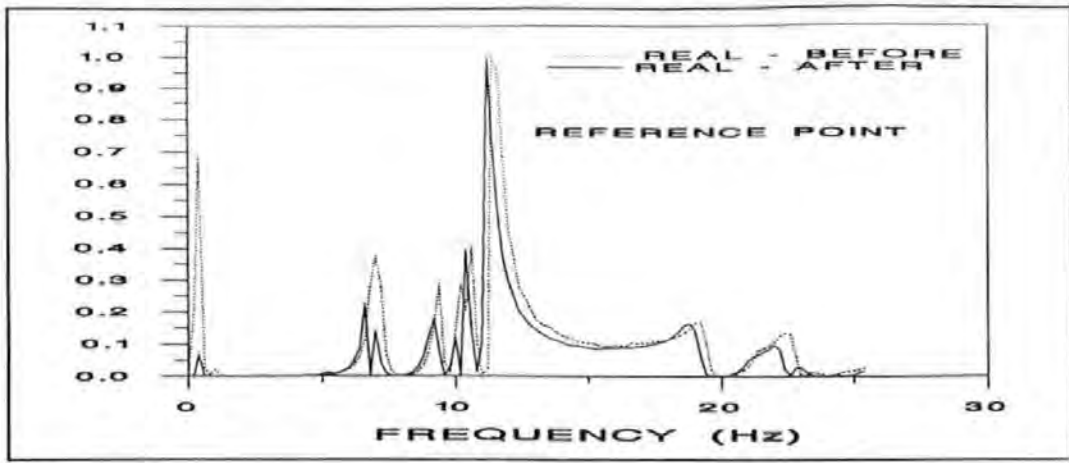


(b) Measurements from the east side

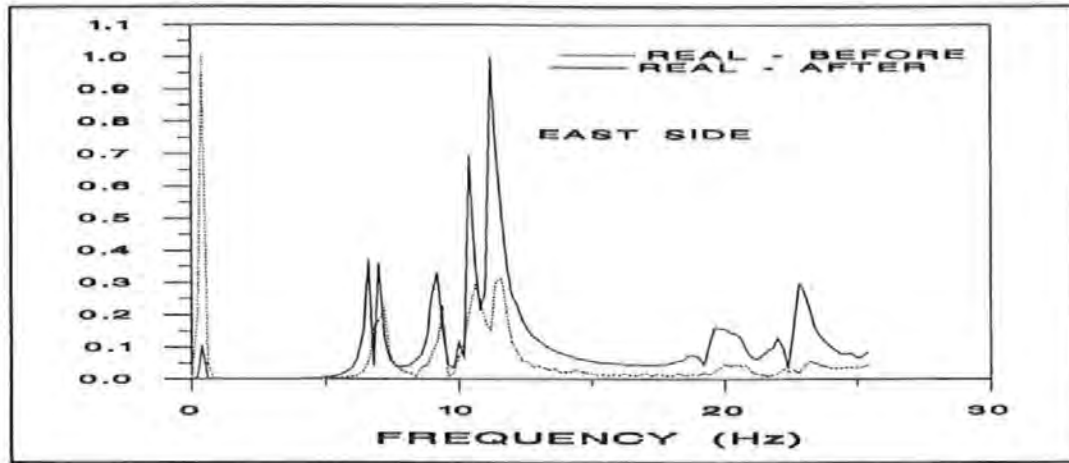


(c) Measurements from the west side

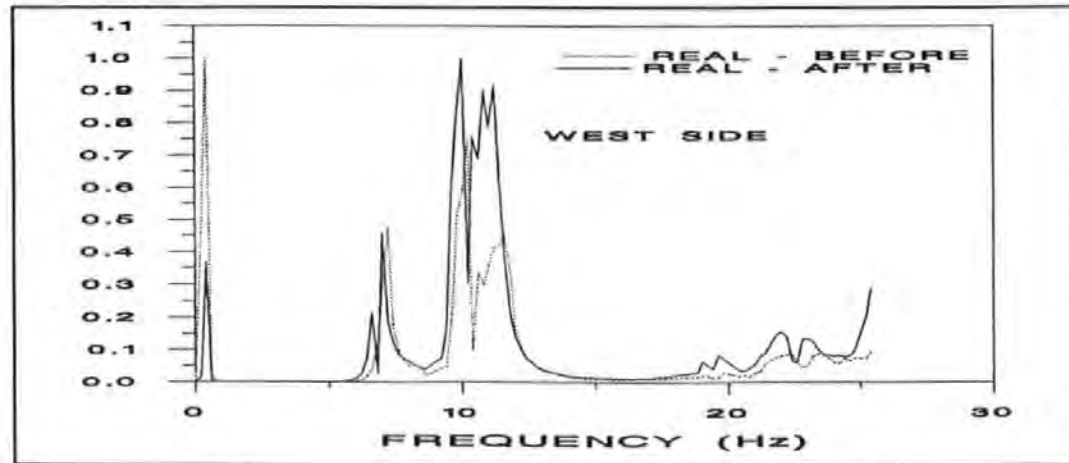
**Figure 7.17 Comparison of the squares of the imaginary part : Deep Lane bridge**



(a) Measurements from the reference point



(b) Measurements from the east side



(c) Measurements from the west side

**Figure 7.18 Comparison of the squares of the real part : Deep Lane bridge**

### 7.7.2 Natural frequencies and damping values

Table 7.2 shows a comparison of the natural frequencies and modal damping ratios obtained before and after the repairs. The maximum covariance of identified natural frequencies is 1.4% while that of the damping ratios is 14.2%. The frequencies reduced while there was no definite trend in the damping values. The large scatter usually observed in estimated damping values precludes their usage in integrity assessment. This point has been discussed in chapter three (section 3.5).

However, the observation (Ågårdh, 1991) that marginal change in the modal damping ratio implies that the damaged area lies within a nodal line of the corresponding mode shape can be used to approximately deduce the repaired areas. Using this criterion, points around the nodal lines of modes 2, 6 and 7 (modes with 0% change) would be expected to lie within the repair zones. Excluding the mode shape of mode 2 (for reasons explained earlier in section 7.6 and later in sub-section 7.7.3), the following points (see Figures 7.4 and 7.19) are identified as being affected by the repairs: west side - 5 (span CD), 13 & 14 (span DE), 23 & 24 (span EF); east side - 31 & 32 (span CD), 41 (span DE) and 50 & 51 (span EF). Only points 13 & 14 and 41 are close to the affected points (11, 38 and 39). Though the identification is poor, the approach may be used for a rough initial indication of possible damage sites.

**Table 7.2 Comparison of natural frequencies and damping ratios obtained before and after repairs to Deep Lane bridge**

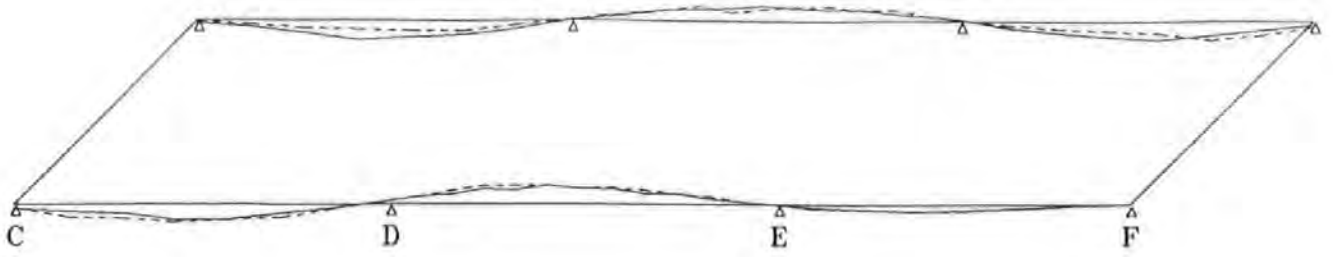
Mode Number	Natural Frequency			Viscous Damping Ratio		
	Before (Hz)	After (Hz)	Change (%)	Before	After	Change (%)
1	7.0 (0.004)*	6.8 (0.003)	-2.9	0.016 (0.075)	0.024 (0.107)	50
2	8.4 (0.006)	8.3 (0.014)	-1.2	0.018 (0.095)	0.018 (0.103)	0
3	9.5 (0.005)	9.4 (0.004)	-1.1	0.016 (0.142)	0.017 (0.105)	6
4	10.4 (0.005)	10.3 (0.004)	-1.0	0.017 (0.084)	0.016 (0.021)	-6
5	11.4 (0.003)	11.1 (0.004)	-2.6	0.021 (0.068)	0.019 (0.10)	-10
6	19.3 (0.004)	19.0 (0.002)	-1.6	0.017 (0.108)	0.017 (0.094)	0
7	22.7 (0.002)	22.3 (0.002)	-1.8	0.018 (0.083)	0.018 (0.052)	0

\* Covariance = standard deviation ÷ mean

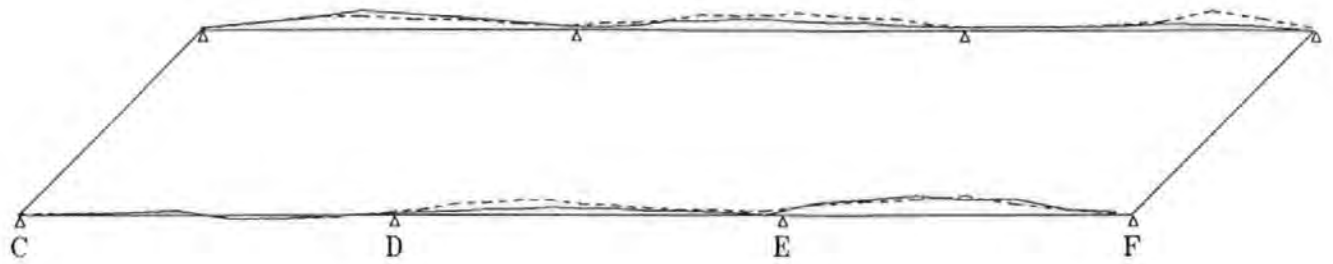
The maximum frequency reduction is less than 3%. This slight reduction in frequency is due to the nature of the repairs. As described earlier, the repairs were mainly concerned with increasing, by a short length, a few of the top reinforcement bars at two small sections of the deck. Since the concrete volume was also not altered, there were no large changes in the overall mass and stiffness of the bridge. Thus, significant changes in frequency are unlikely. For the approach adopted in this research, frequency changes less than 5% are regarded as insignificant.

### **7.7.3 Mode shapes, MAC and MSV**

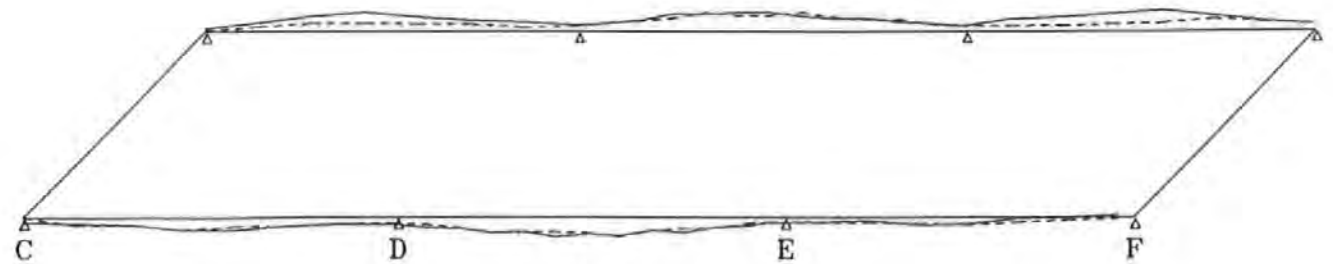
Since the modifications to the bridge were localized, mode shapes offer a better alternative for identifying the altered areas (Salawu and Williams, 1994a). This is due to the fact that the greatest changes in mode shapes are expected to occur in the vicinity of the modifications. The mode shapes before and after the repairs are compared in Figure 7.19. As mentioned earlier, the full mode shape for mode 2 was not identified because the vibrator was located close to a node of this mode. Thus, mode 2 has been omitted from Figure 7.19 and will not be referred to in subsequent discussions. Figure 7.19 shows differences in the mode shapes at the repaired span DE especially for modes 6 and 7. However, differences, though to a lesser extent, are also present in spans CD and EF.



(a) Mode 1: — Before (7.0 Hz); - - - After (6.8 Hz).

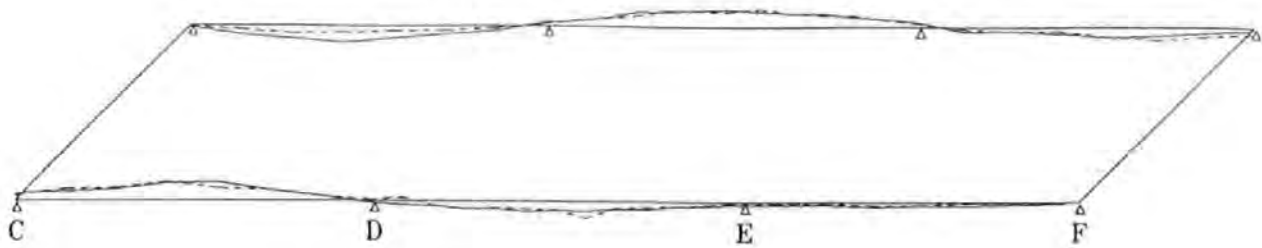


(b) Mode 3: — Before (9.5 Hz); - - - After (9.4 Hz).

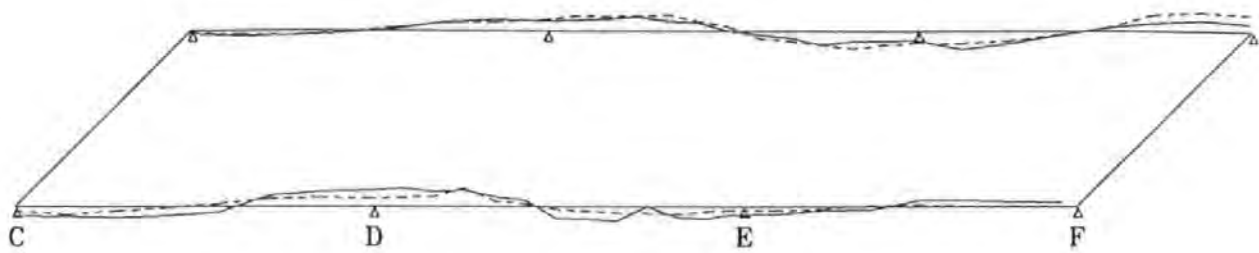


(c) Mode 4: — Before (10.4 Hz); - - - After (10.3 Hz).

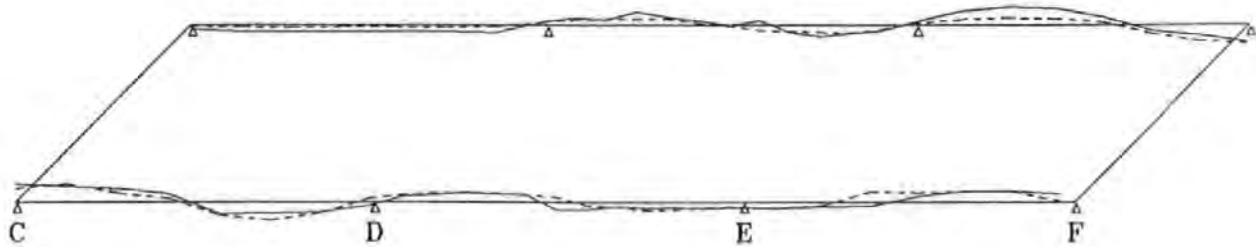
Figure 7.19 Comparison of mode shapes before and after repairs: Deep Lane bridge



(d) Mode 5: — Before (11.4 Hz); - - - After (11.1 Hz).



(e) Mode 6: — Before (19.3 Hz); - - - After (19.0 Hz).



(f) Mode 7: — Before (22.7 Hz); - - - After (22.3 Hz).

**Figure 7.19 Comparison of mode shapes before and after repairs: Deep Lane bridge (continued)**

After detecting changes in the structure's response functions and mode shapes, Modal Sensitivity Values (MSV) and Modal Assurance Criterion (MAC) values are useful parameters for determining to what extent the different modes have been affected. Details of MSV and MAC and their application to damage detection have been discussed in chapter four.

The diagonal elements of the MAC matrix should be 1 if there were no changes in the structure since the modes would essentially be the same. All the off-diagonal elements should be very close to zero. Figure 7.20 shows the MAC values. The off-diagonal elements underlined in the figure merely show that the corresponding modes (1 and 5; 3 and 4) have a degree of similarity. This can be seen to be the case by observing the mode shapes in Figure 7.19. The MAC values of 0.83, 0.83 and 0.73 for modes 3,6 and 7, respectively, indicate existence of changes in the bridge and the higher sensitivity of these modes (3, 6 and 7) to the modifications.

The MSV indicate the relative degree of influence of any alterations on the structure's vibration modes. The most affected mode has an index value of 100. Table 7.3 shows MSV of the bridge. The table suggests that modes 3,6 and 7 are most affected by the repairs. This is similar to the result from the MAC values.

		BEFORE REPAIRS					
		1	3	4	5	6	7
AFTER REPAIRS	1	<u>0.92</u>	0.09	0.09	<u>0.72</u>	0.02	0.00
	3	0.01	<b>0.83</b>	<u>0.53</u>	0.07	0.00	0.09
	4	0.08	<u>0.70</u>	<b>0.92</b>	0.04	0.02	0.01
	5	<u>0.77</u>	0.17	0.10	<b>0.89</b>	0.00	0.02
	6	0.02	0.01	0.00	0.00	<b>0.83</b>	0.01
	7	0.00	0.03	0.00	0.03	0.00	<b>0.73</b>

**Figure 7.20 Modal Assurance Criterion (MAC) values of Deep Lane bridge**

**Table 7.3 Modal Sensitivity Values (MSV) of Deep Lane bridge**

Mode	MSV
1	44.9
3	78.7
4	48.6
5	14.4
6	100
7	57.4

#### 7.7.4 COMAC and Integrity Indices

The Coordinate Modal Assurance Criterion (COMAC) values obtained at the measurement points are shown in Table 7.4. A COMAC value close to 1 indicates good correlation (thus no changes), at the measurement point, between the two data sets. Results of tests by Creed (1989) have suggested that measured mode shape ratios are only repeatable to within 35% to 40% while Friswell and Penny (1992) and Lubber and Lotze (1990) have stated that a 20% error in a particular element of the mode shape vector would be typical. In addition, obtaining very high quality data from full-scale tests is difficult. Taking these factors into account, it is necessary to define a threshold value (for COMAC) below which occurrence of "defects" at the relevant measurement point can be inferred. A value of 0.8 is suggested here for large civil engineering structures. COMAC values less than 0.8 have been underlined in Table 7.4.

From Table 7.4 (and using the criterion just described), points 38, 39, 41 and 50 are identified as being within the repair zone. These points can be compared with points 11, 38 and 39 which actually lie in the repair zone (span DE). The identification of two out of three points is reasonably good. It is of interest to note that the two identified points lie on the same side as the vibrator (see Figure 7.4). This would suggest that better identification could be achieved if the response is measured on the same side as the vibrator position, thus requiring at least two (one on either side) vibrator locations. This observation also favours using multiple excitation techniques (Allemang and Brown, 1985; Zaveri, 1984) in which more than one vibrator is used to simultaneously excite the test structure. Multiple excitation provides a better energy distribution, excites all the modes in the range of interest and allows for repeated roots to be detected. However, resource constraints usually preclude the use of more than one vibrator since multiple excitation

requires sophisticated equipment for excitation and analysis.

**Table 7.4 Coordinate Modal Assurance Criterion (COMAC) values of Deep Lane bridge**

Location	COMAC	Location	COMAC	Location	COMAC
1	0.85	19	0.94	37	0.84
2	0.90	20	0.96	38	<u>0.61</u>
3	0.90	21	0.94	39	<u>0.75</u>
4	0.94	22	0.90	40	0.90
5	0.96	23	0.90	41	<u>0.68</u>
6	0.96	24	0.87	42	0.87
7	0.88	25	0.83	43	0.85
8	0.95	26	0.93	44	0.82
9	0.93	27	0.91	45	0.91
10	0.97	28	0.93	46	0.83
11	0.94	29	0.95	47	0.84
12	0.96	30	0.85	48	0.93
13	0.95	31	0.90	49	0.97
14	0.95	32	0.86	50	<u>0.53</u>
15	0.87	33	0.92	51	0.91
16	0.96	34	0.92	52	0.85
17	0.94	35	0.97	53	0.86
18	0.95	36	0.88	54	0.87

A Global Integrity Index of 0.98 was obtained. The larger the difference between the Global Index and unity, the higher the degree of "deterioration" experienced by the structure. The value of 0.98 further shows that the effect of the remedial works on the overall stiffness of the bridge was very minimal. The Local Integrity Indices are shown in Table 7.5. The higher the Index, the higher the probability of the corresponding point being within the repair zone. Two zones were identified on each side of the bridge i.e. westside - points 10, 11 and 12; points 25, 26 and 27; eastside - points 38 and 39; points 52, 53 and 54. Points 25, 26, 27 (westside) and 52, 53, 54 (eastside) are close to support line F (see Figure 7.4) and are not within the repair zone. During the second series of tests, the slip road to Plymouth (under span EF) was being upgraded and fitted with crash barriers. This involved some excavation and drilling close to the piers on support line F and could have affected the results. It should however be noted that the effects of this road upgrading was not apparent in the results obtained using COMAC.

The points (10, 11, 12, 38 and 39) in the other two identified zones contain points 11, 38 and 39 which lie within the repaired zones. If results from points close to support line F are excluded, based on the reason given in the previous paragraph, the identification is satisfactory. Even if all the zones are considered, a closer investigation of the points will reveal the correct areas. Detailed investigation of four zones (containing 11 points) is cheaper, faster and more efficient than an overall survey of the whole bridge involving 54 points, assuming the measurement pattern used in the tests is adopted.

**Table 7.5 Local Integrity Indices of Deep Lane bridge**

WEST SIDE			EAST SIDE	
Location	Index		Location	Index
1	34.1		28	13.5
2	1.2		29	11.1
3	38.5		30	3.0
4	31.5		31	16.9
5	40.3		32	14.4
6	5.9		33	5.2
7	12.5		34	10.4
8	23.4		35	8.7
9	29.3		36	12.0
<b>10</b>	<b>100</b>		37	38.8
<b>11</b>	<b>68.4</b>		<b>38</b>	<b>62.0</b>
<b>12</b>	<b>64.1</b>		<b>39</b>	<b>74.2</b>
13	33.9		40	17.4
14	23.3		41	13.4
15	22.1		42	57.6
16	22.3		43	22.8
17	14.6		44	6.8
18	20.9		45	25.6
19	30.0		46	22.2
20	41.3		47	11.7
21	42.6		48	10.6
22	35.1		49	9.0
23	0.80		50	3.4
24	25.6		51	3.0
<b>25</b>	<b>59.1</b>		<b>52</b>	<b>100.0</b>
<b>26</b>	<b>52.2</b>		<b>53</b>	<b>68.6</b>
<b>27</b>	<b>57.9</b>		<b>54</b>	<b>55.2</b>

**(Global Integrity Index = 0.98)**

## 7.8 Conclusions

Results from the full-scale tests have shown that sufficient excitation forces can be generated by the excitation system developed. Dynamic response, as a result of the induced excitation, yielded data from which modal parameters were obtained. Good correlation, within limits of the available structural details of the bridge, was obtained between the measured and calculated natural frequencies and mode shapes. The average error between calculated and measured natural frequency (excluding mode 4) is 6.4%. More confidence can be placed in future usage, for various purposes, of a validated analytical model.

The natural frequencies of the bridge did not change significantly while there was no definite trend in the changes in damping values after structural repairs to the bridge. The localised nature of the repairs was the reason for the modest changes in frequency. Comparison of the components of the normalised cumulative frequency response function was able to give an indication of the changes in the bridge's condition. MAC and MSV also indicated changes and suggested the modes that were most influenced by the repairs.

The mode shapes before and after structural repairs, COMAC values and Integrity Indices were found to give good indications of the presence and location of the repairs. The incomplete experimental identification of the mode shape for mode 2 has emphasised the need for a pre-test analysis so that suitable excitation and measurement locations are selected in order that all modes of interest can be observed.

## CHAPTER EIGHT

### FULL-SCALE TESTING OF HOLWAY ROAD BRIDGE

#### 8.1 Introduction

In this chapter, results from forced vibration testing and finite element analysis of Holway Road bridge, Taunton, Somerset, are presented and discussed. The bridge was chosen because results of a recent structural inspection showed that the deck had inadequate bending capacity while the vertical rating of the support bearings (at the abutments) was less than full applied vertical loading. The studies reported in this chapter refer to the bridge's condition before and after installation of new bearings. It was originally intended to conduct another test after strengthening work to improve the deck's bending capacity but the date for this work was still undetermined as at the end of this research project.

As far as the author is aware, results of vibration testing before and after installation of new bearings on a highway bridge has not been reported in the literature. It was therefore intended to investigate the effects of the new bearings on the bridge's modal parameters. Correlation of the experimental results with finite element analysis predictions was also conducted to further demonstrate the effects of bearing replacement on the bridge's dynamic response and to validate the analytical models.

#### 8.2 Description of Bridge

Holway Road bridge is a four span structure that carries an unclassified road over the M5 Birmingham to Exeter motorway between junctions 25 and 26 (Blackbrook to Chelston

section of the M5). The side elevation and deck cross-section of the bridge are shown in Figure 8.1. Built in 1971/72, it is of insitu concrete construction with the deck being continuous. The spans are skewed at  $20^\circ$  while the square span lengths are 11.8m, 18.2m, 18.2m and 11.8m. The carriageway width over the bridge is 6m. Like Deep Lane bridge (chapter seven), the deck has circular voids except in the vicinity of the piers and abutments where it is of solid section. There are six voids each of diameter 600mm. The overall depth of the deck is 1000mm. The verges are supported by a cantilever section which has an average depth of 275mm and incorporates a service bay.

The abutments are of a skeletal type founded on cast insitu concrete driven piles. The deck is supported by four bearings at each abutment. At each of the three intermediate support positions, there are two columns (piers) which are monolithic with the deck. The columns have rectangular cross-section and are founded on piles similar to those used for the abutments. Each column is 7.135m in height and has a cross-sectional dimension of 1m  $\times$  0.5m.

### **8.3 The Repair Work**

Results of structural inspections carried out in 1990 by Somerset Consultant Engineers, SCE (the consulting division of the Environment Department, Somerset County Council) revealed that the deck had inadequate assessment live load capacity due to insufficient reinforcement to resist the midspan bending moments in spans 1 and 4. It was also found that both abutments have rotated away from the motorway (see Figure 8.1) causing the bearings to exceed their maximum allowable movement. At the most heavily loaded bearing, the dead load was found to exceed the permissible bearing capacity by 14%. Lane and weight restrictions have been in force on the bridge since the inspection.

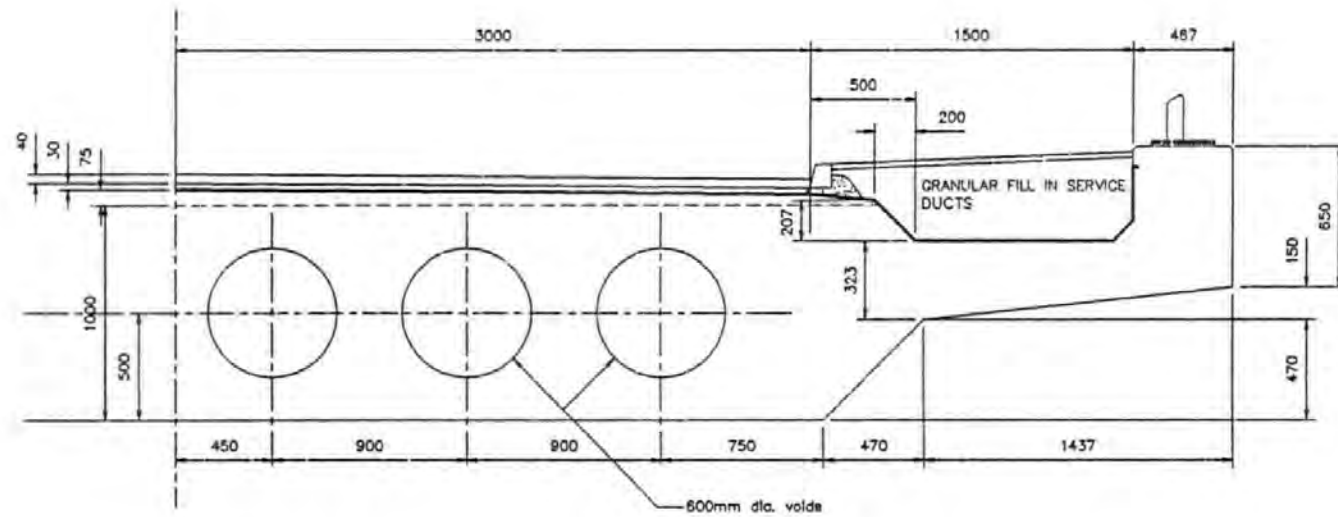
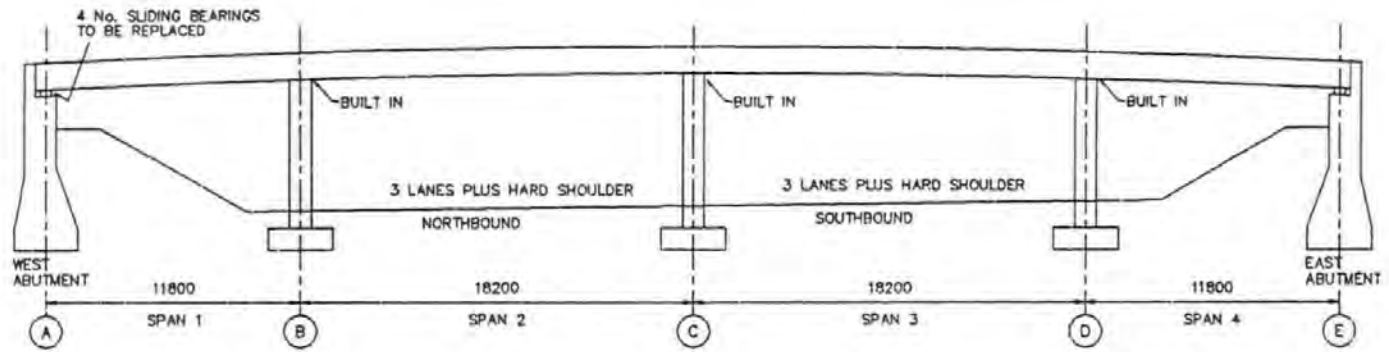


Figure 8.1 Side elevation and deck cross-section of Holway Road bridge. (dimensions in mm)

It was decided to replace the bearings and increase the bending capacity of the deck by bonding plates to the deck soffit in spans 1 and 4. Only the bearing replacement (which, in this chapter, will sometimes be referred to as the repairs) scheme is described in this section since no firm date has been fixed for the plate bonding contract (it was originally scheduled for autumn/winter 1993). In addition to the obvious requirement that the vertical rating of the new bearings exceed the applied vertical load, the bearings were also required to allow greater longitudinal movement, of up to say 50mm.

The sequence of work started with jacking of the bridge deck up to a level that would allow removal of existing bearings and installation of new ones. The jacking was conducted such that differential lifts did not exceed 1.0mm. The existing bearings were removed and the concrete in the existing plinths broken out. Existing plinth reinforcement was straightened, new reinforcement cages added and new plinths constructed. The new bearings were installed and the deck lowered. After the (new) plinth concrete grout and mortar had reached the specified strength, load was transferred from the jacks onto the new bearings. The replacement work was done in January/February 1994.

#### **8.4 Finite Element Modelling and Pre-Test Analyses**

Two-dimensional linear elastic models of the bridge were created with plate (element type QF4) and grillage (element type GRIL) elements using the finite element program LUSAS. The grillage elements were only used to model the parapet upstand beams. Free vibration analyses were conducted on models which represented the bridge's condition before and after bearing replacement. Only the deck slab was modelled and all the four spans were included (Figure 8.2). Each element has three degrees of freedom (DOF) - one translation (vertical) and two rotations (about the transverse and longitudinal axes) - at each node. 396

quadilateral plate elements, 72 grillage elements and 444 nodes were used for each model.

The elements in the finite element mesh had varying thicknesses to represent the different stiffnesses of sections (solid parts, verges, upstand beam and voided parts) of the bridge deck. Similar considerations as for Deep Lane bridge (chapter seven - section 7.5) were adopted for the effective material and inertia values. The deck's longitudinal and transverse stiffnesses were assumed to be equal i.e. orthotropic. This assumption is acceptable since the depth of the voids does not exceed 60% of the overall depth of the deck (Hambly, 1991). A similar orthotropic behaviour was assumed for Deep Lane bridge.

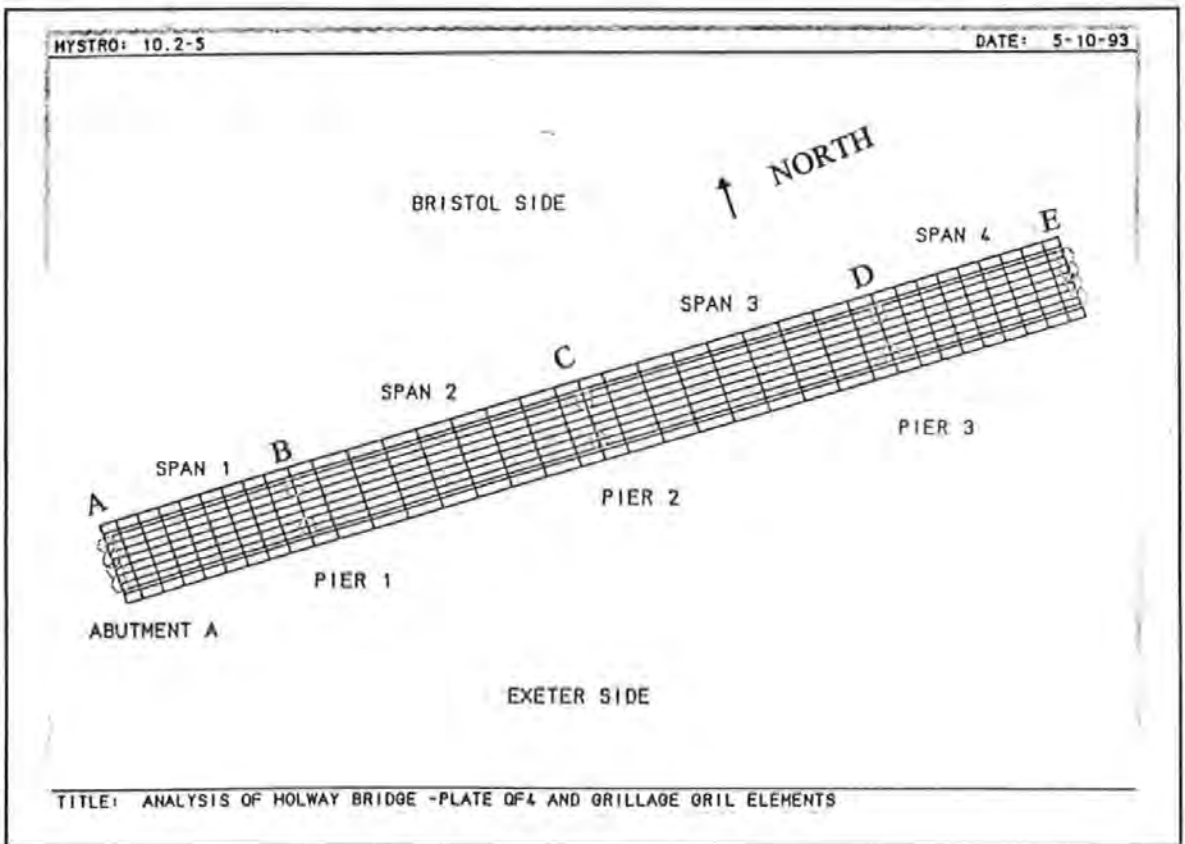


**Figure 8.2 Finite element model of Holway Road bridge**

At the abutments, free movement was allowed for the rotational DOFs while the vertical DOF was represented as either sprung or fully fixed. The built in piers were represented by a combination of vertical and rotational springs at the appropriate support nodes. The spring stiffness values were obtained from SCE.

Pre-test analyses were conducted on two different models of the bridge so as to : 1) obtain suitable measurement locations; 2) have a 'feel' for the nature and magnitudes of the changes likely to result due to the repairs; 3) identify modes most likely to be influenced by the repairs; and 4) choose a position for the vibrator so that the modes of interest can be observed. The first model represented the bridge before the bearings were replaced. In this model, the vertical DOFs at the abutments were represented as sprung. The second model simulated conditions after the repairs and had the vertical DOFs at the abutments fully fixed. This boundary condition was adopted since, according to the manufacturers and SCE, the stiffness of the new bearings is such that full vertical restraint is recommended.

Table 8.1 shows the modal frequencies and diagonal elements of the MAC matrix (MAC has been discussed in sub-section 4.2.1) from the two models. The frequencies increased, as would be expected, with the largest increases occurring within the frequency range 11Hz - 16Hz. Correlation between corresponding mode shapes, as represented by values in the last column of Table 8.1, decreases appreciably after the third mode. The full MAC matrix (Table 8.2) shows that cross-correlation of modes, represented by large values of off-diagonal elements (italized in the table), has occurred. This further demonstrates the significance of accurate representation of boundary conditions.

**Table 8.1 Comparison of frequencies for partial and full vertical restraint at abutments**

Mode Number	Frequency (Hz)			Diagonal Elements of MAC Matrix
	Sprung Stiffness ( $126 \times 10^6$ N/m)	Full Fixity	Difference (%)	
1	5.90	6.06	5.7	1.0
2	8.12	8.56	5.4	1.0
3	11.05	12.58	13.8	1.0
4	11.98	13.99	16.8	0.18
5	12.18	14.05	15.4	0.58
6	12.48	14.94	19.7	0.26
7	14.10	20.31	44.0	0.01
8	15.71	21.42	36.4	0.0
9	20.17	21.62	7.2	0.03
10	21.34	22.43	5.1	0.01

**Table 8.2 MAC matrix for partial and full vertical restraint at abutments**

	Partial Vertical Restraint									
	<b>1.0</b>	0.1	0.65	0.02	0.05	0.58	0.0	0.02	0.01	0.22
Full Vertical Restraint	0.1	<b>1.0</b>	0.44	0.1	0.07	0.05	0.05	0.0	0.16	0.03
	0.06	0.82	<b>1.0</b>	0.01	0.11	0.07	0.01	0.02	0.01	0.22
	0.01	0.0	0.15	<b>0.18</b>	0.80	0.06	0.0	0.0	0.38	0.04
	0.01	0.0	0.05	0.44	<b>0.58</b>	0.13	0.01	0.01	0.26	0.07
	0.0	0.0	0.22	0.45	0.07	<b>0.26</b>	0.11	0.0	0.04	0.46
	0.06	0.61	0.19	0.11	0.10	0.02	<b>0.01</b>	0.08	0.36	0.07
	0.8	0.09	0.07	0.04	0.02	0.5	0.0	<b>0.00</b>	0.02	0.13
	0.0	0.02	0.0	0.0	0.02	0.05	0.89	0.08	<b>0.03</b>	0.10
	0.01	0.0	0.01	0.01	0.0	0.00	0.08	0.93	0.25	<b>0.01</b>

Results from the pre-test analyses suggested that measurable changes should occur in the bridge. From the experience of using the data acquisition and analysis systems (chapter six), it was realised that not more than six to seven modes within the frequency range 0 - 25 Hz are likely to be identified. The analyses results were therefore used to select measurement points and vibrator location that would allow reasonably accurate identification of six modes. It was also considered important to identify a mode within the 14Hz - 17Hz frequency range (most affected range shown in Table 8.1). Using pre-test analyses in this way to select measurement points also meant the points could be selected to coincide with some of the analytical nodes and thus facilitate easy comparison of experimental and theoretical modal models.

### **8.5 Measurement Procedures**

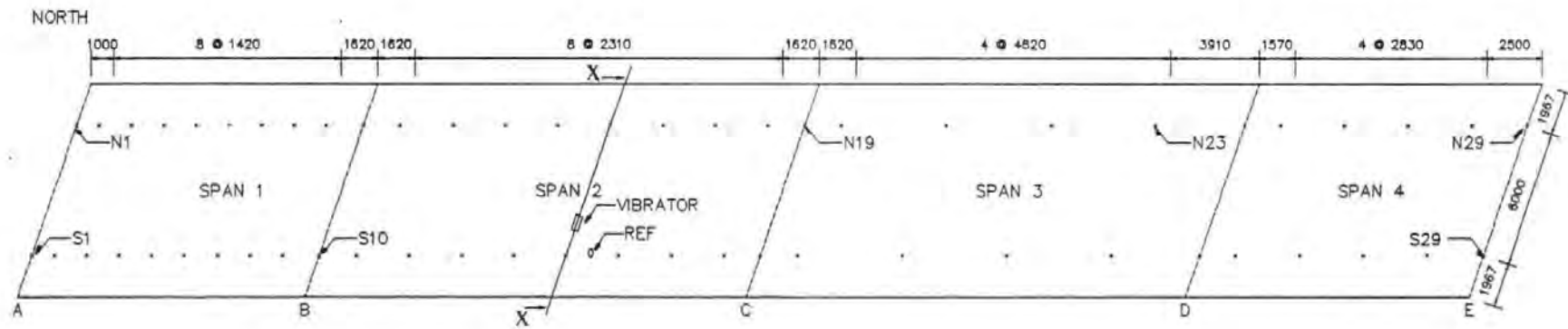
Two series of full-scale tests were conducted on the bridge. The equipment, experimental and data analysis procedures adopted for each series were the same and have been described in chapters six and seven. A test frequency range of 0 - 25 Hz was adopted as mentioned in the last paragraph. The first series of tests was conducted on November 2nd and 3rd 1993 while the second series was carried out on March 21st and 22nd 1994. The first series was initially scheduled for October 26th and 27th 1993. After setting up the equipment and operating them for about 40 minutes on October 26th, the vibrator control unit stopped working and all efforts to get it working failed. The tests were thus called off on the 27th and redone the following week after repairing the control unit in the laboratory at Plymouth. This problem was one of many encountered and illustrates the difficulties of full-scale field testing.

The measurement locations used are shown in Figure 8.3. The vibrator (see Figure 8.3b)

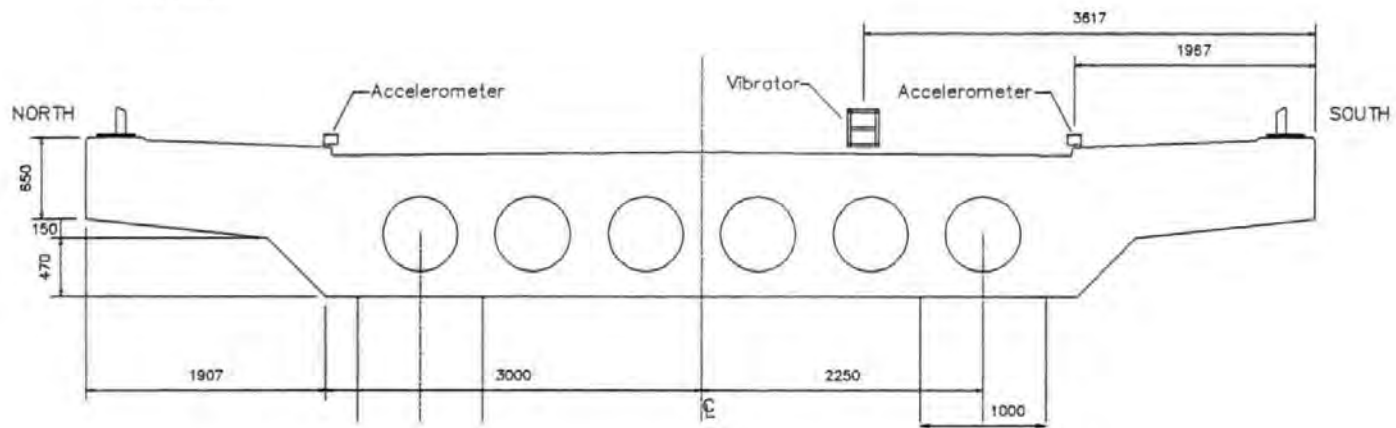
was placed on the roadway rather than the footpath to avoid the input force being damped as a result of the presence of granular fill underneath the footway (see Figure 8.1). For the same reasons, the accelerometers were placed just by the road edge (Figure 8.3b). 58 measurement points (29 on either side of the bridge deck) were used. The notation adopted was to prefix an N or S (for North and South respectively) before the point number depending on which side of the bridge it (point) lies. Since the bridge is symmetrical, the 'density' of measurement points in spans 3 and 4 is half that of spans 1 and 2. The few points used in spans 3 and 4 were only taken to allow identification of unsymmetrical mode shapes. Use of such a pattern of measurement points was further influenced by results from the initial theoretical analyses which suggested that any changes in mode shapes would be pronounced in the outer spans, as should be expected. A reference point (shown as REF in Figure 8.3a) was also used in the same manner as described in the previous chapter. Typical plots of the response functions obtained from the tests are shown in Figure 8.4 while sample curve-fits are shown in Figure 8.5.

## **8.6 Discussion of Experimental Results**

The experimental results obtained before and after the bearings were replaced are presented and discussed in this section. The procedure followed is similar to that used in section 7.7. Measurements (typical FRFs are shown in Figure 8.6) from the reference point were used to check on the repeatability and consistency of the procedures. As should be expected, the curves in Figure 8.6 are almost identical since they refer to the same location.



(a) Plan.



(b) Section X X showing vibrator position.

Figure 8.3 Layout of measurement points used. (dimensions in mm)

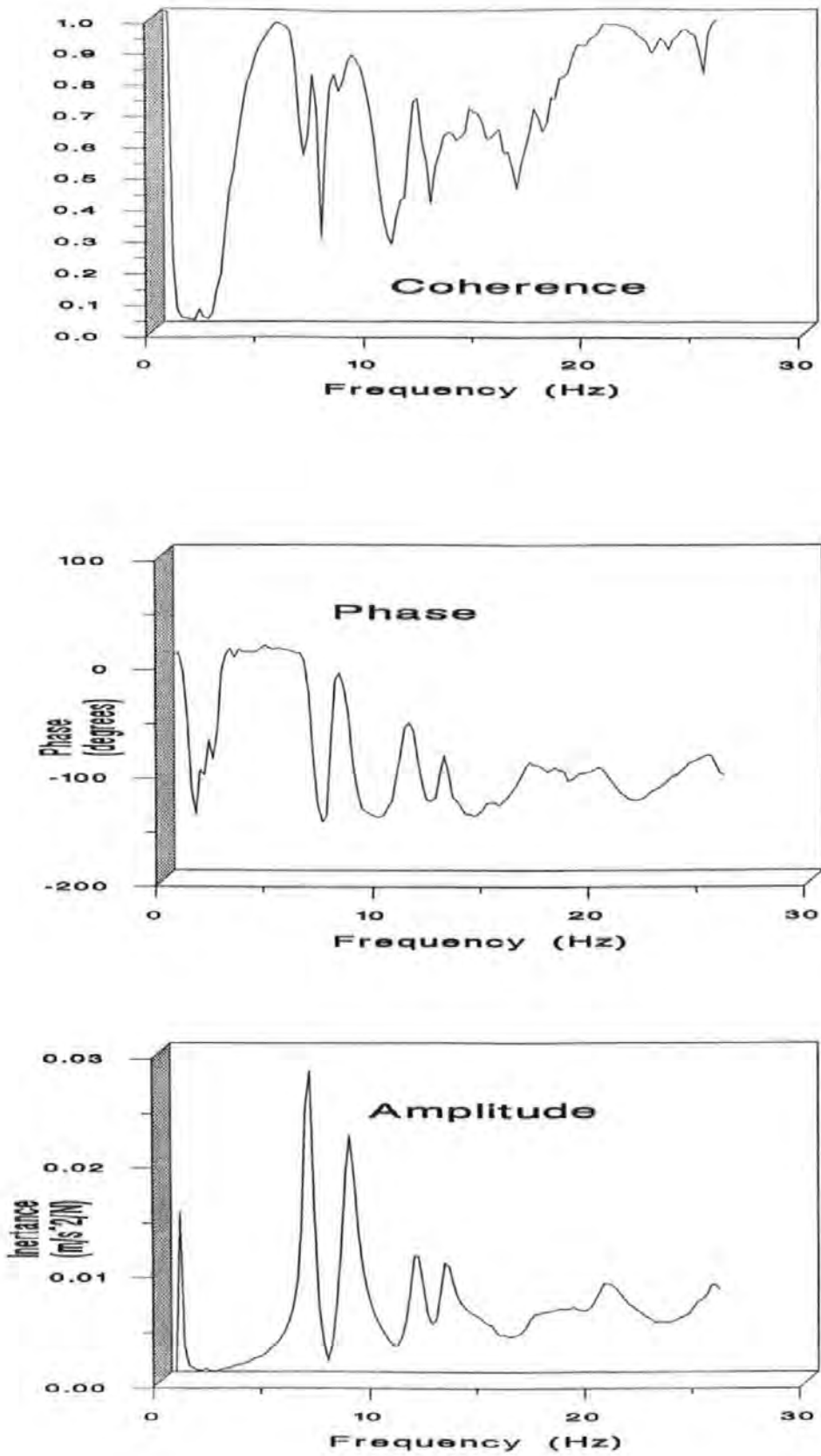
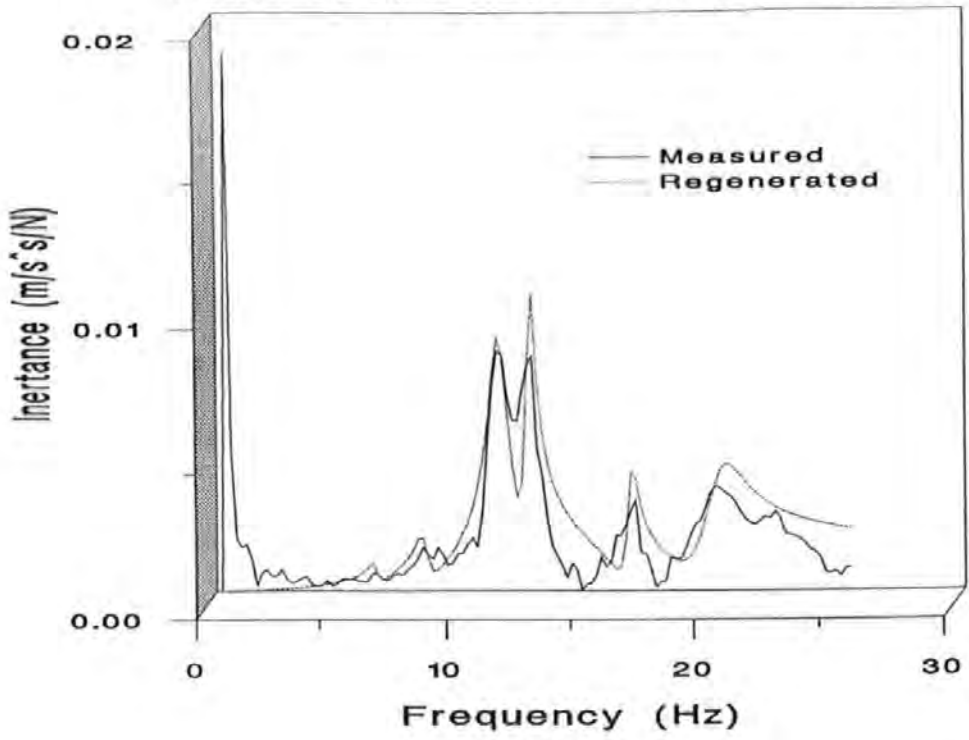


Figure 8.4 Sample FRF plot from tests before bearing replacement

Point S25, before bearing replacement



Point S5, after bearing replacement

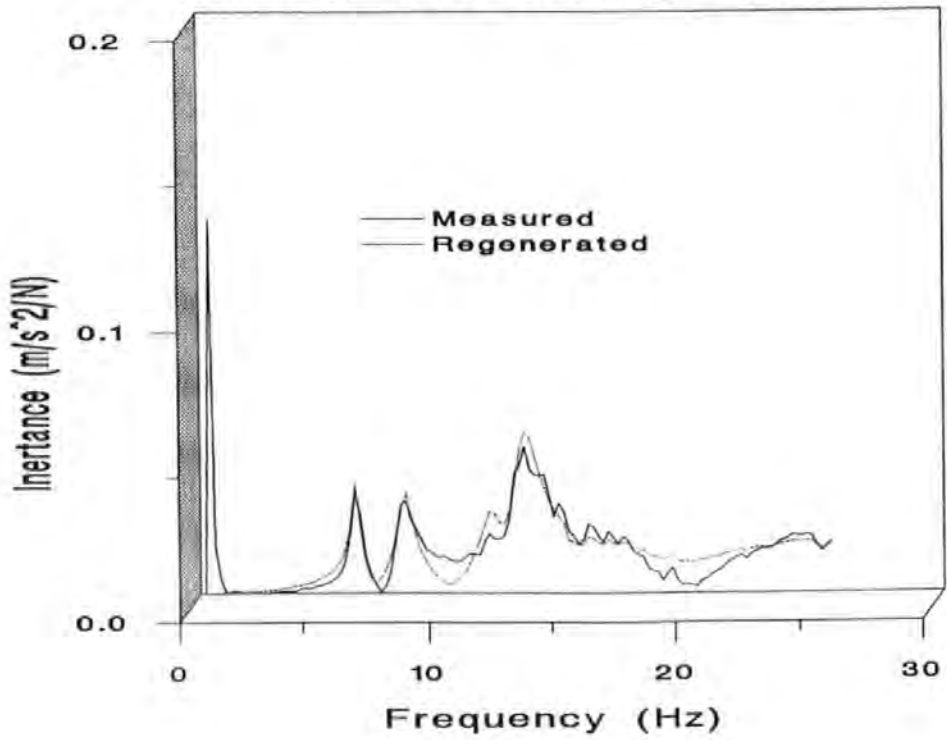
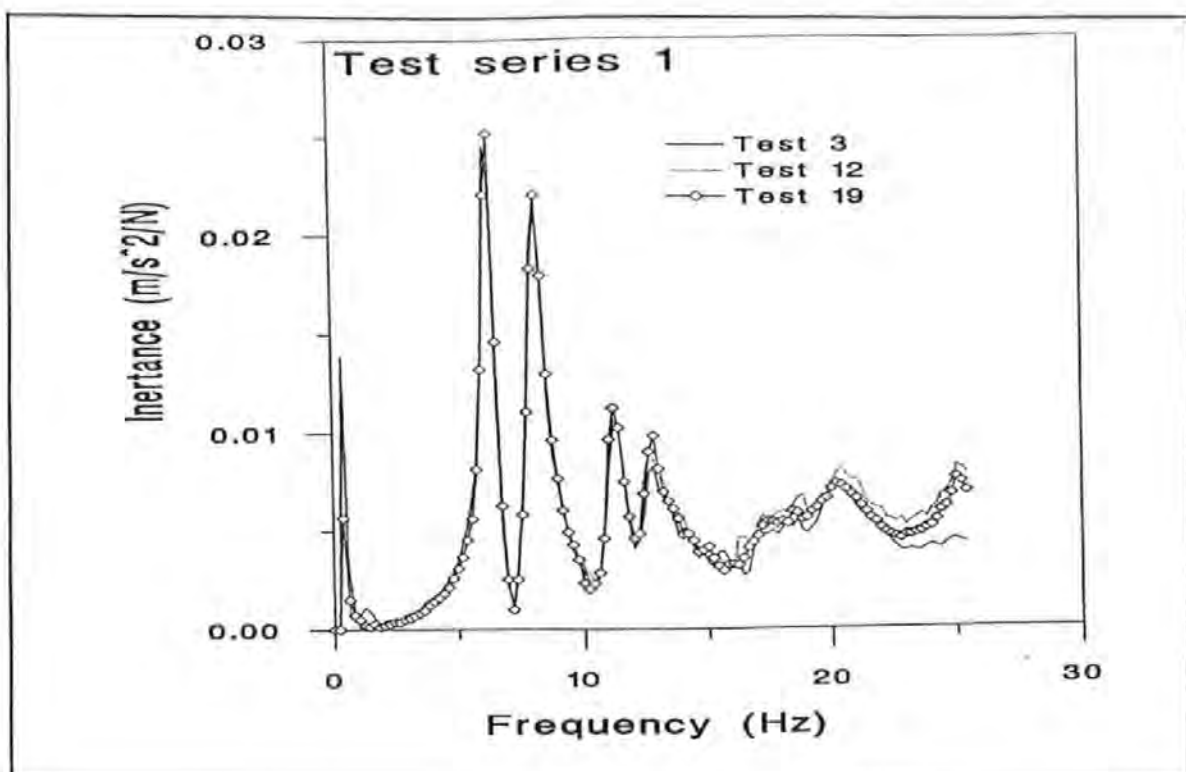


Figure 8.5 Example of curve-fitting



**Figure 8.6 Typical FRFs measured at the reference point**

The comments in the third and fourth paragraphs of section 7.7 as regards the effects of ambient conditions on dynamic parameters are equally appropriate here. The variation in environmental variables at the nearest weather station (Nettlecombe, a distance of about 40km) to the bridge during the test periods is shown in the appendix (Table A.5). Only daily weather summaries are available for the station. The conditions were not dissimilar and were not expected to have significant effects on the identified parameters.

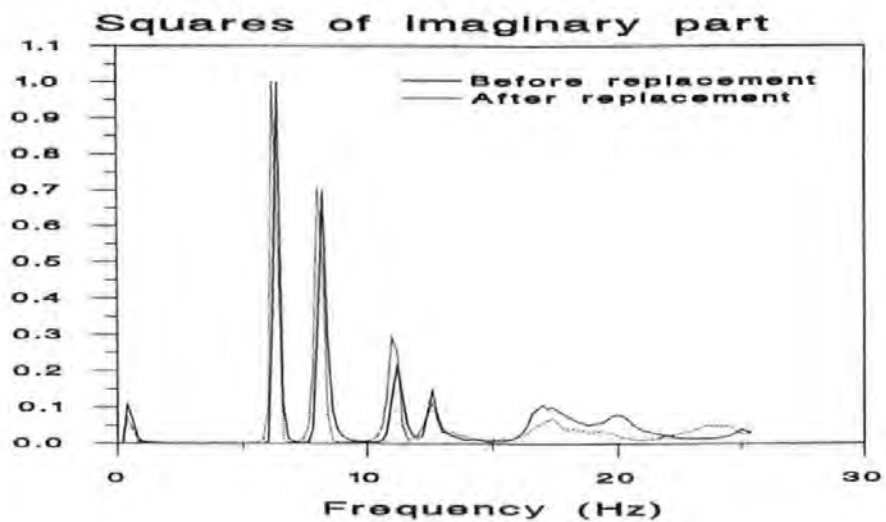
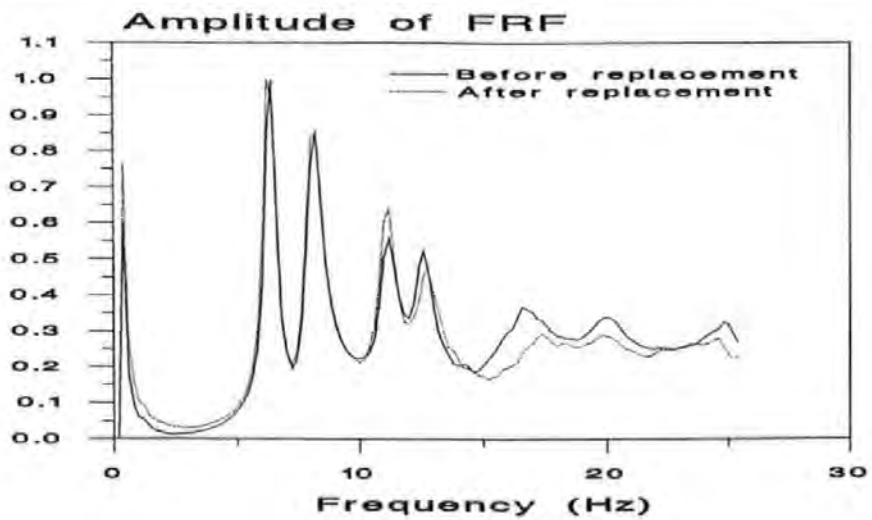
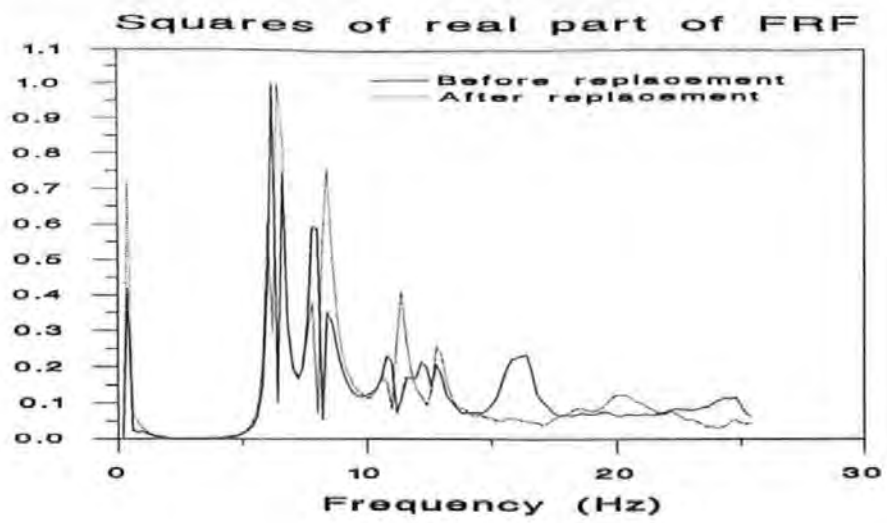
### **8.6.1 Frequency response function (FRF)**

Figure 8.7 shows a comparison of the components of the normalised cumulative (for all measurement points) FRF before and after bearing replacement. As was noticed in subsection 7.7.1, plot of the squares of the real part appears to give the best indication of any changes in the bridge's condition. The differences seem to be more pronounced for modes occurring after 11.0Hz, showing some similarities to results of the pre-test analyses (see section 8.4).

Increasing the bearing stiffness might be expected to lead to some reduction in the vibration level. This would mean the ordinates of the curves corresponding to the second test series should be somewhat lower than those of the first series. This trend is displayed for the higher modes (greater than 11.0Hz) in the amplitude and imaginary components plots. The real part plot does not show a consistent trend. Thus, the plots merely show changes in the two states without giving any firm indication of which state is stiffer. The changes could also have been due to variations in environmental factors and further analysis of the modal parameters is necessary.

### **8.6.2 Natural frequencies and damping values**

The natural frequencies and modal damping ratios obtained are shown in Table 8.3. There was no significant changes in frequency, an average increase of 1.7% being recorded. The main conjecture from this result is that the vertical stiffness of the new bearings is not likely to be high enough to provide full vertical restraint at the abutments. As previously shown in section 8.4, condition of full fixity should lead to increases higher than those observed. This will be further discussed in section 8.7.



**Figure 8.7 Comparison of FRFs before and after bearing replacement**

**Table 8.3 Comparison of natural frequencies and damping ratios obtained before and after bearing replacement on Holway Road bridge**

Mode Number	Natural Frequency			Viscous Damping Ratio		
	Before (Hz)	After (Hz)	Change (%)	Before	After	Change (%)
1	6.3 (0.003)*	6.3 (0.005)	0.0	0.026 (0.044)	0.028 (0.047)	8
2	8.2 (0.002)	8.1 (0.004)	-1.2	0.032 (0.024)	0.030 (0.041)	-8
3	11.2 (0.004)	11.2 (0.004)	0.0	0.027 (0.038)	0.024 (0.044)	-11
4	12.7 (0.004)	12.8 (0.004)	0.8	0.029 (0.042)	0.033 (0.058)	14
5	17.0 (0.018)	17.7 (0.013)	4.1	0.027 (0.065)	0.027 (0.069)	0
6	20.3 (0.006)	19.9 (0.007)	-2.0	0.030 (0.060)	0.038 (0.055)	21

\*Covariance = standard deviation ÷ mean

Increase in bearing stiffness would be expected to reduce the modal damping ratios (section 3.5). Only modes 2 and 3 showed decreased damping ratio with a net (all modes) increase of 24% being observed. This further suggests that the stiffness values (of the new bearings) are not as high as was expected.

### 8.6.3 MAC, MSV and Mode Shapes

Tables 8.4 and 8.5 respectively show the MAC matrix and MSV (sub-section 4.2.1) of the bridge for the two series of tests. The diagonal elements of the MAC matrix are all close to 1.0, suggesting that the conditions of the bridge during both test series are not significantly different. The MSV suggest that modes 3, 4, 5 and 6 are those most affected by the repairs. This is similar to the results from the MAC values and FRF plots shown in Figure 8.7 (sub-section 8.6.1).

**Table 8.4 Modal Assurance Criterion (MAC) values of Holway Road bridge**

	Mode	Before Bearing Replacement					
	Number	1	2	3	4	5	6
After Bearing Replac- ement	1	<b>0.98</b>	0.11	0.13	0.43	0.27	0.04
	2	0.14	<b>0.99</b>	0.69	0.07	0.23	0.13
	3	0.11	0.62	<b>0.97</b>	0.23	0.18	0.06
	4	0.47	0.06	0.20	<b>0.97</b>	0.38	0.02
	5	0.26	0.20	0.20	0.46	<b>0.94</b>	0.23
	6	0.04	0.12	0.07	0.03	0.16	<b>0.95</b>

**Table 8.5 Modal Sensitivity Values (MSV) of Holway Road bridge**

Mode Number	MSV
1	30.1
2	33.9
3	78.1
4	79.1
5	49.2
6	100.0

The mode shapes before and after bearing replacement are compared in Figure 8.8. The two sets of mode shapes are similar with the significant changes occurring in the end spans, particularly for modes 5 and 6. Increased vertical stiffness (of the bearings) would be expected to reduce the mode shape amplitude close to the abutments. This behaviour is displayed in the mode shape (span AB) of mode 5. Since the mode shape amplitude, before the repairs, at the abutments for the other modes were not too large, the improvements due to new bearings (as displayed in mode 5) are not well manifested.

#### **8.6.4 COMAC values and Integrity Indices**

COMAC values and Local Integrity Indices are shown in Table 8.6. Only points S25, N28 and N29 have COMAC values less than 0.8 (0.8 is the value below which changes can be inferred - see sub-section 7.7.4). Two (N28 and N29) of the three points are close to the east abutment (see Figure 8.3). However, the other points (S1, S29 and N1) close to the abutments are not identified.

Only three points (S25, N23 and N29) have Local Integrity Indices greater than 50 with just one (N29) of them close to the abutment. The other Indices are significantly lower as would be expected for all points except those at the abutments. Combining results from the two parameters, only the east abutment can be suspected of having been modified. A global Integrity Index of 1.03 obtained indicates a marginal increase in the overall stiffness. These results further suggest that the stiffness of the new bearings is not as high as the designers thought.

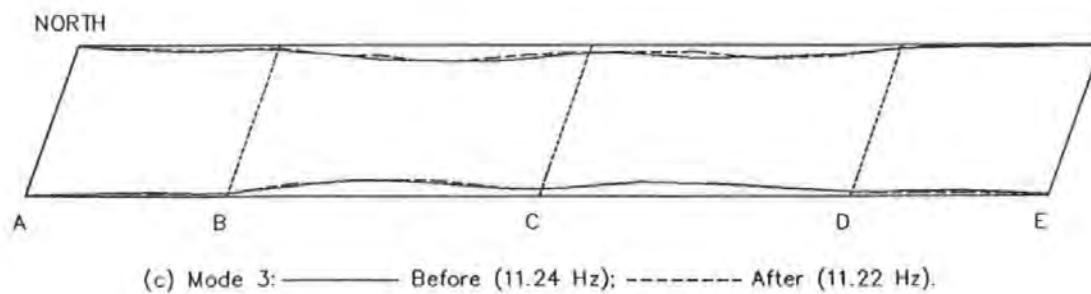
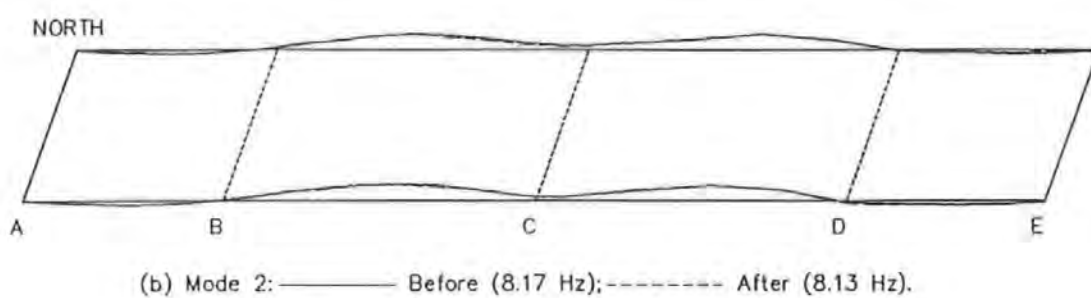
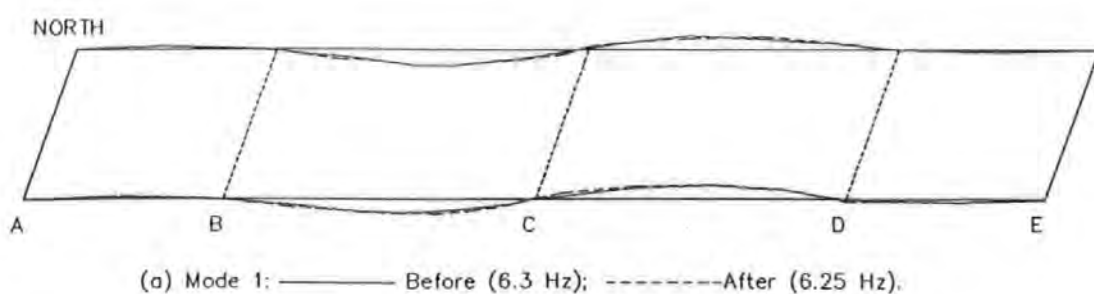


**Figure 8.8 Comparison of experimental mode shapes before and after bearing replacement**

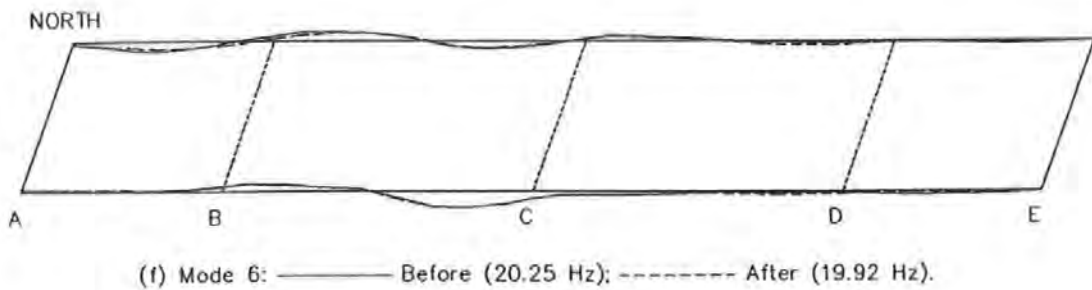
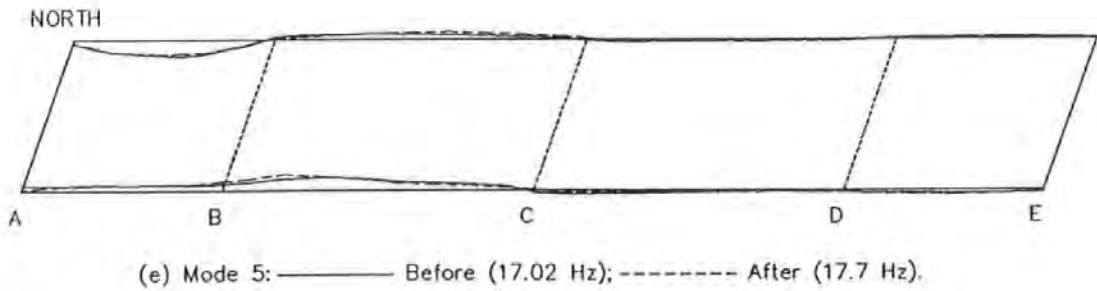
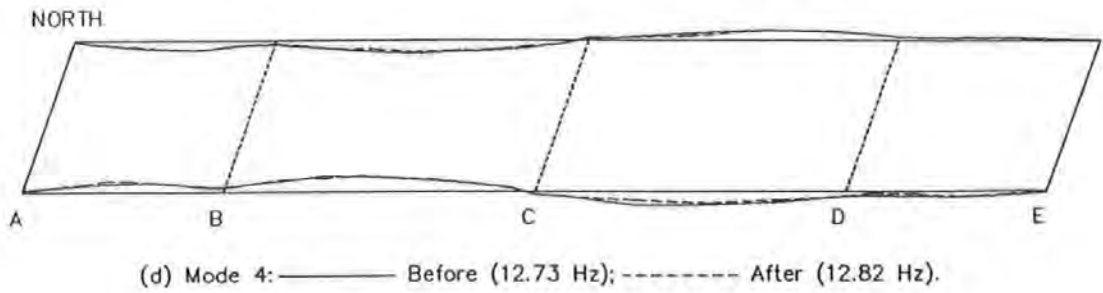


**Figure 8.8 Comparison of experimental mode shapes before and after bearing replacement (continued)**

**Table 8.6 COMAC values and Local Integrity Indices**

SOUTH				NORTH		
Point	COMAC	Local Index		Point	COMAC	Local Index
S1	0.88	24.2		N1	1.00	3.9
S2	0.93	14.3		N2	0.99	7.6
S3	0.94	6.3		N3	0.98	0.4
S4	0.95	23.3		N4	0.97	5.7
S5	0.98	9.4		N5	0.99	5.2
S6	0.95	17.4		N6	1.00	7.0
S7	0.97	3.5		N7	1.00	5.1
S8	0.98	2.9		N8	0.95	28.2
S9	0.99	10.3		N9	0.84	11.3
S10	0.99	18.7		N10	0.98	20.1
S11	0.98	18.7		N11	0.96	18.5
S12	0.99	17.5		N12	0.97	6.8
S13	0.99	1.9		N13	0.98	1.8
S14	1.00	0.2		N14	0.99	22.1
S15	0.99	1.5		N15	0.98	41.2
S16	0.98	5.8		N16	0.98	40.7
S17	0.98	7.4		N17	0.95	42.5
S18	0.98	10.9		N18	0.90	42.7
S19	0.90	4.2		N19	0.85	18.1
S20	0.90	11.4		N20	0.98	6.7
S21	0.94	17.1		N21	0.94	2.9
S22	0.98	28.8		N22	0.98	37.8
S23	0.98	27.1		N23	0.98	100.0
S24	0.85	100.0		N24	0.99	1.2
S25	0.78	1.7		N25	0.98	1.3
S26	0.84	12.4		N26	0.90	36.6
S27	0.92	22.0		N27	0.88	22.5
S28	0.91	4.9		N28	0.79	6.4
S29	0.84	29.5		N29	0.60	54.1

(Global Integrity Index = 1.03)

## 8.7 Comparison of Analytical and Experimental Results

The first ten analytical modes were computed using models corresponding to the two states of the bridge. The mode shapes were visually compared with those of the experimental modes and six matching pairs identified. Comparison of the frequencies (for the situation after the repairs) in Tables 8.1 and 8.3 shows that the experimental model does not correspond to a condition of full vertical fixity at the abutments. The simple updating routine mentioned in section 7.5 was used to obtain a more realistic value of the bearing stiffness. A value of  $567 \times 10^6$  N/m (as compared with  $126 \times 10^6$  N/m for the old bearings) was obtained and subsequently used in the analysis instead of full fixity.

The analytical and experimental natural frequencies are shown in Table 8.7. Average errors of -1.4% and 6% were respectively obtained for the situations before and after bearing replacement. The table shows a generally good agreement between the frequencies. The errors for the condition before the repairs are lower since the stiffness values were more accurately known.

The amplitudes (vertical components only) of the analytical mode shapes at nodes corresponding to the measurement points were extracted to produce reduced models for comparison with the experimental models. The MAC matrices obtained are shown in Tables 8.8 and 8.9 while Table 8.10 shows the MSV. The values in the tables show the modes to be well correlated. The only (minor) exceptions are modes 5 and 6 (before repairs - Table 8.8) and 3 and 6 (after repairs - Table 8.9). The results from MSV computations are identical to the MAC results; further showing the usefulness of MSV as a means of detecting correlated mode pairs and thus its potential application in model updating procedures.

**Table 8.7 Comparison of analytical and experimental frequencies of Holway Road bridge**

Mode Number	Natural Frequency						
	Before Bearing Replacement				After Bearing Replacement		
	Measured (Hz)	Analytical (Hz)	Change (%)		Measured (Hz)	Analytical (Hz)	Change (%)
1	6.3	5.9 <sup>a</sup>	-6.3		6.3	6.0 <sup>a</sup>	-4.8
2	8.2	8.1 <sup>b</sup>	-1.2		8.1	8.5 <sup>b</sup>	4.9
3	11.2	12.2 <sup>c</sup>	8.9		11.2	13.6 <sup>c</sup>	21.4
4	12.7	12.5 <sup>d</sup>	-1.6		12.8	14.5 <sup>d</sup>	13.3
5	17.0	15.7 <sup>e</sup>	-7.6		17.7	17.6 <sup>e</sup>	-0.6
6	20.3	20.2 <sup>f</sup>	-0.5		19.9	20.3 <sup>f</sup>	2.0

a - Analytical mode 1; b - Analytical mode 2; c - Analytical mode 5

d - Analytical mode 6; e - Analytical mode 8; f - Analytical mode 9

**Table 8.8 MAC matrix for analytical and experimental models before bearing replacement**

	Mode	Experimental					
		1	2	3	4	5	6
Analytical	1	<b>0.99</b>	0.10	0.12	0.48	0.46	0.02
	2	0.13	<b>0.94</b>	0.58	0.08	0.14	0.08
	3	0.10	0.44	<b>0.96</b>	0.18	0.11	0.0
	4	0.42	0.03	0.25	<b>0.96</b>	0.46	0.01
	5	0.25	0.21	0.26	0.44	<b>0.85</b>	0.13
	6	0.04	0.12	0.06	0.02	0.18	<b>0.76</b>

**Table 8.9 MAC matrix for analytical and experimental models after bearing replacement**

	Mode	Experimental					
		1	2	3	4	5	6
Analytical	1	<b>0.97</b>	0.10	0.01	0.46	0.32	0.00
	2	0.10	<b>0.91</b>	0.10	0.09	0.18	0.10
	3	0.10	0.47	<b>0.43</b>	0.24	0.17	0.03
	4	0.35	0.04	0.23	<b>0.92</b>	0.43	0.05
	5	0.30	0.27	0.22	0.36	<b>0.95</b>	0.11
	6	0.06	0.14	0.05	0.01	0.16	<b>0.78</b>

**Table 8.10 MSV for analytical and experimental models**

Mode Number	MSV	
	Before	After
1	4.5	45.9
2	7.9	35.0
3	39.3	100.0
4	16.7	6.3
5	44.4	34.2
6	100.0	55.6

The mode shapes are compared in Figures 8.9 and 8.10. The figures show a good degree of correlation except for modes mentioned in the previous paragraph. Modes 1 and 2 are the first and second symmetrical bending modes while modes 3 and 4 are the first and second symmetrical pure torsion modes. Modes 5 and 6 are torsional-bending modes. In mode 5, the end spans are in torsion while the middle spans are in first bending. The middle spans are in second bending in mode 6 with one outer span in pure torsion and the other in pure bending.

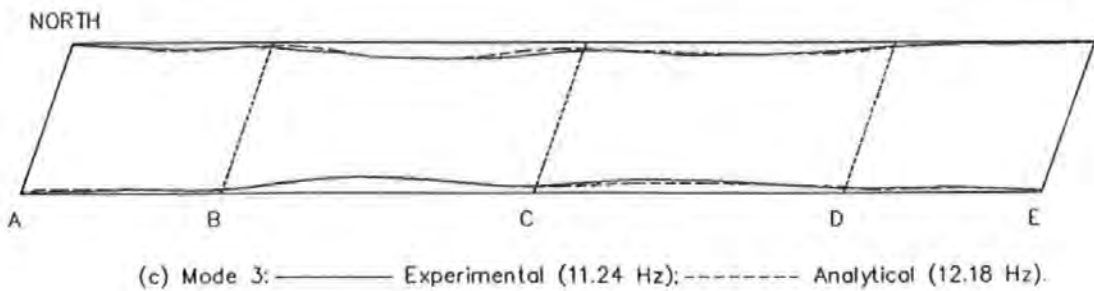
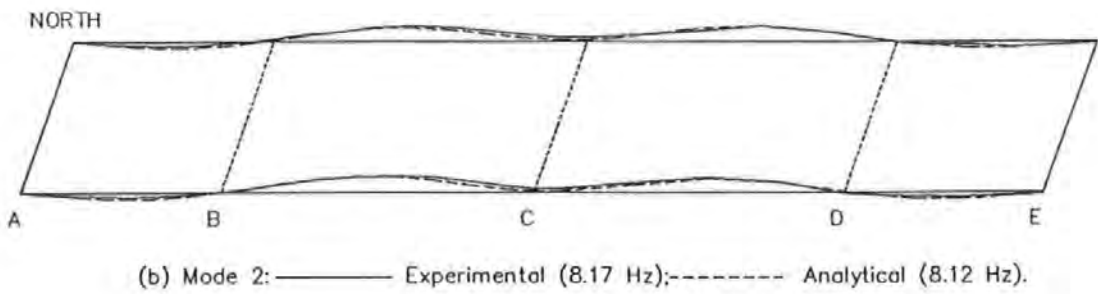
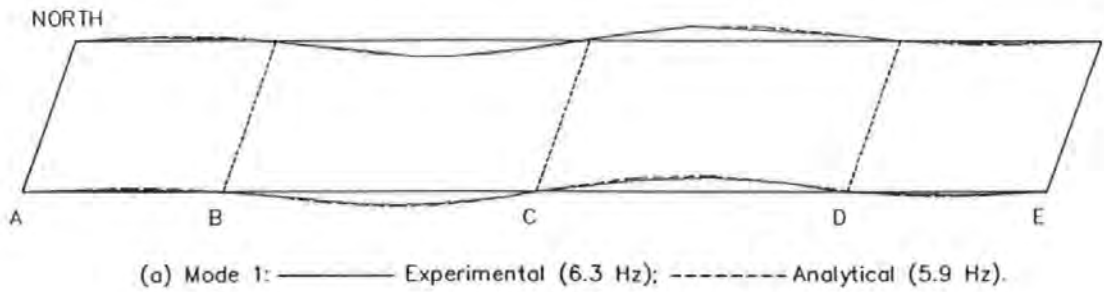


**Figure 8.9 Comparison of analytical and experimental mode shapes before bearing replacement**

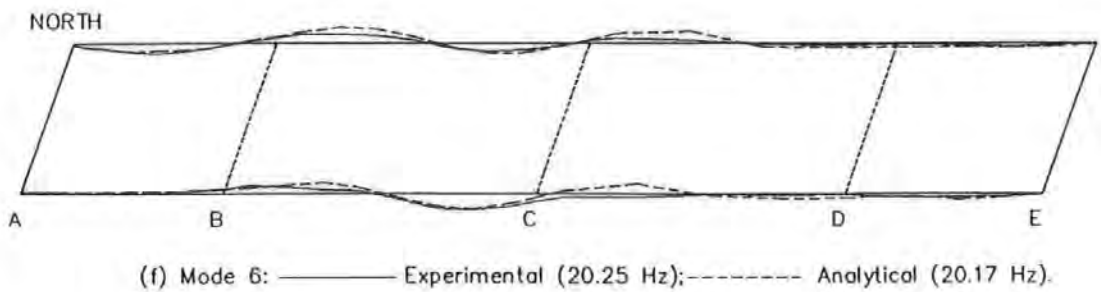
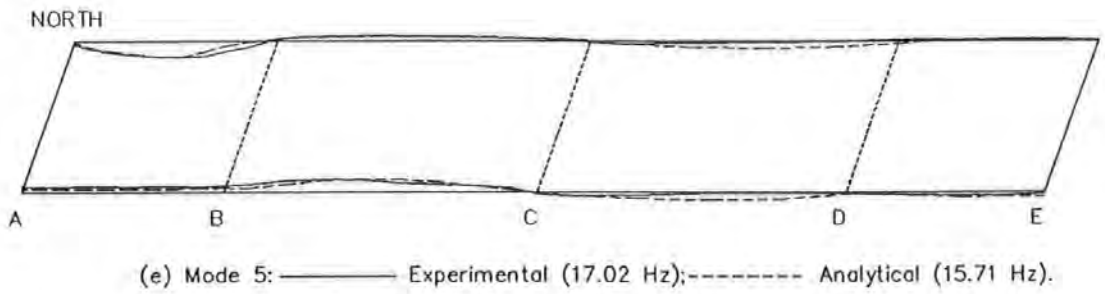
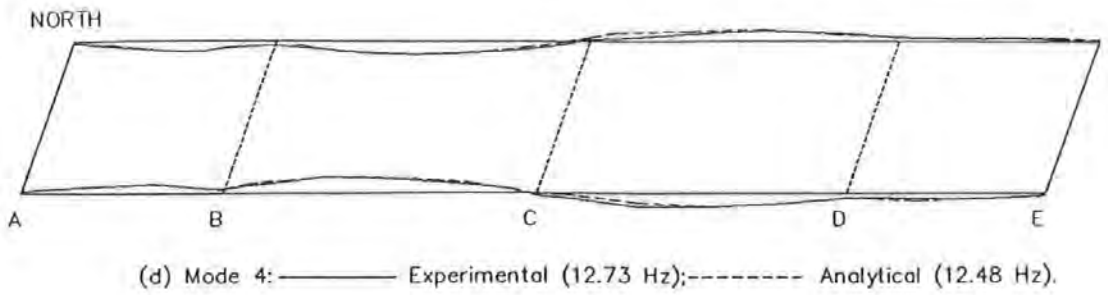


**Figure 8.9 Comparison of analytical and experimental mode shapes before bearing replacement (continued)**

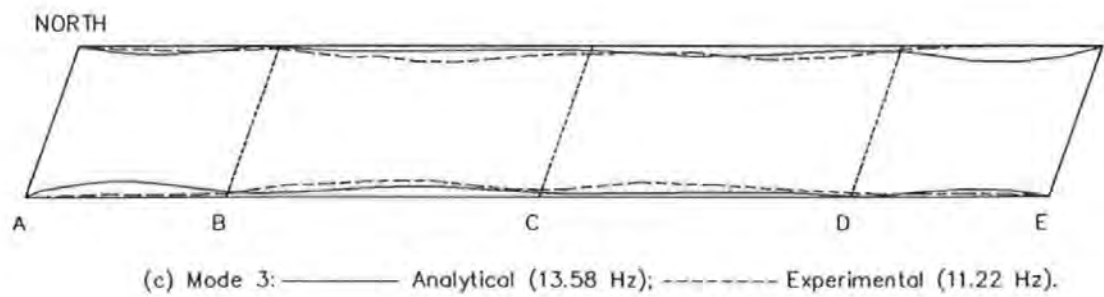
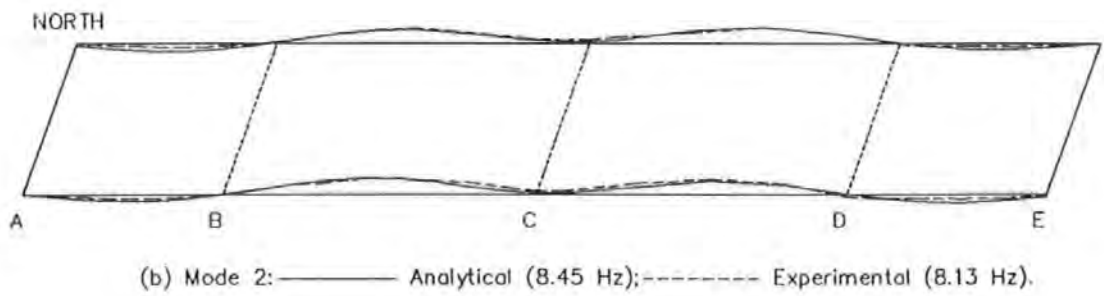
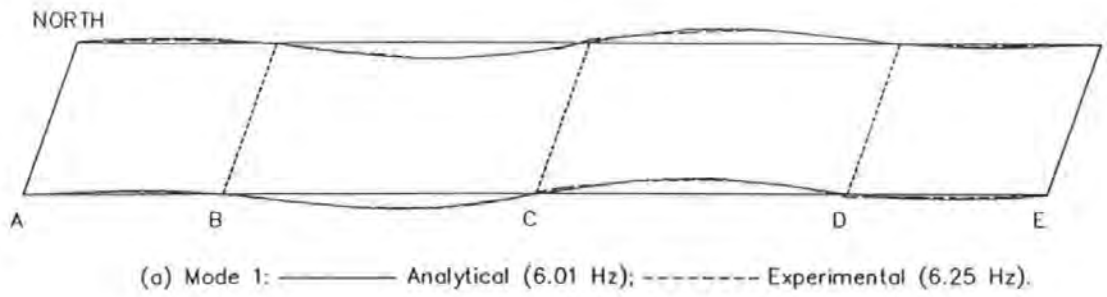


**Figure 8.10 Comparison of analytical and experimental mode shapes after bearing replacement**

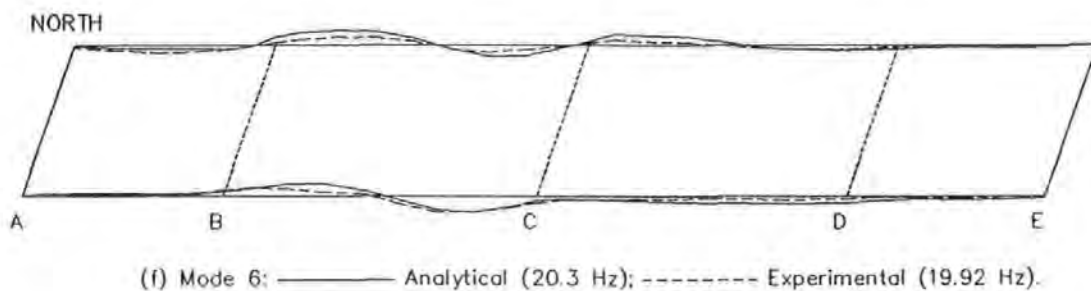
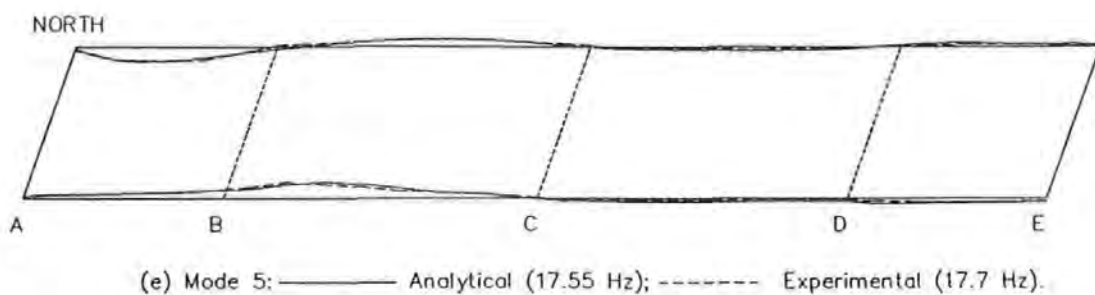
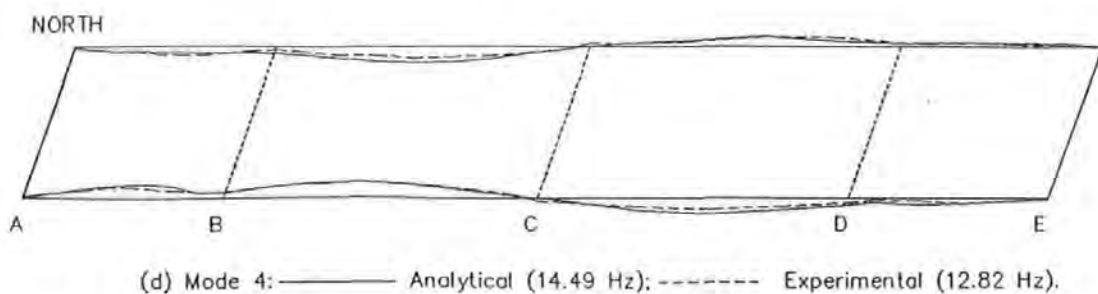


**Figure 8.10 Comparison of analytical and experimental mode shapes after bearing replacement (continued)**

## 8.8 Conclusions

Field results presented and discussed in the chapter have further shown the viability of using dynamic testing to validate theoretical models of civil engineering structures. The average errors in natural frequency from analytical and experimental studies of two different conditions of the test bridge were -1.4% and 6% while the mode shapes were well correlated. The new parameter MSV introduced in chapter four has also been shown to be potentially useful in model updating procedures.

Replacing the bearings at the bridge's abutments did not significantly increase the natural frequencies (of the modes identified) although a marginal increase in global stiffness was obtained using the Global Integrity Index. Comparison of components of the normalised cumulative FRF suggested that the modes with natural frequencies greater than 11.0Hz were more sensitive to the repairs. The same result was also obtained from MSV computations.

COMAC and Local Integrity Indices were only able to indicate one of the abutments as having possibly been modified. All the results obtained firmly indicate that the stiffness of the new bearings are not as high as assumed by the designers. Specifically, the new bearings were found to be about 4½ times stiffer, in the vertical direction, than the old ones. However, they allow more horizontal movement.

## CHAPTER NINE

### SUMMARY, CONCLUSIONS AND RECOMMENDATIONS

In this chapter, brief summaries of, and some conclusions from, the work described in the thesis are presented. Some recommendations for future work on integrity assessment using vibration data are also given.

#### 9.1 Full-Scale Testing

Results from full-scale testing of civil engineering structures add to the database on structural performance and provide information that can be used to monitor service behaviour of built structures. The information obtained from the field tests (chapters seven and eight) conducted during the project will increase the knowledge base on dynamic behaviour of similar structures.

The review of full-scale dynamic testing of bridges presented in chapter two showed that forced vibration testing produces data from which more accurate (as compared with ambient testing) system and modal parameters can be obtained. Forced vibration testing was therefore adopted for the field tests conducted. A hydraulic excitation system was developed for inputting time-varying forces into the test structures. The system (described in chapter six) can be used to induce vertical excitation of highway bridges, long-span floor slabs and similar structures. The maximum force and stroke amplitude that can be generated are respectively  $\pm 5\text{kN}$  and 300mm. The vibrator is robust, can be easily assembled and dismantled on site, and allows utilization of any type of waveform as the input signal. The best operating frequency bandwidth is 5 - 25 Hz. Within this range, the

vibrator produces stable output signals and does not generate unwanted motion. Response functions obtained from field application of the system are satisfactory.

The vibration modes identified from the results of tests conducted were generally in the range 5 - 25 Hz while the damping values, as a percentage of critical damping, ranged from 1.6% to 2.4% for Deep Lane bridge, and 2.4% to 3.8% for Holway Road bridge. The fundamental natural frequencies were respectively 7.0 Hz and 6.3 Hz for Deep Lane and Holway Road bridges. These values are in accordance with previous measurements reported in the literature.

The mode shape for the second mode of Deep Lane bridge was not completely identified because the vibrator was inadvertently placed close to a node of this mode. For Holway Road bridge, full structural details of the bridge were available and initial exploratory analysis was conducted to identify modes likely to be affected by the repair works and appropriate measurement points. The initial analysis was very useful for the successful conduct of the tests. These observations emphasise the need for some form of pre-test analysis so that suitable measurement locations are selected in order that all modes and features of interest can be observed.

## **9.2 Analytical Model Validation**

Validation of analytical models using test data helps to increase confidence in future usage of the models. With the prevalence use of various analysis and design software, many of which are not quality assured, it is now more important to check actual behaviour of built structures so that mathematical models are adequately verified. An analyst will have more confidence in using theoretical models that have been experimentally verified.

Finite element models of the bridges tested were correlated with and validated by the results from the field tests. The correlation and validation are valid within the test frequency range, limits of modelling assumptions and experimental errors. The average error between predicted and measured natural frequencies for both bridges was less than 7%. For Deep Lane bridge, the error in the natural frequency (calculated against measured) for the 4th mode was quite large (43%). This exceptional error was most likely due to the possibly inadequate modelling of the support conditions since full structural details of the bridge were not available. Good agreement was obtained between the calculated and experimental mode shapes. The results also indicate that one of the abutments does not provide free longitudinal movement as was originally designed.

Analytical results for Holway Road bridge show that the stiffness of the new bearings at the abutments are not as high as was assumed in the design. Overall, the results (from both bridges) demonstrate the usefulness of vibration testing as an analytical model verification tool. It is however very important that careful consideration be given to modelling of the boundary conditions and possible sources of experimental errors. An immediate application of the studies would be in the current assessment programme for highway bridges. If a verified model of a bridge is available, then, a more rational analytical investigation of the capacity of the bridge to carry increased loading can be conducted.

### **9.3 Structural Assessment using Vibration Data**

Damage in a structure causes changes in the dynamic properties of the structure. A critical review of the literature (chapter three) revealed the existence of various techniques for relating structural condition and changes in dynamic parameters with the aims of detecting, locating and quantifying damage. Changes in natural frequencies, response functions and

damping (in some cases) can be used to indicate occurrence of structural degradation. Location and quantification of damage is more difficult and may require additional information (typically mode shapes and system matrices). Most of the available methods of damage detection are either limited to specific structural types (or damage event) or require sophisticated models and extensive computations.

Performance evaluation of some damage detection methods (presented in chapter four) suggested that the damage location process could be improved if appropriate modes are included in the computations. The appropriate modes would usually be the ones most affected by damage. A new function, Modal Sensitivity Value MSV, has been proposed (chapter four) for identifying damage sensitive modes. The function uses both frequency and mode shape information and its viability was demonstrated using both simulated and experimental data. Application of the function to data obtained from field testing of Holway Road bridge showed its potential as a means of identifying correlated mode pairs from sets of analytical and experimental results.

A damage detection and location method, Integrity Index Damage Location method, which is applicable to any structure was also proposed (chapter five). The method requires minimal computations and can be configured for specific structural forms, if desired. Any form of structural degradation can be detected and the number of measurement points required depends on how exact the fault location is to be identified. If only structural integrity is to be assessed, without the need to locate faults, only one measurement point is needed. The method was shown to be satisfactory (on both simulated and experimental data) in predicting loss or gain in structural integrity as a result of stiffness changes and also indicating areas affected by damage/defects.

If desired, the Integrity Index method can be used as a pattern recognition tool, especially for pre-cast products or similar structural forms. In such applications, the Global and Local Integrity Indices for various faults, usually associated with the type of structure, are computed and stored in a data base. A simple algorithm can be developed for this task. The Indices would have been correlated with strength properties of the structure so that measurements (and the Indices calculated from them) can be compared with the database in order to determine residual strength. The procedure will provide a simple and efficient diagnostic tool for assessment engineers.

COMAC was found to be useful for identifying damage location although the damage position in the analytical cantilever beam (chapter four) was not well defined. The limitation with COMAC is that differences between the mode shapes at a measurement point become averaged over all the modes. For the Integrity Index method proposed, these differences were magnified by including natural frequencies and weighting factors in the identification algorithm. It was found that successful utilization of COMAC for damage location requires defining threshold values below which damage can be inferred. A value of 0.8 was suggested for large civil engineering structures.

The studies presented in chapter four also showed that model updating and system identification techniques can be used for damage detection and location. This approach is however limited by the fact that model updating methods tend to spread the effect of damage around the structure (as represented by the system matrices), making damage localization difficult. Furthermore, there is no unique solution to the problem of obtaining a set of system matrices from a set of incomplete measured data that would realistically represent the structure.

The natural frequencies of the bridges tested did not change significantly (less than 5%) as a result of repairs carried out on the bridges. The localised nature of the repairs was the reason for the modest changes. There was no definite trend to the changes in damping values. The results from Holway Road bridge was used to deduce that the vertical stiffness of the new bearings is about 4½ times that of the old ones.

Comparison of the components of the normalised cumulative frequency response function was able to give an indication of the changes in the bridges' condition. The real component was found to manifest the changes most. The MAC matrix and MSV also indicated changes and suggested modes that were most influenced by the repairs.

Mode shapes before and after structural repairs, COMAC values and Integrity Indices gave good indications of the presence and location of the repairs. For Deep Lane bridge, two of the affected three points were detected although two spurious locations were also identified. Considering that 54 measurement points were involved, the identification was reasonably good. One of the two abutments at which the bearings were replaced was identified on Holway Road bridge.

In practical applications, the effects of changes in environmental conditions (such as temperature and humidity) on the dynamic response of the structure may have to be considered. For the bridges investigated, the environmental conditions during the test periods were not dissimilar. Assigning specific values to some of these (environmental) events could be difficult as their effect would be dependent on equipment type, test procedures, type and location of structures. These points were discussed in chapter three. Thus, using threshold values for the damage identification parameters is possibly the best (until sufficient numerical information are available) way of accounting for environmental

factors, experimental errors and inaccuracies in data analysis. The values used should be chosen to reflect the importance of the different variables and the degree of accuracy required.

#### **9.4 Recommendations for Future Work**

The procedures exploited in this study can provide useful information as regards the presence, location and extent of damage in a structure. A qualitative assessment of the structure's condition can also be made depending on the quality of the measurements. However, they are not likely to provide quantitative results that can be used for strength evaluation. It would be necessary to relate dynamic parameters to strength and stiffness properties of the structure so that changes can be directly linked to load carrying capacity. Research (involving both experimental and analytical work) into this aspect of structural assessment using vibration testing is required. Another factor that needs to be addressed is the possibility of using results from one series of tests for assessment since current methods require at least two series of tests - one on the pristine structure and another after a period of time. This becomes important when information on the current state of the structure is required and dynamic parameters from prior measurements are unavailable. It is also desirable to conduct long term investigations into the relationships between changes in ambient conditions and dynamic properties.

## REFERENCES

- Abdel-Ghaffar, A. M. and Scanlan, R. H. (1985a). Ambient vibration studies of Golden Gate bridge: I - Suspended structure. *Journal of Engineering Mechanics, ASCE* 111(4), 463-482.
- Abdel-Ghaffar, A. M. and Scanlan, R. H. (1985b). Ambient vibration studies of Golden Gate bridge: II - Pier-Tower structure. *Journal of Engineering Mechanics, ASCE* 111(4), 483-499.
- Adams, R. D., Cawley, P., Pye, C. J. and Stone, B. J. (1978). A vibration technique for non-destructively assessing the integrity of structures. *Journal of Mechanical Engineering Science*, 20(2), 93-100.
- Afolabi, D. (1987). An anti-resonance technique for detecting structural damage. *Proceedings, 5th International Modal Analysis Conference, London*, 1.
- Ågårdh, L. (1991). Modal analyses of two concrete bridges. *Structural Engineering International*, 1(4), 35-39.
- Ågårdh, L. (1994). Impact excitation of concrete bridges. *Proceedings, 12th International Modal Analysis Conference, Honolulu, Hawaii*, 2, 1329-1334.
- Ågårdh, L. and Palm, J. (1992). Modal analysis of a highway concrete bridge excited with impact. *Proceedings, American Concrete Institute Spring Convention, Washington*.
- Aktan, A. E., Lee, K. L., Chuntavan, C. and Aksel, T. (1994). Modal testing for structural identification and condition assessment of constructed facilities. *Proceedings, 12th International Modal Analysis Conference, Honolulu, Hawaii*, 1, 462-468.
- Alampalli, S., Fu, G. and Abdul Aziz, I. (1992). Modal analysis as a bridge inspection tool. *Proceedings, 10th International Modal Analysis Conference, San Diego, California*, 2, 1359-1366.
- Al-Ansary, M. D. and Azayem, K. M. (1986). A modal model for fatigue crack non-destructive testing. *Proceedings, 4th International Modal Analysis Conference, Los Angeles*, 1, 202.
- Allemang, R. J. and Brown, D. L. (1983). A correlation coefficient for modal vector analysis. *Proceedings, 1st International Modal Analysis Conference, Kissimmee, Florida*, 1, 110-116.
- Allemang, R. J. and Brown, D. L. (1985). Multiple-input experimental modal analysis. *Experimental Techniques*, 9(10), 16s-23s.
- Allemang, R. J. and Brown, D. L. (1988). *Experimental modal analysis. Shock and Vibration Handbook* (Harris, C. M., Ed.), McGraw-Hill Inc., New York, 21:1-21:34.
- Alocco, V., Buccino, F., Vitiello, E. and Fava, A. (1993). Evaluation of structural safety margins for existing post-tensioned concrete bridges via dynamic tests. *Proceedings, 5th International Conference on Structural Faults and Repair, University*

of Edinburgh, Edinburgh, 1, 263-271.

Alvarez, R. C., Delibes, A. L., Díaz, J. L. and Fernández, J. G. (1993). Ten years of experience in dynamic testing and assessment of bridges. *Bridge Management 2* (Harding, J. E., Parke, G. A. R. and Ryall, M. J., Eds.), Thomas Telford, London, 815-820.

Armstrong, D. M., Sibbald, A. and Forde, M. C. (1993). Integrity assessment of masonry arches using the dynamic stiffness technique. *Proceedings, 5th International Conference on Structural Faults and Repair, University of Edinburgh, Edinburgh, 3, 297-302.*

Askegaard, V. and Langsø, H. E. (1986). Correlation between changes in dynamic properties and remaining carrying capacity (laboratory tests with reinforced concrete beams). *Matériaux et Constructions, 19(109), 11-20.*

Askegaard, V. and Mossing, P. (1988). Long term observation of RC-bridge using changes in natural frequencies. *Nordic Concrete Research, 7, 20-27.*

Avitabile, P. and Li, P. (1993). Some observations on the difficulties in model updating. *Proceedings, 11th International Modal Analysis Conference, Kissimmee, Florida, 1, 668-675.*

Baalbaki, W., Aïtcin, P. C. and Ballivy, G. (1992). On predicting modulus of elasticity in high-strength concrete. *ACI Materials Journal, 89(5), 517-520.*

Bakht, B. and Jaeger, L. G. (1992). Ultimate load tests of slab-on-girder bridge. *Journal of Structural Engineering, ASCE, 118(6), 1608-1624.*

Baldwin, J. W., Salane, H. J. and Duffield, R. C. (1978). Fatigue test of a three span composite highway bridge. Final Report 73-1, Missouri Highway Research Programme, Columbia, Mo.

Baumgärtner, W. and Naubke, H. (1993). Service life estimation of bridges. *Bridge Management 2* (Harding, J. E., Parke, G. A. R. and Ryall, M. J., Eds.), Thomas Telford, London, 200-210.

Beck, R. T. (1991). Fundamental problems in the application of structural identification procedures to damage detection. Report No. EERL 91-03, Earthquake Engineering research Laboratory, California Institute of Technology, Pasadena, California.

Begg, R. D., Mackenzie, A. C., Dodds, C. J. and Loland, O. (1976). Structural integrity monitoring using digital processing of vibration signals. *Proceedings, 8th Offshore Technology Conference, Houston, Texas, 2.*

Bendat, J. S. and Piersol, A. G. (1980). *Engineering Applications of Correlation and Spectral Analysis.* John Wiley and Sons, New York.

Bendat, J. S. and Piersol, A. G. (1986). *Random Data: Analysis and Measurement Procedures.* 2nd Edn., John Wiley and Sons, New York.

Billing, J. R. (1982). Dynamic test of bridges in Ontario, 1980 : data capture, test

procedures and data processing. MTC Research and Development Report SRR-82-02, Ontario Ministry of Transportation and Communications, Downsview, Ontario.

Billing, J. R. (1984). Dynamic loading and testing of bridges in Ontario. *Canadian Journal of Civil Engineering*, 11(4), 833-843.

Biswas, M., Pandey, A. K. and Samman, M. M. (1990). Diagnostic experimental spectral/modal analysis of a highway bridge. *The International Journal of Analytical and Experimental Modal Analysis*, 5(1), 33-42.

Bolton, A. (1994). *Structural Dynamics in Practice*. 1st Edn., McGraw-Hill International, London.

Bracewell, R. N. (1978). *The Fourier Transform and its Applications*. 2nd Edn., McGraw-Hill, New York.

Brandon, J. A. (1987). Eliminating indirect analysis - the potential for receptance sensitivities. *Journal of Analytical and Experimental Modal Analysis*, April, 73-75.

Braun, S. G. and Ram, Y. M. (1990). Predicting the effect of structural modification: upper and lower bounds due to modal truncation. *Proceedings, 8th International Modal Analysis Conference, Kissimmee, Florida, 2*, 940-945.

Brown, T. A. (1987). The identification of spatial parameter changes via modal analysis. *Proceedings, 5th International Modal Analysis Conference, London*, pp. 267.

Brown, T. A. (1988). A matrix cursor for dynamic model improvement using experimental modes of vibration. *GEC Journal of Research*, 6(3), 139-146.

Brownjohn, J. M. W. (1988). *Assessment of structural integrity by dynamic measurements*. Ph.D Thesis, Department of Civil Engineering, University of Bristol.

Brownjohn, J. M. W., Dumangolu, A. A., Severn, R. T. and Taylor, C. A. (1987). Ambient vibration measurements of the Humber suspension bridge and comparison with calculated characteristics. *Proceedings of the Institution of Civil Engineers: Part 2*, 83, 561-600.

Budiwanto, B. and Jezequel, L. (1990). Comparison of time domain modal identification methods. *Proceedings, 8th International Modal Analysis Conference, Kissimmee, Florida, 1*, 540-546.

Cabrera, J. (1988). Towards a performance index for concrete bridges. *Assessment of Reinforced and Prestressed Concrete Bridges*, The Institution of Structural Engineers, London, 37-42.

Camomilla, G., Donferri, M., Santori, A. G. and Materazzi, L. (1993). Reflectometric and dynamic measurements on the stays of the Polcevera viaduct in Genoa (Italy). *Bridge Management 2* (Harding, J. E., Parke, G. A. R. and Ryall, M. J., Eds.), Thomas Telford, London, 118-127.

Cantieni, R. (1983). *Dynamic load tests on highway bridges in Switzerland*. Report

No. 211, Eidgenossische Material-prufungs-und Versuchsantalt (EMPA), Dubendorf, Switzerland.

Cantieni, R. and Pietrzko, S. (1993). Modal testing of a wooden footbridge using random excitation. Proceedings, 11th International Modal Analysis Conference, Kissimmee, Florida, 2, 1230-1236.

Came, T. G., Lauffer, J. P., Gomez, A. J. and Benjannet, H. (1988). Modal testing an immense flexible structure using natural and artificial excitation. International Journal of Analytical and Experimental Modal analysis, 3(4), 117-122.

Castro, I. P. (1989). An Introduction to the Digital Analysis of Stationary Signals. IOP Publishing Ltd., Bristol, England.

Caudill, M. and Butler, C. (1992). Understanding Neural Networks. MIT Press, Cambridge, Massachusett, U. S. A.

Cawley, P. and Adams, R. D. (1979). The location of defects in structures from measurements of natural frequencies. Journal of Strain Analysis, 4(2), 49-57.

Cawley, P. and Nguyen, D. (1988). The use of the impedance method of non-destructive testing of honeycomb structures. Mechanical Systems and Signal Processing, 2(4), 309-325.

Cempel, C., Natke, H. G. and Ziolkowski, A. (1992). Application of transformed normal modes for damage location in structures. Structural Integrity Assessment, Elsevier Applied Science, London, 246-255.

Chasteau, V. A. L. (1973). The use of tuned vibration absorbers to reduce wind excited oscillations of a steel foot bridge. The Civil Engineer in South Africa, 15(6), 147-154.

Cherng, A. P. and Abdelhamid, M. K. (1993). A signal subspace correlation (SSC) index for detection of structural changes. Proceedings, 11th International Modal Analysis Conference, Kissimmee, Florida, 1, 232-239.

Chondras, T. G. and Dimarogonas, A. D. (1980). Identification of cracks in welded joints of complex structures. Journal of Sound and Vibration, 69(4), 531-538.

Chowdhury, M. R. (1990). Experimental modal testing and analysis of continuously supported structures. Proceedings, 8th International Modal Analysis Conference, Florida, 1, 109-114.

Clements, E. W., Sullivan, J. R. and Vigness, I. (1988). Shock testing machines. Shock and Vibration Handbook (Harris, C. M., Ed.), McGraw-Hill Inc., New York, 26:1-26:20.

Clough, R. W., Ghanaat, Y. and Qiu, X. F. (1987). Dynamic reservoir interaction with Monticello dam. Report No. UCB/EERC 87/21, Earthquake Engineering Research Center, University of California, Berkely.

Cole, M. (1992). A model signature. Construction News, March 12, 1992, pp.16.

Creed, S. G. (1987). Assessment of large engineering structures using data collected

- during in-service loading. Structural Assessment (Garas, F. K., Clarke, J. L. and Armer, G. S. T., Eds), Butterworths, London, 55-62.
- Crema, L., Castellani, A. and Peroni, I. (1985). Modal tests on composite material structures: application in damage detection. Proceedings, 3rd International Modal Analysis Conference, 2, 708-713.
- Curtis, A. J. (1988). Applications of digital computers. Shock and Vibration Handbook (Harris, C. M., Ed.), McGraw-Hill Inc., New York, 27:1-15.
- Davis, A. G. and Dunn, C. S. (1974). From theory to field experience with non-destructive testing of piles. Proceedings of the Institution of Civil Engineers, Part 2, 57, 571-593.
- Deger, Y., Cantieni, R. and Pietrzko, S. (1994). Modal analysis of an arch bridge: experiment, finite element analysis and link. Proceedings, 12th International Modal Analysis Conference, Honolulu, Hawaii, 1, 425-432.
- deSilva, C. W. (1986). The digital processing of acceleration measurements for modal analysis. The Shock and Vibration Digest, 18(10), 3-10.
- DiPasquale, E., Ju, J., Askar, A. and Cakmak, A. S. (1990). Relation between global damage indices and local stiffness degradation. Journal of Structural Engineering, ASCE, 116(5), 1440-1456.
- Doebling, S. W., Hemez, F. M., Barlow, M. S., Peterson, L. D. and Farhat, C. (1993). Damage detection in a suspended scale model truss via model update. Proceedings, 11th International Modal Analysis Conference, Kissimmee, Florida, 2, 1083-1094.
- Doll, H. (1994). Eigenfrequencies and normal modes of the Norderelb bridge near Hamburg: numerical and measuring investigations. Proceedings, 12th International Modal Analysis Conference, Honolulu, Hawaii, 1, 449-455.
- Douglas, B. M. and Reid, W. H. (1982). Dynamic tests and system identification of bridges. Journal of Structural Division, ASCE, 108(ST10), 2295-2312.
- Douglas, B. M. and Richard, J. (1984). Maximum amplitude tests of a highway bridge. Proceedings, 8th World Conference on Earthquake Engineering, Earthquake Engineering Research Institute and International Association for Earthquake Engineering, 6.
- Douglas, B. M., Maragakis, E. A. and Nath, B. (1990). Static deformations of bridges from quick-release dynamic experiments. Journal of Structural Engineering, ASCE, 116(8), 2201-2213.
- Eggers, D. W. and Stubbs, N. (1994). Structural assessment using modal analysis techniques. Proceedings, 12th International Modal Analysis Conference, Honolulu, Hawaii, 2, 1595-1601.
- Ellis, B. R., Jeary, A. P. and Sparks, P. R. (1977). Full scale and model scale studies of the dynamic behaviour of an offshore structure. Proceedings, International Conference on the Behaviour of Slender Structures, City University, London, III.1.1 - III.1.13.

- Ewins, D. J. (1984). *Modal testing: theory and practice*. Research Studies Press Ltd, Letchworth, Hertfordshire, England.
- Eyre, R. (1976). *Dynamic tests on the Cleddau bridge at Milford Haven*. Department of the Environment, TRRL Report SR200 UC, Transport and Road Research Laboratory, Crowthorne.
- Eyre, R. and Smith, I. J. (1977). *Wind and traffic induced dynamic behaviour of some steel box girder bridges*. Symposium on Dynamic Behaviour of Bridges, Transport and Road Research Laboratory, Crowthorne, Berkshire, 56-69.
- Eyre, R. and Tilly, G. P. (1977). *Damping measurements on steel and composite bridges*. Symposium on Dynamic Behaviour of Bridges, Transport and Road Research Laboratory, Crowthorne, Berkshire, 22-39.
- Farrar, C. R., Baker, W. E. and Dove, R. C. (1994). *Dynamic parameter similitude for concrete models*. ACI Structural Journal, 91(1), 90-99.
- FEA (1990). *LUSAS User Manual, Version 10.0*. Finite Element Analysis Ltd., Surrey, United Kingdom.
- Flesch, R. G., Gerasch, W. J. and Kembichler, K. (1991). *The significance of system identification for diagnostic dynamic testing of bridges*. Structural Dynamics, Proceedings of the European Conference on Structural Dynamics - Eurodyn 90, Bochum, Germany, A. A. Balkema, Rotterdam/Brookfield, 1, 419-426.
- Fox, C. H. J. (1992). *The location of defects in structures: a comparison of the use of natural frequency and mode shape data*. Proceedings, 10th International Modal Analysis Conference, San Diego, California, 1, 522-528.
- Friswell, M. I. and Penny, J. E. T. (1992). *The use of vibration data and model updating to detect damage*. Structural Integrity Assessment, Elsevier Applied Science, London, 225-235.
- Galambos, T. and Mayes, R. (1979). *Lessons from dynamic tests of an eleven storey building*. Engineering Structures, 1, Butterworth Scientific Ltd., Surrey.
- Gardner-Morse, M. G. and Huston, D. R. (1993). *Modal identification of cable stayed pedestrian bridge*. Journal of Structural Engineering, ASCE, 119(11), 3384-3404.
- Gomes, A. J. M. A. and Silva, J. M. M. E. (1990). *On the use of modal analysis for crack identification*. Proceedings, 8th International Modal Analysis Conference, Florida, 2, 1108-1115.
- Green, R. (1977). *Dynamic response of bridge superstructures - Ontario observations*. Symposium on Dynamic Behaviour of Bridges, Transport and Road Research Laboratory, Crowthorne, Berkshire, 40-55.
- Green, M. F. and Cebon, D. (1993). *Modal testing of two highway bridges*. Proceedings, 11th International Modal Analysis Conference, Kissimmee, Florida, 2, 838-844.

- Gudmundson, P. (1982). Eigenfrequency changes of structures due to cracks, notches or other geometrical changes. *Journal of Mech. Phys. Solids*, 30(5), 339-353.
- Gudmundson, P. (1984). Changes in modal parameters resulting from small cracks. *Proceedings, 2nd International Modal Analysis Conference*, 2, 690-697.
- Gundy, W. T., Scharon, T. D. and Thomas, R. L. (1980). Damping measurements on an offshore platform. *Proceedings, 12th Offshore Technology Conference*, Houston, Texas, 4.
- Gysin, H. P. (1986). Critical application of the error matrix method for localisation of finite element modelling inaccuracies. *Proceedings, 4th International Modal Analysis Conference*, Los Angeles, California, 2, 1339-1351.
- Hambly, E. C. (1991). *Bridge Deck Behaviour*. 2nd Edn., Chapman and Hall, London.
- Haroun, M. A., Mourad, S. A. and Flynn, N. H. (1993). Modal characteristics of reinforced concrete pier walls before and after cyclic testing. *Proceedings, 11th International Modal Analysis Conference*, Kissimmee, Florida, 2, 1299-1302.
- Hassan, M., Burdett, O. and Favre, R. (1993). Combination of ultrasonic measurements and load tests in bridge evaluation. *Proceedings, 5th International Conference on Structural Faults and Repair*, University of Edinburgh, Edinburgh, U. K., 1, 59-63.
- He, J. (1992). An extended error matrix method. *Proceedings, 17th International Seminar on Modal Analysis*, Leuven, Belgium, September.
- He, J. (1993). Sensitivity analysis and error matrix method using measured frequency response function (FRF) data. *Proceedings, 11th International Modal Analysis Conference*, Kissimmee, Florida, 2, 1079-1082.
- Hearn, G. and Testa, R. B. (1991). Modal analysis for damage detection in structures. *Journal of Structural Engineering*, ASCE, 117(10), 3042-3063.
- Hewlett-Packard (1979). *Operating Manual for Spectrum Analyzer 3582A*. Hewlett-Packard Company, Loveland, Colorado.
- Hewlett-Packard (1990). *Using HPE2080A LIF Utilities for the PC*. HP Part No. E2080-90000, 1st Ed., Hewlett-Packard Company, Palo Alto, California.
- Heylen, W. and Sas, P. (1987). Review of model optimization techniques. *Proceedings, 5th International Modal Analysis Conference*, London, 2, 1177-1182.
- Hoff, C. and Natke, H. G. (1989). Correction of a finite-element model by input-output measurements with application to a radar tower. *International Journal of Analytical and Experimental Modal Analysis*, 4(1), 1-7.
- Hudson, D. E. (1962). *Synchronized vibration generators for dynamic tests of full scale structures*. Research Report, Earthquake Engineering Research Laboratory, California Institute of Technology, Pasadena, California.
- Ibrahim, S. R. and Saafan, A. A. (1987). Correlation of analysis and test in modelling

- of structures - assessment and review. Proceedings, 5th International Modal Analysis Conference, London, 2, 1657-1660.
- Idichandy, V. G. and Ganapathy, C. (1990). Modal parameters for structural integrity of fixed offshore platforms. *Experimental Mechanics*, 30(4), 382-391.
- Iffland, J.S.B. and Birmstiel, C. (1993). Guide to nondestructive test methods. *Bridge Management 2* (Harding, J. E., Parke, G. A. R. and Ryall, M. J., Eds.), Thomas Telford, London, 921-930.
- IMC (1989). User's Guide to Signal Analysis Program FAMOS. IMC Mess-Systeme GmbH, Germany.
- Imregun, M. and Ågårdh, L. (1994). Updating of the finite element model of a concrete highway bridge. Proceedings, 12th International Modal Analysis Conference, Honolulu, Hawaii, 2, 1321-1328.
- Imregun, M. and Visser, W. J. (1991). A review of model updating techniques. *The Shock and Vibration Digest*, 23(1), 9-20.
- James, G. H., Came, T. G., Lauffer, J. P. and Nord, A. R. (1992). Modal testing using natural excitation. Proceedings, 10th International Modal Analysis Conference, San Diego, California, 2, 1209-1216.
- Jeary, A. P. (1992). Establishing non-linear damping characteristics of structures from non-stationary response time-histories. *The Structural Engineer*, 70(4), 61-66.
- Jeary, A. P. and Ellis, B. R. (1984). Non-destructive in-situ testing using dynamic techniques. Proceedings, 3rd International Conference on Tall Buildings (Cheung, Y. K. and Lee, P. K. K., Eds.), Honk Kong and Guangzhou, 76-81.
- Jeary, A. P. and Sparks, P. R. (1977). Some observations on the sway characteristics of concrete structures. *Symposium on Vibrations in Concrete Structures*, New Orleans, USA.
- Jones, R. and Iberle, K. (1986). Structural modifications: a comparison of techniques. Proceedings, 4th International Modal Analysis Conference, Los Angeles, California, 1, 59-65.
- Ju, F. D., Akgün, M., Paez, T. L. and Wong, E. T. (1982). Modal method in diagnosis of fracture damage in simple structures. *Productive Application of Mechanical Vibrations*, Applied Mechanics Division, ASME, 52, 113-126.
- Ju, F. D. and Mimovich, M. (1986). Modal frequency method in diagnosis of fracture damage in structures. Proceedings, 4th International Modal Analysis Conference, Los Angeles, 2, 1168-1174.
- Ju, F. D. and Mimovich, M. (1987). Experimental diagnosis of fracture damage in structures by the modal frequency method. *Modal Testing and Analysis* (Came, T. G. and Simonis, J. C., Eds.) ASME, 29-36.
- Kaouk, M. and Zimmerman, D. C. (1993). Evaluation of the minimum rank update in

damage detection: an experimental study. Proceedings, 11th International Modal Analysis Conference, Kissimmee, Florida, 2, 1061-1068.

Kaouk, M. and Zimmerman, D. C. (1994). Structural damage detection using measured modal data and no original analytical model. Proceedings, 12th International Modal Analysis Conference, Honolulu, Hawaii, 1, 731-737.

Kato, M. and Shimada, S. (1981). Methods of field vibration tests on bridges (in Japanese). Journal of Japan Society of Civil Engineers, 66(2), 28-42.

Kato, M. and Shimada, S. (1986). Vibration of PC bridge during failure process. Journal of Structural Engineering, ASCE, 112(7), 1692-1703.

Kawahito, T. (1974). A study on the inspection method of soundness of expressway bridges by vibration characteristics - part 1 (in Japanese). Report of the Laboratory of Nihon Doro Kodan, 158-167.

Kennedy, J. B. and Grace, N. F. (1990). Prestressed continuous composite bridges under dynamic loading. Journal of Structural Engineering, ASCE, 116(6), 1660-1678.

Kientzy, D., Richardson, M. H. and Blakely, K. (1989). Using finite element data to set up modal tests. Sound and Vibration Magazine, June.

Ko, J. M., Wang, C. W. and Lam, H. F. (1994). Damage detection in steel framed structures by vibration measurement approach. Proceedings, 12th International Modal Analysis Conference, Honolulu, Hawaii, 1, 280-286.

Kohoutek, R. (1993). Tests on bridge over Talbragar river at Dubbo. Proceedings, 11th International Modal Analysis Conference, Kissimmee, Florida, 2, 1168-1174.

Kohoutek, R. and Marshall, P. (1994). Use of modal analysis of Nattai bridge Mittagong bypass. Proceedings, 12th International Modal Analysis Conference, Honolulu, Hawaii, 1, 706-712.

Kroggel, O. (1993). Nondestructive testing of the integrity of bridges: an EC project. Bridge Management 2 (Harding, J. E., Parke, G. A. R. and Ryall, M. J., Eds.), Thomas Telford, London, 727-737.

Kudva, J., Munir, N. and Tan, P. (1992). Damage detection in smart structures using neural networks and finite-element analysis. Smart Materials and Structures, 1, 108-112.

Larson, C. B., Zimmerman, D. C. and Marek, E. L. (1994). A comparison of modal test planning techniques: excitation and sensor placement using the NASA 8-Bay truss. Proceedings, 12th International Modal Analysis Conference, Honolulu, Hawaii, 1, 205-211.

Law, S. S., Waldron, P. and Taylor, C. (1991). Phase component of the FRF as a tool in structural fault diagnosis. Asia-Pacific Vibration Conference '91, Melbourne, Australia.

Law, S. S., Waldron, P. and Taylor, C. (1992). Damage detection of a reinforced concrete bridge deck using the frequency response function. Proceedings, 10th

International Modal Analysis Conference, San Diego, California, 2, 772-778.

Law, S. S., Xun, L. and Ward, H. S. (1990). A vibration technique for structural stiffness identification. Proceedings, International Conference on Vibration Problems in Engineering, Wuhan-Chungqing, 1, 1990, 698-683.

Lee, P. K. K., Ho, D. and Chung, H. W. (1987). Static and dynamic tests of concrete bridges. Journal of Structural Engineering, ASCE, 113(1), 61-73.

Leith, J., Long, A. E., Thompson, A. and Sloan, T. D. (1987). Monitoring the behaviour of a major box girder bridge. Paper 27, Joint I. Struct. E./B.R.E. Seminar on Structural Assessment Based on Full and Large Scale Testing, Building Research Establishment, Garston, Watford.

Leonard, D. R. (1974). Dynamic tests on highway bridges - test procedures and equipment. TRRL Laboratory Report 654, Transport and Road Research Laboratory, Berkshire.

Li, Y. F. (1986). A frequency-time domain modal parameter identification technique. Proceedings, 4th International Modal Analysis Conference, Los Angeles, California, 1, 812-818.

Lieven, N. A. J. and Ewins, D. J. (1988). Spatial correlation of mode shapes, the Coordinate Modal Assurance Criterion (COMAC). Proceedings, 6th International Modal Analysis Conference, Kissimmee, Florida, 690-695.

Lieven, N. A. J. and Ewins, D. J. (1990). Error location and updating the finite element model using singular value decomposition. Proceedings, 8th International Modal Analysis Conference, Kissimmee, Florida, 769-773.

Lieven, N. A. J. and Ewins, D. J. (1992). Effect of incompleteness and noise on error matrix calculations. Proceedings, 10th International Modal Analysis Conference, San Diego, California, 2, 1406-1413.

Lieven, N. A. J. and Waters, T. P. (1994). Error location using normalised orthogonality. Proceedings, 12th International Modal Analysis Conference, Honolulu, Hawaii, 1, 761-764.

Link, M. (1990). Identification and correction of errors in analytical models using test data - theoretical and practical bounds. Proceedings, 8th International Modal Analysis Conference, Kissimmee, Florida, 1, 570-578.

Littler, J. D. (1988). Discussion of 'Ambient vibration measurements of the Humber suspension bridge and comparison with calculated characteristics' by Brownjohn et al. Proceedings of the Institution of Civil Engineers: Part 2, 85, 725-730.

Littler, J. D. and Ellis, B. R. (1987). Ambient vibration measurements of the Humber bridge. International Conference on Flow Induced Vibrations, Bowness-on-Windermere.

Luber, W. and Lotze, A. (1990). Application of sensitivity methods for error localization in finite element systems. Proceedings, 8th International Modal Analysis

Conference, Kissimmee, Florida, 598-604.

Luk, Y. W. (1987). Identification of physical mass, stiffness and damping matrices using pseudo-inverse. Proceedings, 5th International Modal Analysis Conference, London, 679-685.

Maguire, J. R. (1984). The dynamic characteristics of elevated piled tanks and other selected prototype structures. PhD Thesis, University of Bristol, Bristol.

Maguire, J. R. (1992). Construction industry case histories. Structural Integrity Assessment, Elsevier Applied Science, London, 66-75.

Maguire, J. R. and Severn, R. T. (1987). Assessing the dynamic properties of prototype structures by hammer testing. Proceedings of the Institution of Civil Engineers, Part 2, 83, 769-784.

Maia, N. M. M. (1990). Reflections on some SDOF modal analysis methods. Proceedings, 8th International Modal Analysis Conference, Kissimmee, Florida, 1, 658-666.

Mannan, M. A., McHargue, P. and Richardson, M. H. (1994). Continuous monitoring of modal parameters to quantify structural damage. Proceedings, 12th International Modal Analysis Conference, Honolulu, Hawaii, 1, 59-65.

Mannan, M. A. and Richardson, M. H. (1990). Detection and location of structural cracks using FRF measurements. Proceedings, 8th International Modal Analysis Conference, Florida, 1, 652-657.

Marecos, J., Catanheta, M. and Trigo, J. T. (1969). Field observations of Tagus River suspension bridge. Journal of the Structural Division, ASCE, 95(ST4).

Mau, S. T. and Wang, S. (1989). Arch dam system identification using vibration test data. Earthquake Engineering and Structural Dynamics, 18, 491-505.

Mazurek, D. F. and DeWolf, J. T. (1990). Experimental study of bridge monitoring technique. Journal of Structural Engineering, ASCE, 116(9), 2532-2549.

McLamore, V. R., Hart, G. C. and Stubbs, I. R. (1971). Ambient vibration of two suspension bridges. Journal of the Structural Division, ASCE, 97(ST10), 2567-2582.

Meneghetti, U. and Maggiore, A. (1994). Crack detection by sensitivity analysis. Proceedings, 12th International Modal Analysis Conference, Honolulu, Hawaii, 2, 1292-1298.

Milne, R. D. (1980). Applied Functional Analysis. Pitman, London.

Mirza, M. S., Ferdjani, O., Hadj-Arab, A., Joucdar, K., Khaled, A. and Razaqpur, A. G. (1990). An experimental study of static and dynamic responses of prestressed concrete box girder bridges. Canadian Journal of Civil Engineering, 17(3), 481-493.

Mitchell, L. D. (1982). Improved methods for the fast Fourier transform (FFT) calculation of the frequency response function. Journal of Mach. Des., Transactions of

the ASME, 104, April, 277-279.

Mitchell, L. D. (1985). Signal processing and the fast-Fourier-transform (FFT) analyzer. *Experimental techniques*, 9(10), 3s-15s.

Moradalizadeh, M. (1990). Evaluation of crack defects in framed structures using resonant frequency techniques. M. Phil. Thesis, Civil Engineering Department, University of Newcastle Upon Tyne, Newcastle.

Morgan, B. J. and Oesterle, R. G. (1985). On-site modal analysis - a new powerful inspection technique. *Proceedings of the 2nd International Bridge Conference*, Pittsburg, Pennsylvania, 108-114.

Mosley, W. H. and Bungey, J. H. (1990). *Reinforced Concrete Design*. Macmillan Education Ltd., 4th Edn., Basingstoke, Hampshire, England.

Mott MacDonald Ltd. (1990). A38 London to Penzance Trunk Road, Deep Lane Overbridge: Assessment for Construction and Use Loading. Special Services Division, Mott MacDonald Limited, January 1990.

Mott MacDonald Ltd. (1991). A38 London to Penzance Trunk Road, Deep Lane Overbridge: Remedial Work to Deck. Special Services Division, Mott MacDonald Limited, August 1991.

Nalitolela, N. G., Penny, J. E. T. and Friswell, M. I. (1990). Updating structural parameters of a finite element model by adding mass or stiffness to the system. *Proceedings, 8th International Modal Analysis Conference*, Kissimmee, Florida, 836-842.

Newland, D. E. (1975). *An Introduction to Random Vibrations and Spectral Analysis*. Longman Group Ltd., New York.

Ohlsson, S. (1986). Modal testing of the Tjorn bridge. *Proceedings, 4th International Modal Analysis Conference*, Los Angeles, California, 1, 599-605.

Ojalvo, I. U. (1986). Contrasts in two classes of structural dynamic correlation procedures. *Proceedings, 4th International Modal Analysis Conference*, Los Angeles, 1, 81-87.

Okauchi, I., Tanaka, A., Iwaya, K. and Furuyan, N. (1986). Vibration test of Ohnaruto bridge to confirm wind proofness. *IABSE Symposium*, Tokyo.

Olsen, L. O. (1986). Using and understanding electromagnetic shakers in modal applications. *Proceedings, 4th International Modal Analysis Conference*, Los Angeles, California, 2, 1160-1167.

Owen, J. S. and Blakeborough, A. (1993). The prototype testing of Kessock bridge: modal survey. *International Conference on Structural Dynamics Modelling: Test, Analysis and Correlation*, Milton Keynes, UK.

Pabst, U. and Hagedorn, P. (1994). Model correction by identification of local parameters. *Proceedings, 12th International Modal Analysis Conference*, Honolulu, Hawaii, 1, 844-849.

- Pandey, A. K., Biswas, M. and Samman, M. M. (1991). Damage detection from changes in curvature mode shapes. *Journal of Sound and Vibration*, 145(2), 321-332.
- Pardeon, G. C., Carr, A. J. and Moss, P. J. (1981). Bridge modal identification problems. *Proceedings, 2nd ASCE Engineering Mechanics Division Specialty Conference on the Dynamic Response of Structures: Experimentation, Observation, Prediction and Control*, Atlanta, 29-45.
- Park, Y. S., Park, H. S. and Lee, S. S. (1988). Weighted-error-matrix application to detect stiffness damage by dynamic characteristics measurement. *International Journal of Analytical and Experimental Modal Analysis*, 3(3), 101-107.
- Penny, J. E. T., Friswell, M. I. and Garvey, S. D. (1992). The automatic choice of measurement locations for dynamic testing. *Proceedings, 10th International Modal Analysis Conference*, San Diego, California, 1, 30-36.
- Penny, J. E. T., Wilson, D. A. L. and Friswell, M. I. (1993). Damage detection in structures using vibration data. *Proceedings, 11th International Modal Analysis Conference*, Kissimmee, Florida, 2, 861-867.
- Proulx, J., Hébert, D. and Paultre, P. (1992). Evaluation of the dynamic properties of a steel arch bridge. *Proceedings, 10th International Modal Analysis Conference*, San Diego, California, 2, 1025-1031.
- Purkiss, J. A., Bailey, M., Friswell, M. I., Penny, J. E. T. and Wood, M. G. (1997a). The dynamic response of prestressed concrete bridge decks. Source: Institution of Structural Engineers Library, London; Ref. X108.
- Purkiss, J. A., Bailey, M., Friswell, M. I., Penny, J. E. T. and Wood, M. G. (1997b). Analysis of the effect of ambient conditions on the dynamic response of prestressed concrete bridge decks. Source: Institution of Structural Engineers Library, London; Ref. X109.
- Rades, M. (1985). Frequency domain experimental modal analysis techniques. *Shock and Vibration Digest*, 17(6), 3-15.
- Raghavendrachar, M. and Aktan, A. E. (1992). Flexibility by multireference impact testing for bridge diagnostics. *Journal of Structural Engineering*, ASCE, 118(8), 2186-2203.
- Raimer, J. H. and Pernici, G. (1979). Dynamic testing of a modern concrete bridge. *Canadian Journal of Civil Engineering*, 6(3).
- Richardson, J. A. and Douglas, B. M. (1987). Identifying frequencies and three-dimensional mode shapes from a full scale bridge test. *Proceedings, 5th International Modal Analysis Conference*, London, 1, 160-165.
- Richardson, M. H. and Mannan, M. A. (1992). Remote detection and location of structural faults using modal parameters. *Proceedings, 10th International Modal Analysis Conference*, San Diego, California, 1, 502-507.
- Richardson, M. H. and Mannan, M. A. (1993). Correlating minute structural faults with

- changes in modal parameters. Proceedings, 11th International Modal Analysis Conference, Kissimmee, Florida, 2, 893-896.
- Rinawi, A. M. and Clough, R. W. (1992). Improved amplitude fitting for frequency and damping estimation. Proceedings, 10th International Modal Analysis Conference, San Diego, California, 1, 25-28.
- Rivas-Gomez, A. (1993). Nondestructive evaluation of bridge design assumptions. Proceedings, 5th International Conference on Structural Faults and Repair, University of Edinburgh, Edinburgh, 1, 53-58.
- Rizos, P. F., Aspragathos, N. and Dimarogonas, A. D. (1990). Identification of crack location and magnitude in a cantilever beam from the vibration modes. Journal of Sound and Vibration, 138(3), 381-388.
- Roberts, G. P. (1990). ADEPT version 4 - user manual. Report No. G8705.010, Issue 2, WS Atkins Engineering Services, Almondsbury, Bristol.
- Rubin, S. and Coppolino, R. N. (1983). Flexibility monitoring of offshore jacket platforms. Proceedings, OTC4535, 201-208.
- Rytter, A. and Kirkegaard, P. H. (1994). Vibrational based inspection of a steel mast. Proceedings, 12th International Modal Analysis Conference, Honolulu, Hawaii, 2, 1602-1608.
- Salane, H. J. and Baldwin, J. W. (1990). Identification of modal properties of bridges. Journal of Structural Engineering, ASCE, 116(7), 2008-2021.
- Salane, H. J., Baldwin, J. W. and Duffield, R. C. (1987). Dynamics approach for monitoring bridge deterioration. Transportation Research Record, 832, 21-28.
- Salawu, O. S. (1997). Identification of damage sensitive vibration modes. In Preparation.
- Salawu, O. S. and Williams, C. (1992). Design and calibration of equipment for forced vibration testing : test rig and actuator. Research Report No. SCSE 92-009, School of Civil and Structural Engineering, University of Plymouth, Plymouth, UK.
- Salawu, O. S. and Williams, C. (1993). Structural damage detection using experimental modal analysis - a comparison of some methods. Proceedings, 11th International Modal Analysis Conference, Kissimmee, Florida, 1, 254-260.
- Salawu, O. S. and Williams, C. (1994?). Bridge assessment using forced vibration testing. Submitted to Journal of Structural Engineering, ASCE. *(To appear in 1995)*
- Salawu, O. S. and Williams, C. (1994a). Damage location using vibration mode shapes. Proceedings, 12th International Modal Analysis Conference, Honolulu, Hawaii, 1, 933-939.
- Salawu, O. S. and Williams, C. (1994b). An excitation system for dynamic testing of large structures. Journal of Testing and Evaluation, ASTM, 22(4), 370-375.

- Salawu, O. S., Williams, C. and Hewson, P. J. (1994). Comparison of results from vibration testing and finite element analysis of a highway bridge. *Computational Structural Engineering for Practice* (Papadrakakis, M. and Topping, B. H. V., Eds.), Civil Comp Press, Edinburgh, 61-69.
- Samman, M. M. and Biswas, M. (1994a). Vibration testing for nondestructive evaluation of bridges. I: Theory. *Journal of Structural Engineering, ASCE*, 120(1), 269-289.
- Samman, M. M. and Biswas, M. (1994b). Vibration testing for nondestructive evaluation of bridges. II: Results. *Journal of Structural Engineering, ASCE*, 120(1), 290-306.
- Savage, R. J. and Hewlett, P. C. (1978). A new NDT method for structural integrity assessment. *NDT International*, 11, 61-66.
- Schütze, M., Doll, H. and Hildebrandt, P. (1994). Review on an expert system under development - "measurement techniques in civil engineering" - including structural assessment. *Proceedings, 12th International Modal Analysis Conference, Honolulu, Hawaii*, 2, 1349-1355.
- Selberg, H. E. (1966). Aerodynamic stability and related aspects of suspension bridges. *Symposium on Suspension Bridges, Lisbon*.
- Severn, R. T., Jeary, A. P. and Ellis, B. R. (1980). Forced vibration tests and theoretical studies on dams. *Proceedings of the Institution of Civil Engineers: Part 2*, 69, 605-634.
- Shah, P. C. and Udawadia, F. E. (1978). A methodology for optimal sensor locations for identification of dynamic systems. *Journal of Applied Mechanics, ASME*, 45.
- Shahrivar, F. and Bouwkamp, J. G. (1986). Damage detection in offshore platforms using vibration information. *Journal of Energy Resources Technology, Transactions of the ASME*, 108(2), 97-108.
- Shepherd, R. and Reay, A. M. (1967). Some apparatus for the small amplitude dynamic testing of multistorey buildings. *Journal of British Society for Strain Measurements*, 4, 16-21.
- Sibbald, A. (1988). Impact hammer testing of masonry sewers. Ph.D Thesis, University of Edinburgh, Edinburgh.
- Sidhu, J. and Ewins, D. J. (1984). Correlation of finite element and modal test studies of a practical structure. *Proceedings, 2nd International Modal Analysis Conference*, 756-762.
- Slaštan, J. and Pietrzko, S. (1993a). Changes of RC-beam modal parameters due to cracks. *Proceedings, 11th International Modal Analysis Conference, Kissimmee, Florida*, 1, 70 - 76.
- Slaštan, J. and Pietrzko, S. (1993b). Effectiveness evaluation of RC-beam strengthening using CFRP laminates by means of modal analysis. *Proceedings, 5th International*

- Conference on Structural Faults and Repair, University of Edinburgh, Edinburgh, 3, 79-90.
- Sloan, T. D., Kirkpatrick, J., Boyd, J. W. and Thompson, A. (1992). Monitoring the inservice behaviour of the Foyle bridge. *The Structural Engineer*, 70(7), 130-134.
- Snyder, V. W. (1985). Structural modification and modal analysis. *Experimental Techniques*, 9(10), 245-315.
- Springer, W. T., Lawrence, K. L. and Lawley, T. J. (1988). Damage assessment based on the structural frequency response function. *Experimental Mechanics*, 28(1), 34-37.
- Srinivasan, M. G. and Kot, C. A. (1992). Effect of damage on the modal parameters of a cylindrical shell. *Proceedings, 10th International Modal Analysis Conference, San Diego, California*, 1, 529-535.
- Srinivasan, M. G., Kot, C. A. and Hsieh, B. S. (1984). Dynamic testing of as-built civil engineering structures - a review and evaluation. Report No. NUREC/CR 3649, Office of Nuclear Regulatory Commission, USA.
- Stubbs, N. and Osegueda, R. (1990a) Global non-destructive damage evaluation in solids. *International Journal of analytical and Experimental Modal Analysis*, 5(2), 67-79.
- Stubbs, N. and Osegueda, R. (1990b) Global damage detection in solids - experimental verification. *International Journal of analytical and Experimental Modal Analysis*, 5(2), 81-97.
- Sun, X. and Hardy, H. R. (1992a). An investigation on applicability of modal analysis as nondestructive evaluation method in geotechnical engineering. *Proceedings, 10th International Modal Analysis Conference, San Diego, California*, 1, 9-19.
- Sun, X. and Hardy, H. R. (1992b). A study on the operating shapes for nondestructive evaluation in geotechnical engineering. *Proceedings, 10th International Modal Analysis Conference, San Diego, California*, 2, 1237-1244.
- Swamy, N. and Rigby, G. (1971). Dynamic properties of hardened paste, mortar and concrete. *Matériaux et Constructions*, 4(1), 13-40.
- Tang, J. P. and Leu, K. M. (1988). Vibration measurement and safety assessment of bridges. *US-Taiwan Joint Seminar on Rehabilitation of Public Works, Taipei, Taiwan*, 55-69.
- Tang, J. P. and Leu, K. M. (1989). Vibration tests and damage detection of P/C bridges. *Proceedings of the 5th International Conference on Structural Safety and Reliability, ICOSSAR '89, ASCE*, 2263-2266.
- Taškov, L. A. (1988). Dynamic testing of bridge structures applying forced and ambient vibration methods. Paper 6, *Conference on Civil Engineering Dynamics, Society for Earthquake and Civil Engineering Dynamics, London*.
- Tilly, G. P. (1977). Damping of highway bridges : a review. *Symposium on Dynamic Behaviour of Bridges, Transport and Road Research Laboratory, Crowthorne, Berkshire*,

- Tilly, G. P. (1988). Research into assessment of concrete bridges. Assessment of Reinforced and Prestressed Concrete Bridges, The Institution of Structural Engineers, London, 4-7.
- Tracy, J., Dimas, D., Pardoen, G. (1984). Advanced composite damage detection using modal analysis techniques. Proceedings, 2nd International Modal Analysis Conference, 2, 655-660.
- Tsai, W. H. and Yang, J. C. S. (1988). Nondestructive evaluation of composite structures using system identification technique. Journal of Engineering Materials and Technology, Transactions of the ASME, 110(2), 134-139.
- Tsang, W. F. and Rider, E. (1988). Modelling of structures using experimental forced vibration data with a particular application in force prediction. RNEC Research Report RNEC-RP-88023, Royal Naval Engineering College, Plymouth.
- Tsang, W. F. and Williams, C. (1988). Application of experimental modal analysis to full-scale civil engineering structures. Paper 88, 3rd International Conference on Recent Advances in Structural Dynamics, University of Southampton, Southampton.
- Tsang, W. F. and Williams, C. (1990). A comparison of some methods of modal parameter extraction. Proceedings, 8th International Modal Analysis Conference, Kissimmee, Florida.
- Ulm, S. C. (1986). Investigations into the effective use of structural modification. Proceedings, 4th International Modal Analysis Conference, Los Angeles, California, 2, 1276-1286.
- Unholtz, K. (1988). Vibration testing machines. Shock and Vibration Handbook (Harris, C. M., Ed.), McGraw-Hill Inc., New York, 25:1-25:26.
- Uzgider, Z., Sanli, A. K., Piroglu, F. and Caglayan, D. B. (1993). Identification of railway bridges using locomotive-induced vibrations. Bridge Management 2 (Harding, J. E., Parke, G. A. R. and Ryall, M. J., Eds.), Thomas Telford, London, 833-841.
- Vandiver, J. K. (1977). Detection of structural failure on fixed platforms by measurements of dynamic response. Journal of Petroleum Technology, 305-310.
- Vanhonacker, P. (1994). Linking analysis and test: dynamic behaviour of a steel bridge. Proceedings, 12th International Modal Analysis Conference, Honolulu, Hawaii, 1, 713-717.
- Ventura, C. E., Felber, A. J. and Prion, H. G. L. (1994). Seismic evaluation of a long span bridge by modal testing. Proceedings, 12th International Modal Analysis Conference, Honolulu, Hawaii, 2, 1309-1315.
- Vincent, G. S. (1958). Golden gate bridge vibration studies. Journal of the Structural Division, ASCE, 84(ST6).
- Ward, H. S. (1984). Traffic generated vibrations and bridge integrity. Journal of

Structural Engineering, ASCE, 110(10), 2487-2498.

Williams, C. (1983). Vibration monitoring of some civil engineering structures. B.S.S.M./I.MeEch.E. Joint Conference on Measurement in the Vibration Environment, British Society for Strain Measurement, Durham.

Williams, C. (1990). The effects of vibration on large structures and the determination of dynamic characteristics. International Conference on Engineering Integrity through Testing, Birmingham, 441-452.

Williams, C. (1992a). Testing of large structures using vibration techniques. Structural Integrity Assessment, Elsevier Applied Science, London, 290-299.

Williams, G. T. (1992b). A doubtful detail. *The Structural Engineer*, 70(15), 277-278.

Wills, J. (1977). Correlation of calculated and measured dynamic behaviour of bridges. Symposium on Dynamic Behaviour of Bridges, Transport and Road Research Laboratory, Crowthorne, Berkshire, 70-89.

Wolff, T. and Richardson, M. H. (1989). Fault detection in structures from changes in their modal parameters. Proceedings, 7th International Modal Analysis Conference, Las Vegas, Nevada, 87-94.

Wood, M. G., Friswell, M. I. and Penny, J. E. T. (1992). Exciting large structures using a bolt-gun. Proceedings, 10th International Modal Analysis Conference, San Diego, California, 1, 233-238.

Worden, K., Ball, A. D. and Tomlinson, G. R. (1993). Neural networks for fault location. Proceedings, 11th International Modal Analysis Conference, Kissimmee, Florida, 1, 47-54.

Wu, X., Ghaboussi, J. and Garrett, J. H. (1992). Use of neural networks in detection of structural damage. *Computers and Structures*, 42, 649-659.

Yang, J. C. S., Chen, J. and Dagalakis, N. G. (1983). Damage detection in offshore structures by the random decrement technique. 2nd International Offshore Mechanics and Erotic Engineering Symposium.

Yang, J. C. S., Dagalakis, N. and Hirt, M. (1980). Application of the random decrement technique in the detection of an induced crack on an offshore model. *Computational Methods for Offshore Structures*, ASME, Publication AMD37, 55-68.

Yang, J. C. S., Tsai, T., Pavlin, V., Chen, J. and Tsai, W. H. (1985a). Structural damage detection by the system identification technique. *Shock and Vibration Bulletin*, 55(3), 57-66.

Yang, J. C. S., Tsai, T., Tsai, W. H. and Chen, R. Z. (1985b). Detection and identification of structural damage from dynamic response measurement. ASME 4th International Symposium on Offshore Mechanics and Arctic Engineering, Dallas, Texas.

Yar, M. and Hammond, J. K. (1987). Parameter estimation for hysteretic systems.

Journal of Sound and Vibration, 117(1), 161-172.

Yuen, M. M. F. (1985). A numerical study of the eigenparameters of a damaged cantilever. Journal of Sound and Vibration, 103(3), 301-310.

Yuen, M. M. F. (1986). Eigenparameter analysis of beams with different end conditions. Proceedings, 4th International Modal Analysis Conference, Los Angeles, 2, 1572-1576.

Zaveri, K. (1984). Modal analysis of Large Structures - Multiple Exciter Systems. Bruel and Kjaer Publication.

Zhang, K. Y., Gu, A. J. and Li, J. W. (1992). Diagnosis of a slot fault on a frame structure. Proceedings, 10th International Modal Analysis Conference, San Diego, California, 1, 549 - 553.

Zhang, K. Y., Cheng, L. J. and Jin, T. X. (1993). Research on the diagnosis of defect on a building foundations pile. Proceedings, 11th International Modal Analysis Conference, Kissimmee, Florida, 1, 690-695.

Zhang, Z. (1994). Error study of bridge tests for the purpose of structural identification. Proceedings, 12th International Modal Analysis Conference, Honolulu, Hawaii, 1, 433-441.

## **APPENDIX**

### **METEOROLOGICAL DATA DURING FULL-SCALE TESTS**

Plymouth Weather Station (for Deep Lane bridge):      Pages 280-282

Nettlecombe Weather Station (for Holway Road bridge): Page 283

Table A.1 Environmental variables for Wednesday, 14th October 1992

Time (GMT)	Wind		Temp. (°C)	Rainfall (mm)	Relative Humidity (%)
	Direction (°; clockwise from north)	Speed (knots)			
0050	340	0	4.5	0.0	87
0150	340	1	4.4	0.0	89
0250	30	0	4.7	0.0	90
0350	300	0	5.7	0.0	89
0450	340	0	6.1	0.0	87
0550	330	0	6.7	0.0	90
0650	270	0	7.6	0.0	86
0750	310	1	8.3	0.0	83
0850	300	0	9.2	0.0	85
0950	280	5	10.7	0.0	76
1050	270	9	11.1	0.0	74
1150	270	11	11.4	0.0	73
1250	310	12	11.1	0.0	76
1350	290	11	11.7	0.0	73
1450	290	14	11.6	trace	75
1550	280	16	11.1	trace	79
1650	280	15	11.1	trace	77
1750	280	13	11.0	trace	80
1850	270	15	10.5	trace	85
1950	270	15	11.1	trace	80
2050	270	15	10.7	0.0	90
2150	270	16	10.4	0.2	94
2250	270	13	9.7	0.2	91
2350	340	8	9.0	1.0	95

GMT - Greenwich Mean Time

The data refer to measurements made during the hour ending at the times shown.  
trace = rainfall less than 0.2mm but greater than 0.0mm

Table A.2 Environmental variables for Thursday, 15th October 1992

Time (GMT)	Wind		Temp. (°C)	Rainfall (mm)	Relative Humidity (%)
	Direction (°; clockwise from north)	Speed (knots)			
0050	340	8	8.6	trace	87
0150	340	10	7.6	0.0	78
0250	330	10	6.6	0.0	76
0350	320	5	6.0	0.0	78
0450	320	5	6.2	0.2	80
0550	350	9	6.1	0.2	80
0650	320	6	5.8	0.0	86
0750	320	11	6.4	trace	83
0850	310	11	7.8	0.0	75
0950	330	14	9.4	0.0	66
1050	340	19	9.7	trace	68
1150	350	18	8.9	trace	74
1250	340	15	8.6	1.0	73
1350	320	12	9.8	trace	66
1450	340	12	9.0	trace	65
1550	330	10	8.7	0.0	64
1650	330	12	8.1	0.0	65
1750	340	5	6.8	0.0	71
1850	330	7	6.3	0.0	77
1950	340	5	5.5	0.0	80
2050	340	7	5.8	0.0	81
2150	340	4	4.8	0.0	86
2250	360	3	3.5	0.0	91
2350	60	3	2.3	0.0	93

GMT - Greenwich Mean Time

The data refer to measurements made during the hour ending at the times shown.  
trace = rainfall less than 0.2mm but greater than 0.0mm

Table A.3 Environmental variables for Tuesday, 25th May 1993

Time (GMT)	Wind		Temp. (°C)	Rainfall (mm)	Relative Humidity (%)
	Direction (°; clockwise from north)	Speed (knots)			
0050	30	2	12.4	0.0	94
0150	20	0	12.5	0.0	94
0250	10	0	12.5	0.0	93
0350	350	0	12.3	0.0	94
0450	220	0	12.2	0.0	95
0550	210	0	12.8	0.0	93
0650	80	4	15.1	0.0	81
0750	80	12	13.9	3.2	95
0850	70	12	14.3	0.6	93
0950	80	13	14.0	3.6	95
1050	70	13	14.8	1.6	92
1150	80	14	15.7	trace	87
1250	80	18	17.3	0.0	80
1350	90	18	17.2	0.0	80
1450	90	17	16.1	0.0	85
1550	90	14	17.2	0.0	82
1650	80	17	16.2	trace	88
1750	90	16	15.2	0.4	94
1850	90	15	15.1	0.2	95
1950	90	13	14.8	0.4	96
2050	80	11	14.5	0.2	95
2150	80	12	14.8	trace	92
2250	80	13	15.3	0.4	94
2350	70	12	15.2	10.0	96

GMT - Greenwich Mean Time

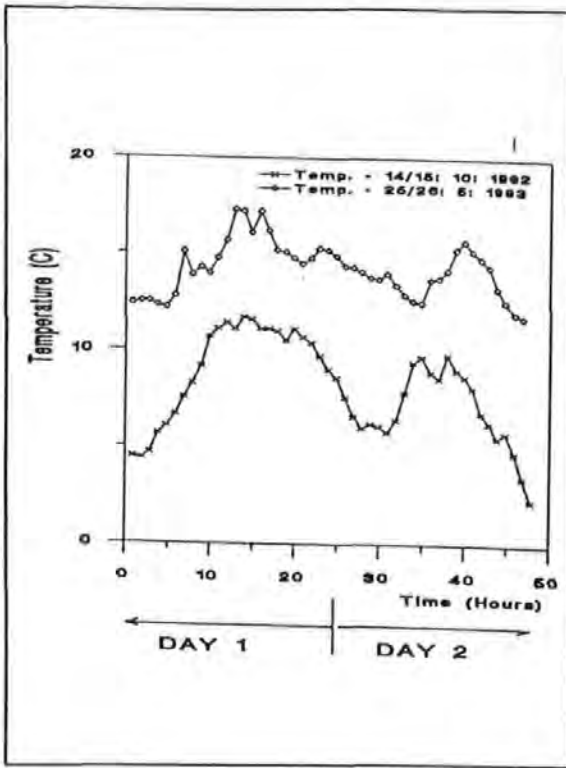
The data refer to measurements made during the hour ending at the times shown  
 trace = rainfall less than 0.2mm but greater than 0.0mm

Table A.4 Environmental variables for Wednesday, 26th May 1993

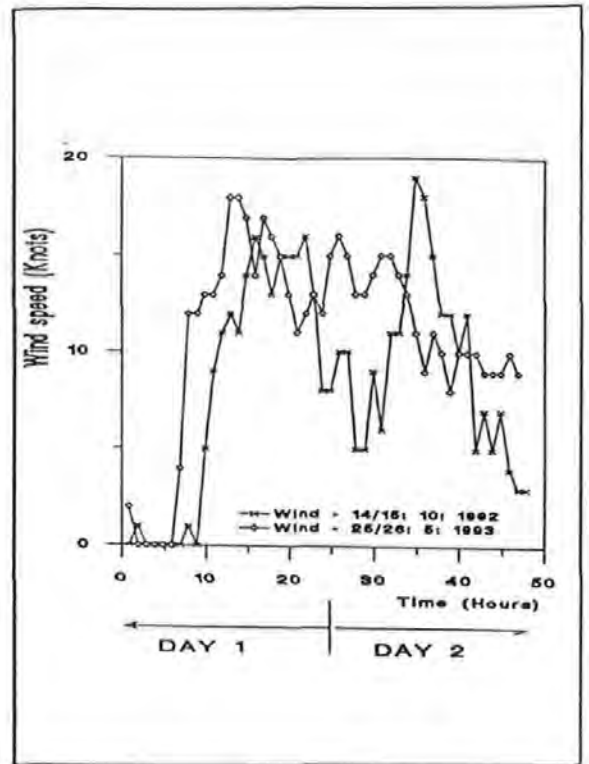
Time (GMT)	Wind		Temp. (°C)	Rainfall (mm)	Relative Humidity (%)
	Direction (°; clockwise from north)	Speed (knots)			
0050	90	15	14.9	9.8	94
0150	90	16	14.4	trace	95
0250	90	15	14.3	0.0	93
0350	90	13	14.1	0.0	93
0450	90	13	13.8	0.0	91
0550	90	14	13.7	0.0	91
0650	90	15	14.0	0.0	88
0750	90	15	13.4	0.6	93
0850	90	14	12.9	5.0	95
0950	80	13	12.6	0.2	95
1050	90	11	12.5	3.2	97
1150	90	9	13.7	1.4	96
1250	90	11	13.8	0.0	98
1350	100	10	14.2	0.0	97
1450	80	8	15.3	0.0	92
1550	100	10	15.7	0.0	89
1650	80	10	15.2	0.0	89
1750	90	10	14.8	0.0	92
1850	80	9	14.4	4.6	96
1950	140	9	13.3	1.8	97
2050	170	9	12.6	0.0	100
2150	200	10	12.0	0.0	100
2250	230	9	11.8	0.0	96
2350					

GMT - Greenwich Mean Time

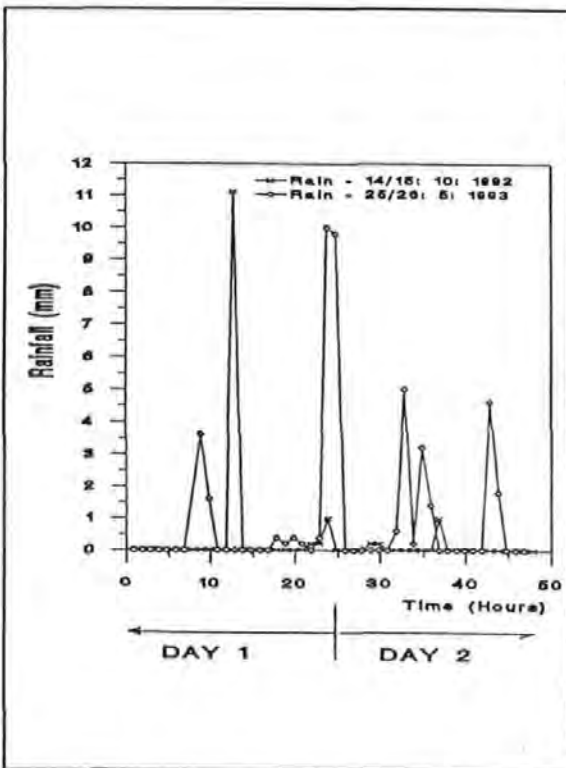
The data refer to measurements made during the hour ending at the times shown  
 trace = rainfall less than 0.2mm but greater than 0.0mm



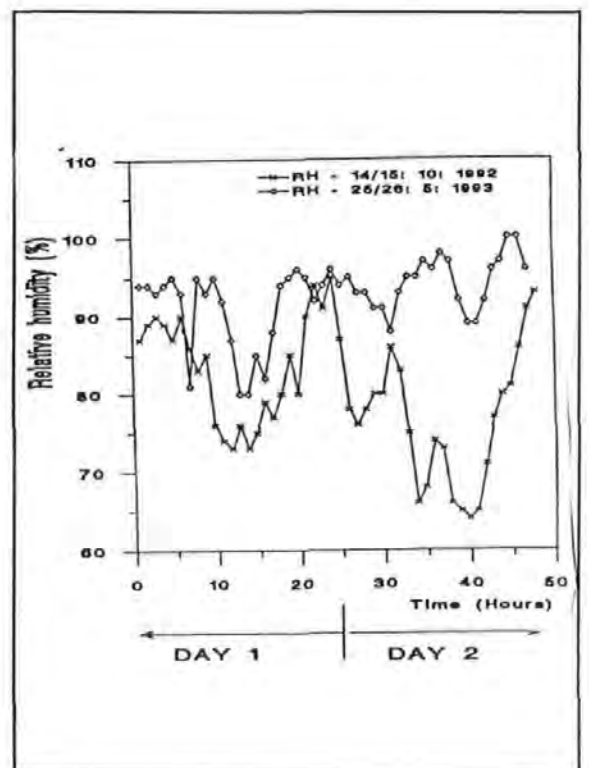
(a) Temperature



(b) Wind speed



(c) Rainfall



(d) relative humidity

Figure A.1 - Variations in ambient conditions in Plymouth during tests on Deep Lane bridge

**Table A.5 Meteorological data during tests on Holway Road bridge**

Date	Temperature (deg. C)			Rain-fall Daily Total (mm)	Sun-shine Daily Total (hr)	Wind			Rel. Humidity at 0900 GMT (%)
	Max	Min	Mean			Mean Speed for Day	Speed at 0900 GMT (kn)	Direction at 0900 GMT (deg.)	
2/11/93	8.0	2.0	5.0	8.0	-	-	2	90	92
3/11/93	10.6	3.0	6.8	1.8	-	-	2	160	100
21/3/94	7.5	2.2	4.8	1.6	-	-	19	360	93
22/3/94	11.8	2.1	6.9	2.2	-	-	13	270	92